TECHNISCHE UNIVERSITÄT DRESDEN

Faculty of Environmental Sciences

Modelling Net Primary Productivity and Above-Ground Biomass for Mapping of Spatial Biomass Distribution in Kazakhstan

Dissertation for awarding the academic degree
Doktoringenieur (Dr.-Ing.)

Submitted by
Dipl.-Ing. Christina Eisfelder

Supervisor:

Prof. Dr. phil. habil. Manfred F. Buchroithner
Technische Universität Dresden, Institute for Cartography

Prof. Dr. rer. nat. habil. Stefan Dech
German Aerospace Center, German Remote Sensing Data Center

Prof. Dr. Martin Kappas
Georg-August-Universität Göttingen, Institute of Geography

Date of submission: 20 December 2012

Dresden, 20 June 2013

Erklärung des Promovenden

Die Übereinstimmung dieses Exemplars mit dem Original der Dissertation zum Thema:

"Modelling Net Primary Productivity and Above-Ground Biomass for Mapping of Spatial Biomass Distribution in Kazakhstan"

wird hiermit bestätigt.

.....
Ort, Datum

.....
Unterschrift

This dissertation was prepared at the German Remote Sensing Data Center (DFD) of the German Aerospace Center (DLR), Oberpfaffenhofen

Acknowledgements

The completion of this dissertation would not have been possible without the valuable support from various people and institutions to whom I would like to express my sincere gratitude.

First of all, I would like to thank my supervisor Prof. Dr. Manfred Buchroithner from Dresden University of Technology for his supervision and interest in this work. He always supported this thesis with helpful advice.

I am also grateful to Prof. Dr. Stefan Dech, director of the German Remote Sensing Data Center (DFD) of the German Aerospace Center (DLR) for his role as co-reviewer and for giving me the opportunity to pursue this study under the Network EOS (Integrated Earth Observation System) PhD Program at DLR-DFD. It has been a great pleasure for me to work at his institute at the German Aerospace Center, Oberpfaffenhofen.

Many thanks also to Prof. Dr. Martin Kappas for taking over the third review.

I would especially like to express my sincere thank to Dr. Claudia Künzer, team leader of the team 'Land Surface Dynamics' at DFD and supervisor of this thesis at DLR, for her constant support, advice, and constructive discussions. Her steady interest in this work and encouragement gave me strength to stay the course.

I am also grateful to Andreas Müller, head of the 'Land Surface' department, for facilitating the accomplishment of this work in his department, and to my colleagues from the team 'Land Surface Dynamics' for the always friendly, helpful, and motivating atmosphere.

Particularly, I would like to sincerely thank Igor Klein for his invaluable support during my field campaign to Kazakhstan in June 2011. Without his translating and assistance the extensive field campaign would not have been possible. Many thanks also for translating the abstract to Russian.

Moreover, I would like to thank my colleagues Markus Niklaus and Markus Tum for their cooperation and help regarding processing with BETHY/DLR and for commenting on various parts of this thesis. Thanks also to Ursula Geßner for advice with error propagation.

I am also grateful to several people from Kazakhstan, who helped me during my field campaign. First of all, very warm thanks to Prof. Dr. Farida Akiyanova from the Institute of Geography of the Academy of Sciences, Almaty, for her friendly advice and help with finding field assistants and providing equipment for the field campaign. Thanks also for providing the vegetation map from the National Atlas of the Republic of Kazakhstan and permission to use the map within this thesis.

I would especially like to thank my field assistants Aruzhan Bekkulieva and Zhandos Kanafin from the Institute of Geography, as well as Arman Ashirbaev for always keeping up an enjoyable atmosphere despite the hard work and long working hours during the field campaign.

Moreover, I am very grateful to Dr. Kazbek Toleubayev from the Kazakh Research Institute for Plant Protection and Quarantine, Almaty, and his laboratory staff for oven drying of my biomass samples from both field campaigns in 2010 and 2011.

I am also grateful to Thomas Eiglsperger and Alexander Kotenkov for collecting biomass samples in Central Kazakhstan during a field campaign to Kazakhstan carried out on behalf of DLR in December 2010.

Many thanks also to Prof. Dr. Martin Kappas and Dr. Pavel Propastin from University of Göttingen for offering me the opportunity to join their field trip to Kazakhstan in June 2010.

I would like to extend my gratitude to Dr. Miriam Machwitz for advice with pre-processing of input data for the RBM and model application, as well as to Dr. Jochen Richters for advice regarding the RBM and interpretation of results from the model comparison.

Many thanks go to Pierre Hiernaux from the Centre d'Etudes Spatiales de la Biosphère, Toulouse, for his advice with *in situ* measurements.

I would also like to thank Dr. Niels Thevs and Allan Buras from the working group 'Landscape Ecology and Ecosystem Dynamics' of the Ernst-Moritz-Arndt-Universität Greifswald for general advice with field work in Central Asia, literature recommendations, and providing allometric equations.

Thanks also to Ulrike Dittmann for help with digitising of field protocols, Moritz Mössner for assistance with downloading and pre-processing of MODIS data and digitising of field protocols, and Thomas Baldauf for assistance with downloading and preparation of climate station data.

Furthermore, I would like to thank Thomas Hahmann, Dr. Danielle Hoja, and Stefan Hahmann for proofreading and commenting on various parts of this thesis, as well as Dr. Beatrix Weber and Steve and Lesley Hoad for proofreading of English language.

Very special thanks deserves my boyfriend Thomas Hahmann for his constant support, endless patience, and encouragement. Your love and understanding helped me through the challenging times during the preparation of this thesis.

Finally, I would like to express my gratitude to my parents for their support during my studies that led me here.

Abstract

Biomass is an important ecological variable for understanding the responses of vegetation to the climate system and currently observed global change. In semi-arid areas it especially influences environmental processes, such as the hydrological cycle, soil erosion and degradation. It is therefore essential to develop accurate and transferable methods for biomass estimation in these areas. The quantification of biomass for large areas and long time periods is necessary to identify and monitor those areas under high risk of degradation and desertification. This can only be achieved using data collected from satellite remote sensing.

The impact of changes in vegetation biomass on the global ecosystem is of high relevance and may have a critical influence on the future evolution of the climate. Modelling net primary productivity (NPP) is an important instrument for analysing carbon exchange between atmosphere and vegetation. It allows for quantification of carbon sinks and sources. The analysis of NPP time-series and their spatio-temporal patterns helps us to understand ecological functioning and potential disturbances.

The vegetation in the arid and semi-arid environments of Kazakhstan faces extreme climatic conditions. Land degradation and desertification already pose large ecological challenges. The region is expected to be affected particularly strongly by future climate change. In Central Asia further rises in temperature and an intensification of aridity are predicted. In the context of diverse anthropogenic and climatic influences on the Kazakh environment, it is of great interest to observe large-scale vegetation dynamics and biomass distribution.

In this dissertation, previous research activities and remote-sensing-based methods for biomass estimation in semi-arid regions have been comprehensively reviewed for the first time. The review revealed that the biggest challenge is the transferability of methods in time and space. Empirical approaches, which are predominantly applied, proved to be hardly transferable. This lack of transferability hinders a repeated or operational application of biomass estimation methods. Remote-sensing-based NPP models, on the other hand, allow for regional to continental modelling of NPP time-series and are potentially transferable to new regions.

This thesis thus deals with modelling and analysis of NPP time-series for Kazakhstan and presents a methodological concept for derivation of above-ground biomass (AGB) estimates based on NPP data. The focus for the methodological development was on biomass estimation for natural and semi-natural environments, which cover about 70% of the area of Kazakhstan. For validation of the results, biomass field data were collected in June 2011 in three study areas in Central, South, and West Kazakhstan. Additionally, field data was also collected in Central Kazakhstan in December 2010.

For the selection of an appropriate model, two remote-sensing-based NPP models were applied to a study area in Central Kazakhstan. The first is the Regional Biomass Model (RBM), a light-use-efficiency model. The second is the Biosphere Energy Transfer Hydrology Model adapted by DLR (BETHY/DLR), which is a soil-vegetation-atmosphere-transfer model. Both models calculate the NPP on a regional scale of approximately 1 km² spatial resolution and were applied to Kazakhstan for the first time in this dissertation.

Differences in the modelling approaches, intermediate products, and calculated NPP, as well as their temporal characteristics were analysed and discussed. The model BETHY/DLR calculated higher NPP (mean annual NPP 2010 and 2011: 136.9 g C m^{-2} and 106.7 g C m^{-2}) than the RBM (62.1 g C m^{-2} and 54.6 g C m^{-2}) and showed stronger inter-annual changes. The comparison to field data from 2011 yielded better results for BETHY/DLR, though the results

from both models were highly correlated to the field observations (BETHY/DLR: R=0.97, RMSE=8.4 g C m^{-2}; RBM: R=0.99, RMSE=22.5 g C m^{-2}).

The model BETHY/DLR was then applied with a regional land cover map to calculate NPP for Kazakhstan for 2003–2011. The results were analysed regarding spatial, intra-annual, and inter-annual variations. Such detailed analyses of NPP time-series for Kazakhstan have not been available before in the literature. The mean annual NPP for Kazakhstan is 143 g C m^{-2}. The three most important natural land cover classes in Kazakhstan and their mean annual NPP are: grassland with 140 g C m^{-2}, sparse vegetation with 120 g C m^{-2}, and open shrubland with 112 g C m^{-2}. The maximum productivity is reached in June. NPP anomalies occurred most often in agricultural areas in the North of Kazakhstan. Natural semi-arid and arid ecosystems showed a low inter-annual NPP variability.

In addition, the correlation between NPP and meteorological parameters was analysed. Correlation between NPP and temperature as well as between NPP and photosynthetically active radiation showed correlation coefficients of R>0.6 for more than 90% of the land area. The reaction of vegetation growth to precipitation was delayed one to two months.

In the last part of this dissertation, a methodological concept for derivation of above-ground biomass estimates of natural vegetation from NPP time-series has been developed. The procedure aims at estimating the above-ground biomass of herbaceous (grass/herbs) and woody (shrubs) vegetation for Kazakhstan for the period of maximum vegetation growth. The methodological concept is based on the NPP time-series, information about fractional cover of herbaceous and woody vegetation, and plants' relative growth rates (RGRs). It has been the first time that these parameters are combined for biomass estimation in semi-arid regions.

The developed approach was finally applied to estimate biomass for the three study areas in Kazakhstan. The validation with field data showed the high importance of accurate fractional cover information. This information is especially important for estimation of woody biomass. With constant fractional cover values for individual land cover classes, the resulting woody biomass showed a weak linear correlation to biomass field data. Using fractional cover information from field observations, the developed approach yielded results that showed a strong correlation to woody biomass from field data (R=0.83, RMSE=24.4 g C m^{-2}).

The validation for herbaceous biomass revealed a moderate correlation to biomass field data (R=0.64, RMSE=25.4 g C m^{-2}). An underestimation of herbaceous biomass was observed for most validation sites, which was accounted for by an underestimated NPP. A classification of different herbaceous vegetation communities is needed for a better representation of the NPP variability. This in turn will improve the herbaceous biomass estimates.

The results of this dissertation provide information about the vegetation dynamics in Kazakhstan for 2003–2011. This is valuable information for a sustainable land management and the identification of regions that are potentially affected by a changing climate. Furthermore, a methodological concept for the estimation of biomass based on NPP time-series is presented. The developed method is potentially transferable. Providing that the required information regarding vegetation distribution and fractional cover is available, the method will allow for repeated and large-area biomass estimation for natural vegetation in Kazakhstan and other semi-arid environments.

Kurzzusammenfassung (Abstract in German)

Biomasse ist eine bedeutende ökologische Variable und ihre Beobachtung ist entscheidend für das Verständnis der Reaktion von Vegetation auf den gegenwärtig zu beobachtenden globalen Wandel. Sie beeinflusst ökologische Prozesse wie den Wasserkreislauf, Bodenerosion und Degradation, insbesondere in semi-ariden Gebieten. Daher besteht eine große Notwendigkeit an präzisen und übertragbaren Methoden zur Quantifizierung von Biomasse für diese Regionen. Eine Abschätzung der Biomasse für große Gebiete und lange Zeiträume ist entscheidend für das Erkennen und Überwachen von Gebieten mit einem hohen Degradations- und Desertifikationsrisiko. Dies kann nur mit Hilfe der Satellitenfernerkundung geleistet werden.

Die Auswirkungen von Veränderungen der Vegetationsbiomasse auf das globale Ökosystem sind ebenfalls von hoher Relevanz und können einen entscheidenden Einfluss auf die zukünftige Entwicklung des Klimas nehmen. Ein wichtiges Instrument für die Analyse des Kohlenstoffaustauschs zwischen Atmosphäre und Vegetation ist die Modellierung der Netto-Primär-Produktion (NPP). NPP-Modellierung ermöglicht die Quantifizierung von Kohlenstoffsenken und -quellen. Die Analyse von NPP-Zeitreihen sowie ihrer raum-zeitlichen Änderungen trägt zum Verständnis ökologischer Funktionsweisen und deren möglichen Beeinträchtigungen bei.

Die Vegetation in den ariden und semi-ariden Gebieten Kasachstans unterliegt extremen klimatischen Bedingungen. Bodendegradation und Wüstenbildung stellen bereits heute große ökologische Herausforderungen dar. Die Region wird voraussichtlich besonders stark von zukünftigen Klimaänderungen betroffen sein – für Zentralasien werden ein weiterer Temperaturanstieg sowie eine Intensivierung der Trockenheit prognostiziert. Im Kontext vielfältiger anthropogener und klimatischer Einflüsse auf die Umwelt Kasachstans ist die großräumige Beobachtung der Biomasse sowie der Vegetationsdynamik von großem Interesse.

Zu Beginn dieser Dissertation wurde eine umfassende Literaturstudie zu bestehenden Forschungsaktivitäten und fernerkundungsbasierten Methoden zur Abschätzung von Biomasse in semi-ariden Gebieten vorgenommen, welche in dieser Form zuvor nicht verfügbar war. Die Auswertung ergab, dass die größte Herausforderung in der räumlichen und zeitlichen Übertragbarkeit der angewandten Methoden besteht. Die überwiegend genutzten empirischen Ansätze erwiesen sich als kaum übertragbar, was eine wiederholte oder operationelle Anwendung verhindert. Fernerkundungsbasierte NPP-Modelle ermöglichen hingegen die Modellierung von NPP-Zeitserien auf regionaler bis kontinentaler Ebene und sind potentiell auf andere Regionen übertragbar.

Diese Dissertation befasst sich daher mit der Modellierung und Analyse von NPP-Zeitreihen für Kasachstan und präsentiert ein methodisches Konzept zur Abschätzung der oberirdischen Biomasse (AGB) basierend auf NPP-Daten. Der Fokus für die Entwicklung der Methodik liegt auf natürlichen und naturnahen Ökosystemen, die ca. 70% der Fläche Kasachstans ausmachen. Zur Validierung der Ergebnisse wurden im Juni 2011 in drei Untersuchungsgebieten in Zentral-, Süd- und West-Kasachstan Biomasse-Felddaten aufgenommen. Zusätzlich wurden Felddaten im Dezember 2010 in Zentral-Kasachstan erfasst.

Für die Auswahl eines geeigneten Modells wurden zwei fernerkundungsbasierte NPP-Modelle für ein Untersuchungsgebiet in Zentral-Kasachstan angewendet: das Regionale Biomasse-Modell (RBM), ein Lichtnutzungseffizienz-Modell, und das vom DLR adaptierte ‘Biosphere Energy Transfer Hydrology Model‘ (BETHY/DLR), ein Boden-Vegetations-

Atmosphären-Transfer-Modell. Beide Modelle berechnen die NPP auf regionaler Ebene mit ca. 1 km² räumlicher Auflösung und wurden in dieser Arbeit erstmals für Kasachstan angewendet.

Unterschiede in den Modellansätzen, Zwischenprodukten und NPP-Ergebnissen sowie deren zeitliche Ausprägung wurden ausgewertet und diskutiert. Das Modell BETHY/DLR berechnete höhere NPP-Werte (mittlere jährliche NPP 2010 und 2011: 136,9 g C m^{-2} und 106,7 g C m^{-2}) als das RBM (62,1 g C m^{-2} und 54,6 g C m^{-2}) und zeigte stärkere jährliche Veränderungen auf. Der Vergleich zu Felddaten ergab bessere Ergebnisse für BETHY/DLR. Die Korrelation der Ergebnisse zu den Feldbeobachtungen war jedoch für beide Modelle hoch (BETHY/DLR: R=0,97; RMSE=8,4 g C m^{-2}; RBM: R=0,99; RMSE=22,5 g C m^{-2}).

Das Modell BETHY/DLR wurde anschließend unter Verwendung einer regionalen Landbedeckungskarte zur Berechnung der NPP für Kasachstan für die Jahre 2003–2011 angewendet. Die Ergebnisse wurden in Bezug auf räumliche sowie zeitliche Variationen analysiert. Derartig detaillierte Analysen von NPP-Zeitreihen für Kasachstan sind in der Literatur bisher nicht existent. Die mittlere jährliche NPP für Kasachstan beträgt 143 g C m^{-2}. Die drei wichtigsten natürlichen Landbedeckungsklassen in Kasachstan und ihre mittlere jährliche NPP sind Grasland mit 140 g C m^{-2}, spärliche Vegetation mit 120 g C m^{-2}, und offenes Buschland mit 112 g C m^{-2}. Die maximale Produktivität wird im Juni erreicht. NPP-Anomalien zeigten sich am häufigsten in landwirtschaftlich genutzten Gebieten im Norden Kasachstans. Natürliche semi-aride und aride Ökosysteme wiesen eine geringe jährliche NPP-Variabilität auf.

Zudem wurde die Korrelation zwischen der NPP und meteorologischen Parametern untersucht. Zu Temperatur und photosynthetisch aktiver Strahlung (PAR) ergaben sich Korrelationskoeffizienten von R>0,6 für mehr als 90% der Landfläche. Die Reaktion der NPP auf die Niederschlagswerte zeigte eine Verzögerung von ein bis zwei Monaten.

Im abschließenden Teil der Dissertation wurde ein methodisches Konzept zur Abschätzung der oberirdischen Biomasse von natürlicher Vegetation auf Basis von NPP-Zeitreihen entwickelt. Das Verfahren zielt auf die Ableitung von krautiger Biomasse (Gras/Kräuter) und holziger Biomasse (Sträucher) für Kasachstan für den Zeitraum des maximalen Vegetationswachstums. Das methodische Konzept basiert auf der NPP-Zeitserie, Informationen zur prozentualen Bodenbedeckung von krautiger und holziger Vegetation sowie relativen Wachstumsraten (RGRs) der ansässigen Pflanzengattungen. Diese Parameter wurden erstmals für die Abschätzung von Biomasse in semi-ariden Gebieten kombiniert.

Die entwickelte Methodik wurde anschließend für die Abschätzung der Biomasse in den drei Untersuchungsgebieten in Kasachstan angewendet. Die Validierung mit Felddaten zeigte die große Bedeutung genauer prozentualer Bedeckungsgrade, welche insbesondere für die Abschätzung der holzigen Biomasse von hoher Relevanz sind. Mit konstanten Bedeckungsgraden pro Landbedeckungsklasse wurde für holzige Biomasse eine schwache lineare Korrelation zu Biomasse-Felddaten beobachtet, mit prozentualen Bedeckungswerten aus Feldbeobachtungen zeigten die Ergebnisse eine hohe Korrelation zu den Felddaten (R=0,83, RMSE=24,4 g C m^{-2}).

Für krautige Biomasse ergab die Validierung eine mittlere Korrelation zu den Biomasse-Felddaten (R=0,64, RMSE=25,4 g C m^{-2}). Für die meisten Validierungspunkte wurde eine Unterschätzung der krautigen Biomasse festgestellt, welche zum Teil auf eine Unterschätzung der NPP zurückgeführt werden kann. Eine Klassifizierung verschiedener krautiger Vegetationszusammensetzungen ist – bereits für die NPP-Modellierung – notwendig um die Variabilität der Biomasse krautiger Vegetation besser abbilden zu können.

Die Ergebnisse dieser Dissertation geben Aufschluss über die Vegetationsdynamik in Kasachstan im Zeitraum 2003–2011. Diese Informationen stellen eine wichtige Grundlage für ein

nachhaltiges Landmanagement und die Identifizierung potentiell vom Klimawandel betroffenener Regionen dar. Außerdem wird ein methodisches Konzept für die Abschätzung von Biomasse auf Basis von NPP-Zeitserien vorgestellt. Die entwickelte und potentiell übertragbare Methodik ermöglicht bei Verfügbarkeit von Informationen zu räumlicher Vegetationsverteilung und Bedeckungsgraden die wiederholte und großflächige Abschätzung der Biomasse natürlicher Vegetation in Kasachstan und anderen semi-ariden Regionen.

Резюме (Abstract in Russian)

Биомасса является важним параметром экосистемы и её наблюдение имеет решающее значение для понимания реакции растительности на наблюдаемые глобальние изменения. Биомасса влияет на экологические процессы, такие как круговорот воды, эрозиию и деградациию почв, особенно в полузасушливых районах. Таким образом, существует большая потребность в точных и широко применимих методах для количественной оценки биомассы в этих регионах. Оценка биомассы для широкомасштабных территорий и удолгосрощном периоде имеет решающее значение для выявления и обнаруживания районов с высоким риском деградации почв и опустинивания. Это задача может быть достигнутатолько с помощью спутникового дистанционного зондирования.

Влияние изменении в растительной биомассе на глобальные экосистемы является также знашимой и может оказать решающее влияние на дальнейшее изменение климата. Важным инструментом для анализа обмена углерода между атмосферой и растительностью является моделирование Net Primary Productivity (NPP). Моделированье NPP позволяет количественно определить поглотителей и источники углерода. Анализ временных рядов NPP и их пространственно-временные изменения вносит свой вклад в понимание экологических функций и возможних факторов влияюших на эти функции.

Растительност в пустынных и полупустынных регионах Республики Казахстана подвержена экстремальным климатическим условиям. В настоящие время деградация почв и опустынивание являются одними из основных экологических проблем в этих регионах. В будущем регионы Республики Казахстана предположительно будит в значителной мере подвершени изменениям климата. Для стран Центральной Азии ожидается дальнейшее повышение температуры, а также ожидается усиление засух. В контексте различных антропогенных и климатических воздействий на окружающую среду в Республике Казахстан имеется большой интерес к широкомасштабноми мониторинги биомассы и динамики растительности.

В начале диссертации был проведен обширный обзор литературы о существующих исследованиях по дистанционноми зондированию и оценке биомассы в полузасушливых регионах. Такой обзор не был доступен до настоящего времени. Анализ показал, что самой большой проблемой явльаетса перенос методов в пространственном и временном измерением. Использованые эмпирические подходы оказались непременимими к другим территориям или временним отружкам, что преруатствиет их повторному или оперативному использованию. NPP модели основанные на дистанционном зондировании позволяют однако моделирование временных рядов NPP на региональном и континентальном уровне, а также имеют потенциал их исползования в других регионах.

Эта диссертация таким образом представльет моделирование и анализ временных рядов NPP в Казахстане и предлагает методический подход для оценки поверхностной биомассы (AGB) основивайсь на данных NPP. Для разработки методики основное внимание было назеленно на природные и приближенние к природным экосистемам, на долю которых приходится около 70% территории Республики Казахстан. В июне 2011 года в трех регионах Центральном, Южном и Западном Казахстане были проведени работы по сбору биомассы с целью оценки получшенних результатов. Кроме того, полевые данные были собраны в декабре 2010 года в Центральном Казахстане.

Для выбора подходящей модели, две NPP модели основанные на дистанционном зондировании были исследовани в центральном раёне Казахстана: Региональная модель биомассы (RBM) основання на принципе ефективного исположание енергии солнешного излучения и адаптированной в DLR модели "Биосфера Передача энергии Гидрологии" (BETHY/DLR) – модель описиваюшей почвы растительности, и взаимодействие с атмосферой обе модели вычисляли NPP на региональном уровне с пространственним разрешением в 1 км², и в этой работе были впервые использованы впервие для Центрально-Азиатского региона.

Различия в моделних подходах, полученних результатах NPP и их временные характеристики были проанализированы и описани. Модель BETHY/DLR вычислила более высокие значения NPP (среднегодовое NPP 2010 и 2011: 136,9 г С $м^{-2}$ и 106,7 г С $м^{-2}$) хем RBM (62,1 г С $м^{-2}$ и 54,6 г С $м^{-2}$) и показала большие ежегодные изменения. Сравнение с данными 2011 года показали лучшие результаты для BETHY/DLR. Но корреляция результатов с данними полевых наблюдений, однако, была высока для обеих моделей (BETHY/DLR: R=0,97, RMSE=8,4 г С $м^{-2}$, RBM: R=0,99, RMSE=22,5 г С $м^{-2}$).

Впоследствии модель BETHY/DLR была выброна, и с помощью региональной карты почв и растителного покрова были вычислиные NPP по Казахстану с 2003 до 2011 года. Полученные результаты были проанализированы с точки зрения пространственных и временных изменений. Такой подробный анализ временных рядов NPP в Казахстане до сих пор отсутствует в научноей литературе. Среднегодовое NPP в Казахстане составляет 143 г С $м^{-2}$. Три самых основных природных класса почвенно-растительного покрова в Казахстане и их среднегодовой NPP это пастбища с 140 г С $м^{-2}$, редкая растительность с 120 г С $м^{-2}$, и открытие земли покритие кустарником с 112 г С $м^{-2}$. Максимальная продуктивность достигается в июне. Аномалии NPP чаще всего встречаются в сельскохозяйственных районах на севере Казахстана. Природные полузасушливые и засушливые экосистеми показали относительно невисокие годовые изменения NPP.

Кроме того, были исследовани корреляции между NPP и метеорологическими параметрами. Для температури и фотосинтетической активной радиации (PAR) были определени коэффициенты корреляции R>0,6 для более чем 90% территории страны. NPP показало реаксию на количество осадков с задержкой от одного до двух месяцев.

В заключительной части диссертации был разработан методический подход для оценки поверхностной биомассы естественной вегетации на основее временных рядов NPP. Етот метод предназнашен для определения травянистои биомассы (травы / ботвы) и древесной биомассы (кустарники) в Казахстане в период максимального роста растительности. Данние методологический подход основивается на временых рядах NPP, информации о доле покрытия земляной поверхности травянистой и древесной растительностью а также на относительных темпах роста (RGRs) местных видов растений. Эти параметры были впервыесовокурно исползовани для оценки биомассы.

Представленний метод был в итоге применен для оценки биомассы в трех исследуемых регионах Республики Казахстан. Проверка с полевими данными показала большую важность точного процентуального покрытия, которые особенно важны для оценки древесной биомассы. При использовании постоянноі доли покрытия в каждом почвенно-растительном классе для древесной биомассы была определена очень слабая линейная корреляция с данными биомассы полевых измерений в то время как при изполозований даннах полевых наблюдений по доли покритья результаты показали высокую корреляцию (R=0,83, RMSE=24,4 г С $м^{-2}$).

Для травянистой вегетации проверка показала среднею корреляцию (R=0,64, RMSE=25,4 г С $м^{-2}$) между результатами разшётов и данними полевых измерений. Для большинства точек в которых осушествилалась проверка, была найдёна бедооценка доли травянистой вегетации, шточастично обйсняется недооценкои разшитанного NPP. Классификация различных композиций травянистой растительности, използуемой уже на етапе моделирования NPP, имиет важное значение для определенеления изменчивости биомассы травянистой растительности.

Результаты данной работы выявили динамику растительности в Республике Казахстан за период с 2003 по 2011 год. Эта информация является важной основои для устойчивого управления земельными ресурсами и для выявления потенциальных областей, которые могут быть подвержени измененим климата. А также представлен методический подход для оценки биомассы основанний на анализе временных рядов NPP. Разработанная методика которая может быть применена и в других регионах, позволяет при наличии данних о доле покрития вегетацией земной поверхности проводит неоднократние оценки биомассы естественной растительности в Казахстане и в других полузасушливых регионах на большой территори.

Table of Contents

List of Figures

List of Tables

Acronyms / Abbreviations / Symbols

10U	10 metre eastward wind component (ECMWF parameter)
10V	10 metre northward wind component (ECMWF parameter)
2T	2 metre temperature (ECMWF parameter)
ADB	Asian Development Bank
AET	Actual Evapotranspiration
AGB	Above-Ground Biomass
AIRSAR	Airborne polarimetric C-/L-/P-Band SAR sensor
ALOS PALSAR	Phased Array type L-band SAR sensor aboard the Advanced Land Observing Satellite (2006-2011)
APAR	Actual Photosynthetically Active Radiation
Aqua	NASA research satellite launched in 2002
ArcGIS	GIS software developed by the US based company Esri
ASI	Italian Space Agency (Agenzia Spaziale Italiana)
AVHRR	Advanced Very High Resolution Radiometer sensor aboard various NOAA satellites (from 1979 onwards)
B	Biomass
BA	Basal Area
BD	Dry weight above-ground Biomass
BETHY/DLR	Biosphere Energy Transfer Hydrology Model - adapted by DLR
BF	Fresh weight above-ground Biomass
BGB	Below-Ground Biomass
BIOME3	Equilibrium Terrestrial Biosphere Model
BIOME-BGC	Ecosystem Process Model - BioGeochemical Cycles
bNDVI	broad band NDVI
BRDF	Bidirectional Reflectance Distribution Function
BSh	Hot semi-arid climate (Köppen-Geiger climate classification system)
BSk	Cold semi-arid climate (Köppen-Geiger climate classification system)
BT	Brightness Temperature
C	Carbon
C1/C2	Weighting factors for EVI calculation
C_3 plant	Plant that uses the C_3 pathway for carbon fixation in photosynthesis
C_4 plant	Plant that uses the C_4 pathway for carbon fixation in photosynthesis
CA	Crown Area
CAIAG	Central-Asian Institute of Applied Geosciences
CARBOEUROPE	Coordination and dissemination of carbon research results in light of the implementation of Kyoto Protocol in Europe
CASA	Carnegie-Ames-Stanford Approach
CAWa	Regional Research Network Water in Central Asia
CC	Canopy Coverage
CDM	Clean Development Mechanism
CENTURY	Grassland and Agroecosystem Dynamics Model developed by Parton and Rasmussen (1994)
CESBIO	Centre d'Etudes Spatiales de la BIOsphère in Toulouse

CF	Conversion Factor
C-Fix	Ecosystem model developed by Veroustraete et al. (1994)
CGER	Commission on Geosciences, Environment and Resources
CLM	Community Land Model (based on the Common Land Model, Dai et al. 2003)
CO_2	Carbon Dioxide
CP	Convective precipitation (ECMWF parameter)
$CR_{B991–B1306}$	Accumulated Continuum Removal for bands between 991 and 1306 nm
CYCLOPES	Name of a European Union (FP5) funded research project
DAIS	Digital Airborne Imaging Spectrometer
DBH	Diameter at Breast Height
DEM	Digital Elevation Model
DFD	German Remote Sensing Data Center (Deutsches Fernerkundungsdatenzentrum) of DLR
DLR	German Aerospace Center (Deutsches Zentrum für Luft- und Raumfahrt e.V.)
DM	Dry Matter
DMSP	Defense Meteorological Satellite Program
DOI	Digital Object Identifier
DOY	Day of the Year
DPM	Disc Pasture Meter
DTED	Digital Terrain Elevation Data
DWD	German Meteorological Service (Deutscher Wetterdienst)
ECMWF	European Centre for Medium-Range Weather Forecasts
Envisat ASAR	Advanced Synthetic Aperture Radar instrument aboard ESA's Environmental Satellite (2002–2012)
EOC	Earth Observation Center of DLR-DFD
EOS	Integrated Earth Observation System PhD Program
ERA	ECMWF Re-Analysis project
EROS	USGS Center for Earth Resources Observation and Science
ERS-1/-2	European Remote Sensing satellites (1991-2011)
ESA	European Space Agency
ESDB	European Soil Database
ET	Evapotranspiration
EU	European Union
EVI	Enhanced Vegetation Index
FAO	Food and Agriculture Organization
FAO74	FAO's soil classification system (dating from 1974)
FAO90	FAO's soil classification system (dating from 1990)
FC	Fractional Cover
FP	Framework Programmes for Research and Technological Development of the European Union
FPAR	Fraction of absorbed Photosynthetically Active Radiation
FTP	File Transfer Protocol
G	Grass
G	Soil heat flux

GAC	Global Area Coverage (related to AVHRR data)
g C m^{-2}	grams of Carbon per square metre
g DM m^{-2}	grams of Dry Matter per square metre
GCOS	Global Climate Observing System
GEMI	Global Environmental Monitoring Index
GHCN	Global Historical Climatology Network
GIS	Geographic Information System
GLAS	Geoscience Laser Altimeter System aboard NASA's ICESat satellite (2003–2010)
GLC2000	Global Land Cover 2000 project coordinated by JRC
GLCF	Global Land Cover Facility, funded by NASA, provides e.g. Landsat, MODIS, SRTM data
GLOBCOVER	ESA initiative to produce global land cover maps from 300 m spatial resolution MERIS data
GLO-PEM	Global Production Efficiency Model developed by Prince (1991)
GPCC	Global Precipitation Climatology Centre
GPP	Gross Primary Productivity
GPS	Global Positioning System
GTOPO30	Global 30 Arc-Second Elevation Data Set
GTOS	Global Terrestrial Observing System
GTZ	German Technical Cooperation (Deutsche Gesellschaft für Technische Zusammenarbeit)
GVD	Green leaf biomass Volumetric Density
GVI	Global Vegetation Index (related to AVHRR data)
H	Height
H	Herb
H_C	Height to the base of the crown
HCC	High Cloud Cover (ECMWF parameter)
h_{ECMWF}	ECMWF reference height
HWSD	Harmonized World Soil Database
HYBRID	General Ecosystem Model developed by Friend et al. (1997)
HyMap	Airborne Hyperspectral Sensor with 125 spectral bands
IEEE	Institute of Electrical and Electronics Engineers
IGCOS	Integrated Global Carbon Observing System
IIASA	International Institute for Applied Systems Analysis
InSol	Incoming Solar radiation
IPCC	Intergovernmental Panel on Climate Change
ISA	International Standard Atmosphere
ISRIC	International Soil Reference and Information Centre
ISSCAS	Institute of Soil Science – Chinese Academy of Sciences
IUSS	International Union of Soil Sciences
J_C	Function describing carboxylation rate
J_E	Function describing electron transport rate
J_{max}	maximum electron transport rate
JERS-1	Japanese Earth Resources Satellite (1992–1998)
JRC	Joint Research Centre of the European Commission

k	scale factor
L	canopy background adjustment term
L	Length
LAC	Local Area Coverage (related to AVHRR data)
LAI	Leaf Area Index
Landsat ETM+	Landsat Enhanced Thematic Mapper Plus
Landsat TM	Landsat Thematic Mapper
LAT	Latitude
LC	Land Cover
LCC	Low Cloud Cover (ECMWF parameter)
LCC	Land Cover Classification
LCCS	Land Cover Classification Scheme
LiDAR	Light Detection and Ranging
LON	Longitude
LPJ	Lund-Potsdam-Jena Dynamic Global Model developed by Bondeau et al. (2007)
LSP	Large-Scale Precipitation (ECMWF parameter)
LST	Land Surface Temperature
LUE	Light Use Efficiency
LULUCF	Land Use, Land-use Change and Forestry
m ASL	metres Above Sea Level
m BSL	metres Below Sea Level
MCC	Medium Cloud Cover (ECMWF parameter)
MCD12Q1	Land Cover Product derived from MODIS data
MCD43A3	Albedo product derived from MODIS data
MEAB	Millennium Ecosystem Assessment Board
MedAPE	Median Absolute Percentage Error
MERIS	MEdium Resolution Imaging Spectrometer instrument aboard ESA's Envisat satellite (2002–2012)
METEOSAT	Series of geostationary Meteorological Satellites (from 1977 onwards)
mg g^{-1} d^{-1}	milligrams per gram per day (unit for RGR)
MIR	Mid InfraRed
mm/a	annual precipitation in millimetre
MOD05/MYD05	Total Precipitable Water Product derived from MODIS data based on Terra/Aqua observations
MOD13A2/MYD13A2	Vegetation Indices product derived from MODIS data based on Terra/Aqua observations
MOD35	Cloud mask product derived from MODIS data
MOD44B	Vegetation Continuous Fields product derived from MODIS data
MODIS	Moderate-resolution Imaging Spectroradiometer (Sensor aboard the Satellites Terra and Aqua)
MRT	MODIS Reprojection Tool
MSAVI	Modified Soil-Adjusted Vegetation Index
MVC	Maximum Value Composite (related to AVHRR data)
MYD11A2	LST/Emissivity product derived from MODIS data
MYD15A2	LAI and FPAR product derived from MODIS data

NASA	US National Aeronautics and Space Administration
NCDC	NOAA's National Climatic Data Center
NDSVI	Normalized Senescent Vegetation Index
NDVI	Normalized Difference Vegetation Index
$NDVI_{BAmax}$	Background-Adjusted $NDVI_{max}$
$NDVI_{Cum}$	Cumulative NDVI until peak
$NDVI_{CumRat}$	Cumulative NDVI until 1.53 times peak
$NDVI_{max}$	Maximum NDVI
NDWI	Normalized Difference Water Index
NEP	Net Ecosystem Productivity
NGA	National Geospatial-Intelligence Agency
NGDC	NOAA's National Geophysical Data Center
NIR	Near InfraRed
nNDVI	narrow band NDVI
No.	Number
NOAA	US National Oceanic and Atmospheric Administration
NPP	Net Primary Productivity
NPV	Non-Photosynthetically active Vegetation
ø	Average
ORCHIDEE	Organizing Carbon and Hydrology in Dynamic Ecosystems model developed by Krinner et al. (2005)
p	Level of Significance
PAR	Incoming Photosynthetically Active Radiation
PES	Payment for Environmental Services
PET	Potential Evapotranspiration
PPAR	Potential Photosynthetically Active Radiation
PV	Photosynthetically active Vegetation
q	Atmospheric transmission
r	Correlation coefficient
$r_{Est./Seed}$	ratio of RGR of Established plants and Seedlings
$r_{AGB/TPB}$	ratio of RGR of Above-Ground Biomass and Total Plant Biomass
R^2	Coefficient of determination
R_a	autotrophic respiration
RBM	Regional Biomass Model developed by Richters (2005a)
RBM+	RBM version adapted by Machwitz (2010)
R_d	dark respiration
REDD	Reducing Emissions from Deforestation and Forest Degradation in Developing Countries
R_g	Global Radiation
RGR	Relative Growth Rate
RGR_{AGB}	Relative Growth Rate of Above-Ground Biomass
$RGR_{Est.}$	Relative Growth Rate of Established plants
RGR_{max}	maximum Relative Growth Rate
RGR_{mean}	mean Relative Growth Rate
RGR_{Seed}	Relative Growth Rate of Seedlings
RGR_{TPB}	Relative Growth Rate of Total Plant Biomass
R_h	heterotrophic respiration

RMSE	Root Mean Square Error
R_n	net irradiance
RVI	Ratio Vegetation Index (=NIR/Red)
S	Shrub
S	Solar constant
SAR	Synthetic Aperture Radar
SARVI	Soil-Adjusted and Atmospherically Resistant Vegetation Index
SAVI	Soil-Adjusted Vegetation Index
SBA	Stand Basal Area
SeaWiFS	Sea-viewing Wide Field-of-view Sensor aboard the OrbView-2 satellite (1997–2010)
SiB2	Simple Biosphere Model developed by Sellers et al. (1996a,b)
SIR-C	Spaceborne Imaging Radar – C Band instrument aboard SRTM
SLC	Scan Line Corrector in the Landsat ETM+ instrument
S_N	Number of Stems
SOTER	Soil and Terrain database
SOTWIS	Harmonized continental SOTER-derived database
SPIE	International Society for Optical Engineering (formerly Society of Photographic Instrumentation Engineers)
SPOT-VGT	VEGETATION instrument aboard the Satellite Pour l'Observation de la Terre (SPOT)
SR	Simple Ratio of NIR to visible reflectances
SRTM	Shuttle Radar Topography Mission (Radar system aboard Space Shuttle Endeavour in February 2000)
SSM/I	Special Sensor Microwave radiometer/Imager
STEP	Sahelian Transpiration, Evaporation and Productivity model developed by Lo Seen et al. (1995) and Mougin et al. (1995)
SVAT	Soil-Vegetation-Atmosphere-Transfer model
SWIR	Short-Wave InfraRed
t	time of day
T	atmospheric Transmission
T	mean daily Temperature
TCI	Temperature Condition Index (related to AVHRR data)
T_{ECMWF}	ECMWF Temperature
Terra	NASA research satellite launched in 1999
TERRABITES	Terrestrial Biosphere in the Earth System research network
TIR	Thermal InfraRed
TPB	Total Plant Biomass
TURC	Continental GPP and NPP model developed by Ruimy et al. (1996)
T_ε	Temperature stress
UN	United Nations
UNEP	United Nations Environment Programme
UNEP–WCMC	United Nations Environment Programme – World Conservation Monitoring Centre
UNESCO	United Nations Educational, Scientific and Cultural Organization
UNFCCC	United Nations Framework Convention on Climate Change
UNSO/UNDP	United Nations Sahelian Office/United Nations Development Programme

USGS	United States Geological Survey
USSR	former Union of Soviet Socialist Republics (1922–1991)
UTC	Coordinated Universal Time
UTM	Universal Transverse Mercator coordinate system
V_{max}	maximum carboxylation rate
VCF	Vegetation Continuous Fields dataset derived from MODIS data
VCI	Vegetation Condition Index (related to AVHRR data)
VH	Vegetation Health
VI	Vegetation Index
VPM	Vegetation Photosynthesis Model developed by Xiao et al. 2004a,b
W	Width
WCM	Water-Cloud Model
WGS84	World Geodetic System (dating from 1984)
WorldClim	Dataset of global climate layers with a spatial resolution of ca. 1 square kilometre
WRB	World Reference Base for Soil Resources
WRI	World Resources Institute
WSC	Wind Scatterometer instrument aboard the ERS satellite
W_{ε}	Water stress
X-SAR	X-Band Synthetic Aperture Radar instrument aboard SRTM
Z	Surface geopotential (ECMWF parameter)
α_a	advective parameter
γ	solar altitude
γ	psychrometric constant
Δ	saturation vapour pressure
ε_{eff}	biophysical conversion factor
ε_{max}	maximum Light Use Efficiency
ρ	reflectance
σ	Standard deviation

1 Introduction

1.1 The Importance of Biomass Information

Biomass is an important ecological variable for understanding the responses of vegetation to the climate system and currently observed global change. Its analysis – especially in the context of past, present and future climate change – is one of the most important environmental challenges of the twenty-first century. The impact of changes in vegetation biomass on the greenhouse gas balance as well as the future evolution of climate change is critical (cf. e.g. Global Terrestrial Observing System (GTOS) 2009). The uptake of carbon dioxide (CO_2) by vegetation is perhaps the only sustainable way of reducing the atmospheric CO_2 (United Nations Environment Programme World Conservation Monitoring Centre, UNEP–WCMC 2008).

Uptake or release of CO_2 can be quantified by the net primary productivity (NPP) of plants. NPP is the biomass production by green vegetation per unit area and unit time. It is most often measured in mass of carbon per unit area per year (g C m^{-2} $year^{-1}$). NPP describes the net flow of carbon from the atmosphere into plants. It provides information on the removal of carbon by vegetation from the atmosphere and the potential delivery of stored carbon (Field et al. 1995). This allows for the quantification of CO_2 fluxes as required, for example, in emissions trading. NPP is a key variable for ecological monitoring activities and a sensitive indicator of climate and environmental change (Niemeijer 2002, Schimel 1995). Long-term analyses may allow for better understanding of environmental processes especially in arid and semi-arid regions (cf. e.g. Propastin and Kappas 2009). NPP has therefore been identified by the Commission on Geosciences, Environment and Resources as a primary variable for observing ecological functioning and ongoing degradation processes (CGER 2000).

The present amount of biomass provides an estimate of terrestrial carbon stocks. Thus, the observation of biomass change is a direct measurement of carbon sequestration or loss. Figure 1-1 illustrates the meanings of the terms standing biomass and NPP.

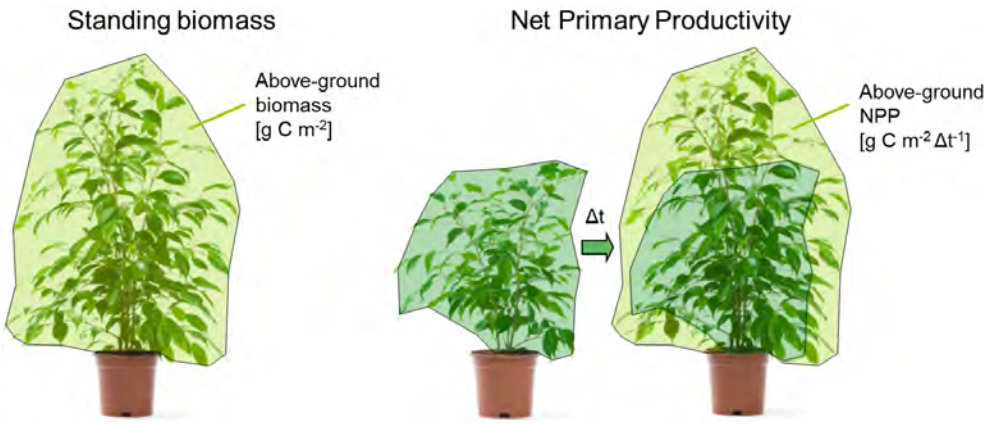

Figure 1-1: Schematic illustration showing the meaning of the terms standing above-ground biomass (AGB) and net primary productivity (NPP).

Standing biomass is the vegetation biomass per unit area at a definite point in time. It is usually measured in mass of carbon per unit area (e.g. in g C m^{-2}) or in mass of dry matter (DM) per unit area (e.g. in g DM m^{-2}). The illustration in figure 1-1 highlights the above-ground biomass (AGB). NPP is always related to a time-period. It describes the growth of vegetation, commonly in terms of carbon gain or loss. The above-ground growth, i.e. carbon gain, of vegetation is schematically shown in figure 1-1.

Obtaining information on AGB and NPP has several benefits with regard to the effort to understand the climate system (Global Climate Observing System, GCOS 2006). Vegetation and biomass are important factors influencing the biodiversity and environmental processes such as the hydrological cycle, soil erosion, and degradation (e.g. Fabricius et al. 2003, Lu 2006). Other important relations exist between biomass and ecosystem variability and resilience. Maintaining biomass, especially woody vegetation, is important (Segoli et al. 2008, Verón et al. 2010) and ecosystem exploitation should not go below the critical resilience thresholds (cf. e.g. Propastin 2006). Information on biomass and NPP helps to quantify the resilience of dryland systems and is thus essential for a sustainable land-use management (Baumann 2009).

The important role biomass plays in the global ecosystem has long been recognized (e.g. Bazilevisch and Ye Rodin 1967, Bolin et al. 1979), but carbon sequestration and emission as well as the influences of changes in biomass on the environmental processes are not yet fully understood. To reduce these uncertainties, it is necessary to accurately estimate the biomass distribution from local to global scales as well as its variation in time (CESBIO 2010, Lu 2006). Both the GTOS and the GCOS recommend producing biomass estimates on an annual basis (GCOS 2006, GTOS 2009).

According to the GCOS, biomass is one of the essential climate variables that are feasible for global implementation and have a high impact on the United Nations Framework Convention on Climate Change (UNFCCC) requirements (e.g. GCOS 2005). Reporting on carbon stock levels is needed, for example, for Kyoto protocol commitments. These include projects in the framework of Clean Development Mechanism (CDM), Reducing Emissions from Deforestation and Forest Degradation in Developing Countries (REDD), and Payment for Environmental Services (PES) (e.g. Costanza et al. 1997, Millennium Ecosystem Assessment Board (MEAB) 2005, World Resources Institute (WRI) 2008). To be successful in voluntary carbon markets or via the post-Kyoto climate change agreement, a universal, robust, low-cost technique to measure and monitor carbon stocks over large areas and through time is essential (e.g. Gibbs et al. 2007, Grassi et al. 2008, Mitchard et al. 2009, Pfaff et al. 2000, Rosenqvist et al. 2003).

Definitions of different types of biomass

The terrestrial vegetation biomass can be divided into above-ground living biomass (AGB), below-ground living biomass (BGB), dead mass and litter. Total plant biomass (TPB) is the sum of AGB and BGB. According to the Intergovernmental Panel on Climate Change (IPCC, 2003) Good Practice Guidance for Land Use, Land-use Change and Forestry (LULUCF) and the Guidelines for National Greenhouse Gas Inventories (IPCC 2006), the AGB pool includes all above-soil living vegetation biomass (stems, stumps, branches, bark, seeds and foliage). The BGB is the mass of all living roots. The dead biomass pool comprises all non-living biomass that is located on the ground or below-ground. Non-living biomass smaller than a specified minimum size (10 cm) is referred to as litter. Distinction to soil components is usually based on particle size (IPCC 2003, 2006).

1.2 The Specific Need for Biomass Research in Semi-arid Areas in Kazakhstan

Semi-arid areas are characterized by alternating arid and humid conditions. Both monthly and annual rainfall show great variations. The native vegetation of semi-arid regions comprises a variety of mainly drought-resistant species. Vegetation cover is mostly sparse. The landscape, however, may show a high diversity in terms of land forms, soils, flora, and water balance (Food and Agriculture Organization, FAO 1989). Steppes, herbaceous vegetation, grass and rangeland are the typical and dominant landscape types for the semi-arid environments (e.g. Liu et al. 2003, Vanamburg et al. 2006). Low trees and bushes, savannah, and open woodland can also be found (e.g. Diouf and Lambin 2001, Montès et al. 2002, Nori 2012, Adam 2010). Figure 1-2 shows a detail of Holdridge's life zone system for the classification of land areas. This classifies semi-arid zones as one humidity province and lists typical ecosystems.

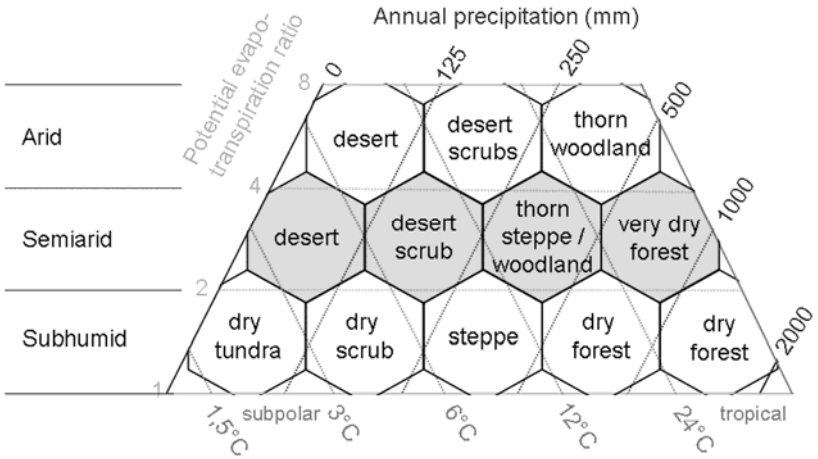

Figure 1-2: Life zones of semi-arid regions and adjacent aridity zones (modified after Holdridge 1967).

According to the FAO, almost one-third of the terrestrial world is arid land, with 12.2% being classified as semi-arid (FAO 2010). According to the United Nations Sahelian Office/United Nations Development Programme (UNSO/UNDP 1997), semi-arid zones even extend over 18% of the land surface and cover 23,739,000 km². In total, the drylands of the Earth are home to more than two billion people (WRI 2003). An overview of the semi-arid regions of the world according to three different climate classification systems is given in figure 1-3.

Arid, semi-arid and sub-humid lands are especially susceptible to environmental degradation and desertification. This is a reduction of the biological potential of the land (e.g. Biro 2011, Biro et al. 2010, 2011, Eswaran et al. 2001, Mulligan 2009, UN 1994, Verstraete 1986). The reduction in plant biomass lowers the soil quality and fertility which in turn reduces the capacity for agriculture and keeping livestock (e.g. Buchroithner 2009). Reduction in biomass therefore has a negative effect on human well-being (e.g. Köchy et al. 2008, UNEP 1999).

Environmental degradation has been identified as one of the major threats by the High Level Panel on Threats, Challenges and Change of the United Nations (UN 2004). The vegetation cover in semi-arid and arid regions is of high importance for protection against wind and deflation. The level of soil protection provided by shrubs is directly proportional to their biomass/cover (Calvão and Palmeirim 2004). The quantification of biomass is essential to identify and monitor those areas under high risk of degradation and desertification (Hirata et al. 2001, Moleele et al. 2001). Quantification of biomass is also essential when assessing the

degradation status of semi-arid regions (e.g. Baumann 2009, Liu et al. 2003). Moreover, semi-arid regions are potentially interesting for restoration or cultivation projects (Bayramov et al. 2012a,b, Field et al. 2008, Mills et al. 2007, Wiskerke et al. 2010). The vegetation biomass per unit area is rather low in semi-arid regions and these biomass levels do not change as much as in other climate zones (UNEP 1999). Nevertheless, the large surface area of drylands gives carbon sequestration in these regions a global significance; even more so when soil carbon is also considered (UNEP-WCMC 2008).

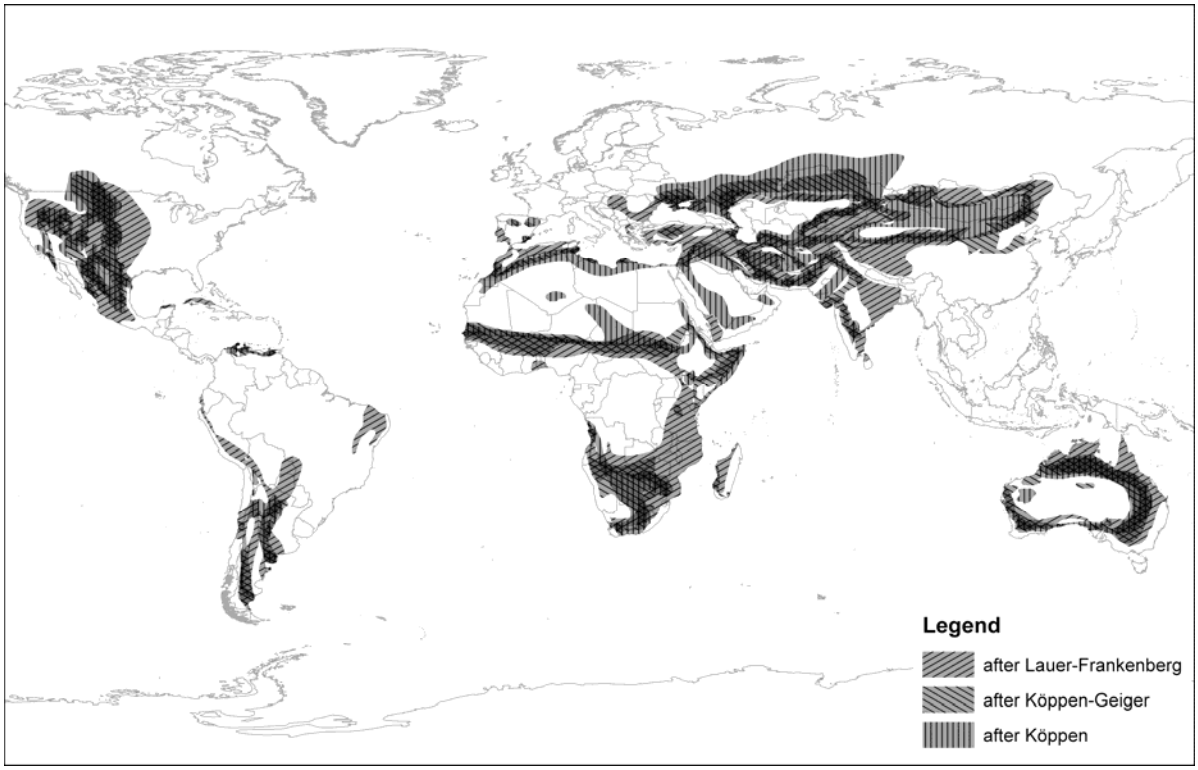

Figure 1-3: Expansion of semi-arid regions as presented in three different maps with distinct underlying classification systems: after Lauer-Frankenberg (Source: Diercke 1992, modified), after Köppen-Geiger (Source: Strahler and Strahler 1984, modified), and after Köppen (Source: Philip's 2003, modified).

Remote sensing of biomass in semi-arid regions provides important information for several applications, and has been used for a variety of studies. Table 1-1 gives an overview of major areas which need regular biomass estimation. The diversity of applications shows the large potential of the topic of biomass estimation for further research. Especially remote-sensing-based analysis is one key focus.

Large areas in Kazakhstan are characterized as arid or semi-arid (Eisfelder et al. 2012, Lioubimtseva and Adams 2004). The country is land-locked and its climate is extremely continental. Kazakhstan has experienced varying human influences and political decisions with dramatic ecological and environmental consequences. Most prominent is the decline of the Aral Sea due to water extraction for agricultural usage. Much larger areas, however, were undergoing land cover change, especially during the second half of the 20th century. In 1953 the 'Virgin Lands Programme' was initiated to transform large areas of the traditional pasture lands of the Kazakh Steppe into crop agriculture (de Beurs and Henebry 2004). This resulted in large scale land cover changes in northern Kazakhstan. Between 1950 and 1960 the cultivated area of Kazakhstan increased from 7.8 million to 28.5 million hectares (Asian Development Bank, ADB 2010). The extensive land use led to dramatic steppe deterioration. Eventually, after the

breakdown of the Soviet Union, vast areas of ploughed land were abandoned. In recent years, the grazing impact on vegetation has decreased and undergrazing rather than overgrazing was reported. This was due to a reduction in the livestock population (de Beurs and Henebry 2004, Lioubimtseva et al. 2005).

In addition to the human impacts on the environment, there are also the effects of changing climate. Increased annual and winter temperatures have been recorded since the beginning of the 20th century. Temperatures in Central Asia are expected to further increase 1–2°C by 2030–2050 (Lioubimtseva et al. 2005). Aridity is expected to intensify, especially in western Kazakhstan. The increase of atmospheric concentration of CO_2 is likely to affect plants in semi-arid and arid Central Asia, by reducing their sensitivity to drought stress. Trends in precipitation are highly variable, but indicate a small overall decrease (Lioubimtseva and Henebry 2009). De Beurs and Henebry (2004) observed higher normalized difference vegetation index (NDVI) values at the start of the growing season in northern Kazakhstan. This indicates a shift to an earlier growing season. Due to the climatic situation and human influence, the most threatening natural hazards in Kazakhstan are land degradation and desertification (ADB 2010).

In the context of these diverse anthropogenic and climatic influences on the Kazakh environment, it is of great interest to observe large-scale vegetation dynamics and biomass distribution. It is also important to obtain knowledge about spatial and temporal patterns of NPP and its relationship to climate. This information may help to identify regions that are more vulnerable to changing climate, and thus support sustainable land management.

Table 1-1: Major areas with need for regular biomass quantification in semi-arid regions and possible applications.

Area	Possible applications	Example studies
Sustainable land-use management	- Support drought detection - Advice to farmers regarding good grazing places - Information on amount, quality, and distribution of forage - Understanding of wildlife feeding patterns - Management guidelines regarding the suitability of habitats - Quantifying the effect of grazing intensities - Crop forecasting - Locust forecasting and hatching	Dech et al. 2003, Du Plessis 1999, Kawamura et al. 2005, Kogan et al. 2004, Mutanga and Rugege 2006, Qi and Wallace 2002, Rosema 1993, Wylie et al. 1995
Fire risk assessment	- Fire risk assessment for savannah ecosystems - Selection of sites for controlled burning - Development of early warning systems for fire management - Fuel modelling and fire behaviour simulation	Kraus and Samimi 2002, Mutanga and Rugege 2006, Pereira et al. 1995, Sannier et al. 2002, Verbesselt et al. 2006
Climate change and degradation	- Understand the exchange of energy and CO_2 between vegetation and the atmosphere - Understand the role these regions play in the biochemical cycles - Examine yield and food production - Assess both degradation and ecosystem recovery - Plan protective measures for areas under high risk of desertification - Assist the decision-making process for the declaration of areas experiencing drought exceptional circumstances	Collins et al. 2009, Diouf and Lambin 2001, Hirata et al. 2001, McVicar and Jupp 1998, Moleele et al. 2001, Pickup 1996, Rosema 1993, Running et al. 1995, Shoshany 2000
Reporting	- For CDM of the Kyoto Protocol and inventory improvement - Develop predictions of future trends - Input to climate models, environmental models and hydrological models	FAO 2006, Grippa and Woodhouse 2002, Ozdemir 2008, Wylie et al. 2002

1.3 Objectives of this Dissertation

As documented in the previous sections, biomass and NPP are important parameters regarding the vegetation and its carbon storage, as well as sensitive indicators of environmental change and ecological functioning. Monitoring of biomass and NPP is especially important in arid and semi-arid regions, because these areas are susceptible to environmental degradation. However, semi-arid regions have been rarely analysed in remote-sensing based biomass or NPP studies, particularly in comparison with other ecosystems.

The arid and semi-arid environments in Kazakhstan are expected to be especially affected by a changing climate. Therefore, it is of special interest to observe biomass distribution and vegetation dynamics in these areas. The main goals of this thesis are therefore the modelling and the analysis of large-area NPP time-series, as well as the development of an approach for biomass estimation for semi-arid regions in Kazakhstan.

To approach these goals, the first objective of this dissertation is to perform a sound review on methods for remote-sensing based biomass estimation for semi-arid environments, which had not been available before. The aim of the review is to identify major challenges and the most promising approaches that can be recommended for future research.

The second objective of this dissertation is the comparison of two selected regional remote-sensing-based NPP models for a study area in Kazakhstan. Both models have not been applied to Kazakhstan before. Thus, the major aims of the comparison are to identify differences between the models' results and to analyse the applicability of the models for the study area.

The third objective of this thesis includes the modelling of NPP time series for Kazakhstan for the period 2003–2011 and the analysis of the obtained NPP data. The major aims of the analysis are to investigate spatial, intra-annual, and inter-annual NPP patterns, as well as to identify regions with high NPP variability and possible NPP anomalies. Such detailed analyses based on NPP dynamics are not available for Kazakhstan yet. A further aim is to investigate the correlation between the NPP and meteorological parameters.

The final objective of this dissertation is to develop a methodological approach for biomass estimation in semi-arid natural environments based on the NPP data. The aim is to apply the developed approach for selected study areas in Kazakhstan and to validate the results with field data that are to be collected in the course this thesis.

In summary, the following research objectives are addressed in this dissertation:

1) Sound review on methods for remote-sensing based biomass estimation for semi-arid regions, including the identification of major challenges and the most promising approaches.
2) Detailed comparison of two selected NPP models for a study area in Kazakhstan, including the analysis of differences between the models and investigation of their applicability to semi-arid environments in Kazakhstan.
3) Modelling of NPP time series for Kazakhstan for 2003–2011 and analysis of the results regarding spatial and temporal NPP patterns, as well as investigation of the correlation between the NPP data and meteorological parameters.
4) Development of a methodological approach for derivation of biomass estimates for natural environments based on NPP data and the application of this approach to selected study areas in Kazakhstan.

1.4 Structure of the Thesis

This thesis consists of eight chapters which are outlined as follows.

Chapter 1 introduces the topic of biomass. It addresses the importance of biomass mapping and NPP derivation, especially for semi-arid regions in general and for Kazakhstan in particular. This is followed by the definition of research objectives for this thesis and a short outline of the structure of the thesis.

Chapter 2 presents a sound review on methods and data applied to estimate biomass for semi-arid regions based on remote-sensing. It gives detailed discussion of observed difficulties and challenges. A brief introduction to primary productivity modelling and a description of the major aspects of the two models applied in this thesis are provided.

Chapter 3 provides information about Kazakhstan and the three study areas in Central, South, and West Kazakhstan. The geographic locations of the study areas as well as criteria for the study area selection are specified. A description of major characteristics regarding geology and geomorphology, climatic influences, dominating soil patterns, and typical zonal and azonal vegetation follows. Furthermore, socio-economic characteristics are briefly introduced.

Chapter 4 gives an overview and short description of the different input data applied within this thesis. This includes meteorological data, remote-sensing based products, land cover and soil maps, elevation models, collected field data, and additional data. In addition, a quality assessment of the meteorological data is presented. In this chapter also the method for biomass field data collection is described.

Chapter 5 presents results of the comparison of NPP models for the study area in Central Kazakhstan. Necessary steps for the harmonization of input data are described. A detailed analysis and comparison of input data, intermediate products, and NPP results follows. A comparison with NPP estimates from other studies, the validation with field data, and the discussion of the results complete the model comparison chapter.

Chapter 6 presents the results from NPP modelling for Kazakhstan. This includes mean annual and monthly NPP results, NPP anomalies, and variability. The NPP estimates are analysed and discussed with respect to spatial and temporal patterns. Furthermore, the relation to meteorological variables is investigated and discussed.

Chapter 7 presents the developed approach for derivation of standing biomass estimates based on NPP data. Relative growth rate, an important parameter for the biomass derivation method, is introduced and the methodological concept of the approach is described. The derivation of suitable relative growth rate values is explained and possible factors influencing the accuracy of the biomass estimate are discussed. Finally, results from the application of the developed approach to the study areas in Kazakhstan are presented. Preparations of field data for validation, as well as the validation results for biomass estimates are summarized. A discussion closes this chapter.

Chapter 8 provides comprehensive conclusions with respect to the research objectives of this thesis. This also includes an outlook with recommendation for future studies.

Parts of this thesis have been published in international peer-reviewed journals or presented at international scientific conferences and workshops:

EISFELDER, C., KUENZER, C. and DECH, S. (2010). A review on derivation of biomass information in semi-arid regions based on remote sensing data. *Proceedings of the SPIE*, Vol. 7831, 20–23 September 2010, Toulouse, France, pp. 78310L, DOI: 10.1117/12.868505.

EISFELDER, C., KUENZER, C. and DECH, S. (2012). Derivation of biomass information for semi-arid areas using remote sensing data. *International Journal of Remote Sensing*, 33(9), pp. 2937–2984, DOI: 10.1080/01431161.2011.620034.

EISFELDER, C. and KUENZER, C. (2012). NPP modelling based on remote sensing data – comparing two models for Kazakhstan. *2nd TERRABITES Symposium*, Modelling the terrestrial biosphere: From Ecological Processes to Remote Sensing Observations, 06–28 February 2012, Frascati, Italy.

EISFELDER, C., KUENZER, C., DECH, S. and BUCHROITHNER, M.F. (in print). Comparison of two Remote Sensing based Models for Regional Net Primary Productivity Estimation – a Case Study in Semi-arid Central Kazakhstan. *IEEE Journal of Selected Topics in Applied Earth Observations and Remote Sensing*, DOI: 10.1109/JSTARS.2012.2226707.

EISFELDER, C., KLEIN, I., NIKLAUS, M. and KUENZER, C. (2012). Remote Sensing based net primary productivity modelling for semi-arid Kazakhstan. *IEEE International Geoscience and Remote Sensing Symposium,* IGARSS 2012, 22–27 July 2012, Munich, Germany.

EISFELDER, C., KLEIN, I., NIKLAUS, M. and KUENZER, C. (under review). Net primary productivity in Kazakhstan, its spatio-temporal patterns and relation to meteorological variables. *Journal of Arid Environments*.

2 Theoretical Background

2.1 Review of Biomass Derivation based on Remote Sensing for Semi-arid Regions

The following elaborations have been published in the International Journal of Remote Sensing (Eisfelder et al. 2012). This chapter contains major parts of the published article.

Remote-sensing-based biomass studies have been carried out since the early 1980s. The large majority of these have focused on forests. A reasonable number of efforts have also been undertaken for the estimation of the biomass in semi-arid regions; however, a summary of these studies has not been available before. This chapter provides an overview of the remote-sensing-based research activities for AGB estimation in semi-arid regions using optical data, radar data, combined multi-sensor approaches, and modelling approaches. Additionally, a summary and a discussion of the commonly observed difficulties and challenges to be overcome in the future are given.

2.1.1 Role of Remote Sensing for Biomass Mapping

Traditional techniques for measuring the amount of biomass are based on field data collection (e.g. Brown 2002, Etienne 1989, Parresol 1999, Radloff and Mucina 2007, Tucker 1980). These methods are accurate, but time and labour intensive, often difficult to implement and only practicable for small areas (e.g. Chen et al. 2009, García et al. 2010, Lu 2006). Therefore, remote-sensing-based techniques became an alternative to obtain such data. The main advantages of remote sensors are the possibility to monitor large areas and to capture the spatial variability of the land surface, as well as the repeatability of data collection that offers the possibility for time-series analyses. Moreover, remote sensing has the capacity for systematic observations at different scales from global to local and the potential of using historical data.

Although remote sensing does not allow direct measurements of biomass, the signals are sensitive to vegetation structure and influenced by, for example, vegetation cover, density, shadow and texture (Baccini et al. 2008). These parameters are correlated with AGB and thus allow the indirect prediction of biomass levels.

Table 2-1: Overview of the parts of AGB derived within remote-sensing studies in semi-arid regions.

Part of biomass derived	Example Studies
Total AGB	Chen et al. (2009), Holm et al. (2003)
Woody biomass	Chopping et al. (2008), Dong et al. (2003), Franklin and Hiernaux (1991), Wang and Qi (2008)
Foliage biomass	Franklin and Hiernaux (1991), Le Maire et al. (2008), Means et al. (1999)
Herbaceous/shrub biomass	Aranha et al. (2008), Mutanga and Rugege (2006), Verbesselt et al. (2006), Wessels et al. (2006)
Green leaf volumetric density (GVD)	Svoray et al. (2001), Svoray and Shoshany (2003)

Most remote-sensing-based research focuses on terrestrial vegetation AGB. Below-ground biomass (BGB) cannot be directly detected by remote observations and allometric equations have to be used (Næsset and Gobakken 2008). The AGB, however, can be estimated with some accuracy over large areas based on remote-sensing data. Some studies derive total AGB while others focus on a specific part of the biomass (cf. table 2-1).

In recent years, remote sensing has become widely used for biomass estimation, especially for boreal and tropical forests, and is recognized as offering the most suitable tool to obtain spatially continuous data sets on biomass (e.g. Lu 2006, Nijland et al. 2009, Rahman et al. 2008). Research on remote-sensing-based biomass estimation for other ecosystems is comparatively scarce. When remote-sensing-based methods are developed further, they will become increasingly important for biomass monitoring in the future, especially for global AGB information provision (Integrated Global Carbon Observing System (IGCOS) 2004, GCOS 2003, GTOS 2009). However, so far, remote-sensing-based methods for biomass estimation are still at an experimental stage, not used operationally and often applied with uncertain accuracy; appropriate methods still need to be developed (e.g. García et al. 2010, GCOS 2005, GTOS 2009, Mitchard et al. 2009). Suitable methods are lacking, especially for non-forest ecosystems, and robust and transferable methods to map biomass in semi-arid regions still need to be developed (e.g. Diouf and Lambin 2001, Mangiarotti et al. 2008, Svoray and Shoshany 2002, Verbesselt et al. 2006).

Table 2-2: Review articles covering the topic of remote-sensing-based biomass estimation.

Article	Topic
Tucker (1980)	Non-destructive estimation of standing crop biomass
Tueller (1987)	Application of remote sensing in arid environments
Kasischke et al. (1997)	Use of imaging synthetic aperture radar (SAR) for woody plant biomass estimation and other applications
Shoshany (2000)	Satellite remote sensing of vegetation in Mediterranean areas, includes a section on biomass and primary productivity studies
Brown (2002)	Status of carbon measurements in forests, including the future role of remote sensing
Rosenqvist et al. (2003)	Remote-sensing approaches in support of Kyoto Protocol reporting, including AGB estimation
Patenaude et al. (2005)	Remote-sensing approaches in support of Kyoto Protocol reporting, including AGB estimation, focus on forest carbon estimation
Lu (2006)	Biomass estimation using remote sensing, focus on forests
Frolking et al. (2009)	Spaceborne remote sensing of AGB and canopy structure in the context of forest disturbance and recovery
Goetz et al. (2009)	Mapping and monitoring of carbon stocks using satellite observations, focus on forest applications

The majority of studies for remote-sensing-based biomass estimation have focused on forests, which is mirrored by the existing review papers (cf. table 2-2). Reasonable effort has also been undertaken for biomass estimation in semi-arid regions; however, a summary of these studies is not available yet. The approaches applied in arid regions may differ from those used for more densely vegetated areas like forests.

Thus, the aim of this study is to provide an overview and a critical analysis of the remote-sensing research activities for AGB estimation in semi-arid regions and areas of comparable vegetation structure, published during the last two decades. A summary of previous efforts on AGB estimation in semi-arid regions and a discussion of observed problems are valuable for

understanding the relation between remote sensing data and AGB and can, thus, support the development of successful strategies and suitable models for satellite-based AGB estimation.

2.1.2 Biomass Derivation for Semi-arid Areas based on Optical Data

Optical remote-sensing uses passive sensors that record the visible and near-infrared (NIR) reflectances from the Earth. Their radiometry is influenced by the vegetation structure, texture and shadow and thus indirectly correlated with AGB. The red, NIR and, especially, short-wave infrared (SWIR) bands are particularly sensitive to vegetation (e.g. Baccini et al. 2008). Figure 2-1 shows the spectral reflectance curves for typical land cover of semi-arid environments. The specific characteristics of these reflectance curves form the basis for vegetation discrimination using vegetation indices (VIs). Optical data at medium to high spatial resolution provide information suited for studies on a local to regional scale, while data at medium to coarse resolution can be useful for studies at regional to continental scale. Coarser spatial sensors often provide more frequent observations, thus allowing for time-series analyses.

Table 2-3 provides an overview of the most commonly used optical sensors applied to estimate biomass in semi-arid regions over the past 20 years. In the following section, the different approaches will be presented according to spatial resolution: coarse resolution (e.g. AVHRR, Moderate-resolution Imaging Spectroradiometer (MODIS); section 2.1.2.1), medium resolution (e.g. Landsat Thematic Mapper (TM)/Enhanced Thematic Mapper Plus (ETM+); section 2.1.2.2), high-resolution spaceborne and airborne imagery (e.g. IKONOS, QuickBird, HyMap; section 2.1.2.3), as well as ground based spectra and imagery (section 2.1.3).

Table 2-3: Specifications of optical satellite sensors that have been used for biomass estimation in semi-arid regions.

Sensor	Mission	Maximum spatial resolution	Spectral range [nm]	Swath width [km]	Revisit time [days]	Temporal coverage
AVHRR	NOAA-6 to NOAA-18, MetOp-A	1.1 km	580–680, 720–1100, 3550–3950, 10300–11300, 11500–12500	2600	2	1979–today
VEGETA-TION	Spot-4, -5	1.15 km	430–470, 610–680, 790–890, 1580–1750	2200	2	1998–today
MODIS	Terra, Aqua	1 km, 0.5 km, 0.25 km	total: 36 bands, for land applications: 459–479, 545–565, 1230–1250, 1628–1652, 2105–2155	2330	2	1998–today
TM/ ETM+	Landsat-5/ Landsat-7	0.03 km (VIS-SWIR), 0.06 km (TIR, ETM+) / 0.12 km (TIR, TM), 0.015 km (panchromatic, ETM+)	450–520, 520–600, 630–690, 760–900, 1550–1750, 2080–2350, 10420–12500 (TIR)	185	16	TM: 1984–2004, ETM+: 1999–2003 (with SLC)
IKONOS	IKONOS	4 m, 0.82 (panchromatic)	445–516, 506–595, 632–698, 757–853	11	1–3	1999–today
Quick Bird	QuickBird	2.4 m, 0.61 m (panchromatic)	450–520, 520–600, 630–690, 760–900	16.5	1–3.5	2001–today
HyMap	Airborne	2–10 m	125 spectral bands, bandwidth of approx. 16 m, wavelength range: 400–2500	-	-	-

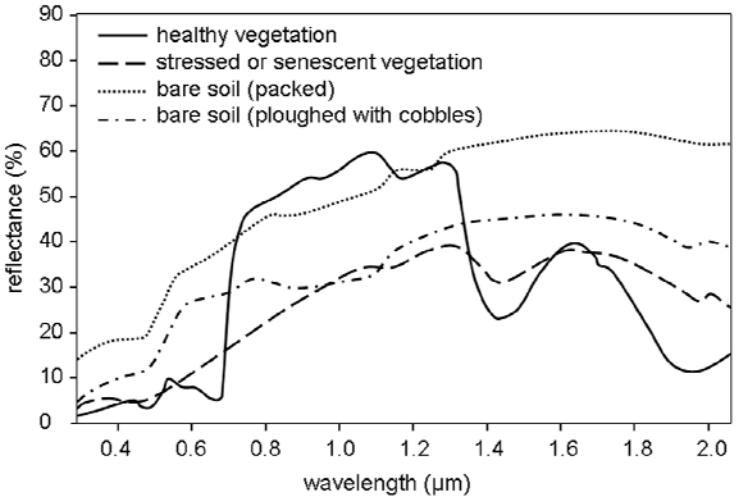

Figure 2-1: Simplified spectral reflectances for land cover in semi-arid regions (modified after Baban 2005).

2.1.2.1 Biomass Derivation for Semi-arid Areas based on Low-resolution Optical Data (>1 km)

Low-resolution optical data have been available for a long time. Among the first satellite sensors used for biomass retrieval was the AVHRR sensor. Further, the sensors VEGETATION, MODIS, as well as METEOSAT (Meteorological satellite) data, have been used. Table A-1 (appendix) provides an overview of the research activities using low-resolution optical data. Please refer to this table for details on, for example, the study area and accuracy. In the following, studies using empirical relationships with spectral bands or VIs are summarized first, followed by studies applying other approaches.

The most common approach for biomass estimation based on low-resolution optical data includes regression equations and the use of VIs or integrated VIs. Several of the early studies were based on such an approach (cf. table A-1). For example, Tucker et al. (1985) found a strong correlation between the integrated normalized difference vegetation index (I-NDVI = sum of NDVI (normalized difference vegetation index) values over time) as well as the maximum NDVI ($NDVI_{max}$) and end-of-growing season herbaceous AGB. However, an apparent lack of sensitivity below ~250 kg ha^{-1} of total biomass production was observed. This observation could not be confirmed by Wylie et al. (1991, 1995), who found no visible increase in the point scatter below 300–400 kg ha^{-1} (Wylie et al. 1991). Hobbs (1995), who correlated the biomass field measurements with four VIs, found that linear relationships between biomass and the VIs break down at biomass levels >1000 kg ha^{-1}. Exponential relationships with $NDVI_{max}$ were the best predictors of herbage growth in this study. Cumulative NDVIs provided only weak relationships to herbage biomass, though they were commonly used for primary production assessment in other studies (Diallo et al. 1991, Prince 1991, Wylie et al. 1991).

Almost two decades after the first studies with AVHRR data, Diouf and Lambin (2001) tested whether the previously observed linear relationship between I-NDVI and herbaceous primary production was robust over a 10-year period. Separate regressions for each year resulted in good relationships. However, the strong inter-annual variations in the regression parameters lead to the conclusion that the I-NDVI is not a robust proxy variable for biomass in the semi-arid study area. Possible reasons may have been influences of the soil type and the coarse resolution of AVHRR (Diouf and Lambin 2001). Similar results had already been observed by Wylie et al. (1991), who had found considerably different relationships for different years due

to more or less drought conditions. Nevertheless, the I-NDVI was successfully applied in later studies. Holm et al. (2003) used the I-NDVI together with rainfall data to assess landscape degradation. Remotely sensed estimates of total phytomass were compared to models based on field data, rainfall and landscape characteristics. Linear regression and correlation analyses resulted in a good (for I-NDVIs) to moderate (for $NDVI_{max}$ and maximum minus minimum NDVI) agreement (Holm et al. 2003).

Wessels et al. (2006) also chose an approach using the I-NDVI for herbaceous biomass retrieval using a geometric means regression between the I-NDVI and biomass field data. The regression results varied considerably for individual sites and were generally lower for landscape groups, due to landscape variations within the groups. The results of this study suggest that separate regression equations for each year based on annual field measurements increase prediction accuracy. While the I-NDVI was successful at estimating inter-annual variation in the biomass at single sites, it was not strong enough to reliably derive the biomass on an annual basis from all the sites (Wessels et al. 2006). A possible explanation for the weak relationship is that the biomass field sampling sites were too small and not representative of the AVHRR pixels. Senescent material of the previous growth season may have also weakened the I-NDVI–biomass relationship (Wessels et al. 2006). The addition of tree cover information only slightly improved the I-NDVI–biomass relationship for some landscape groups.

A similar study has been undertaken by Verbesselt et al. (2006), who used Satellite Pour l'Observation de la Terre VEGETATION (SPOT-VGT) time-series data. The mean herbaceous biomass amounts at the end of the rain season were related to both single-date and integrated VIs. In this study, the integrated VI approaches reached significantly better correlation coefficients than the single-data approach indices (cf. table A-1).

In other studies, the use of single-date VIs was preferred, such as by Sannier et al. (2002), who observed a high correlation between the field measurements of biomass and the NDVI for individual vegetation cover classes (grassland, steppe, savannah). However, the authors suggested using different regressions when the woody biomass proportion reaches a certain level.

Kawamura et al. (2005) used NDVI data to derive the plant biomass in a semi-arid steppe. The observed exponential relationship showed a moderate correlation (cf. table A-1). To attain higher coefficients, the authors suggest applying another sampling technique, using a more suitable VI, or calibrating for geographical effects (Kawamura et al. 2005).

A large-scale study incorporating MODIS-NDVI data has been carried out by Xu et al. (2008), who monitored grass production over China. The country was divided into six regions, for which separate models were established. The exponential function, power function and linear models resulted in highest correlation coefficients (cf. table A-1). For the whole of China, the best model had exponential form. When applied to MODIS data, the models yielded good accuracies for single regions; the national model showed a significantly lower performance (Xu et al. 2008).

The studies presented so far used common VIs or integrated VIs for biomass estimation. In some single studies, other approaches have also been applied, which will be shortly summarized in the following. Details on accuracies and study areas can again be found in table A-1. One attempt has been made by Rosema (1993) to use daily visible and thermal infrared from noon and mid-night METEOSAT data to simulate herbaceous biomass development on the basis of daily total evapotranspiration.

The METEOSAT-derived biomass estimates performed as well as the National Oceanic and Atmospheric Administration (NOAA)-NDVI estimates (Rosema 1993). Another approach for biomass mapping has been investigated by Kogan et al. (2004), who evaluated the derivation of pasture biomass from the vegetation health (VH) indices. Biomass anomalies were compared to

the VH values and the results showed that the VH indices can be used as proxies for biomass production estimation. Mutanga and Rugege (2006) combined remote-sensing data with spatial statistics to predict herbaceous biomass. Individual MODIS bands, as well as VIs and principal components, were used for correlation with field data. The biomass distribution was modelled using ordinary kriging and cokriging with the field data and the band showing the highest correlation. The results showed that the combination of remote-sensing data with field biomass and geostatistics improves the estimation accuracy compared to a conventional stepwise linear regression. However, the drawbacks of these techniques are the need for large amounts of field observations and extensive time consumption.

One of the few studies that cover large study areas is that by Baccini et al. (2008), who used MODIS data for the mapping of AGB of tropical Africa. Large parts of the study area were covered by tropical forest, but the range of ecosystems also included xeric shrubland. A random forest (Breiman 2001) regression tree model was developed with spectral bands and field biomass training data. Comparison with a traditional multiple regression model showed better results for the random forest model. Combinations of spectral bands, other MODIS products (NDVI, enhanced vegetation index (EVI), leaf area index (LAI)), climate data and topography data were also tested, but the gain of adding this information was limited and accompanied by negative effects.

2.1.2.2 Biomass Derivation for Semi-arid Areas based on Medium-resolution Optical Data (>5 m, <1 km)

Medium-resolution data, mainly from the Landsat series, have also been used in several studies for biomass estimation purposes. Due to their long-term availability, Landsat data have been used from the late 1980s to most recent studies. Table A-2 (appendix) gives an overview of major studies based on medium-resolution data.

In 1991, Franklin and Hiernaux (1991) applied TM data and a radiative transfer model to predict tree size and density. This information was used within allometric equations to derive foliage and woody AGB. Reflectance models, as used in the study by Franklin and Hiernaux (1991), have not been used very often with optical data for biomass estimation in semi-arid regions. Much more common is the use of VIs.

Anderson et al. (1993), for example, evaluated the association of three VIs (cf. table A-2) and AGB using different approaches: sample point (average VI value for a 3 pixel × 3 pixel area), spectral class (classification into 5 classes) and greenness strata approach (7–8 greenness classes). The latter was found to be the most suitable. A direct pixel-based regression was impractical due to small field sites, image registration and field plot location inaccuracies.

A combination of VIs has been used by Qi and Wallace (2002) to circumvent the problems of biomass estimation in semi-arid regions due to sparse and senescent vegetation cover. They used the NDVI to compute green fractional vegetation cover and introduced an additional indicator, named normalized senescent vegetation index (NDSVI, Qi et al. 2000), which was based on the reflectance in the red SWIR region and provides complementary information on fractional senescent vegetation cover. Further, information on canopy height is derived from the NIR reflectance. A multivariate regression was then used to relate canopy biomass to Landsat imagery, which showed a strong correlation.

Wylie et al. (2002) used the NDVI in a multi-scale approach. First, field biomass measurements were converted to ground estimates for 30 m×30 m plots using field radiometer NDVI and geostatistical kriging. Then, a quadratic regression between the plot estimates and

Landsat-TM NDVI data was used. The parameters were finally scaled to NOAA-AVHRR resolution for homogeneous areas.

Landsat-TM spectral bands and NDVI have also been used to derive different components of the AGB in a study by Calvão and Palmeirim (2004). In this study, a least-squares linear regression was used to relate the remote-sensing parameters with field data. The correlation of TM bands with leaf biomass was low; the NDVI performed slightly better. Higher correlation coefficients were found for woody biomass, total living biomass, total biomass and litter, mainly with the mid-infrared (MIR, seven), red (three) and green (two) TM bands.

A comprehensive analysis of the suitability of the spectral bands and VIs from Landsat data for empirical biomass estimation of savannah ecosystems has been investigated by Samimi and Kraus (2004). Several indices were extracted and averaged for each test site. Non-linear regression equations were then derived for indices showing high correlations with different types of AGB. A number of indices were highly correlated to grass biomass and foliage biomass. Most suitable were combinations with the following ETM+ bands: bluegreen (one), green (two) and MIR (five, seven). No significant correlation could be found for woody biomass, nor – consequently – for total AGB. Indices calculated from the radiance or reflectance correlated more than indices derived from digital numbers. The tasselled cap wetness index proved useful for grass biomass calculation and the brightness index for estimating total foliage biomass. NDVI did not correlate with dry grass biomass. The extension of the model to a fourth additional region improved the coefficients of determination. Thus, it was concluded that a regional model for savannah ecosystems could be found (Samimi and Kraus 2004).

Aranha et al. (2008) also used NDVI to estimate the AGB of shrubs. They integrated NDVI and forest inventory data and applied a stepwise regression analysis to develop the AGB estimation models. The regression with dry shrub biomass yielded a rather low correlation coefficient in this study.

The studies summarized so far were based on the use of VIs. An alternative to VIs might be the use of stand structural attributes, such as stand basal area (SBA), canopy coverage (CC) and LAI. Suganuma et al. (2006) analysed the suitability of these parameters for biomass estimation in open woodlands. The study is included in this review although no remote-sensing data are used, because its findings are relevant for application to remote-sensing data. The biomass estimation accuracy was slightly higher by using SBA than CC or LAI, but only CC and LAI are considered to be applicable for a remote-sensing-based estimation. The authors suggest utilizing biomass estimation regression equations with vegetation classifications on the dominant species level. Medium-resolution or more detailed spatial resolution data could be used for the CC and, thus, biomass estimation (Suganuma et al. 2006).

2.1.2.3 Biomass Derivation for Semi-arid Areas based on High-resolution Optical Data (< 5 m)

This section includes studies based on both spaceborne and airborne sensors. High spatial resolution spaceborne sensors are available since the launch of IKONOS-2 (1999) and QuickBird (2001) and have a spatial resolution of less than 5 m. They are especially useful for detailed biomass studies of small areas. For vegetation types with low ground cover, such as open forest, the data even allow for derivation of single tree attributes (e.g. Ozdemir 2008). The high-resolution airborne sensors used include HyMap and aerial photography. In contrast to low- and medium-resolution optical data, rather little research on biomass estimation based on high-resolution imagery has been published so far. A summary of the studies is given in table A-3 (appendix).

One study using IKONOS data has been published by Thenkabail et al. (2004), who estimated biomass in oil palm plantations. The best empirical models between field data and IKONOS imagery were exponential and involved the red band or normalized indices with the red and blue bands using dry season images. The best model for the pooled data of two study sites was based on the NDVI. For further improvements, the authors suggest to use improved models and additional wavebands, for example, the MIR band (Thenkabail et al. 2004).

Another approach has been applied by Ozdemir (2008), who used pan-sharpened QuickBird data to extract tree attributes (crown area, tree shadow), which were then used for stem volume estimation. A conventional least-squares linear regression was applied for the relationship between stem volume and the image variables. The models using shadow area reached higher correlation coefficients than those based on the crown area.

Airborne data have also been applied for biomass estimation in semi-arid areas, though not very frequently. An early study was that by Dancy et al. (1986), who estimated the amount of biomass of semi-arid rangelands applying true-colour aerial photographs. The photographs were used for estimation of the percentage ground cover, which was then converted to biomass using exponential calibration equations with good results for grass/bush plots.

In recent years, the HyMap sensor has been used in some studies on biomass estimation. Addink et al. (2007), for example, tried to find an optimal object segmentation size and the optimal band combination for AGB and LAI estimation. Cho and Skidmore (2009) studied the robustness of VIs and red-edge positions for monitoring of Mediterranean grass/herb biomass production using HyMap imagery. High-regression correlations with frequently used indices were found for a single year, but the predictive capability for the other year was weak. Models using red-edge positions were more robust and resulted in lower prediction errors.

Nijland et al. (2009) analysed the effect of spatial resolution on the retrieval of AGB and LAI in a Mediterranean environment using a regression model between HyMap spectral bands and log-transformed AGB field data. The authors found optimal pixel sizes of 95 m (overall) and 65 m (for separate vegetation types: herb and shrub AGB, dense shrub AGB). The use of the optimal pixel size resulted in a significant error reduction compared to a pixel size of 5 m. However, resampling a high-resolution image should be preferred over the use of coarse-resolution imagery (Nijland et al. 2009).

2.1.3 Studies Investigating Field Spectra and Ground-based Imagery

Field-based studies, including those that use *in situ* field spectra and other ground-based remote imaging techniques, are not in the focus of this review. However, some findings might also be relevant for airborne and spaceborne remote-sensing techniques and shall, therefore, shortly be presented here.

Regarding the use of VIs, Filella et al. (2004) found good relationships between the NDVI derived from field spectra and the biomass for dry shrubland types with low LAIs and vegetation cover. The NDVI did not saturate and was sensitive to biomass changes. Mutanga and Skidmore (2004), however, found that the standard NDVI performed poorly in biomass estimation compared to narrow-band VIs for grassland with high canopy density. The simple ratio calculated from the bands in the shorter and longer red-edge portions showed better correlation with biomass. Also, Beeri et al. (2007) found that VIs using only the red and NIR regions are less accurate as the proportion of non-photosynthetical vegetation increases. Vanamburg et al. (2006) investigated the potential of field-based nadir RGB (red, green, blue) imagery to estimate the green biomass on semi-arid grassland and found that plant phenology significantly affected the relationship and was an important factor needed to explain biomass

variability. Further, it was assumed that the nadir RGB imagery failed to represent the vertical stratification of the vegetation. The use of a narrow-band sensor system is recommended for more accurate ground-based biomass estimation in the shortgrass prairie.

2.1.4 Biomass Derivation for Semi-arid Areas based on Radar Data

Radar data, in particular, SAR, have been widely used to map AGB, especially in forested areas (cf. section 2.1.1). The transmitted energy of the active SAR systems penetrates into the vegetation and the amount of backscatter depends on the canopy structure. The SAR return is especially influenced by the dielectric constant of the vegetation, which is made up of the individual leaves, branches, trunks and bark that altogether represent the total biomass. Additionally, the volume fractions, distribution and orientation of the vegetation parts relative to the incidence vector determine both the magnitude and phase of the backscattered energy (e.g. Cronin 2004). Thus, the signal is related to vegetation biomass but it is also influenced by other parameters, such as soil moisture and roughness.

SAR systems operate at different wavelengths, which are sensitive to the different components of the vegetation (e.g. Cronin 2004). For biomass estimation in semi-arid zones, the use of SAR systems is not as prevalent as for forest areas. Table 2-4 gives an overview of the radar sensors that have been used for biomass estimation in semi-arid regions. In the following, the main findings of the studies are summarized, first for spaceborne sensors (C- and L-bands) and then for airborne sensors (multipolarimetric). Details of the studies can be found in table A-4 (appendix).

Table 2-4: Specifications of radar sensors that have been used for biomass estimation in semi-arid regions.

Sensor	Mission	Band	Polarization	Maximum spatial resolution	Swath width [km]	Revisit time [days]	Temporal coverage
SAR	ERS-1/2	C	VV	30 m	100	35 (global)	ERS-1: 1991–2000 ERS-2: 1995–today
WSC	ERS-1/2	C	VV	0.25°	400	35 (global)	ERS-1: 1991–2000 ERS-2: 1995–today
ASAR	ENVI-SAT	C	VV, HH, VV/HV, HV/HH, VH/VV	950, 150, 30 m	400, 100, 5	35 (global)	2001–today
SAR	JERS-1	L	HH	18 m	75	44 (global)	1992–1998
PALSAR	ALOS	L	Quad	7–100 m in various modes	30–350 in various modes	46	2006–today
SSM/I (passive)	DMSP	19.35, 22.235, 37.0, 85.5 [GHz]	H, V	12.5–25 km	1394	Several hours	1987–today
AIRSAR	Air-borne	C + L + P	Quad	-	-	-	-

Frison et al. (1998) used European Remote Sensing (ERS) satellite wind scatterometer (WSC) data and a semi-empirical backscattering model (soil and vegetation) in combination with an ecosystem grassland model (Sahelian transpiration, evaporation and productivity model, STEP model; Lo Seen et al. 1995, Mougin et al. 1995). Radar data acquired at 20° were found to be mainly related to soil characteristics, whereas 45° data provided information about the vegetation (Frison et al. 1998, Frison and Mougin 1996). The developed model was inverted and used for biomass estimation, resulting in an error of 33%. However, for heterogeneous agro-pastoral sites with low herbaceous cover, 45° ERS-WSC data were found to be dominated by bare soil contribution (Zine et al. 2005).

The use of special sensor microwave radiometer/imager (SSM/I) data has also been tested, but poor results were obtained compared to ERS-WSC data, mainly due to strong atmospheric effects (Frison et al. 2000). Moreover, SSM/I data were mainly linked to soil parameters, while WSC response was directly sensitive to the biomass (Frison et al. 2000). A systematic exploration of the relationship between ERS-WSC data, herbaceous AGB and soil moisture by Jarlan et al. (2002) revealed that a wide range of admissible parameters exists and that additional data are necessary to narrow the parameter domain.

In a further study, the combined use of a water balance model, a radiative transfer model and ERS scatterometer data was applied (Jarlan et al. 2003). Temporal information on soil moisture from METEOSAT rainfall data was used as an additional input for the radiative backscattering model. Then, a non-linear inversion was applied to ERS data to retrieve the AGB. The relationship between retrieved and field-measured herbaceous biomass showed a good agreement. The algorithm was successfully applied to obtain herbaceous biomass of on area of 350,000 km^2.

Svoray et al. (2001) assessed the empirical relationship between ERS-2 backscatter and biomass and observed that large differences in the AGB of different vegetation formations resulted in low backscatter variation. The green leaf biomass volumetric density (GVD) was introduced, which showed a significantly higher correlation to ERS-2 backscatter, leading to the conclusion that the backscatter is highly correlated with the green leaf biomass.

While previous studies made use of C-band SAR data, Santos et al. (2002) used L-band SAR (Japanese Earth Resources Satellite, JERS-1) to map the biomass of forest–savannah contact zones with the empirical relationships. A sigmoid function responded best to biomass variations at abrupt contact zones, while a logarithmic equation was best for gradual transition zones. The authors found a general influence of vegetation density on the radar backscatter. However, soil texture and structure were also found to contribute to backscatter variation, especially in savannah sites.

Advanced Land Observing Satellite (ALOS) phased array type L-band SAR (PALSAR) also provides L-band SAR data, which have been used by Mitchard et al. (2009) to predict woody AGB over Africa. The study area was not in a typical semi-arid environment, but included forest–savannah transition zones. The obtained AGB described only larger woody AGB and excluded shrubs, grasses and BGB. Strong relationships between AGB field measurements and cross-polarized (HV) radar backscatter were found for four sites. Saturation was obvious between 150 and 200 Mg ha^{-1}. Logarithmic and quadratic logarithmic models fitted the biomass–HV relationship best. Consistency of the relationship was tested by predicting the AGB of each side by applying a regression equation developed from the other sites. The root mean square error (RMSE) increased by only 12–30% and remained low for sites with AGB < 150 Mg ha^{-1}.

Not only spaceborne, but also airborne SAR data have been used for biomass estimation. Airborne polarimetric SAR (AIRSAR) data were, for example, applied by Cronin (2004) for

biomass mapping of woodlands. The empirical relationships between the SAR backscatter and total AGB showed considerable scatter, due to the large range of species present. A non-linear function was found to be more efficient than logarithmic and polynomial functions. For the three frequencies obtained with AIRSAR (C-, L-, P-bands), the HV polarization at P- and L-bands was considered most suited for biomass estimation. Similar results were obtained for relationships to trunk biomass and leaf and small branch biomass. The relationship also varied with incidence angle; here, best results were obtained at high incidence angles (~57°–60°). The empirical relationships for biomass mapping were limited above 60–100 Mg ha^{-1}, due to SAR saturation. Cronin (2004) also investigated a SAR backscattering model. The C-HV signal was found to interact almost exclusively with foliage and small branches. The author (Cronin) suggested obtaining pixel-based measures of canopy and trunk biomass by considering all SAR frequencies and polarizations and using SAR inversion models.

A further study based on aerial multifrequency polarimetric AIRSAR data for biomass estimation in semi-arid zones has been presented by Collins et al. (2009). The radar backscatter was correlated with the basal area using simple linear regression. The basal area was then converted to the AGB by applying allometric equations. In this study, the C-band was not utilized due to findings of insufficient canopy penetration in previous studies. The L-HV channel showed the strongest relationship to tree biomass. The corresponding model was inverted and applied to predict the AGB of 15 test plots reserved for model validation with good results.

2.1.5 Biomass Derivation for Semi-arid Areas based on the Synergetic Analysis of Optical and Radar Data

Most previous studies concentrated on the use of either optical or radar data. Rather little attempts have been made so far to use a combination of both for biomass estimation in semi-arid areas. Nevertheless, encouraging results have been obtained.

One study is presented by Svoray and Shoshany (2002, 2003), who combined ERS-2 C-band and Landsat-TM data to retrieve herbaceous AGB. The empirical relationship between the ERS-2 SAR backscatter alone and AGB was moderate. Application of the water-cloud model yielded a higher accuracy, which could be further increased by applying a modified model that included fractional cover information from Landsat data. The authors concluded that semi-arid herbaceous vegetation cannot be assumed as a homogeneous vegetation layer (Svoray and Shoshany 2002), but that the water-cloud model can be adapted to sparse canopies when it is combined with additional vegetation cover information.

Cronin (2004) investigated the benefits gained with integrating AIRSAR and optical data and concluded that the latter could help to discriminate woodland communities and, thus, help to understand the interaction of microwaves with different vegetation structures. She especially recommends the use of a combination of ALOS PALSAR and Landsat ETM+-derived Foliage Projected Cover (FPC) for biomass mapping below 100 Mg ha^{-1} (Cronin 2004) and a combination of FPC with C-band HV or L- or P-band for mapping of woody regrowth.

The information contained in optical and radar data was also found to be coherent by Mangiarotti et al. (2008), who combined optical and radar data within a coupled vegetation dynamics – radiative transfer/backscatter model (cf. section 2.1.6). Another study showing the advantages of a combined approach over the use of optical and radar data alone has been published by Chen et al. (2009). They investigated the Landsat ETM+, JERS-1 data and a combination of both for biomass estimation over western Canada. The strongest correlation between the natural logarithm of AGB and single remote-sensing data was found for the SAR

backscatter; the second strongest predictor was the simple ratio VI with NIR and MIR bands. However, the best overall performance was reached by a model combining JERS and TM data ([1], number refers to accuracies given in table A-5 (appendix). A 'two-step approach' with separate models for three land cover types (grass, shrub, sparse woodland) further improved the AGB estimation ([2]). The transfer of the methods to a second study area resulted in good (one-step approach, [3]) to moderate (two-step approach, [4]) accuracies. In this study, the combination of L-band SAR data with VIs using NIR and MIR data clearly improved the biomass estimation compared to the use of each of the two data sets individually.

2.1.6 Biomass Derivation for Semi-arid Areas based on Modelling Approaches

A number of different models have been developed to derive biomass estimates incorporating different data sources and following different approaches (e.g. Dech et al. 2001). Especially, vegetation dynamics models have recently been used in combination with remote-sensing data to predict temporal variations on vegetation parameters and primary production. The variety of models for primary production estimation is not presented here, as this is a topic of its own and should be the subject of an individual review. In the following, some examples of modelling approaches that make use of remote-sensing data and derive standing AGB or show limitations and potentials of this kind of approach for semi-arid areas are reviewed. An overview of the considered studies is included in table A-5 (appendix).

Mougin et al. (1995) and Lo Seen et al. (1995) combined remote-sensing data, canopy and soil reflectance models and an ecosystem model (STEP model) for semi-arid grassland. Temporal profiles of NDVI were simulated by the coupled model and compared to AVHRR NDVI data (Lo Seen et al. 1995). I-NDVI was also compared to net primary productivity and a linear relationship was found for high-rainfall areas. The model has been used for several studies: for example, by Jarlan et al. (2008) with SPOT-VGT data, and by Mangiarotti et al. (2008), who coupled it with radiative transfer (for optical data) and backscatter (for radar data) models for both soil and herbaceous vegetation. The coupled models were used to simulate the AGB, which predicted well the actual biomass (Jarlan et al. 2008).

Nouvellon et al. (2001) also used a combination of a grassland ecosystem and a radiative transfer model for the simulation of carbon and water budgets of semi-arid grasslands. NDVI data were used for calibration of the initial parameters (living root biomass, maximum light use efficiency); this significantly improved the simulated AGB.

Another modelling approach for AGB estimation of semi-arid grasslands has been proposed by Feng et al. (2005). Their model is based on field measurements, but the surface parameters could be inversed from remote-sensing data. The authors observe a strong logarithmic correlation between LAI and AGB. However, a different logarithmic regression equation was retrieved for any time period considered. Thus, coverage (to express degradation) and time (to express the growth period) were introduced as additional parameters. The new model was superior to the use of constant allometric ratios and VIs (Feng et al. 2005).

2.1.7 Discussion

In the previous sections, an overview of the remote-sensing research activities for AGB estimation in semi-arid regions has been given. In this section, a summary of the efforts is presented and repeatedly observed problems are discussed. Common difficulties and future challenges of remote-sensing-based biomass estimation in semi-arid areas are presented.

2.1.7.1 Comparison of Methods for Remote-sensing-based Biomass Estimation in Semi-arid Areas

Several different methods and parameters have been applied for remote-sensing-based biomass estimation in semi-arid areas. About 85% of the reviewed studies were based on empirical relationships between remote-sensing-derived indices and biomass field measurements, while only few studies investigated other methods or compared different approaches.

The empirical relation can be formulated as a direct or indirect relationship, when intermediate variables (e.g. LAI, shadow area or fractional vegetation cover) are correlated to biomass. In most studies, VIs are used and linear or exponential curves fitted (cf. tables A-1 to A-3 (appendix A). With SAR data, the backscatter is usually applied (cf. table A-4). Nonparametric empirical models such as regression trees (e.g. Baccini et al. 2008) have also been used to account for the non-linear relationship between the biomass and spectral bands, along with multiple regression (e.g. Chen et al. 2009) and geometric mean regression (Wessels et al. 2006).

Especially, the NDVI was found to be closely related to the biomass and, particularly, to green biomass (Diouf and Lambin 2001, Filella et al. 2004, Sannier et al. 2002). However, the performance of VIs such as NDVI in semi-arid areas is not consistent and some studies also report poor results that might be induced by a strong influence of varying soil types (Duncan et al. 1993, Ringrose et al. 1994). The findings from ground-based studies also suggest that narrow-band VIs or indices using red-edge channels could be more effective for biomass estimation in semi-arid landscapes than traditional VIs (cf. section 2.1.3).

The relationship between fractional cover and biomass was also found to be site specific (Franklin and Hiernaux 1991); however, fractional vegetation cover proved suitable in combination with vegetation height information and VIs (Qi and Wallace 2002). Moreover, it was found to be useful in studies combining optical and radar data (cf. section 2.1.5).

Several studies based on coarse-resolution data made use of integrated VIs (cf. table A-1). While some authors received good results (e.g. Holm et al. 2003, Wylie et al. 1991), others concluded that the I-NDVI was not a robust proxy for herbaceous biomass (Diouf and Lambin 2001). Only few studies compared the performance of the integrated versus single-date indices, again with inconsistent findings (cf. Hobbs 1995, Holm et al. 2003, Sannier et al. 2002, Tucker et al. 1985, Verbesselt et al. 2006). There is obviously no common agreement on whether a single-date or integrated approach should be favoured. The integrated VIs may be most suitable for annual vegetation (e.g. Tucker et al. 1985).

Other approaches than empirical regressions have only been used in a minority of studies (e.g. Kogan et al. 2004, Rosema 1993). Radiative transfer models have been applied with Landsat data (Franklin and Hiernaux 1991), SAR data (Cronin 2004, Frison et al. 1998, Jarlan et al. 2003) and within a combined approach (Svoray and Shoshany 2002, 2003). Modelling approaches in combination with remote-sensing data have also been applied rarely (e.g. Mangiarotti et al. 2008, Nouvellon et al. 2001). In figure 2-2, an overview of the different approaches for remote-sensing-based biomass estimation in semi-arid regions is given.

The limits of the empirical models, due to their strong dependency on field data, limited transferability and over-simplification of the relationship, have often been discussed (e.g. Anderson et al. 1993, GTOS 2009, Svoray and Shoshany 2002). Nevertheless, empirical models are commonly used, because they are convenient to use, easy to implement and often give accurate results for the study area for which they have been trained (Nijland et al. 2009).

The dominance of empirical approaches can also be explained by the difficulties that inhere in more complex models. For example, radiative transfer models are often difficult to handle

due to the under-determined and ill-posed nature of the inversion problem (e.g. Baret and Buis 2008, Nijland et al. 2009) and require a detailed description of the vegetation canopy (Svoray and Shoshany 2002). However, physical models might allow for more robust and accurate biomass estimation than empirical approaches (Diouf and Lambin 2001). Vegetation and ecosystem models, on the other hand, depend on several additional input parameters, which are often not available at fine scales. Moreover, to be able to represent the complex environmental mechanisms, the models need to introduce assumptions that limit the accuracy of the derivation of biomass amounts and distribution (GTOS 2009). Nevertheless, previous studies showed that such models can successfully be used in combination with remote-sensing data to simulate AGB.

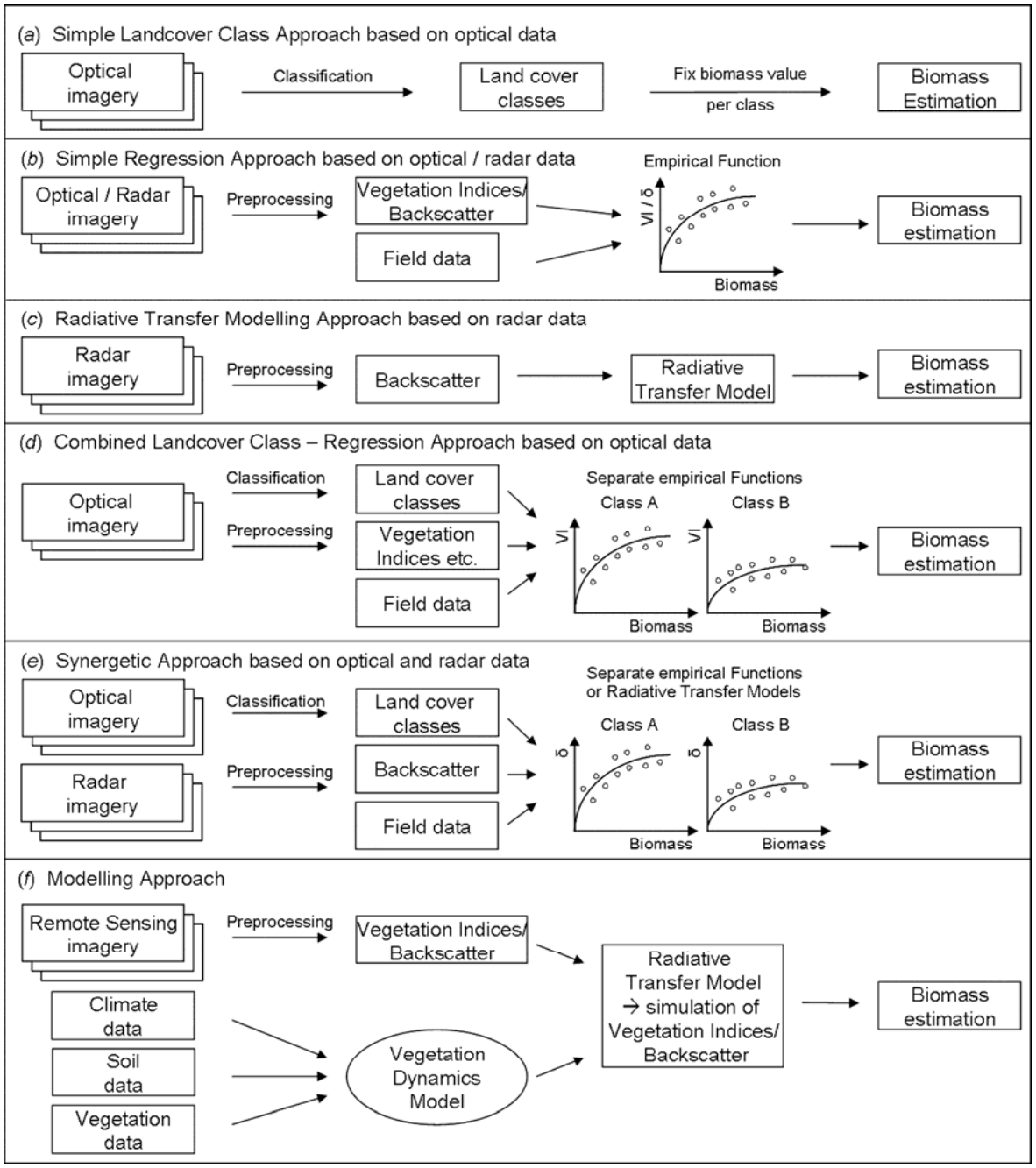

Figure 2-2: The way from satellite data to biomass estimation: different approaches typically applied for biomass estimation in semi-arid regions.

2.1.7.2 Challenges for Biomass Estimation Resulting from the Characteristics of Semi-arid Areas

As observed in many of the research studies, remote-sensing-based approaches for biomass estimation in semi-arid regions are problematic due to the sparse vegetation cover and often senescent vegetation (e.g. Beeri et al. 2007, Svoray and Shoshany 2003, Wessels et al. 2006). The spectral response used for vegetation characterisation is highly influenced by soil background, shadow, different species, standing dead vegetation and litter. The signals from vegetation are often much smaller than those from soil background and have low spectral contrast (Calvão and Palmeirim 2004). Moreover, senescent vegetation cannot be related to traditional spectral VIs (Qi and Wallace 2002). Indices based on MIR bands may be more suitable for areas dominated by senescent vegetation (Moleele et al. 2001, Qi and Wallace 2002). The reflectance of soil background and its variation should be explicitly considered for biomass assessment in semi-arid regions (Elvidge and Lyon 1985, Huete et al. 1985, Montandon and Small 2008).

Moreover, the phenomenon of vegetative darkening has been repeatedly observed and seems to be a common effect on the NIR reflectance in semi-arid and arid ecosystems (e.g. Calvão and Palmeirim 2004, Graetz et al. 1988, Moleele et al. 2001, Musick 1984, Otterman 1996). Vegetation shadows may also contribute to this effect (Graetz and Gentle 1982, Jakubauskas et al. 2001, Okin et al. 2001) and, in case of bright soils, the overall brightness may be influenced more by shadowing effects than by radiation directly reflected by the vegetation (Garcìa-Haro et al. 1996). Thus, changes in fractional vegetation cover might have a stronger influence on the optical signal than changes in the thickness of the canopy (Calvão and Palmeirim 2004, Verstraete and Pinty 1991).

Several researchers reported difficulties in retrieving vegetation information in areas of low (<30%) cover (Okin et al. 2001, Tueller 1987). According to Okin et al. (2001), possible reasons for this might be not only the soil background, but also the non-linear mixing due to multiple scattering, the spectral characteristics of desert plants, a strong spectral variability within the same species and the open canopies.

The vegetation in semi-arid areas, especially annuals and grass, is also highly variable throughout the year, depending on the distribution and amount of precipitation. The total primary production of a year may occur within a very short time period; thus, a high temporal resolution of the remote-sensing data might be more important than the spatial resolution (e.g. Tucker et al. 1985). Shrubs are less dependent on the highly variable precipitation and, thus, a more stable component of the overall biomass (Calvão and Palmeirim 2004).

2.1.7.3 Challenges of Data Availability, Costs and the Suitability of Source Data

The choice of source data is not only determined by the scale of the desired assessment, required accuracy and specific compulsory periods for biomass mapping but also by the availability of data and their price. High-resolution data are generally quite expensive. This limits their use for many projects, especially if larger areas are to be observed. Some satellite imagery, for example, MODIS data and recently also the Landsat archive, is available for free and therefore accessed and used by a wide community.

Low-cost availability and global coverage allow the testing of developed methods over large areas and by a wide community. This is a great advantage, especially for the development of operational services. Some methods also need time-series information, for example, for calculation of integrated indices. These studies build on low-resolution sensors with high acquisition repetitivity. For areas with frequent cloud cover, the acquisition repetitivity of

optical sensors is also relevant or SAR data are used instead. Modelling approaches usually also need input data in short time intervals, but, here, often long-term data availability is a prerequisite, and thus low-resolution data, such as NOAA-AVHRR, satisfy the requirements best.

Although the problem of remote-sensing signal saturation is not prevalent in semi-arid regions, it might have to be considered for the choice of source data, for example, for semiarid woodlands. VIs from red and NIR reflectance generally saturate earlier than VIs from NIR and MIR reflectances or the red-edge position (e.g. Boyd et al. 1996, Filella and Peñuelas 1994, Nelson et al. 2000). For radar data, it can be generalized that longer wavelengths saturate later and are more sensitive to larger components of the vegetation; polarization of SAR also plays a role (e.g. Chen et al. 2009, Cronin 2004).

Different remote-sensing observations are more or less sensitive to the AGB in specific environments or for different AGB densities. Due to the lower vegetation height, density and biomass in semi-arid regions, optical data are especially useful, while some other methods that are frequently applied for biomass estimation of forests, such as light detection and ranging (LiDAR) and polarimetric SAR interferometry, have not been applied to semi-arid zones.

Some benefits of the different remote-sensing sensors are given in table 2-5. However, any single sensor has its limitations and no single sensor can be expected to provide consistently infallible biomass information (Goetz et al. 2009). Therefore, some authors suggest using different data sources in a synergistic way, to overcome the limitations of each (e.g. Chen et al. 2009, Goetz et al. 2009).

Table 2-5: Benefits and limitations of different remote sensing sensors for biomass estimation in semi-arid areas.

Data	Benefits	Limitations
Optical	- Large areas can be covered - Regular mapping is possible - Simple correlation with, for example, land cover - Red, NIR and SWIR reflectance valuable for biomass estimation - Historical data available for some sensors - Relatively low cost, some sensor data free of charge	- Weather dependent - Saturation at relatively low biomass levels (LAI 2–3) that might affect biomass estimation in more densely vegetated semi-arid areas - Influenced by soil background reflectance
SAR	- Weather and daylight independent - Large areas can be covered - Medium to long wavelengths suitable for typical semi-arid vegetation - Combination of wavelengths and polarizations contains additional information on vegetation biomass	- Speckle reduces effective spatial resolution - Influenced by soil moisture and topography - Only sensitive above a certain vegetation density
LiDAR	- Three-dimensional profile of the vegetation - Most suitable for dense forest with large height differences	- Very high costs - Rarely available - Only local data acquisition possible - No regular mapping possible - Not operational on satellite platform (except GLAS)

2.1.7.4 Challenges of Strongly Varying Accuracy for Biomass Estimation in Semi-arid Areas

It is obvious that the regression quality varies strongly. Coefficients of determination (R^2), for example, for empirical regressions based on coarse-resolution optical data were in the range from 0.32–0.95. Contrary findings have also been reported, for example, for the sensitivity of Landsat bands and NDVI to woody and leaf biomass (Calvão and Palmeirim 2004, Samimi and Kraus 2004). These inconsistent findings hamper a straightforward conclusion on the most appropriate regression approaches for biomass estimation. On the other hand, it can be concluded that the performance of regression models is obviously very site specific.

It might be advisable to further explore approaches such as regression tree models (Baccini et al. 2008), multivariate regression including complementary information (Qi and Wallace 2002), multi-scale approaches (Wylie et al. 2002) or greenness strata approaches (Anderson et al. 1993). These methods yielded good results, but general conclusions cannot be drawn, because they have only been applied in a few studies.

The reported accuracies from studies based on radar data present a similar picture. Good results were, for example, obtained for empirical regressions with SAR backscatter (Collins et al. 2009, Svoray et al. 2001) and a combination of a radiative transfer model with a water balance model (Jarlan et al. 2003). Svoray and Shoshany (2002) reported superiority of a backscatter model compared to empirical relationships.

Very few studies have investigated the synergetic use of optical and SAR data so far. However, the results obtained seem to be very promising and outperformed the results obtained using one of these data types alone (cf. Chen et al. 2009, Svoray and Shoshany 2002). Thus, synergetic approaches should clearly be in the focus of future research.

Due to the individual conditions and different methods for validation, the results reported for different studies cannot be absolutely compared. It should also be considered that the field data that are used for validation are themselves error-prone. Especially, for coarse-resolution data, collection of adequate field data that represent the biomass at pixel scale is difficult. In most studies, a relatively small number of field plots was available. Exceptionally extensive ground data were available for the studies carried out in the Kruger National Park, which could base on long-term observations of numerous field plots (Mutanga and Rugege 2006, Verbesselt et al. 2006, Wessels et al. 2006). Other studies based on comprehensive field data are, for example, those by Baccini et al. (2008), Mitchard et al. (2009), and Xu et al. (2008).

For the reasons mentioned above, it is difficult to conclude that one approach or database is superior to another. The strongly varying accuracies and even contrary findings hinder a clear ranking of the different techniques. Further research is necessary to investigate the causes for the variable accuracy observed. Unfortunately, studies that apply and compare different approaches are very rare. Comparative analyses of both – different approaches for one study area and one approach over different study areas – would significantly help to understand the shortcomings and advantages of each.

2.1.7.5 Challenges of Transferability of Methods for Biomass Estimation in Semi-arid Areas

The largest challenge in biomass estimation based on remote-sensing data seems to be the transfer of the methods in time (repeatability) and space (portability). Unfortunately, an adequate field database that allowed for testing the transferability of developed models was seldom available. Thus, only few studies were able to give an assessment on this important issue.

Regarding the repeatability, previous studies reported considerable differences in the relationships between the biomass and the remote-sensing signals for different years and strong inter-annual variations in the regression parameters (Diouf and Lambin 2001, Wylie et al. 1991). Therefore, such regressions provided poor results if applied to another year (Cho and Skidmore 2009, Wessels et al. 2006). Only in one study, promising results regarding a repeated application were reported using a greenness strata approach (Anderson et al. 1993). These findings suggest that empirical approaches are not very robust in time.

Portability is also considered a major problem with remote-sensing-based models for biomass estimation. For example, regression approaches lost accuracy when applied to all sites of a study area compared to separate vegetation types (Sannier et al. 2002) and even showed to be strongly affected by variations within one landscape group (Wessels et al. 2006). Xu et al. (2008) also found that individual models for separate regions performed better than a national model. Thus, the portability of the applied empirical approaches is obviously limited. However, promising results have been obtained regarding the portability of empirical regression models for biomass estimation in semi-arid regions (Samimi and Kraus 2004) and a model that was based on a combination of SAR and optical data (Chen et al. 2009). Mitchard et al. (2009) also were optimistic that a generally applicable relationship for biomass estimation based on ALOS PALSAR data could be established.

According to Franklin and Hiernaux (1991), radiative transfer models are not a beneficial alternative regarding the portability, as the necessary assumptions on stand characteristics need to be calibrated at each site. Nevertheless, Jarlan et al. (2003) reported promising results for the large-area application of a combined water balance model and a radiative transfer model based on SAR data. For ecosystem models, which are especially established to cover large areas and often rely on several additional input data, a better performance regarding transferability can be expected. Promising results were, for example, reported by Mangiarotti et al. (2008) and Nouvellon et al. (2001).

The above results show that large challenges and problems exist regarding the transferability of models for biomass estimation. Especially, empirical relationships seem to provide weak results when applied to another point in time or to another study area. Difficulties have also been reported for modelling approaches. Unfortunately, only few studies were able to analyse the aspects of transferability. Thus, a lot of further research on this topic for remote-sensing-based methods for biomass estimation, especially in semi-arid areas, is required.

2.1.8 Conclusions

The concern and interest in biomass estimation of the Earth's ecosystems has been growing rapidly in the past years and is expected to increase in the future. Remote-sensing techniques offer a unique possibility for fast, cost-efficient and large-scale biomass estimation and a great need exists for the development of accurate and transferable methods for this task. While an immense number of studies have been carried out for forests, semi-arid areas – which cover 18% of our planet's land surface – have been rather neglected. The natural vegetation of semi-arid areas is predominantly discontinuous and consists of a great number of different species. Additionally, the soil background highly influences the remotely sensed signals due to the scarce vegetation cover. Therefore, remote-sensing-based biomass estimation for semi-arid areas requires a lot of additional research.

The majority of studies for semi-arid areas were based on low- and medium-resolution optical or radar data. High-resolution data have only been used in individual cases. The most intensively used have been the sensors AVHRR and TM/ETM+ as well as ERS-1/2 data. The

accuracies obtained with optical and radar data were comparable. Only few studies have investigated synergetic approaches; however, these reported a significant improvement when a combination of optical and SAR data was used.

The great majority of studies applied empirical relationships between remote-sensing-derived indices and biomass field data. The accuracy of these regression approaches varied largely, but they are obviously hardly transferable in time or space. Rather little effort has been invested in more complex approaches like radiative transfer models or the combination of remote-sensing data and ecosystem models. These, however, would have a better potential for transferability.

Several studies also reported problems with the validation of the results, due to inconsistencies in the scale between satellite and field data. As the economic constraint is a major issue and is often hindering extensive, large-area field sampling, rapid, labour-saving and inexpensive field sampling techniques need to be developed. Furthermore, standardized ground sampling schemes would allow for better comparability of the different studies.

Future research should be directed towards a better understanding of the several influences on the relationship between AGB and remote-sensing signals in semi-arid regions. Regarding the use of sensors, more research is especially needed on the synergetic use of optical and SAR data, for which promising results have been obtained. From the methodological point of view, additional research on more complex approaches, such as radiative transfer models or the use of ecosystem models is recommended. Comparative studies would help to understand advantages and shortcomings of different approaches. Future research should especially be directed towards the development of robust models that allow for better transferability – one of the greatest challenges of remote-sensing-based biomass estimation in semi-arid areas. This topic is especially important, because the limited transferability is the major constraint hindering the operational application of remote-sensing-based biomass estimation approaches. However, operational monitoring systems would be a big step forward in understanding the changes in biomass in semi-arid areas and in providing an essential tool for sustainable resources management, the derivation of possible climate change related trends or value-added carbon storage products.

2.2 Net Primary Productivity Models Used in this Study

2.2.1 Introduction to Primary Productivity Models

In contrast to the estimation of standing above-ground biomass (Eisfelder et al. 2012, GTOS 2009), NPP has been widely modelled on global scale (Awaya et al. 2004, Cramer et al. 1999, Potter et al. 2003, Running et al. 1999, Running et al. 2004). Also several regional models have been developed (Crabtree et al. 2009, Feng et al. 2007, Liu et al. 2005, Wißkirchen 2005, Yu et al. 2009). Many studies focus on estimation of vegetation growth by modelling gross primary productivity (GPP) and NPP (Hilker 2008, Yu et al. 2009).

GPP describes the gross carbon uptake by plants during photosynthesis. A fraction of the energy uptake is used by the plants for maintenance (maintenance respiration) and growth (growth respiration). Maintenance and growth respiration add up to the autotrophic respiration. The remaining fixed carbon is referred to as NPP, which can thus be derived from GPP by subtracting autotrophic respiration, i.e. total respiratory losses. Some studies are also interested in the net ecosystem productivity (NEP), which is the net carbon uptake of a land ecosystem. NEP can be calculated from the NPP by subtracting heterotrophic respiration, i.e. carbon dioxide (CO_2) emission of the soil (Wißkirchen 2005).

Many global vegetation productivity models are driven by simulated climate data and use constant leaf area index (LAI) values. For regional models, however, spatially explicit inputs are important to capture the spatial distribution of the vegetation productivity. This information can be derived from satellite data. Especially the LAI and the fraction of absorbed photosynthetically active radiation (FPAR) characterize the vegetation canopy and the energy absorption capacity and can be used as key driving variables for NPP models (Myneni et al. 2002). Several models exist for NPP estimation based on remote sensing, which differ in approach and complexity, data needs, flexibility, spatial and temporal resolution (Cramer et al. 1999, Coops et al. 2009).

One major group of NPP models commonly driven by remote sensing data, are light use efficiency (LUE) models (Liu and Cheng 2010, Xiao 2006). These calculate NPP from light interception, based on the concept of Monteith (1972). The idea behind this approach is that the carbon uptake of well watered and fertilized plants is linearly related to the absorbed photosynthetically active radiation. Models that follow the concept of Monteith (1972), calculate GPP or NPP dependent on the absorbed photosynthetically active radiation and a vegetation-type-specific light use efficiency (LUE). The variability of LUE is controlled by stress factors, such as temperature and water stress as well as nitrogen availability. Examples of this type of model are CASA (Potter et al. 1993, Field et al. 1995), C-Fix (Veroustraete et al. 1994, Verstraeten et al. 2006), GLO-PEM (Prince 1991, Prince and Goward, 1995), TURC (Ruimy et al. 1996), and VPM (Xiao et al. 2004a, Xiao et al. 2004b).

More complex process models can also be driven by parameters derived from remote sensing (Feng et al. 2007, Wißkirchen 2005). Dynamic models calculate uptake and release of carbon in a physically consistent way regarding conservation of energy and impulse. They are based on plant physiological ecology principles and explicitly represent ecosystem carbon and water exchanges and vegetation dynamics (Cramer et al. 2001). Examples for dynamic models are e.g. CENTURY (Parton and Rasmussen 1994), LPJ (Bondeau et al. 2007), and HYBRID (Friend et al. 1997). Some models use remote sensing based vegetation structure parameters (e.g. LAI) as input, e.g. BIOME-BGC (Thornton et al. 2002, White et al. 2000). Others include calculation of phenology and LAI or fractional cover, e.g. BIOME3 (Haxeltine and Prentice 1996), HYBRID, and ORCHIDEE (Krinner et al. 2005). A special type of dynamic vegetation models are soil-vegetation-atmosphere-transfer (SVAT) models. They deal with the interface between soil, vegetation and atmosphere (Göttlicher et al. 2009), simulate land surface processes in detail and then integrate over the canopy (Cramer et al. 1999). Remote sensing based SVAT model are e.g. SiB2 (Sellers et al. 1996a,b) and CLM (Dai et al. 2003).

2.2.2 Description of the Model BETHY/DLR

BETHY/DLR is based on the SVAT model 'Biosphere Energy Transfer Hydrology Model' (BETHY), developed by Knorr (1997) at the Max-Planck-Institute for Meteorology (cf. also Knorr 2000, Knorr and Heimann 2001). BETHY simulates the photosynthesis of vegetation within a full energy and water budget of the Earth's surface.

BETHY simulates the CO_2 uptake by vegetation as a process that is limited by light intensity, heat, soil water availability, and nitrogen (Knorr 1997). Incoming and absorbed photosynthetically active radiation are computed to describe light limitation. Heat limitation is considered by energy and water balance at the vegetated surface and water limitation is calculated with a soil water model (Knorr 1997, Knorr and Heimann 2001). Figure 2-3 gives an overview of the structure of BETHY and the linkage between the four model components, which describe energy and water balance, photosynthesis, phenology, and carbon balance.

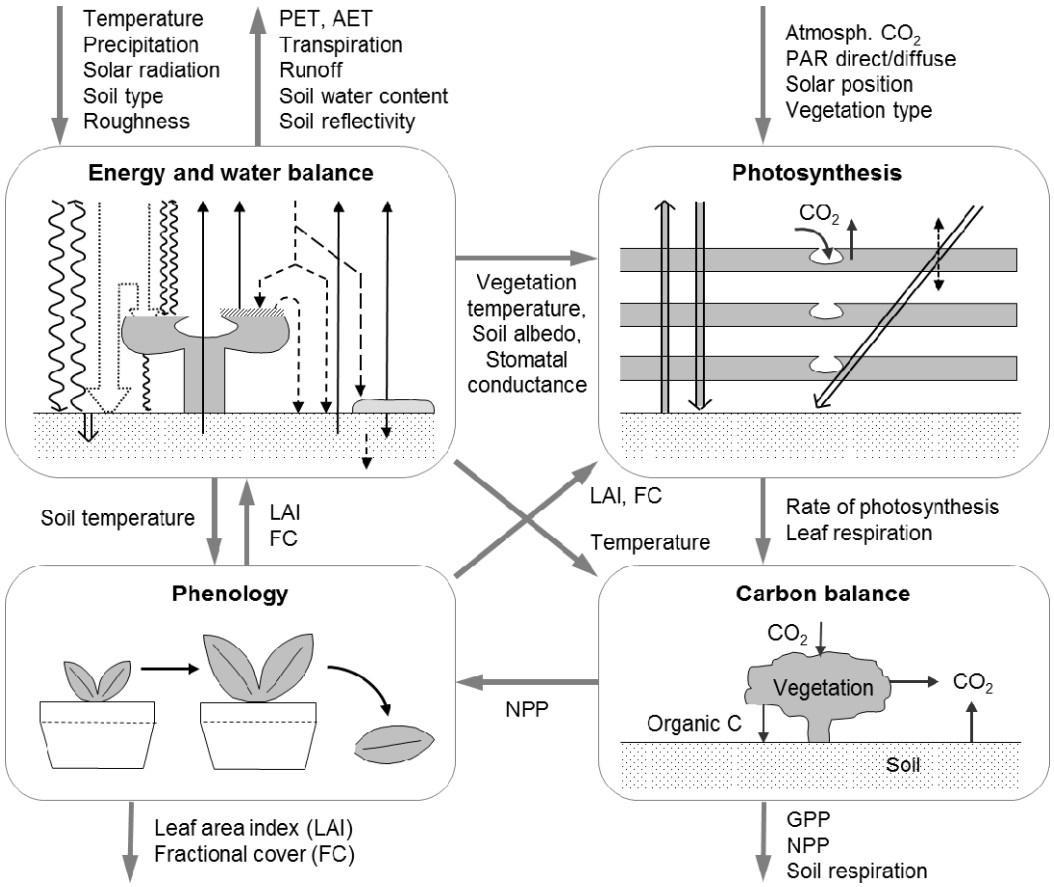

Figure 2-3: Structure of BETHY showing input and output parameter as well as information flow between the four major model components (adapted from Knorr 1997).

The energy balance is calculated hourly based on temperature, precipitation, solar radiation, and soil parameters (texture, albedo, roughness). LAI and fractional vegetation cover are further required to calculate surface albedo, net radiation, latent and sensible heat flux, and air moisture. Soil water and snow balance are calculated daily (Knorr 1997). Evapotranspiration is calculated separately for wet (unlimited ET) and dry (limited ET) vegetation according to the approach by Penman-Monteith (Monteith 1965b) and the resistance concept of Garrat (1992). The energy balance can be described generally based on the net radiation R_0, the latent and sensible heat fluxes E_0 and H_0, and the soil heat flux G (Wißkirchen 2005).

$$R_0 - H_0 - E_0 - G = 0 \qquad (2\text{-}1)$$

Input data for the photosynthesis module comprise PAR, solar angle, soil albedo, atmospheric CO_2 concentration, and information on vegetation types. Input from other model components are LAI, fractional vegetation cover, air moisture, and transpiration rate. Output products are hourly PAR absorption and GPP. The parameterization of the photosynthesis is based on a combined enzyme kinetic approach after Farquhar et al. (1980) and Collatz et al. (1992), for C_3 and C_4 plants respectively. This approach parameterizes the enzyme kinetics on leaf level. The differentiation between C_3 and C_4 plants is important, as C_4 plants are able to fix more atmospheric CO_2 at high temperatures. Unter these conditions, the photosynthesis of C_3 plants is already saturated.

The rate of photosynthesis is then extrapolated from leaf to canopy level. The vegetation canopy is regarded to consist of three layers, for which radiation absorption in the canopy (two-flux approximation, Sellers 1985) is calculated (Knorr 1997). The photosynthesis rate A is

calculated as the minimum of two functions, which describe the carboxylation rate J_C and the electron transport rate J_E, minus dark respiration R_d.

$$A = \min(J_C; J_E) - R_d \qquad (2\text{-}2)$$

For the calculation of photosynthesis, plant specific parameters are needed. Therefore, it is necessary to differentiate between plant functional types and to define vegetation types, for which the individual parameters are defined. The actual model internal vegetation types and their specific parameters are given in Table 2-6.

Table 2-6: Vegetation types in BETHY/DLR and their specific parameters: V_{max}: maximum carboxylation rate at 25°C [µmol(CO_2) m^{-2} s^{-1}], J_{max} (for C_3): maximum electron transport rate at 25°C [µmol(CO_2) m^{-2} s^{-1}], k (for C_4): CO_2 specificity at 25°C [µmol(CO_2) m^{-2} s^{-1}], h: vegetation height [m], d_r: rooting depth [m], X: C_4 plant, otherwise C_3. (Sources for individual parameters are provided in Knorr 1997 and Tum 2008).

Number	Vegetation type	V_{max}	J_{max};k	h	d_r	C_4
1	Tropical broad-leaved evergreen trees	62	118	30.0	6.9	
2	Tropical broad-leaved deciduous trees	90	179	15.0	3.7	
3	Temperate broad-leaved evergreen trees	41	82	15.0	3.0	
4	Temperate broad-leaved deciduous trees	35	70	15.0	3.0	
5	Evergreen coniferous trees	29	52	15.0	3.9	
6	Deciduous coniferous trees	53	95	15.0	1.5	
7	Evergreen shrubs	52	102	1.0	3.5	
8	Deciduous shrubs	160	266	1.0	3.5	
9	C_3 short grass	42	80	0.3	1.8	
10	C_3 long grass	42	80	2.0	1.8	
11	C_4 short grass	8	140	0.3	1.8	X
12	C_4 long grass	8	140	2.0	1.8	X
13	Tundra vegetation	20	37	0.3	0.5	
14	Swamp vegetation	20	37	0.3	0.5	
15	Arable crops	117	220	0.6	1.8	
16	Irrigated crops	123	227	0.6	1.8	
17	Tropical tree crops	60	106	2.0	6.9	
18	Citrus crops	60	106	2.0	3.7	
19	Temperate deciduous tree crops	123	227	2.0	3.0	
20	Sugar cane	39	700	2.0	1.8	
21	Maize	39	700	2.0	1.8	
22	Rice	98	190	0.3	0.3	
23	Cotton	123	227	2.0	2.0	
24	Sugar beet	129	226	0.5	1.8	X
25	Soy	94	168	0.8	1.8	X
26	Sunflower	80	213	2.0	2.7	
27	Barley	68	169	1.2	1.8	
28	Wheat	83	193	1.5	1.8	
29	Rape	61	187	1.0	1.8	
30	Beech trees	46	109	15.0	4.0	
31	Oak trees	40	72	15.0	4.0	
32	Spruce, Fir trees	10	24	15.0	2.8	
33	Pine trees	17	30	15.0	4.0	
34	No vegetation	-	-	-	-	

The list provided in table 2-6 is an extended version of the vegetation types distinguished by Knorr (1995). For each vegetation type, the following biochemical parameters are defined: maximum carboxylation rate V_{max}, maximum electron transport rate J_{max} and other plant specific parameters, i.e. maximum rooting depth d_r and maximum height h.

Available land cover types, which are used as model input, have to be translated to these inherent vegetation types. For each grid cell, two model internal vegetation types can be defined. A weighting factor gives the relative importance of the primary and the secondary vegetation type.

The carbon balance model (cf. figure 2-3) uses model internal parameters from the photosynthesis model (GPP) and the energy balance model (soil water and leaf area temperature), as well as external data (air temperature and plant specific nitrogen content) to calculate autotrophic (from plants) and heterotrophic (from soil) respiration. Autotrophic respiration is modelled as the sum of maintenance respiration, which is mainly determined by the plant specific dark respiration, and growth respiration. The latter is defined to be proportional to the difference between GPP and maintenance respiration.

Further details on the calculation can be found in Knorr (1997), Knorr and Heimann (2001) and Wißkirchen (2005). Finally, NPP is calculated hourly as the difference of total carbon assimilation GPP and autotrophic respiration R_A. The hourly values are aggregated to daily data. The general equation for NPP calculation is given as follows:

$$NPP = GPP - R_A \tag{2-3}$$

BETHY/DLR additionally calculates NEP by subtracting heterotrophic respiration R_H from NPP (Wißkirchen 2005).

$$NEP = NPP - R_H \tag{2-4}$$

BETHY was originally designed for global simulations with output products generated monthly with a standard resolution of 0.5° latitude by longitude (Knorr 1997, Knorr and Heimann 2001). It was adapted by Wißkirchen (2005) at the German Aerospace Center for regional modelling based on remote sensing data with the aim to create a basis for operational, remote sensing based CO_2 balance modelling. The new version of the model was named BETHY/DLR. The spatial resolution of the model outputs was improved from 0.5° to 1 km due to the use of remote sensing data. The continuous time-series of daily climatic input data allows for a higher temporal resolution of the NPP results. In contrast to the original model, phenology is not calculated within the model, but satellite derived LAI data is used to describe vegetation phenology. Furthermore, the diurnal variation of the temperature is calculated from meteorological data, because the calculation from daily minimum and maximum temperatures, as done with BETHY, was found to lead to a systematic underestimation of the daily mean temperature (Wißkirchen 2005).

Scaled diurnal variations of PAR (at location x and time t) are calculated based on global radiation R_G and a constant scale factor k. R_G is derived according to the approach by Burridge and Gadd (1974), based on longitude LON, latitude LAT, time of day t, day of the year DOY, solar constant S, atmospheric transmission T, and solar altitude γ. Atmospheric transmission is calculated from daily mean cloud cover, which is based on European Centre for Medium-Range Weather Forecasts (ECMWF) data for three cloud heights (Wißkirchen 2005). The scale factor

k=0.48 describes the part of the global radiation that is used for photosynthesis (Wißkirchen 2005).

$$PAR_{x,t} = R_G(LAT, LON, t, DOY, T)_{x,t} \cdot S \cdot \gamma_{x,t} \cdot k \quad (2\text{-}5)$$

BETHY/DLR model outputs are GPP, NPP, and NEP. Spatial resolution of the output products depends on the resolution of LAI and land cover input data. The temporal resolution of modelled parameters is one day. BETHY/DLR was used by Wißkirchen (2005) for regional simulation of the CO_2 balance of Europe. Sensitivity analyses showed that model results are most strongly affected by CO_2 concentration, LAI, vegetation classification, and precipitation (in order of decreasing influence). Further details on the model and performed analyses can be found in Wißkirchen (2005).

The model BETHY/DLR was recently applied for derivation of NPP of agricultural plants for Germany and Austria (Tum and Günther 2011). Validation with statistical data on harvest showed good results (for Germany: R^2 0.79 and 0.58, for Austria: R^2 0.74 and 0.78, for 2000 and 2001 respectively; Tum and Günther 2011). For aboveground NPP for forests in Germany for the years 2000 and 2001 also high coefficients of determination were found to statistical data (coniferous forest: R^2 ~0.94, deciduous forest: R^2 ~0.75; Tum et al. 2011). A new soil water model was also implemented for BETHY/DLR (Tum and Borg submitted). The sensitivity of the model to different input data has also been analysed by Tum et al. (2012) and Niklaus (in preparation). BETHY/DLR has further been used for NPP calculation in Namibia (Dokupil 2008) and for South Africa (Niklaus et al. 2010a,b, Niklaus et al. 2012).

Input Data for BETHY/DLR

BETHY/DLR is driven by remote sensing and meteorological data. Operational data on air temperature, wind speed, and cloud coverage are available from the European Centre for Medium-Range Weather Forecasts (ECMWF) ERA-Interim reanalysis with a spatial resolution of 0.25° × 0.25° and a six hour interval (cf. section 4.1.1). Precipitation is available twice per day.

Remote sensing based LAI is a main driving parameter and needed with a high spatial resolution. LAI composites from CYCLOPES (Baret et al. 2007, Weiss et al. 2007) were usually utilized with BETHY/DLR (e.g. Tum et al. 2011, 2012). For the application of BETHY/DLR for Kazakhstan in this study, however, MODIS LAI data were used (Knyazikhin et al. 1999, see section 4.1.2.1). The MODIS LAI data were preferred, as CYCLOPES data contained gaps in the arid regions of Kazakhstan due to problems with neural network classification and were not available for 2008 and 2009.

Furthermore, the model requires information about land cover and land use to describe the spatial variability of vegetation types. In previous studies, the land cover classification included in the CYCLOPES database for the year 2000, the Global Land Cover 2000 (GLC2000, Bartholomé et al. 2002, Di Gregorio and Jansen 2001) provided this information. Within this study, two different land cover maps were used. For the model comparison (chapter 5) a MODIS land cover classification was used (cf. section 4.1.2.6). For the derivation of 9-year time-series for Kazakhstan (chapter 6), a regional land cover and land use classification was chosen (Klein et al. 2012, see section 4.1.3).

Further input data for BETHY/DLR comprise soil types from the FAO soil map (FAO et al. 2009) and topography from the latest version of the NOAA/NGDC GTOPO30 product (USGS 1996). For BETHY/DLR, the input data are made available as global datasets. Detailed information on the available input data for this study is provided in chapter 4.

2.2.3 Description of the Model RBM

The Regional Biomass Model (RBM) was developed by Richters (2005a) for derivation of NPP on a regional scale in a semi-arid research area in north-western Namibia. It was developed for use with MODIS data on a 10-day interval with 1 km spatial resolution. It is based on the model CASA (Carnegie-Ames-Stanford Approach, Potter et al. 1993, Field et al. 1995), which uses a combination of a remote sensing based and a process oriented approach (Richters 2005a).

RBM is a light use efficiency model, also called production efficiency model. The parameterization of the photosynthesis is based on the theory of Monteith (1972). This basic physical theory assumes a linear relationship between absorbed photosynthetically active radiation and plant production. Absorbed photosynthetically active radiation can be described as the product of FPAR and incoming photosynthetically active radiation (PAR, e.g. Running et al. 2000). The product of FPAR and PAR is scaled by the biophysical conversion factor ε_{eff}, the so-called light use efficiency (LUE). The LUE has to be specifically adapted to different vegetation types and study regions (Monteith 1972).

$$NPP = \varepsilon_{eff} \cdot FPAR \cdot PAR \tag{2-6}$$

PAR describes the part of incoming solar radiation that can be used for photosynthesis by plants. It is one of three central parameters for calculation of NPP. Within the RBM, the PAR (at location *x* and time *t*) is calculated from incoming solar radiation *InSol* that depends on the potential incoming solar radiation, latitude *LAT* of the study area, relief (*Slope* and *Aspect*), and the day of the year *DOY*. It is further determined by the atmospheric transmission *q*, which can be calculated from mean cloud cover, and scaled by the part *k* of radiation that can be used for photosynthesis. Equation 2-7 summarizes the parameters needed for PAR calculation (Richters 2005a, Dokupil 2008). The routine for derivation of InSol was adopted from Swift (1976) and is described in detail by Richters (2005a).

$$PAR_{x,t} = InSol(LAT, Slope, Aspect, DOY)_{x,t} \cdot q_{x,t} \cdot k \tag{2-7}$$

The efficient biophysical conversion factor ε_{eff} is according to Richters (2005a) calculated from the maximum LUE ε_{max} and the two scaling factors temperature stress T_ε and water stress W_ε.

$$\varepsilon_{eff}(x,t) = T_\varepsilon(x,t) \cdot W_\varepsilon(x,t) \cdot \varepsilon_{max}(x,t) \tag{2-8}$$

The maximum LUE ε_{max} integrates the effects of relief (slope, aspect, and elevation), soil (texture and nutrient), and vegetation cover. It is calculated annually (Richters 2005a). The needed vegetation cover information describes the treated biome regarding the different coverage of grass, tree, and bare soil. This information is provided by MODIS vegetation continuous fields (VCF) fractions.

T_ε and W_ε reflect the actual climatic conditions and are thus calculated for each modelled time step. Temperature stress is derived from mean daily temperature *T* as given in equation 2-9. Water stress is calculated from actual evapotranspiration *AET* and potential evapotranspiration *PET* as given in equation 2-10.

$$T_\varepsilon(x,t) = 0.8 + 0.02 \cdot T(x,t) - 0.0005 \cdot (T(x,t))^2 \tag{2-9}$$

$$W_\varepsilon(x,t) = 0.5 + 0.5 \cdot \frac{AET(x,t)}{PET(x,t)} \quad (2\text{-}10)$$

The potential evapotranspiration is derived from an evaporation model based on temperature, emissivity, albedo, and potential insolation using the approach by Priestley and Taylor (1972). The following equation is applied for PET calculation in the RBM, with advective parameter α_a, saturation vapour pressure Δ, the psychrometric constant γ, net irradiance R_n and soil heat flux G. Further descriptions of the formulations for PET calculation within the RBM can be found in Richters (2005a).

$$PET = \alpha_a \frac{\Delta}{\Delta + \gamma}(R_n - G) \quad (2\text{-}11)$$

AET is not calculated within the RBM. For this parameter, MODIS water vapour data are used, which present the amount of water content in the atmosphere (King et al. 1992, Gao and Kaufman 1998). According to Richters (2005a), a lot of climatologic studies in the semi-arid tropics, for which the model was designed, showed that rainfall events are primarily caused by convective processes and not by cyclones. Thus, the measured water vapour column of each raster cell from MODIS is used as estimate for AET (Richters 2005a). Figure 2-4 shows a flowchart of NPP calculation within the RBM.

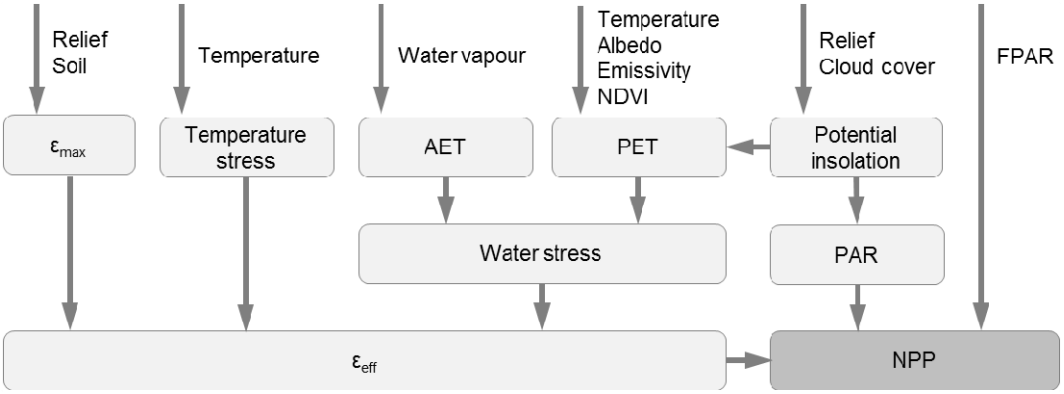

Figure 2-4: Flowchart of NPP calculation within the RBM (Source: Richters 2005b).

RBM was applied by Richters (2005a, 2005b) to calculate NPP in Namibia based on MODIS 10-day composites. Comparison to field data showed a linear correlation (Richters 2005b). The model was modified by Machwitz (2010) to be used with 232 m spatial resolution data on a 16-day basis (model was renamed to RBM+). The more detailed scale allowed consideration of the fine scattered landscape of West Africa (Machwitz et al. 2009). Instead of estimating FPAR on basis of the NDVI (normalized differenced vegetation index), a downscaled MODIS-FPAR product was used as input parameter (Machwitz 2010). RBM+ was applied by Machwitz (2010) to analyse carbon stocks in West Africa. A sensitivity analysis showed that model results are most strongly influenced by FPAR, vegetation fractions, PAR, potential, and actual evapotranspiration (in order of decreasing influence) (Machwitz 2010). Without special preprocessing, the spatial and temporal resolutions of the necessary MODIS parameters limit the modelled NPP to a 16-day temporal and a ~926.6 spatial resolution with the current version of the RBM.

Input Data for the RBM

The RBM is based on parameters that can almost entirely be derived by remote sensing. For the applied version of the model the following data are needed on a 16-day interval: albedo, cloud cover, emissivity, FPAR, land surface temperature, and water vapour (Frey et al. 2012, Justice et al. 1998, Leinenkugel et al. submitted, Shuai et al. 2008, Wan 2008, Yang et al. 2006). These data are available as MODIS standard products at a spatial resolution of ~926.6 m or higher as 16-day or 8-day composites. Additional information that is fed into the model as annual or constant data comprise a MODIS VCF dataset with information on bare, herbaceous, and woody vegetation cover (DeFries et al. 2000, Hansen et al. 2002b, Hansen et al. 2003), soil data from the Harmonized World Soil Database (HWSD, FAO et al. 2009), and a digital elevation model (DEM) from the SRTM mission (Rabus et al. 2003). The used input data for this study are described in chapter 4.

3 Study Areas

3.1 Selection and Geographic Location of Study Areas

The Republic of Kazakhstan is situated in the centre of the Eurasian continent. The country is landlocked, approximately equidistant from the Atlantic and Pacific Oceans. Kazakhstan is the world's ninth largest country with an area of 2.72 million km². It spreads between 40°–56°N and 45°–88°E reaching from the Caspian Sea and Volga plains in the West to the Altay Mountains in the East. To the South and South-east the country is bordered by the Tian Shan Mountains. To the North the geologically diverse steppe, with its gentle hilly plains, plateaus, and flat low plains, reaches the Western Siberian lowland (ADB 2010). The northern border is shared with Russia. To the South, Kazakhstan borders onto Turkmenistan, Uzbekistan, Kyrgyzstan and China (cf. figure 3-1). The widest distance east-to-west is approximately 3,000 kilometres and the longest distance north-to-south is 1,500 kilometres.

Figure 3-1: Overview map of Kazakhstan.

For the selection of possible study areas within Kazakhstan several criteria were defined that comprise both thematic and practical restrictions. Thematic restrictions concern the suitability for the envisaged investigations of the study, i.e. the areas should be covered by natural vegetation and not be primarily managed land. The parameters applied to exclude unsuitable areas were fractional vegetation cover in combination with land cover and land-use information. Practical restrictions concern the suitability for field data collection, i.e. topographic and political restrictions. The parameters height and slope as well as the extent of nature reserves and restricted or risky accessible areas, including border areas, were chosen to further exclude these areas. The criteria applied for the individual parameters are listed in table 3-1.

Table 3-1: Parameters and criteria used for the exclusion of areas not suitable for the envisaged investigation.

Parameter	Exclusion criteria (values not excepted)	Data source
Height	> 3000 m	SRTM, 2000 (Rabus et al. 2003)
Slope	> 10° (22%)	SRTM, 2000 (Rabus et al. 2003)
Bare cover	< 100%	MODIS VCF 2001 (Hansen et al. 2003)
Herbaceous cover	> 0%	MODIS VCF 2001 (Hansen et al. 2003)
Irrigation area	Irrigated area	Siebert et al. 2007
Land cover	Cropland, Forest, Regularly flooded areas, Salt hardpans, Water, Snow/ice, Artificial areas	GLOBCOVER 2006 (Bicheron et al. 2006)
Nature reserve	Nature Reserve	CAIAG
Border areas	Five kilometres buffer area	CAIAG
Restricted or risky accessible areas	Baikonur, Nuclear test sites, Mining areas, Oil/gas fields	UNEP/GRID-Arendal 2005, 2007

Figure 3-2 shows the result of the GIS analysis. The Altai Mountains in the very East of Kazakhstan, as well as some areas within the Tian Shan mountains along the south-eastern border of Kazakhstan are not suitable for the study due to mountainous topography, partly forest, and permanent snow/ice cover.

Large parts in the South-West, especially the major parts of the Ustyurt Plateau and the Kyzylkum Desert, also have to be excluded as the vegetation cover is too low due to very dry conditions, and thus these areas are not suitable for biomass estimation studies. Agricultural areas are dominant in the north-central part of Kazakhstan, where rain-fed agriculture is the primary land-use. Irrigation areas are common along the rivers, such as the Syr-Darya in South Kazakhstan, and also in the pre-mountainous plains in South-east Kazakhstan. These agricultural areas are not suitable for the envisaged investigation. Some nature reserves exist in Kazakhstan (e.g. Korgalzhyn Nature Reserve around Lake Tengiz), where field data collection is restricted. The Baikonur rocket launching site is also not accessible. Further restricted sites include nuclear testing sites of which the most widely known is Semipalatinsk-Kurchatov located south-east of Semey (Semipalatinsk). Mining and oil and gas field areas are also excluded. These occur mainly in the low-lying areas of Kazakhstan east of the Caspian Sea.

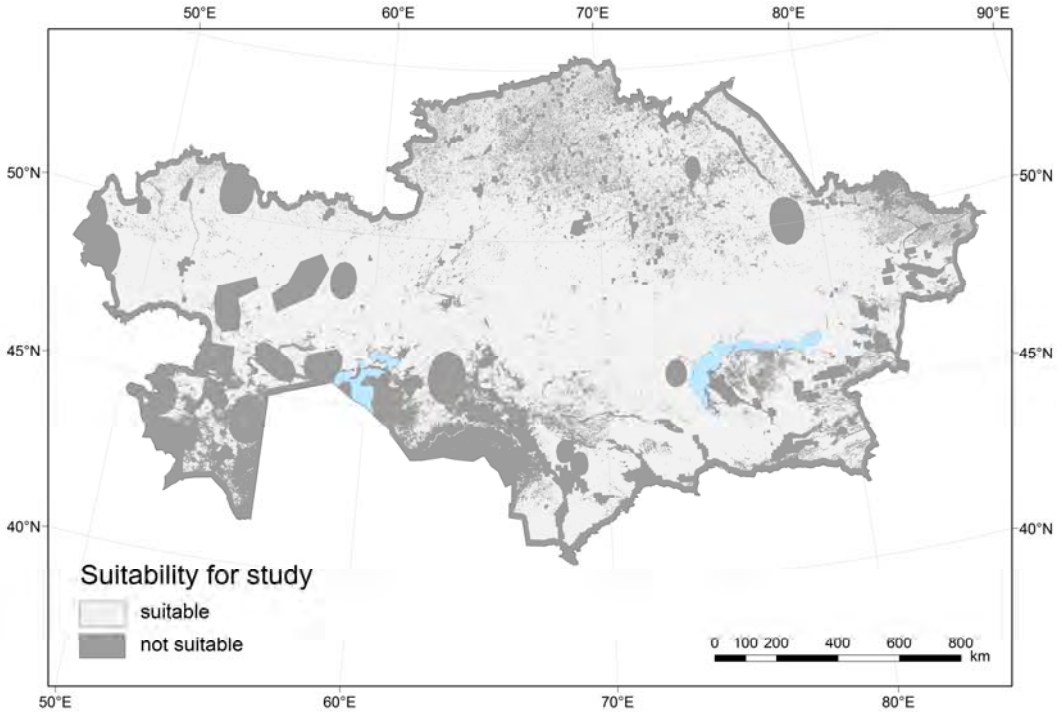

Figure 3-2: Map showing the result of the GIS analysis for Kazakhstan. The light grey regions of Kazakhstan are suitable study areas. Regions with dark grey colour are not suitable as at least one of the exclusion criteria applies.

The remaining area within Kazakhstan, which is suitable for the study according to the applied criteria, covers an area of about 2,160,600 km² (cf. Figure 3-2). This is 79 % of the area of Kazakhstan and corresponds to 6 times the area of Germany. The largest contiguous part of the suitable area spreads within a strip running from West to East over Central Kazakhstan.

Figure 3-3 shows the expansion of semi-arid regions as given in three different maps based on distinct underlying classification systems. In the widely used Köppen-Geiger climate classification system the semi-arid climates are divided into two variations, hot semi-arid climate (BSh) and cold semi-arid climate (BSk). The classification is based on average annual and monthly temperatures, precipitation and the seasonality of precipitation (McKnight and Hess 2000). The semi-arid steppe climate is assigned when the mean annual precipitation is within a certain range depending on mean annual temperature and the season of precipitation. The hot and cold steppe climates are separated by a mean annual temperature of ≥18°C vs. <18°C (Peel et al. 2007, Kottek et al. 2006). In Kazakhstan a cold semi-arid climate is present. The classification after Lauer-Frankenberg applies different criteria. It assigns semi-arid climates in warm temperate to tropical conditions if the number of humid months within a year is between three and five.

As can be seen in figure 3-3 the areas classified as semi-arid in the three classification schemes largely overlap. Areas that are semi-arid in at least two classifications spread from West Kazakhstan to the East and cover large parts of Central Kazakhstan. From East Kazakhstan the semi-arid climate spreads to the South along a small strip at the northern edge of the mountain ranges through South Kazakhstan.

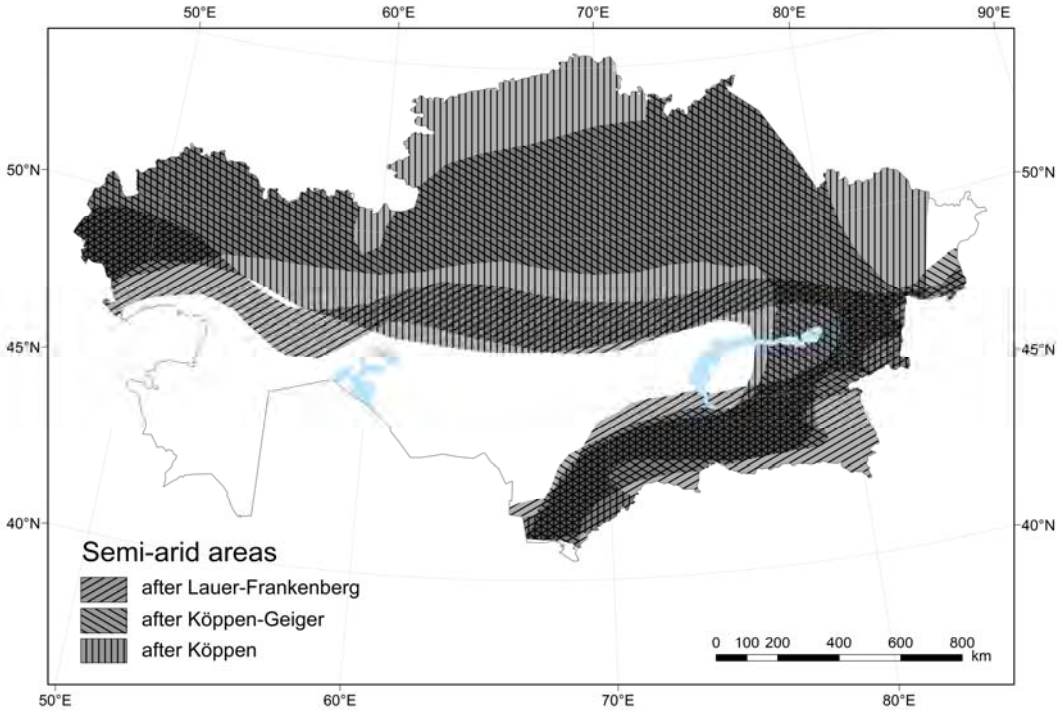

Figure 3-3: Expansion of semi-arid areas in Kazakhstan as presented in three different maps with distinct underlying classification systems: after Lauer-Frankenberg (source: Diercke 1992, modified), after Köppen-Geiger (source: Strahler and Strahler 1984, modified), and after Köppen (source: Philip's 2003, modified).

The result of the GIS-analysis and the map of expansion of semi-arid regions in Kazakhstan were combined and three study areas were chosen and classified as suitable for the study. These are mainly characterised by semi-arid climate and covered by predominantly natural vegetation. The location of the three study areas is shown in figure 3-4.

The first study area lies in Central Kazakhstan in the Karaganda oblast between the cities of Balkhash and Karaganda, between 46°–50°N and 72°–76°E. The second study area is situated in South Kazakhstan in the Zhambyl oblast. Geographically, the region is limited between 43°–45°N and 72°–75°E. A third study area was defined in West Kazakhstan. This study area spreads along the Ural River between the cities of Atyrau, at the northern shore of the Caspian Sea, and Chapaev near Kazakhstan's northern border to Russia. This study area belongs to the oblasts West Kazakhstan and Atyrau and spreads between 47°–51°N and 50°–53°E.

The most important characteristics of Kazakhstan in general and the three study areas in particular are described in the following sections. These sections cover the following topics: geologic, geomorphologic and hydrographic characteristics, climatic characteristics, distribution of main soils, and distribution of natural vegetation cover. A brief description of socio-economic characteristics is also provided.

Further information about the study areas and test sites is provided in the appendices. Appendix B shows a map of vegetation communities' distribution produced by Volkova et al. (2010) for the study areas, appendix C summarizes major information on the individual test sites, and appendix D provides photo tables for the test sites.

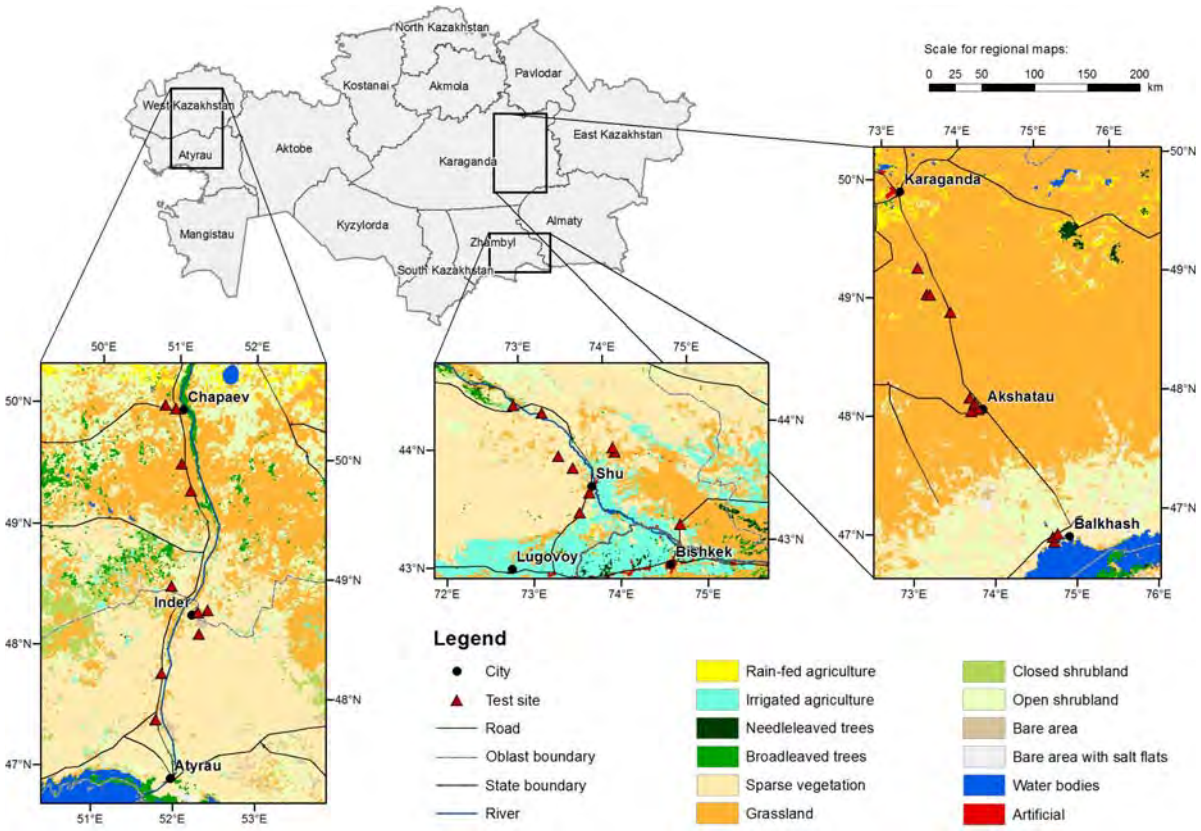

Figure 3-4: Map showing the location of the three study areas within Kazakhstan. The individual test sites are marked with red triangle signatures. The Central Asia land cover and land use map (Klein et al. 2012) illustrates the land cover in 2009.

3.2 Geologic and Geomorphologic Characteristics

More than 80% of the area of Kazakhstan is flat land with heights below 500 m above sea level. In the South-East of the country important mountain ranges are the Tian Shan, the Dzungarian Alatau, and the Altay. Remains of the Kazakh Uplands are located south-west of Karaganda in Central Kazakhstan. A map that shows the topography of Kazakhstan is provided in figure 3-1. The lowest point of the country is at the bottom of the Karagiye depression near the Caspian Sea at 132 m BSL. The highest point is Pik Khan-Tengri in the Tien Shan at 7010 m. Several large rivers cross the country, of which the Syr-Darya and the Ural River are most prominent. Other major rivers are the Shu, Ili, Yrtysh, Ishim, Emba, Tobol and Nura. Disregarding the Caspian Sea, the largest water bodies are the remaining parts of the Aral Sea and lakes Balkhash, Alakol, Tengiz and Zaisan (ADB 2010). In the following, regional characteristics of the three study areas are summarized.

Central Kazakhstan

The largest part of Central Kazakhstan is a remnant plateau of a former mountain range that has been eroded. In the Caledonian orogeny (about 505 million years ago, late Cambrian) as well as in the Variscan orogeny (approx. 380 to 280 million years ago) intensive folding processes took place (Berg 1959). Since the end of the Palaeozoic (Permian) to the beginning of the Tertiary these areas were emerging land. During this long period the mountain ranges have been continuously eroded (Berg 1959). Only low spurs and isolated inselbergs still remain. The products of weathering accumulate around the mountains as they are not carried away by water.

The denuded bare rocks are of granites, Palaeozoic sandstones, conglomerates, clay shales, limestone, and volcanic lava. In the Oligocene (about 34 million to 23 million years ago) the area was covered by an ocean. Former valleys were filled by calcareous muds and clays of a Tertiary sea (Walter and Breckle 1989), which are still deposited horizontally (Berg 1959).

The geomorphology of the remnant landscape is complicated (Walter and Breckle 1989). The northern and central part of the study area in Central Kazakhstan is nowadays characterised by a plateau of rolling upland. A landscape made up of several small hills spreads over the whole study area, from Karaganda to Lake Balkhash (Berg 1959). The hills and ridges that stick out of the rubble generally reach heights of not more than 100 m relative to the surroundings. They are made up of primary rocks, such as quarcite, granite, porphoryte, or diorite (Berg 1959). In the granite mountains north of Lake Balkhash also single higher mountains remain that reach altitudes up to 1500 m (Walter and Breckle 1989). The mountains near Karkaralinsk in the very North-east of the Central Kazakhstan study area are one example of the remaining solitary higher mountain ranges (Berg 1959).

In the Carboniferous era large anthracite coal deposits formed, which are now of great economical importance for the region. The mines around Karaganda form one of the biggest coal mining areas of Kazakhstan. Near the northern shore of Lake Balkhash, in Kounradski, rich copper deposits are mined, which are embedded in extrusive rocks of quartz diorite porphyry (Berg 1959).

Large rivers are not present in the study area. Rivers in the very northern part of the study area belong partly to the Yrtysh River catchment; some end in depressions with no outlet (Berg 1959). In the South of the study area Lake Balkhash is situated, around which the lowest terrain heights, of about 340 m, occur. Lake Balkhash has a length of about 600 km, but is shallow with a mean depth of only 6 m. It has no outflow. The western part of the lake, where the Ili River discharges, contains fresh water, while the eastern part is slightly salty (Berg 1959).

West Kazakhstan

The study area in West Kazakhstan is situated in the Caspian Lowland and has been largely influenced by the Caspian Sea. The Caspian Sea is a huge salt lake with an area of about 380,000 km² of water. It is the largest closed water body on Earth (e.g. Bayramov and Mamedov 2008).

The sea level of the Caspian Sea is nowadays around 28 m below sea level, but in earlier periods it has been both several metres higher and lower. The expansion of the Caspian Sea in the Quaternary can be reconstructed from different deposit layers. The lower khazaric deposits reach till heights about 0 m ASL. The higher chwalynic deposits, which result from the latest transgression of the Caspian Sea, reach up to 50 m ASL, i.e. 78 m above the current Caspian Sea level. On the northern shore of the Caspian Sea several geologically young sea level rises can be proved, which occurred after the chwalynic transgression (Berg 1959).

As a result of the former Caspian Sea level rises, the whole study area in West Kazakhstan is very flat with a high groundwater table. The terrain is characterized by a mosaic of slightly raised areas and very shallow depressions. The southern part of the study area lies below sea level. Terrain heights reach between –30 m in the South and 100 m in the North-east. Undrained salt lakes, such as Lake Inder, are common. At the banks of Lake Inder Permian deposits with high levels of gypsum and rock salt reach the surface and are the source of the high salinity level in the lake. In summer the lake bed is dry and covered by a salty crust (Berg 1959).

The Ural River, which forms the border between Europe and Asia, runs through the study area from North to South. Along with the Volga River it is one of the major rivers feeding the

Caspian Sea. Water level is highest in April and May when the spring floods widen the river to more than 10 km. The discharge gets lower in summer, autumn and winter.

South Kazakhstan

The area north of the Shu River belongs to the Betpak-Dala, the south-western part of the Mujunkum desert. The Betpak-Dala plateau is about 130 m high and consists of horizontal layers of clay and sand from the Tertiary. In the inner Betpak-Dala there are no rivers, but ground water is not very deep (Berg 1959).

In the desert zone, e.g. the Mujunkum south of the Shu River, Takyrs are common. These are flat clay areas that are formed by aggradation, i.e. the deposition of clay materials by water. They dry out in summer and are typically not covered by vegetation (Berg 1959).

The southernmost part of the study area can be described as slightly oblique mountain foreland. It is rich of Aeolian silt deposits on which very fertile light grey soils formed.

The Shu River, which flows through the study area, has largely influenced topography and attracted human settlements and agriculture. It is formed in the Naryn Province in the Tian Shan mountains in Kyrgyzstan. Much of the rivers' water is diverted to irrigate agricultural areas on the fertile black soils of the Shu Valley. Moreover, the Shu River looses water by evaporation and infiltration. Thus, in summer the river becomes small and disappears in the Mujunkum sands in Southern Kazakhstan (Berg 1959).

3.3 Climatic Characteristics

The climate of Kazakhstan is extremely continental, due to its location in the centre of the Eurasian continent. High summer temperatures and freezing winters are typical for most parts of the country. Mean January and July temperature for Kazakhstan are shown in figure 3-5. Spring starts first in the South and takes up to two months to reach the North of the country.

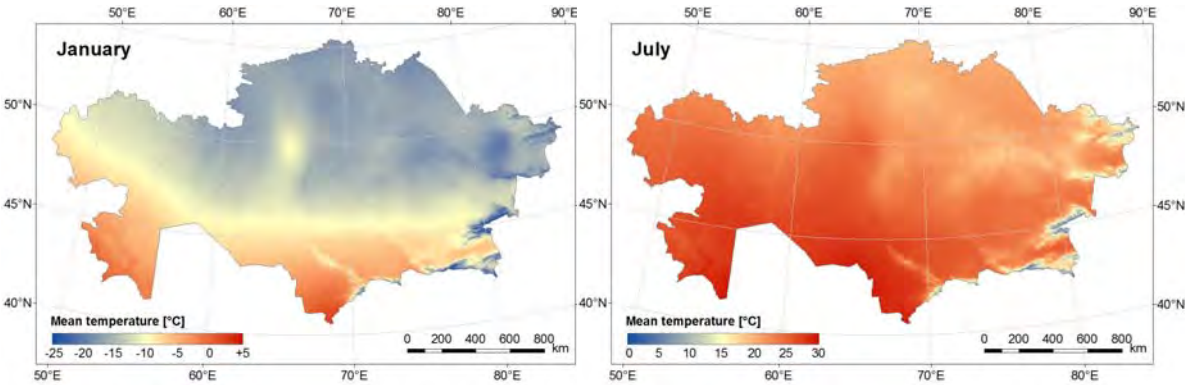

Figure 3-5: Mean January and July surface temperatures for the period 1950-2000. Temperature data source: Hijmans et al. (2005), ©WorldClim, v1.4 (http://www.worldclim.org).

Precipitation shows an irregular distribution for different regions of the country. Annual precipitation ranges between 100 and 400 mm, except for the mountainous regions in the South and East, where precipitation reaches up to 1000 mm per year. Figure 3-6 shows mean seasonal precipitation for Kazakhstan. In the following, the climatic characteristics are described in more detail for the three study areas in Central, West and South Kazakhstan.

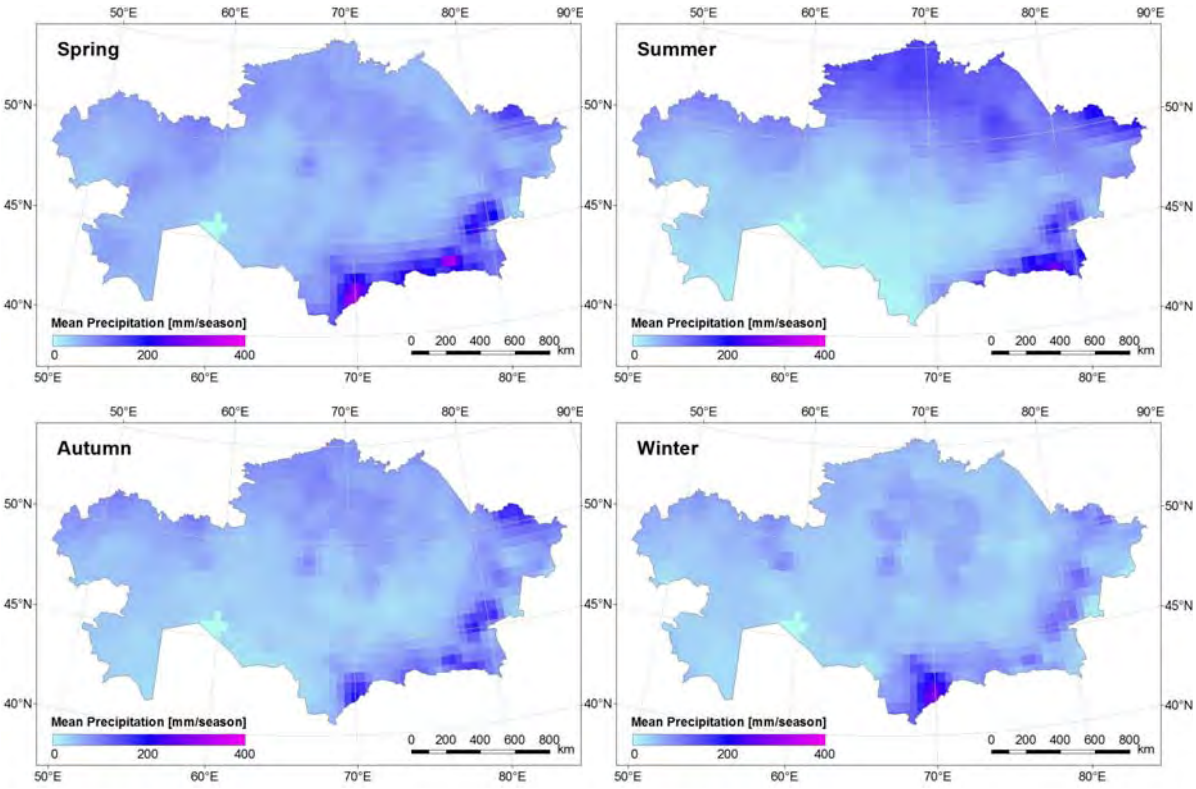

Figure 3-6: Mean seasonal precipitation for the period 1990-2009. Precipitation data source: Rudolf et al. (2010), Rudolf and Schneider (2005), ©GPCC 2001 (http://gpcc.dwd.de).

Central Kazakhstan

The larger northern part of the study area in Central Kazakhstan can be characterised as steppe, while the southern part is semi-desert. The climate is semi-arid and high continental. Mean annual temperature varies in response to elevation, but generally increases from North to South from about 3.4°C (for Karaganda) to 5.8°C (for Balkhash). July average temperatures reach 20.8°C (Karaganda) to 24.4°C (Balkhash).

In the Kazakh steppes temperature maxima can reach more than 40°C in summer and minima less than –50°C in winter. Daily temperature amplitudes are also large and can reach more than 15–20°C (Berg 1959). In the southern semi-desert temperatures rise more quickly and spring is very short, if existent at all (Berg 1959).

Frosts already hinder plant development in late autumn and early spring. Temperature minima in winter usually exceed –20°C, but snowfall is not very high in steppes (Berg 1959). In cold winters with mean January temperatures of –15 to –20°C snow cover lasts from November until spring with generally not more than 20–30 cm height (e.g. Dietz et al. submitted).

Mean annual precipitation shows a gradient from about 260 mm/a in the North to 150 mm/a in the South (cf. figure 3-7). In the steppe zone a period of dryness is clearly apparent which turns into drought in late autumn. In the semi-desert zone the drought lasts throughout the growing period (Walter and Breckle 1989).

Most of the precipitation in the steppe zone falls in June (Berg 1959). Annual precipitation amounts vary largely. In the northern semi-desert the maximum of precipitation generally falls in June, while in the southern semi-desert the maximum lies in May. A second maximum of precipitation can often be observed in autumn. Monthly precipitation amounts vary largely in different years (Berg 1959).

Optimal growth conditions with favourable temperatures, long daily sunshine, and good water supply obtain for four months, from April until end of July (Walter and Breckle 1989).

At the northern edge of the steppe zone anticyclones are common from October through March. The anticyclonic winds from northern directions bring cold Arctic airmass, which leads to strong frost in the Central Kazakhstan study area. In the steppes dry winds from N, NE, or E are typical and precipitation is low. Anticyclones also prevail in summer. The weather in this period is governed by continental airmass from SW directions. Summers are warm and rather dry. End of May and June the intrusion of boreal airmass leads to heavy rain and thunderstorms.

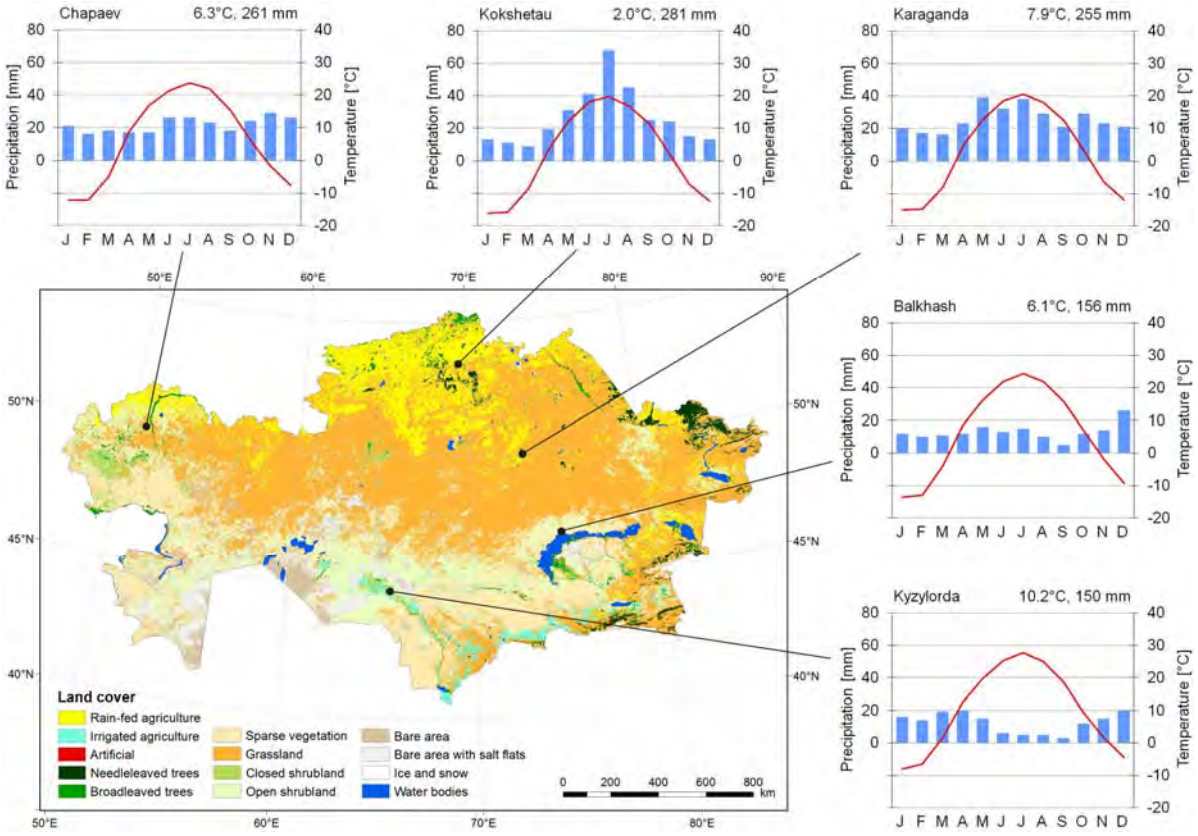

Figure 3-7: Land cover and land use map of Kazakhstan (Klein et al. 2012) and representative precipitation and temperature diagrams (extracted from Hijmans et al. 2005).

West Kazakhstan

The Caspian Lowland is arid with very cold winters. Aridity increases and rainfall decreases from North to South (Walter and Breckle 1989). The northernmost part belongs to the steppe zone, while the larger southern part can be characterized as semi-desert. The climate of the West Kazakh steppe is similar to that described for Central Kazakhstan.

The climate of the semi-deserts is more continental than in the steppe zones. Summer temperatures are higher and the mean temperature in July is typically 24–26°C with high daily amplitudes. Winters are cold with mean January temperatures around –16 to –12°C. Maximum daily high temperatures can reach 40°C in summer and minimum temperatures of –40°C are reached in winter. Temperatures rise quickly and spring is very short, if it exists at all (Berg 1959).

Precipitation in the semi-desert is also lower than in the steppe zone. It reaches 160–250 mm per year. Maximum precipitation falls in June in the northern parts, or May in the southern parts. A second maximum precipitation can often be observed in autumn. Monthly

precipitation varies largely in different years (Berg 1959). Snow cover is usually very low in the semi-deserts (Berg 1959).

The southernmost part of the study area in West Kazakhstan shows characteristics of deserts, which are described in the following section on South Kazakhstan. In the semi-deserts near the Caspian Sea easterly winds dominate in summer and autumn, at other times winds from North and West are common (Berg 1959). Similar to Central Kazakhstan the anticyclonic winds lead to heavy frosts in the West Kazakhstan study area.

South Kazakhstan

In the study area around Shu large deserts can be found. The Betpak-Dala is an arid desert having a spring or bi-seasonal rainy season with an annual precipitation of 100–150 mm. The Mujunkums climate is arid to semi-arid and usually features a bis-easonal rainy season with precipitation amounts of 170–300 mm (IPCC 1997).

Summers are very dry, cloudless, and hot. Mean July temperatures reach 26–30°C with large daily amplitudes (up to 20°C) and the soil gets very hot. Winters in the northern deserts are cold and harsh, but shorter and milder in the South (Berg 1959).

The winds in the desert are generally weak and show a typical diurnal variation with maximum speeds in the afternoon and lighter winds at night. In winters, Siberian anticyclones and westerly winds dominate. The study area around Shu that lies further south is characterised by mild winter conditions. In summer North winds are typical, only at the beginning of summer, cyclones from West and South-west are common (Berg 1959).

3.4 Soil Characteristics

Kazakhstan is relatively rich in soils. Most of the forest-steppe zone in the North grows on Chernozems, which turn to dark Kastanozem, light Kastanozem, and brown soils further South. The deserts and semi-deserts are mainly characterised by Solonchaks. A soil map of Kazakhstan, showing the main soils of the country, is presented in figure 4-12 in section 4.2.2. The following paragraphs provide a more detailed description of the soil characteristics for the three study areas in Central, West and South Kazakhstan.

Central Kazakhstan

The soils in the northern part of the study area in Central Kazakhstan are made up of dark Kastanozems. The humus content in these soils is according to Berg (1959) about 3–4.5% due to the low amount of plant substances. These areas are commonly described as southern or dry steppes. The thickness of the humus horizon varies between 55 and 80 cm. At a depth of 12–20 cm a higher calcium carbonate content is typical and at a depth of 40–140 cm the soil is compacted by calcium and magnesium carbonates, which accumulates during the process of soil formation (Berg 1959).

The southern part of the Central Kazakhstan study area shows typical characteristics of the semi-desert. The soils are very complex and consist of light Kastanozems as well as Solonetz and decalcified Kastanozems in depressions. The humus content and horizon are low due to the dry conditions and low vegetation cover. Chemical processes in the soil occur slowly, so that the soils contain large amounts of calcium and magnesium salts as well as natrium and kalium salts. Argillaceous soils are more prone to salinization than sandy soils. Moreover, changes in soil humidity strongly affect the soil and the vegetation cover. This can often lead to patchy vegetation cover (Berg 1959).

The light Kastanozem, which is typical for the semi-desert, contains natrium. The humus horizon is 30–40 cm thick, but the humus content very low (at the surface only 1–3%). The lower part of the soil profile contains dissolved salts and is similar to Solonchak. Below 50 cm the carbonate content is very high and at a depth of 1.80 m usually gypsum is common (Berg 1959). In areas with high salt content Solonetz and Solonchak occur (Berg 1959). These soil types are more common in the West Kazakhstan study area and thus described in the following section. The distribution of different soil types for the three study areas is also shown in figure 3-8.

West Kazakhstan

The soils in the north-eastern part of the study area in West Kazakhstan are made up of dark Kastanozems, similar to those described in the section about Central Kazakhstan. In the central part characteristic soils of the semi-desert are typical. These have been described above for Central Kazakhstan.

The soils of the Caspian Depression, to which belongs the West Kazakhstan study area, also show special characteristics. They can in general be characterised by saliferous clay areas, several Solonchaks, and large sand areas (Berg 1959). In the northern part of the Caspian Lowland mother soils are heavy loams and in the southern part light sands. These were deposited by the Ural and Volga rivers.

In the northern part of the study area the variety of slightly raised areas and shallow depressions leads to a mosaic of soil types. In the shallow depressions snow accumulates and moistens the soil. Chernozem-like soil profiles develop. On the raised ground solonetz-like soils develop (Walter and Breckle 1989).

The semi-desert contains several salt lakes, Solonchak and Solonetz (black alkali soil) areas. Solonchaks occur when the ground water reaches the land surface, evaporates and deposits salt on the surface. They are thus common near lakes and in valleys (Berg 1959). Solonetz, however, develops when ground water can not rise, but salt is moved downwards (percolation) and contains a nitric horizon in the upper 100 cm. Solonetz dries out in summer, but puddles form in spring after snow melt and rainfalls. Solonetz is a characteristic soil of semi-deserts and present in different parts of the West Kazakhstan study area.

In the southern part of the study area, which lies below sea level, the zonal soil type is Burozem (arid brown earth), but sand cover is common. The sands derive from post-Tertiary sea deposits and alluvial deposits from the Ural River. Heavy clays beneath the sand lead to a high groundwater table. The psammobiomes of this area are favourable for the growth of plants (Walter and Breckle 1989). The area west of the Ural River is also influenced by salt, which originates from the salt deposits in the region, the transgression deposits of the Caspian Sea, together with salt that has been transported by winds from the Caspian Sea.

South Kazakhstan

Desert soils are typical for the study area in South Kazakhstan. They are poorly developed due to the low levels of water and vegetation for soil development. In contrast to the steppe soils, desert soils have only low humus content which results in a light, grey colour (Berg 1959).

Typical soils for this study area are especially calcisol and gleysol. Both soil types occur in dry regions and are according to the World Reference Base for Soil Resources (WRB) formed by accumulation of less soluble salts or non-saline substances. Calcisols are widespread in arid and semi-arid regions and common in highly calcareous parent materials (IUSS Working Group WRB 2006) and accumulated calcium carbonate.

Gleysols are wetland soils that were drained or saturated with ground water long enough to develop a gleyic colour pattern. They accumulated gypsum and typically occur in depression areas with shallow ground water (IUSS Working Group WRB 2006).

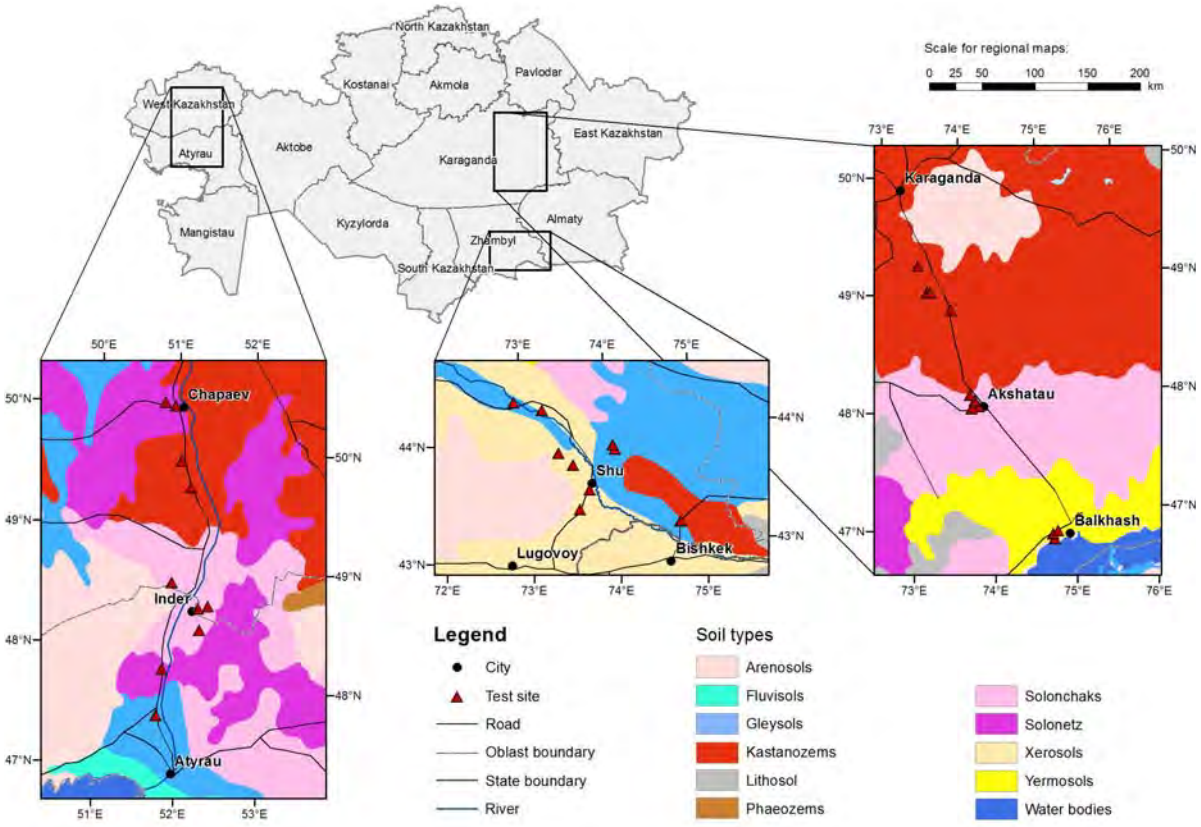

Figure 3-8: Soil types within the three study areas in Kazakhstan. Soil map data source: HWSD (FAO et al. 2009).

3.5 Characteristics of Natural Vegetation

The vegetation zones of Kazakhstan show a pronounced north-to-south distribution. A small strip in the North belongs to the forest steppe. Further south follow large areas of steppe and semi-desert, which can be divided in northern steppe, dry steppe and northern semi-desert. The South of Kazakhstan belongs mainly to the southern semi-desert zone. In the mountainous areas of the Altai and Tian Shan, montane deserts and steppes developed (cf. figure 3-9). A more detailed description of the vegetation for the three study areas is provided in the following sections. Addionally, figure B-1 (appendix) provides a detailed map of plant communities' distribution within the study areas.

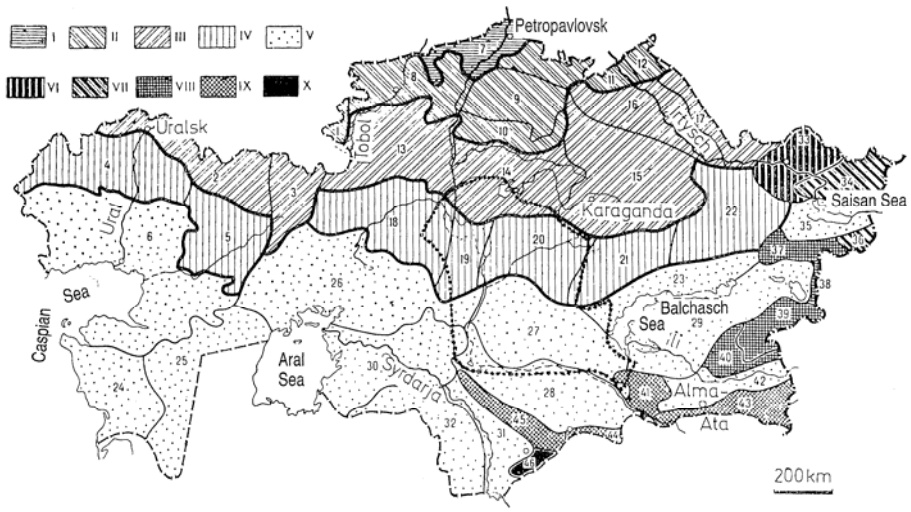

Figure 3-9: Vegetation zones of Kazakhstan. I: forest steppe, II: steppe, III: dry steppe, IV: semi-desert (desert-steppe), V: desert (southern semi-desert), VI-X: montane deserts and steppes. Numbers 1 to 46 refer to different rayons which correspond to biomes (Source: Walter and Breckle 1989).

Central Kazakhstan

The northern part of the study area in Central Kazakhstan belongs to the southern or dry steppe. The term 'steppe' refers to treeless grasslands of temperate, semi-arid climatic zones (Walter and Breckle 1989). In these zones grasses and woody plants do not coexist. The grasses of the temperate zone develop a dense root system that prevents seedlings of deciduous trees from establishing themselves. In the wet, northern steppe perennial herbs are common, which however, occur only sporadically in the drier southern steppe (Walter and Breckle 1989). Low shrubs can be found in stony areas or on earth mounds thrown up by rodents. Here they were protected from root competition with grasses. Amongst these low shrubs are *Amygdalus nana, Spiraea hypericifoliy* and *Caragana frutex* (Walter and Breckle 1989).

The typical vegetation for the southern steppe or dry steppe is a fescue – feather grass steppe. The feather grasses, such as *Stipa lessingiana* or *Stipa capillata* are adapted to the dry conditions (Berg 1959). In addition to the grass cover shrubs, such as *Caragana frutex,* are characteristic for the steppe. They usually occur on rolling terrain. The shrubs assist snow accumulation and infiltration of moisture into the soil (Berg 1959). In locally defined areas, on Solonetz, sceletal soils and calcareous soils, semi-desert and desert vegetation reaches into the steppe zone (Berg 1959).

The major central part of the study area in Central Kazakhstan belongs to the semi-desert zone. While the ground in the steppe is usually covered completely by vegetation, the semi-desert vegetation is not closed, however more than 50% of the ground is covered and the remained is bare soil. The vegetation is a combination of steppe grasses, such as fescue (*Festuca*) and feather grass (*Stipa*). Semi-shrubs such as *Artemisia,* grow well under dry conditions (Berg 1959).

The semi-desert vegetation can be characterised as Artemisia-steppe. In the northern part grasses, such as *Festuca* and *Stipa* species, dominate, while further south *Artemisia* is dominant. In the southernmost parts of the semi-deserts salt plants are of importance (Berg 1959). The vegetation cover is not closed and plants do not grow high. However, they have a big root system that allows for optimal use of soil moisture. Ephemeral plants that develop in spring and wither quickly are also typical (Berg 1959). On sandy soils steppe grasses grow further south,

while loamy soils are favoured habitats for desert plants. If the soils contain more salt more salt plants occur (Berg 1959).

In the most southern part of the Central Kazakhstan study area grasses are rare and semi-desert is spread around Lake Balkhash. On stony ground *Salsola arbusculiformis, Artemisia, Ferula,* and *Caragana* species are common. In a west-eastern strip north of Lake Balkhash *Salsola arbusculiformisis* becomes the predominant vegetation cover.

The distribution of different plant communities and species in the study areas is shown in figure B-1 (appendix). The land cover gradually turns from steppe vegetation in the northern part to semi desert vegetation in the southern part of the Central Kazakhstan study area. The northern part is covered by fescue – feather grass steppes with dominant species from the genera *Stipa* and *Festuca*. In the northern central part steppes with shrubs from genera *Caragana* are present. These turn into shrub – forb – bunch grass steppes. In the central part vegetation cover changes between sagebrush – feather grass steppes, shrub – forb – bunch grass communities and forb – sagebrush – feather grass steppes with pea-shrubs. The southern part of the study area is dryer and the vegetation gradually turns into open shrub land with dwarf shrubs. North of Lake Balkhash complex grass – black *Salsola* with giant fennel communities are dominant. They alternate with feather grass – sagebrush and grass – black *Salsola* communities (Volkova et al. 2010).

West Kazakhstan

The vegetation in the north-eastern part of the study area in West Kazakhstan belongs to the southern or dry steppe. It is similar to the northern part of Central Kazakhstan. The Caspian lowland belongs to the semi-desert zone. This runs across northern Asia as a strip between the steppes in the north and the deserts in the south (Walter and Breckle 1989). Its vegetation is similar to the semi-desert vegetation described for Central Kazakhstan.

However, in addition to the zonal vegetation, specific land characteristics in West Kazakhstan lead to the formation of a special vegetation distribution. In the generally flat northern part of the study area the mosaic of slightly raised areas and shallow depressions has led to a zonation of the vegetation (Walter and Breckle 1989). In the shallow depressions with chernozem-like soils a typical herb-poor grass steppe vegetation develops with a ground cover of 75–90% (Walter and Breckle 1989). Typical species are *Festuca sulcata, Stipa lessingiana* and *St. capillata*, combined with herbs such as *Medicago romanica, Galium ruthenicum, Galium villosa,* and *Phlomis pungens.*

On the raised ground with solonetz-like soil, the vegetation is typical for deserts. Ground cover reaches only 20–45%, the plants are lower than in the depressions and mean annual production is lower (Walter and Breckle 1989). Spring ephemerals are typical, especially *Poa bulbosa.* Common perennial species are *Artemisia pauciflora* (halophyte), *Kochia prostrata* and *Camphorosma monspeliacum* (chenopodiaceae) (Walter and Breckle 1989). Overgrazing in the semi-desert areas leads to a reduction of steppe grasses and *Artemisia* species spread (Berg 1959).

In the southern part of the study area psammobiomes (sandy soils) are favourable for growth of plants (Walter and Breckle 1989). Ephemerals develop in spring. *Artemisia lercheana* is the dominant perennial species. Grasses such as *Agropyron sibiricum, A. ramosum, A. cristatum, Festuca sulcata* and *Koeleria glauca* are also common (Walter and Breckle 1989). In the northern desert zone, i.e. in the most southern part of the West Kazakhstan study area, *Anabasis salsa* is very common (Berg 1959). The sands were originally completely covered by plants, but increased settlement, with overgrazing and cultivation led to the development of large dune areas by the early 1870's (Walter and Breckle 1989).

The North-South distribution of vegetation zones can clearly be seen from figure B-1 (appendix). The vegetation communities observed are similar to those in Central Kazakhstan, but much more homogeneous. In the most northern part bunch grass steppes in combine with sagebrush communities form the zonal vegetation. South of the town Chapaev combinations of sagebrush – wheat grass – bunch grass, black sagebrush, and locally orach communities are common. Further South this turns into grass – sandy sagebrush and psammophytic shrub communities and east of the Ural River into grass – sagebrush and *Anabasis aphylla* – sagebrush communities. Close to the valley of the Ural River complex communities of *Anabasis salsa* and sagebrush communities as well as complexes of bulbous blue grass – sagebrush, black sagebrush and *Anabasis salsa* communities are common. Within the desert zone local patches of *Halimone verrucifera*, annual saltwort – *Halocnemum strobilaceum* and orach communities can be observed. Within a small strip along the Ural River itself reed grass, shrub and meadow communities, especially halophytic meadows, as well as shrub – willow and poplar forests and meadows (Volkova et al. 2010) have become established.

South Kazakhstan

The desert vegetation does not usually form a closed cover. Bare soil covers more than half of the ground. This is due to low soil moisture, so the plants develop bigger root systems. Only in spring, when ephemerals develop, may the ground be covered completely. The ephemeral plants die in spring and are replaced by Xerophytes, *Artemisia,* along with salt plants (Berg 1959).

The northern desert with the typical grey soil is the transition zone to the semi-deserts. As the very salty gypsum layer is quite high, plants that have adapted to this salinization are common in this area (Berg 1959). *Salsola arbuscula* and *Anabasis salsa* are dominant. The former is a salt shrub that grows 30–50 cm high. In the Betpak-Dala it is replaced by *Salsola laricifolia. Anabasis salsa* is a semi-shrub of 10–15 cm height. *Nanophyton erinaceum* and *Artemisia* also occur in this zone (Berg 1959). *Artemisia* bushes grow 30–50 cm high and on 1 m² 5 to 10 plants may grow. In depressions the shrub *Caragana grandiflora* is common, which can grow up to 1 m height.

Ephemerals are rare, because the maximum precipitation falls quite late – in the second half of spring – and summer heat follows quickly. The distribution of species and communities is influenced by soil and relief and often varies on small scale.

The Mujunkum, south of the Shu River, has many similarities with the southern dune areas. The typical grass is *Aristidy pennata* and the shrub *Calligonum* is also characteristic for these sandy areas, as well as *Agropyrum sibiricum, Stipa* species, and *Artemisia* (Berg 1959).

A further plant growing in the southern part of the study area is Saxaul, of which two species occur: White Saxaul (*Haloxylon persicum* or *acutifolium*) grows on sand and Black Saxaul (*Haloxylon aphyllum*) grows on Solonchak. Both varieties lose their leaves to reduce evaporation (Berg 1959). Thus they alter the uppermost layer of the soil by depositing salt and ash materials. Especially in the Mujunkum south of the Shu River, Black Saxaul covers large areas (Berg 1959). Black Saxaul can reach heights of 4–6 m. The wood is used as firewood as well as to smoke meat. The stems are so hard that they ar difficult to split with an axe.

For the Eastern loess areas at the foot of the mountain ranges *Artemisia*-Ephemeres-vegetation is typical. It shows a dense cover of herbs and several ephemeres in May. Beginning of June *Artemisia* species and *Kochia* develop and in autumn *Artemisia* shrubs reach heights of 30–40 cm.

The floodplains of the rivers are called Tugai and develop a special vegetation. In the Shu valley special meadows develop. The grass (*Lasiogrostis splendens* or *Stipa splendens*) grows up to 1.5 m high (Berg 1959).

3.6 Socio-economic Characteristics

The Kazakh lands have been under varying human influences for a long time. This has strongly influenced the landscapes development. Historically, the Kazakh steppe has been used as range land by nomadic herders. They herded livestock, grew fodder and small grain. This was the main human activity in the past and still remains important today (ADB 2010).

The Caspian Lowland, for example, was already settled in the Stone and Bronze Age. Several nomadic tribes trekked through the region between the rivers Ural and Volga. The Nogai settled the area in the 16th century, but were displaced by the Kalmuks in the 17th. In the beginning of the 19th century the Cossacks arrived with big sheep herds and overgrazing led to the expansion of sand dunes. Even more disastrous were the uncontrolled agricultural practices, which caused big sand deflation (Walter and Breckle 1989).

The conversions of native grasslands into crop-lands progressively increased from the 18th century onward. Nevertheless, crop agriculture stayed uncommon and mostly confined to narrow bands along rivers (ADB 2010). This changed significantly, when the former Soviet Union installed its Virgin Land Scheme in the 1950's. Huge areas of steppe and marginal desert were ploughed and heavy cereal cultivation, mainly wheat, introduced to make the area a breadbasket for the former Soviet Union's populations. About 45% of the steppe zone was used for agriculture by the Soviet Union and about 10.7% of the semi-desert zone was also converted to agricultural land (Berg 1959). Between 1950 and 1960 the cultivated area of Kazakhstan increased from 7.8 million to 28.5 million hectares (ADB 2010). This led to dramatic steppe deterioration. Eventually, vast areas of ploughed lands were abandoned. Heavy seeding with grasses and perennials, such as feather grass and wheat grass, helped to recover parts of these areas. However, according to the Kazakhs Fodder and Pasture Institute, it is assumed that it will take 30 years more for the abandoned steppe regions to fully recover (ADB 2010).

The current land use in Kazakhstan can be divided into four major zones: Cereal farms (wheat, corn) mixed with meat and dairy farming are the major land use in the North-east of the country. The central part of Kazakhstan is primarily used for livestock farming (cattle, sheep, and goats) with occasional land use. The south-western parts are used for meat production, wool farming, and sheep breeding. The south-eastern, partly mountainous, areas are typically used for nomadic and semi-nomadic livestock (cattle, sheep, goats, and camels) (ADB 2010).

Most important natural resources of Kazakhstan are oil, natural gas, chromium, coal, copper, gold, lead, tungsten, and zinc (ADB 2010). The economically very important oil and gas fields are mainly found in the Caspian Sea region. Thias allows Kazakhstan to rank among the top 20 oil producers in the world (in 2008). The countries energy needs are mainly covered by coal power (ADB 2010). The uranium deposits are estimated to be the second largest in the world (ADB 2010). The country's main exports are oil, uranium, ferrous and non-ferrous metals, machinery, chemicals, grain, wool, meat, and coal (ADB 2010).

The agricultural sector is still important for the economy, providing employment for more than 30% of the country's workers. About 22 million hectares are used as arable land and 185 million hectares as pasture, making it the fifth largest pasture land worldwide (ADB 2010). Sheep breeding is dominant, along with cattle, pigs, horses, as well as camels. The most

important crop is wheat, which is mainly grown in the rain-fed agricultural lands of northern Kazakhstan. Irrigated crops are grown along rivers and water bodies, such as the Syr-Darya or Aral Sea. Crops include mainly wheat and rice, along with cereals, fruits, fodder, potatoes, and sugar beet. Wheat production is still of great importance, especially with the aim of food self sufficiency since the country gained independence. The Shu River valley belongs to Kazakhstan's most important areas for irrigated agriculture. The city Shu is an important transportation hub for the whole Southern Kazakhstan and Northern Kyrgyzstan. This is because the east-west Turkestan-Siberia railway is joined here with the railway running north to Astana and Petropavl on the Transsiberian railway. Therefore, Shu's central location allowed it to become a large hub for rail freight.

The ecological problems in Kazakhstan are manifold. Poor irrigation practices have led to severe environmental damage in irrigated agricultural areas. The water resources of the country are often polluted from industrial and agricultural run-off (ADB 2010). A significant proportion of agricultural land has been destroyed by desertification. Actually, due to the climatic situation and human influence, the most threatening natural hazards in Kazakhstan are land degradation and desertification (ADB 2010). The Aral Sea is almost dried out due to water diversion for irrigation. Former nuclear weapon test sites, such as Semipalatinsk, are contaminated by radiation (ADB 2010). Numerous governmental projects have been embarked on to prevent further damage, but still more effort is needed, to overcome the environmental problems of the country. This is especially true regarding its problems of sanitation, air and water quality, irrigation practices, and land degradation (ADB 2010).

Kazakhstan's population was about 16 million in 2009 (cf. table 3-2), with an average annual population growth rate of 1.14 %. The population is relatively heterogeneous. Most people, with 53%, are Kazakh, followed by 30% Russian and 11% Ukrainian. Most live in the North-east and South-east of the country. The population density in Kazakhstan is about six people per square kilometre, one of the lowest in the world (ADB 2010). As most people live in cities, large areas are sparsely populated, such as the Karaganda district in Central Kazakhstan (cf. table 3-2). The city of Karaganda is the main industrial centre with about 475,000 inhabitants. It is the most populated city of the area. The major part of the study area in Central Kazakhstan is only sparsely populated. The most important religions in Kazakhstan are Muslim, primarily Sunni (47%), Russian Orthodox (44%), and Protestant (2%). Kazakh is the official "state" language (spoken by 64%) and Russian is the official "language of interethnic communication" (spoken by 95% of the population) (ADB 2010).

Table 3-2: Socio-economic characteristics for the districts of the study area and entire Kazakhstan (source: National Statistical Agency of Kazakhstan), as well as Germany for comparison.

District	Capital	Area [km²]	Population 1989	Population 1999	Population 2009	Population density 2009 [people/km²]
Atyrau	Atyrau	118,600	424,708	440,286	510,377	4.30
West Kazakhstan	Uralsk	151,300	629,494	616,800	598,880	3.96
Karaganda	Karaganda	428,000	1,745,448	1,410,218	1,341,700	3.13
Zhambyl	Taraz	144,300	1,038,667	988,840	1,022,129	7.08
Total Kazakhstan	Astana	2,724,900	16,222,324	14,981,281	16,009,597	5.88
Germany	Berlin	357,100	-	-	81,802,000	229.07

4 Available Data, Pre-Processing, and Input Data Quality Assessment

4.1 Remote-Sensing based Raster Input Data

Remote sensing time-series are needed as input for the NPP models applied in this study. For BETHY/DLR, meteorological input data are needed at least on a daily basis, as well as LAI time-series. RBM is mainly based on MODIS data and needs FPAR, NDVI, albedo, land surface temperature and emissivity, and water vapour products. Land cover information for both models is also based on remote sensing data and provided by the MODIS land cover classification and the vegetation continuous fields (VCF) product, or the Central Asia land cover and land use map (Klein et al. 2012). All remote-sensing based data that were used in this study are described in the following sections.

4.1.1 Meteorological Data from the ECMWF

The meteorological input data needed for BETHY/DLR are available from the ERA-Interim reanalysis at ECMWF. The ERA-Interim Archive contains meteorological data from the ERA-Interim reanalysis since 1979. The reanalysis continues and the archive is being updated on a monthly basis (Berrisford et al. 2011).

The required datasets belong to the suite of surface level parameters. Table 4-1 gives an overview of the required input parameters from ECMWF, which comprise time-series on air temperature 2 m above the ground, precipitation, wind speed 10 m above the ground and cloud coverage for three cloud strata. The data are available with a spatial resolution of 0.25° × 0.25° (about 25 × 25 km at the equator). Most parameters are available four times daily, at 00, 06, 12 and 18 UTC; precipitation is provided twice per day, at 00 and 12 UTC (Berrisford et al. 2011).

Table 4-1: Meteorological input parameters for BETHY/DLR derived by the ECMWF.

Parameter	Short name	Code number	Units
Surface geopotential	Z	129	$m^2 s^{-2}$
Large-scale precipitation	LSP	142	m of water
Convective precipitation	CP	143	m of water
10 metre eastward wind component	10U	165	$m s^{-1}$
10 metre northward wind component	10V	166	$m s^{-1}$
2 metre temperature	2T	167	K
Low cloud cover	LCC	186	(0–1)
Medium cloud cover	MCC	187	(0–1)
High cloud cover	HCC	188	(0–1)

A primary quality requirement is that the reanalysis products match available observations. Further, estimated parameters have to be consistent with physical laws (Dee et al. 2011). These requirements are achieved by using a sequential data assimilation and forecast model, in which various observation from multiple sources is assimilated (Dee et al. 2011). For each interval of the analysis, available observations are combined with prior information from the forecast model to estimate atmospheric and surface parameters (Dee et al. 2011).

A total of nearly 10^7 observations per day are assimilated globally in ERA-Interim for most recent years. The majority of data originate from satellites (Dee et al. 2011). However, also atmospheric refraction measurements, as well as *in situ* measurements, for example from buoys, radiosondes and land stations, are incorporated in the analysis (Dee et al. 2011). A detailed description of the ERA-Interim reanalysis, including configuration, performance and included observation datasets is provided by Dee et al. (2011).

4.1.1.1 Pre-processing of Meteorological Data

Temperature

Daily mean, minimum and maximum of temperature are calculated from the temperature datasets provided by the ECMWF. Diurnal variation is then calculated by setting the maximum temperature for 2 pm model time and the minimum temperature at the time of sunrise. The fitted temperature curve shows a sinusoidal shape until sunset and a linear decline at night.

Further, the temperature values (T_{ECMWF}) are scaled to the 1 km² resolution of the land cover data. The scaling is based on the difference between the ECMWF reference height (h_{ECMWF}) and the height of each modelled pixel as from a higher-resolution digital elevation model (h_{DEM}, GTOPO30, see section 4.2.1). As scaling factor the gradient of the International Standard Atmosphere (ISA) is applied, which is –6.5K/1000m.

$$T' = T_{ECMWF} \cdot 0.0065 \cdot \frac{K}{m} \cdot (h_{ECMWF} - h_{DEM}) \tag{4-1}$$

Precipitation

As described above, ECMWF provides precipitation data separately for two time periods per day. The water balance, however, is calculated daily in BETHY/DLR, so that daily values of precipitation are needed as model input. Therefore, the two precipitation datasets are summed up to obtain the total daily precipitation sum. This sum provides the daily precipitation input into the water balance model of BETHY/DLR.

Wind

Wind data are provided by the ECMWF four times a day and separated into an eastward and a northward wind component. The wind speed data of the East-West component ($\vec{u}_x$), und the North-South component ($\vec{u}_y$), are combined to derive the absolute value for the wind speed for the four time steps.

$$|u| = \sqrt{\vec{u}_x^{\,2} + \vec{u}_y^{\,2}} \tag{4-2}$$

PAR

Within BETHY/DLR scaled diurnal variations of PAR are calculated based on global radiation as described in section 2.2.2 (cf. equation 2-5). The atmospheric transmission, which is needed for PAR calculation, is influenced by the degree of cloudiness. Therefore, the daily average cloud cover is calculated as weighted sum from the three cloud strata (high, medium and low cloud cover) datasets provided by the ECMWF. The calculation of the PAR based on the ECMWF cloud cover data was found to lead to more exact results than the direct use of the radiation provided by the ECMWF (Wißkirchen 2005).

4.1.1.2 Quality Assessment of Meteorological Input Data

For the quality assessment of the meteorological input data, climate station data from 299 stations with records of temperature and precipitation were available. The data were retrieved from the National Climatic Data Center (NCDC) of the National Oceanic and Atmospheric Administration (NOAA). They were made available through the Global Historical Climatology Network (GHCN)-Daily database, which contains historical daily temperature, precipitation, and snow records. The data base is made up by a composite of climate records from numerous sources that were merged and quality assessed.

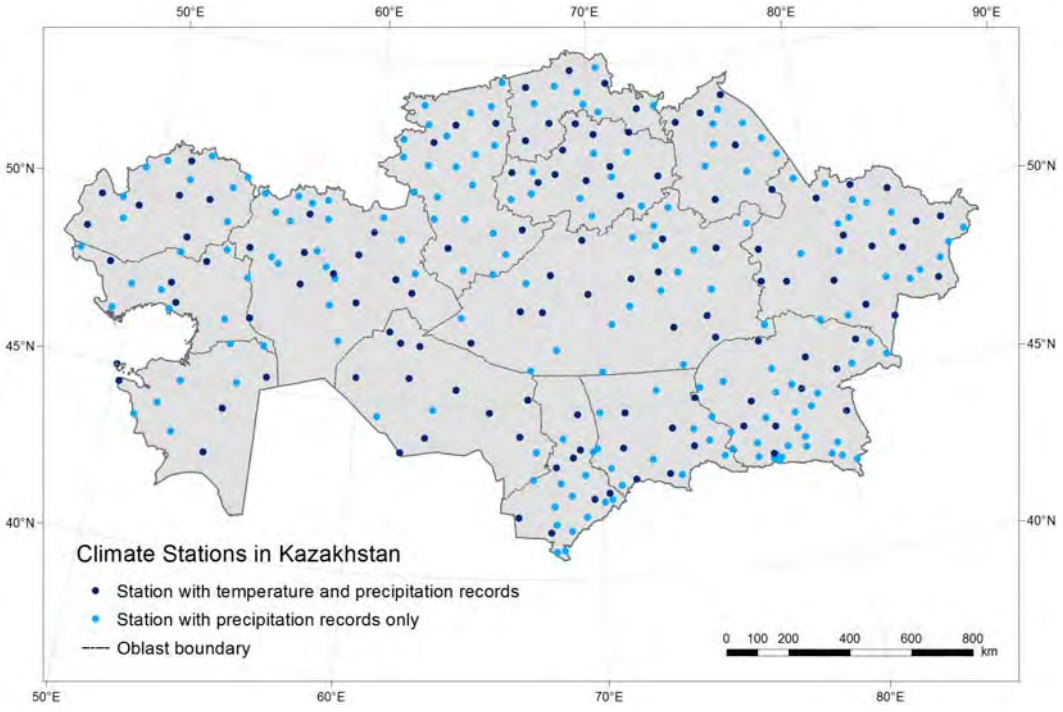

Figure 4-1: Distribution of the 299 available climate stations with data records of temperature and precipitation over Kazakhstan.

The distribution of the climate stations over Kazakhstan is shown in figure 4-1. The data are well distributed over the country with slight accumulation in North Kazakhstan and clusters in the south-eastern mountainous regions. Precipitation records were available for all of the 299 climate stations, while temperature records were only available from 119 stations. Measurements of the other meteorological parameters, which are needed as model input (PAR and wind speed), were not available. The climate station records were provided as daily measurements for minimum temperature, maximum temperature and precipitation. Not all of

the stations provided continuous records for the time span 1989–2011, but for each parameter more than 300,000 data records were available, which were used for comparison with ECMWF data for temperature and precipitation, as described in the following sections.

Quality assessment of ECMWF temperature data

For the quality assessment of the ECMWF temperature data, records from 119 climate stations in Kazakhstan were available. The number of days with available temperature records for the period 1989–2011 varied from station to station. For minimum daily temperature the number of records per station was between 29 and 7515 and for maximum daily temperature between 226 and 818 records. In total, 334,839 individual records were available for minimum temperature and 433,804 records for maximum temperature.

Figure 4-2 (left) shows the scatterplot of all available daily minimum temperature records from the climate stations and the corresponding ECMWF minimum temperatures. Figure 4-2 (right) shows the frequency distribution of the correlation coefficients obtained for minimum temperature data for the 119 individual climate stations in Kazakhstan. Figure 4-3 shows the corresponding plots for the quality assessment of the daily maximum temperature.

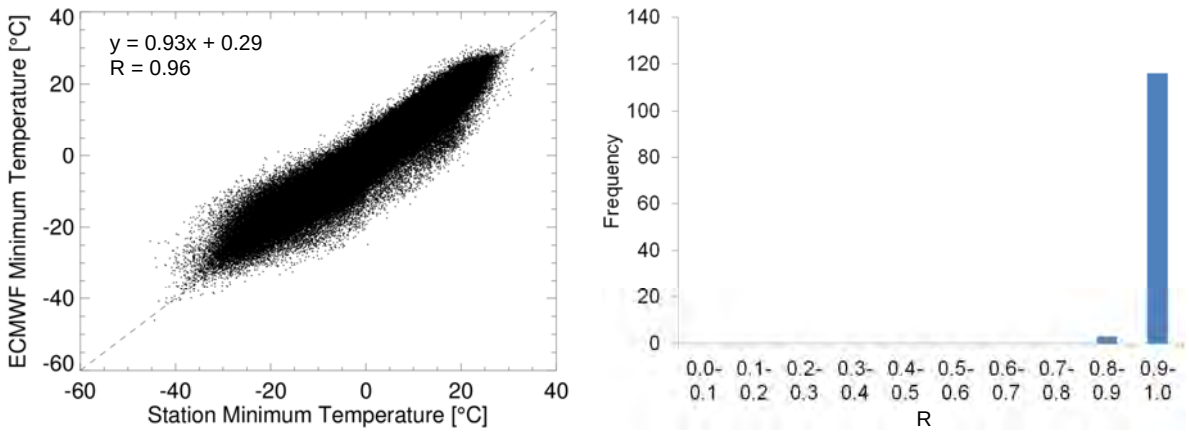

Figure 4-2: Left: Scatter plot of daily minimum temperature records from climate stations and corresponding daily ECMWF temperature minimum data. Right: Frequency distribution of the correlation coefficients obtained for the 119 climate stations in Kazakhstan for the assessment of daily temperature minimum data.

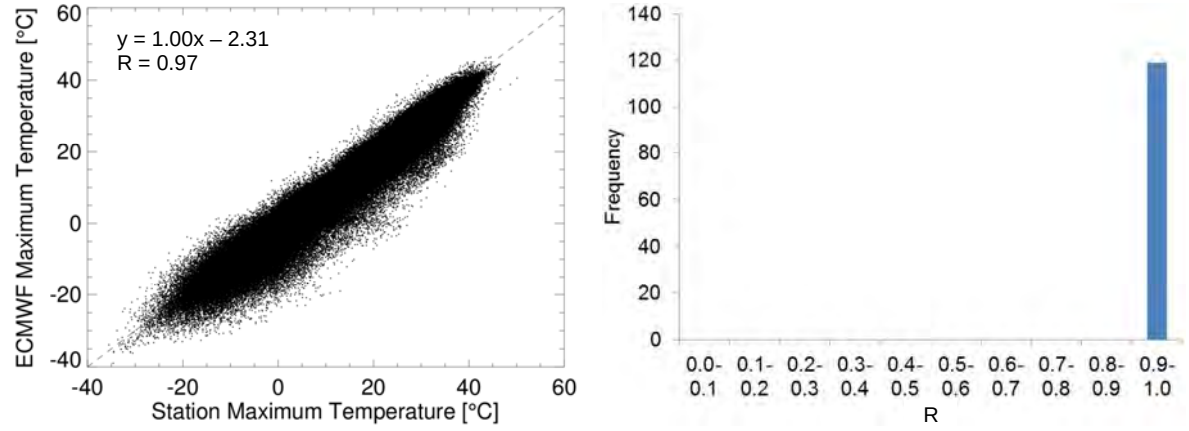

Figure 4-3: Left: Scatter plot of daily maximum temperature records from climate stations and corresponding daily ECMWF temperature maximum data. Right: Frequency distribution of the correlation coefficients obtained for the 119 climate stations in Kazakhstan for the assessment of daily temperature maximum data.

The scatter plots show a very good correlation between the ECMWF data and the climate station records for both minimum and maximum daily temperature (Figures 4-2 and 4-3). The overall correlation coefficients are with R=0.96 for minimum temperature and R=0.97 for maximum temperature very high. From the individual climate stations 97% show R>0.9 for minimum temperature and 100% show R>0.9 for maximum temperature. These results show that the ECMWF temperature data represent very well the temperature records measured at the climate stations over whole Kazakhstan.

Quality assessment of ECMWF precipitation data

For the quality assessment of the ECMWF precipitation data, records from 299 climate stations were available. The number of days with available precipitation records for the period 1989–2011 varied from station to station with a minimum of 242 days and a maximum of 6566 days. In total, 495,483 individual precipitation records were considered for the quality assessment.

Figure 4-4 (left) shows the scatterplot of all available daily precipitation records from the climate stations and the corresponding ECMWF daily precipitation amounts. Figure 4-4 (right) shows the frequency distribution of the correlation coefficients obtained for the 299 climate stations in Kazakhstan. The scatter plot reveals no visible correlation between the daily datasets. The overall correlation is with R=0.33 very low. The correlation coefficients for the individual stations vary between 0.07 and 0.69. In figure 4-5 the obtained correlation coefficients for daily precipitation data are plotted for the individual climate stations. The stations with strong and weak correlations show no obvious systematic geographical distribution.

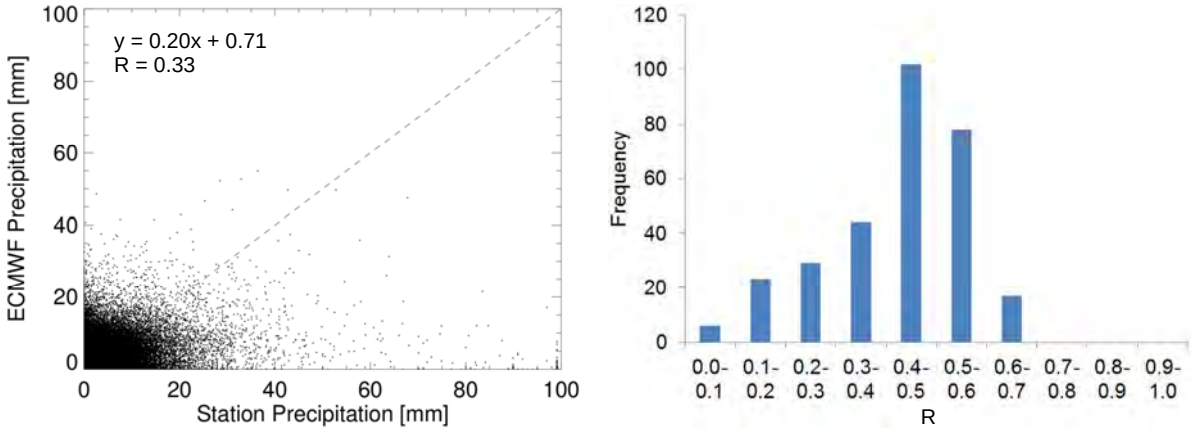

Figure 4-4: Left: Scatter plot of daily precipitation records from climate stations and corresponding daily ECMWF precipitation data. Right: Frequency distribution of the correlation coefficients obtained for the 299 climate stations in Kazakhstan for the assessment of daily precipitation data.

Modelling of precipitation is a challenging task, because accurate representation of the hydrological cycle presents a special challenge (Dee et al. 2011). The ECMWF reanalysis data, however, proved to be reliable when longer time-periods are considered (Balsamo et al. 2010). Errors in the precipitation input data, of course, cause inaccuracies in the modelled NPP with BETHY/DLR. However, errors in daily precipitation are less problematic than errors in seasonal precipitation distribution. The precipitation feeds the soil water model in BETHY/DLR and daily precipitation is not critical, as long as the soil is not completely dry. The distribution of precipitation amounts over the seasons, however, is important for NPP modelling. Therefore, monthly sums of precipitation were generated and also compared to climate station data.

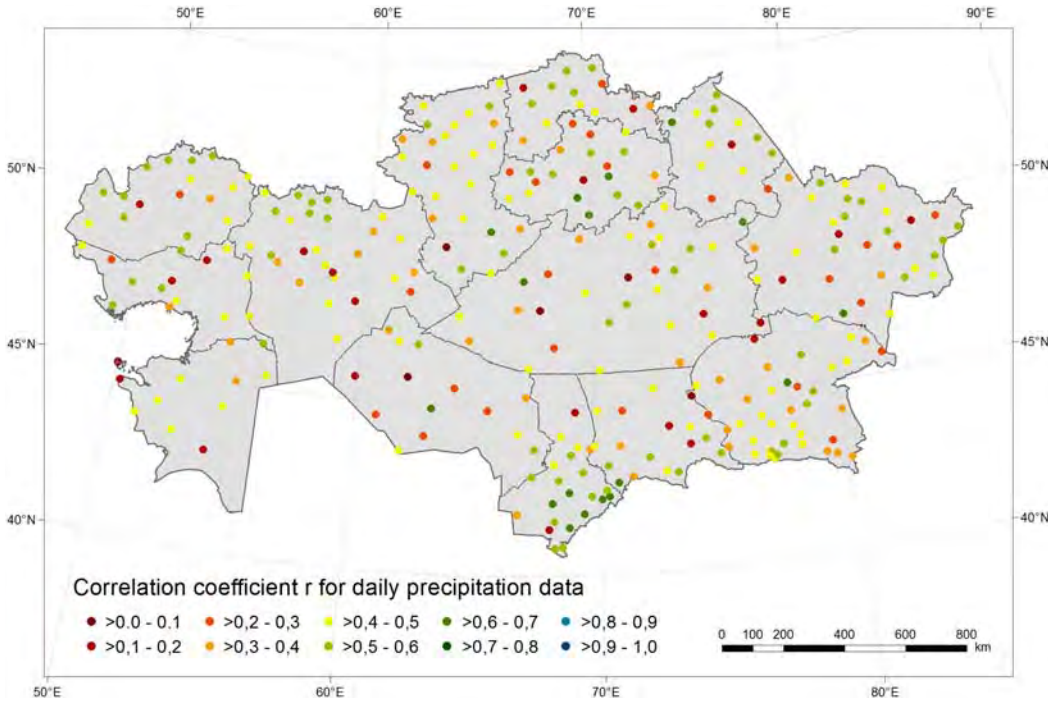

Figure 4-5: Spatial distribution of correlation coefficients between daily precipitation records from climate stations and corresponding daily ECMWF precipitation data.

For the quality assessment of monthly precipitation data, the daily precipitation records were summed and compared to the monthly ECMWF precipitation sums. The number of months with available precipitation records for the period 1989–2011 varied from station to station with a minimum of 9 months and a maximum of 216 months. A total number of 19,981 monthly station records were available for the quality assessment.

Figure 4-6 (left) shows the scatterplot of the monthly precipitation sums from the climate stations and the corresponding ECMWF monthly precipitation amounts. Figure 4-6 (right) shows the frequency distribution of the correlation coefficients obtained with monthly precipitation data for the 299 climate stations in Kazakhstan. The scatter plot shows a significantly stronger correlation than observed with daily precipitation data. The overall correlation reaches R=0.64. However, the precipitation amounts are still underestimated by the ECMWF data by about 36% compared to the climate station data. The correlation coefficients for the individual stations vary between 0.62 and 0.73.

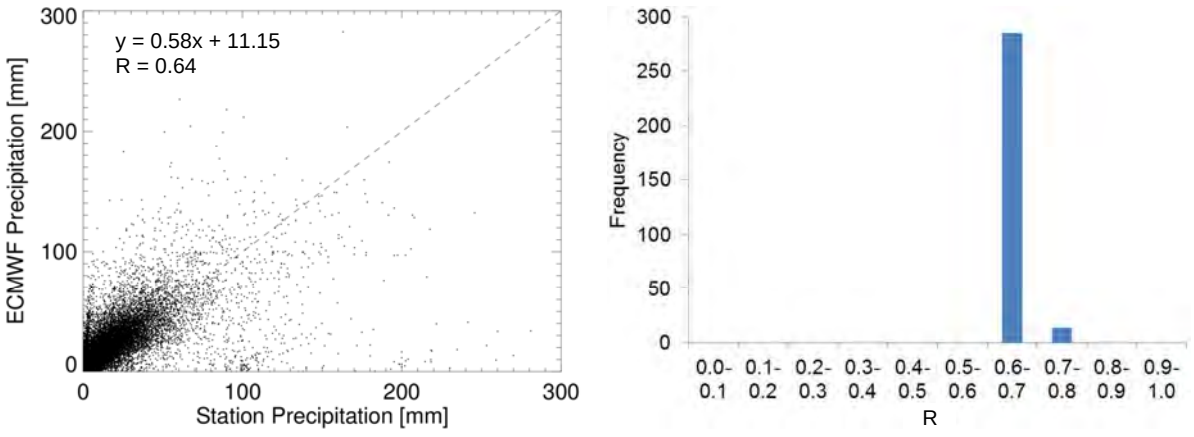

Figure 4-6: Left: Scatter plot of monthly precipitation records from climate stations and corresponding monthly ECMWF precipitation sums. Right: Frequency distribution of the correlation coefficients obtained for the 299 climate stations in Kazakhstan for the assessment of monthly precipitation data.

4.1.2 MODIS Products

Several MODIS products (albedo, cloud cover, emissivity, FPAR, land surface temperature, water vapour, and VCF) are needed for the RBM (cf. section 2.2.3). MODIS LAI and land cover are also used in BETHY/DLR. Most of these datasets are MODIS land products, which are available at 500 m or 1 km spatial resolution as 8-day or 16-day composites. These products are produced in sinusoidal projection as a tiled grid. Only the water vapour product is not available in sinusoidal projection, but in swath format. Figure 4-7 shows the coverage of the Sinusoidal grid tiles. The study area in Central Kazakhstan lies within tiles H22V04 and H23V04. Six tiles are required to cover the area of entire Kazakhstan (cf. figure 4-7).

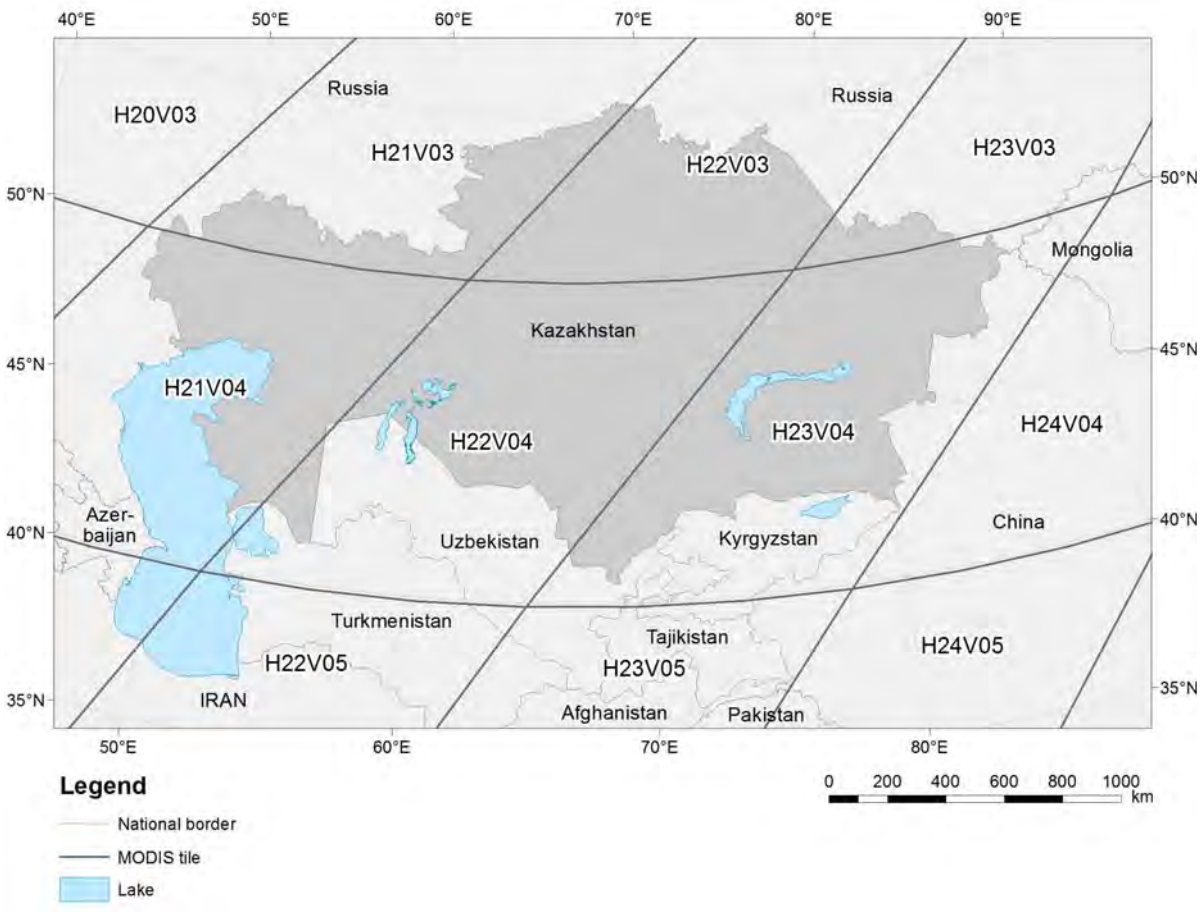

Figure 4-7: MODIS sinusoidal tile coverage for the area of Kazakhstan.

The MODIS data were downloaded from the USGS Data Pool. All data were available as collection 5, except the VCF product of which collection 4 data were retrieved. The MODIS Reprojection Tool (MRT) was used for mosaicking of the MODIS tiles. The mosaics were then subsetted and projected, also with the MRT. For usage with RBM the data were projected to UTM with 928 m resolution, for BETHY/DLR to geographic projection with a spatial resolution of ~0.00833°. A description of the individual MODIS products used within this study, is provided in the subsequent sections.

4.1.2.1 LAI and FPAR

The MODIS LAI and FPAR product provides information on global Leaf Area Index (LAI) and Fraction of Photosynthetically Active Radiation (FPAR) absorbed by vegetation. Per definition

"FPAR is the Fraction of Absorbed Photosynthetically Active radiation that a plant canopy absorbs for photosynthesis and growth in the 0.4–0.7 µm spectral range. FPAR is expressed as a unitless fraction of the incoming radiation received by the land surface." (description of the MOD15 LAI/FPAR product, NASA 2012a) and "LAI is defined as the one-sided green leaf area per unit ground area in broadleaf canopies and as half the total needle surface area per unit ground area in coniferous canopies." (information on LAI, NASA 2012b).

The MODIS LAI/FPAR products from Terra (MOD15A2) and Aqua (MYD15A2) are derived based on atmospherically corrected surface reflectances from sensor data and provide LAI and FPAR information at about 1 km (more exactly ~926.6 m) spatial resolution on an 8-day basis (Knyazikhin et al. 1999). Combined products from Terra and Aqua are also available. The main algorithm exploits the spectral information of MODIS surface reflectances. The back-up algorithm makes use of vegetation indices. A three-dimensional formulation of the LAI/FPAR inverse problem underlies the algorithm and allows describing the natural variability of vegetation canopies (Knyazikhin et al. 1999). The LAI and FPAR retrieval technique is defined to possess the same statistical properties as if they were derived from ground measurements (Knyazikhin et al. 1999).

A structural land cover classification that is compatible with the radiative transfer model used for LAI/FPAR derivation is required for the LAI and FPAR retrieval algorithm. This classification is available from the MODIS land cover product. Further detailed description of the LAI/FPAR product and the algorithm applied is provided by Knyazikhin et al. (1999).

For this study the MYD15A2 product was used. The preprocessing of FPAR and LAI data was done completely identical. First, MODIS tiles were mosaicked. Second, gaps and outliers in the time-series were identified and corrected applying a harmonic analysis, as described by Niklaus et al. (submitted). Any outliers as well as missing data were previously substituted by a mean phenology for that class and MODIS tile (Niklaus et al. submitted). The 8-day LAI data for BETHY/DLR were projected to geographic projection with a spatial resolution of ~0.00833°. To be used as input for the RBM, the FPAR data were projected to UTM projection, subsetted, and rescaled to 928 m. For RBM, the 8-day products were further converted to 16-day datasets by computing the mean LAI from two 8-day products for each 16-day dataset.

4.1.2.2 NDVI

The MODIS Vegetation Indices product is available with a spatial resolution of 1 km as 16-day composites based on Terra (MOD13A2) or Aqua (MYD13A2) data. Higher spatial resolutions are also available. The product contains two vegetation indices (VIs). First, the standard normalized difference vegetation index (NDVI), which is based on red (0.6–0.7 µm) and NIR reflectances (0.7–1.1 µm). Second, the enhanced vegetation index (EVI), which provides improved sensitivity in high biomass regions, minimizes canopy-soil variations, and reduces atmosphere influences (Huete et al. 1999). The following equations show how NDVI and EVI area calculated, with ρ reflectance in blue, red or NIR band, L canopy background adjustment term, and C_1 and C_2 weighting factors.

$$NDVI = \frac{\rho_{NIR} - \rho_{RED}}{\rho_{NIR} + \rho_{RED}} \tag{4-3}$$

$$EVI = 2\frac{\rho_{NIR} - \rho_{RED}}{L + \rho_{NIR} + C_1\rho_{RED} + C_2\rho_{BLUE}} \tag{4-4}$$

Input data for the derivation of the VIs are BRDF adjusted MODIS surface reflectances (blue, red and NIR) that have been corrected for clouds, ozone absorption, and aerosols. A special compositing scheme reduces angular, sun-target-sensor variations (Huete et al. 1999). More details on the algorithm applied to derive NDVI and EVI can be found in Huete et al. (1999). The NDVI data were used as input for the RBM. Preprocessing steps included projection, subsetting, and rescaling, as described in section 4.1.2.1 for FPAR data.

4.1.2.3 Albedo

The MODIS Albedo product is available on a 16-day basis with 500 m (MCD43A3) or 1000 m (MCD43B3) spatial resolution. It includes two albedo measurements, the directional hemispherical reflectance (black-sky albedo) and the bihemispherical reflectance (white-sky albedo). The generation of the albedo product is based on reflectances in seven spectral bands from both Terra and Aqua data. Using a Bidirectional Reflectance Distribution Function (BRDF), angular integrations are performed to derive land surface albedos for each spectral band. The black sky albedo is obtained from integration over the exitance hemisphere for a single irradiance direction. The white sky albedo results from all viewing and irradiance directions (Strahler et al. 1999b). A detailed product description is given by Strahler et al. (1999b).
The albedo data were used as input for the RBM. Actual albedo, which lies between black sky and white sky albedo, was calculated as the mean from these two values. Further preprocessing steps included, as with the other MODIS products, projection, subsetting, and rescaling.

4.1.2.4 Land Surface Temperature and Emissivity

The MODIS Land Surface Temperature (LST)/Emissivity product is available as an 8-day daytime and nighttime product at 1 km spatial resolution. The product MYD11A2, which was used within this study, is based on Aqua data. The day/night algorithm makes use of seven thermal infrared (TIR) bands (bands 20, 22, 23, 29, and 31–33) from both day and night MODIS data. It retrieves daytime and nighttime LSTs and surface emissivities (Wan 1999). Atmospheric transfer simulations were applied to establish a database for MODIS thermal radiances, which was used to produce a look-up table and an interpolation scheme that describes the effects of surface temperature and emissivity, atmospheric water vapour, and temperature profiles on MODIS TIR band radiance (Wan 1999). Emissivities in bands 31 and 32 can be estimated from land cover information and are used as input information. The LST product is retrieved by a generalized view-angle dependent split-window algorithm (Wan 1999). This algorithm is applied to correct for atmospheric and emissivity effects of different land cover types, resulting in a high quality LST and emissivity product (Wan 1999). More detailed information on the algorithm applied for LST and emissivity derivation is provided by Wan (1999).

The temperature and emissivity data were used as input for the RBM. First, the datasets were projected, subsetted, and rescaled, as described above. Second, the 8-day products were converted to 16-day datasets, by calculating the mean value of two 8-day products for each 16-day dataset. Then, mean daily temperature was calculated as the mean from 16-day datasets of day and night temperatures. Mean daily emissivity was retrieved likewise. Finally, the datasets were scaled and converted from Kelvin to °Celsius. Further details on the necessary pre-processing steps are available from Richters (2005a).

4.1.2.5 Water Vapour and Cloud Cover

The MODIS Total Precipitable Water Product (MOD05_L2 from Terra data and MYD05_L2 from Aqua data) is available as daily data with a spatial resolution of 1 km. It provides information on column water vapour amounts. Over land, a near-infrared (NIR) algorithm is applied during daytime, which retrieves observations of water vapour attenuation from NIR solar radiation reflected by surfaces and clouds. This algorithm also includes a correction of aerosol effects (Gao and Kaufman 1998). For the level 2 product, further, an infrared algorithm is applied that derives atmospheric profiles both day and night. Ratios of water vapour absorbing channels are employed to remove the effects of variation of surface reflectance with wavelengths. As a result, atmospheric water vapour transmittances are retrieved. From these, the column water vapour amounts are derived based on radiative transfer calculations and look-up tables. The error in water vapour values is typically between 5% and 10% (Gao and Kaufman 1998). More information on the Retrieval Algorithm can be found in Gao and Kaufman (1998).

The MODIS water vapour product also includes a daily cloud mask, which is identical to the MOD35 Cloud mask product. It is based on several visible and infrared threshold and consistency tests, including an indication of shadow effects. The cloud mask is based on radiometrically accurate radiance of the visible channels (Parkinson and Greenstone 2000).

Within this study, MODIS water vapour data were applied for the RBM. Pre-processing was done with tools provided by Richters (2005a). With these, the swath data were converted to grid data and individual values converted to their physical quantities. Details about the applied procedure are described by Richters (2005a). To be used as input for the RBM in this study, the datasets were finally projected to UTM projection and rescaled to 928 m spatial resolution.

4.1.2.6 Land Cover Classification

The Land Cover Product MCD12Q1 is based on combined Terra and Aqua products and provides five different global land cover classifications with 500 m spatial resolution on a yearly basis. The primary classification scheme identifies 17 land cover classes, including 11 natural vegetation classes (Strahler et al. 1999a). The land cover classification applied for radiative transfer for LAI and FPAR, classification Type 3, identifies the following 11 classes: broadleaf crops, grasses/cereal crops, shrubs, savannah, evergreen broadleaf forest, deciduous broadleaf forest, evergreen needleleaf forest, deciduous needleleaf forest, non-vegetated, urban, and water (cf. figure 4-8).

The land cover product relies on a broad database of MODIS products including a land/water mask, nadir BRDF-adjusted reflectances, spatial texture, directional reflectance information for 16-day periods, EVI, snow cover, land surface temperature and terrain elevation information. Based on this database, the land cover classifications are produced using decision tree and artificial neural network classification algorithms based on training data (Strahler et al. 1999a). Further information on the MODIS land cover products including a full algorithm description is provided by Strahler et al. (1999a).

The MCD12Q1 classification applied for LAI and FPAR derivation for the year 2009 was used as input for BETHY/DLR for the model comparison (cf. chapter 5) in this study. It was projected to geographic projection with a spatial resolution of ~0.00833°.

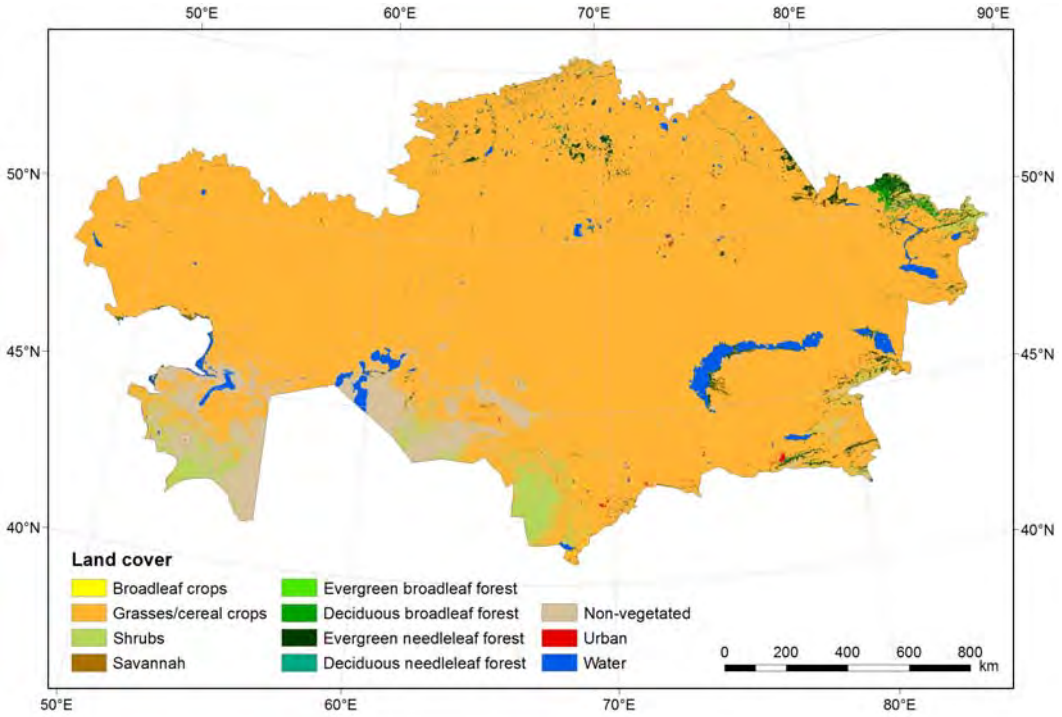

Figure 4-8: MODIS land cover classification Type 3 (LAI/FPAR) for Kazakhstan for the year 2009.

4.1.2.7 Vegetation Continuous Fields

The MODIS Vegetation Continuous Fields (VCF) product (MOD44B) contains proportional cover estimates for woody vegetation, herbaceous vegetation, and bare ground (cf. figure 4-9). The product is derived from monthly composites of the seven MODIS land bands (blue, green, red, near infrared, and three midinfrared bands) with 500 m spatial resolution (Hansen et al. 2003). The MODIS data were transformed into annual phenological metrics. A total of 68 multi-temporal metrics were derived (Hansen et al. 2003). Global training data were derived using high-resolution imagery (Global Land Cover Facility, GLCF 2012). Together with the phenological metrics, the training data are used within a regression tree to derive percent vegetation cover (GLCF 2012). A full description of the approach for deriving the metrics and training data, as well as of the regression tree algorithm is provided by Hansen et al. (2002a,b). The outputs from the regression tree are further modified by a stepwise regression and bias adjustment according to Hansen et al. (2002b) to retrieve the final product that describes the percent canopy cover per 500m MODIS pixel (Hansen et al. 2003).

The first release (collection 3) of the MODIS VCF product with all three layers is available for download for the year 2001 from the global land cover facility (GLCF) website (http://glcf.umiacs.umd.edu/data/vcf/index.shtml). Products for other years, which had first been released, were withdrawn due to implausible changes in fractional cover between the single years. The error associated with the available VCF product for 2001 is quite high (Machwitz 2010, Tum et al. 2011). The current collection 4 is available for the years 2000 until 2005, but so far only contains percent tree coverage. The other layers are planned to be provided in later releases (NASA 2012c). For this study the MODIS VCF collection 3 data were used. In contrast to a discrete classification scheme, the three continuous layers of the VCF product are especially suited to describe areas of heterogeneous land cover (GLCF 2012). The MODIS VCF product was used as input for the RBM. Preprocessing steps included projection, subsetting, and rescaling, as described in section 4.1.2.1 for FPAR data.

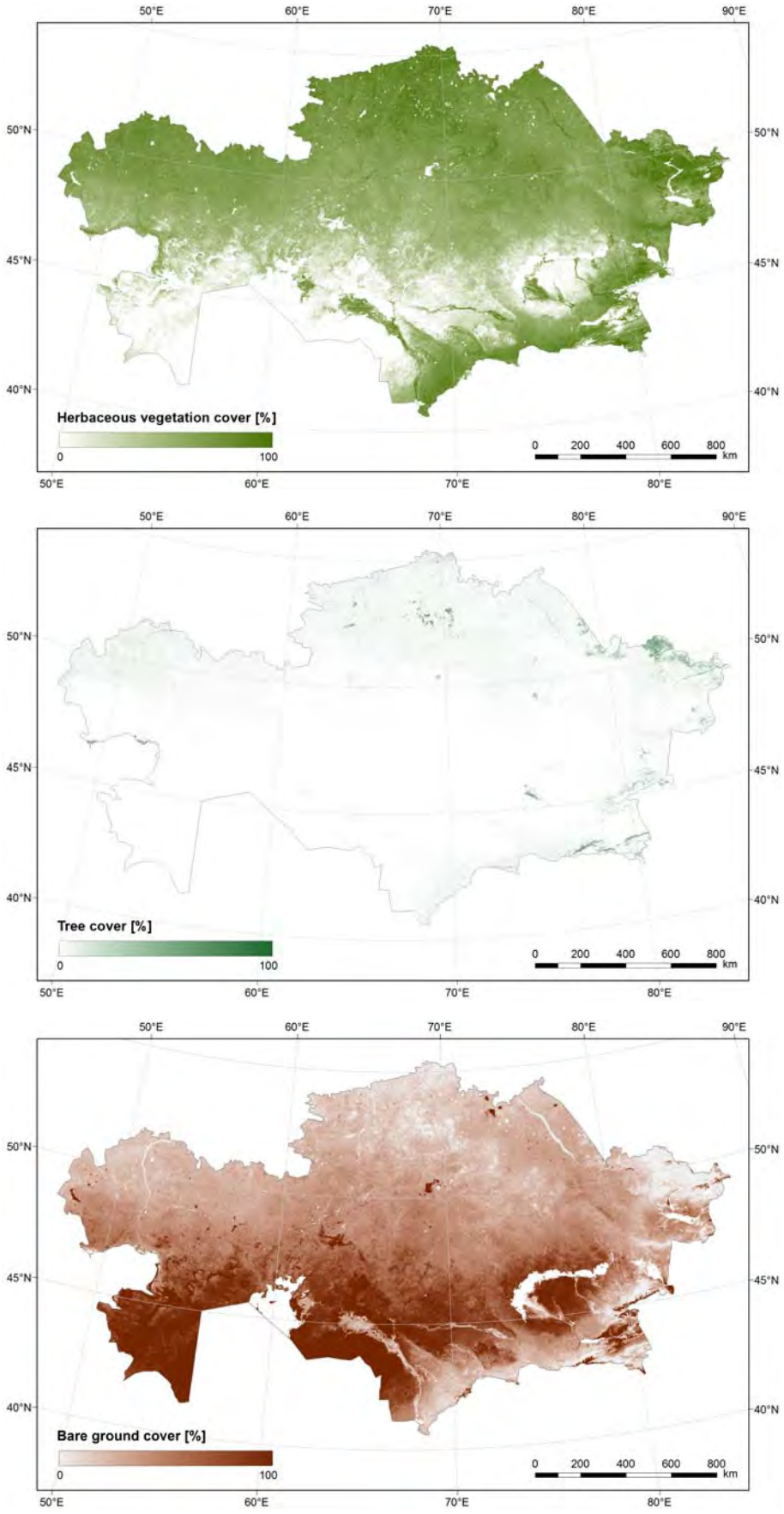

Figure 4-9: MODIS VCF product showing fractional herbaceous vegetation (above), tree cover (middle) and bare ground (below) for Kazakhstan for the year 2001.

4.1.3 Central Asia Land Cover and Land Use Map

As land cover information for BETHY/DLR, a regional land cover and land use map for Central Asia was available from Klein et al. (2012). This land cover map was derived based on a one-year time-series of MODIS NDVI and reflectances of the red and near-infrared bands. The data base was available at a spatial resolution of 250 m. For each of four temporal sections (winter/spring, summer, autumn/winter and full annual cycle), median, minimum, maximum and amplitude metrics were calculated. Metrics that were highly correlated with each other were excluded from the analysis, resulting in a total of 42 MODIS metrics available as features for the following classification process (Klein et al. 2012).

The hierarchical classification scheme was especifically developed for the region of Central Asia and is based on the land cover classification scheme (LCCS) of the Food and Agriculture Organisation of the United Nations Environment Programme (FAO-UNEP). Table 4-2 gives an overview of the land cover classes of the land cover and land use map and their characterisctics.

Table 4-2: Description of land cover classes for Central Asia from the land cover and land use map (Klein et al. 2012).

Class Name	Description
Rain-fed agriculture	Rain-fed agriculture
Irrigated agriculture	Water supply mainly by irrigation
Artificial	Built up and sealed areas
Needleleaved trees	Needleleaved evergreen trees, main layer: trees > 65%
Broadleaved trees	Broadleaved deciduous trees, main layer: trees > 65%
Sparse vegetation	Sparse shrubs (5–15%, 30cm–3m) and sparse herbaceous (5–15%, 30cm–3m)
Grassland	Herbaceous closed to open vegetation: main layer: herbaceous: 15–100% (3cm–3m)
Closed shrubland	Closed medium high shrubland, main layer: shrubs: > 65% (50cm–3m)
Open shrubland	Open medium high shrubland: main layer: shrubs: 15-65% (50cm–3m)
Bare area	Unconsolidated material(s), less than 4% vegetative cover
Bare area with salt flats	Unconsolidated material(s) with salt flats, less than 4% vegetative cover
Ice and snow	Artificial and natural
Water bodies	Artificial and natural

An automatically generated decision tree classifier based on C5.0 algorithm was then applied. This type of classifier has the advantage that it reveals nonlinear and hierarchical relationships between training variables (Huth et al. 2012). The C5.0 empirical learning system uses training samples to extract informative patterns, which are then assembled into a tree structured classifier. The reference samples were collected from high resolution remote sensing imagery for the two years, for which land cover classification maps were produced: 2001 and 2009. The classification process starts with a separation of the reference sample into a training ($2/3^{rd}$) and a validation ($1/3^{rd}$) dataset. A ruleset is generated from the training data and its performance tested on the validation data. Only if the accuracy fits required thresholds, the classifier is used for the classification (Klein et al. 2012).

Some post-classification steps were applied to improve the classification results. Additional information on slope and height from a Shuttle Radar Topography Mission (SRTM) digital elevation model (DEM, see section 4.1.4) and long-term precipitation averages from the Global Precipitation Climatology Centre (GPCC) were included for post-classification. Based on this

additional information, some misclassifications between spectral ambiguous classes, such as 'ice and snow' and 'bare areas with salt flats', 'shadow' and 'water bodies', as well as 'rain-fed agriculture' and 'grassland', could be excluded. The classification results for 2009 were found to show an overall accuracy of 91.26% (Klein et al. 2012). The Central Asia land cover and land use map covers the countries of Kazakhstan, Kyrgyzstan, Uzbekistan, Tajikistan and Turkmenistan. Figure 4-10 shows the land cover and land use classification for the year 2009 for Kazakhstan.

The Central Asia land cover and land use map was rescaled to the same spatial resolution as the LAI input data prior to be used as input dataset for BETHY/DLR. The rescaling was performed with ArcGIS using a majority filter based on a 9×9 pixel matrix. The projection was converted to a geographic WGS84 projection with ~0.00833° spatial resolution.

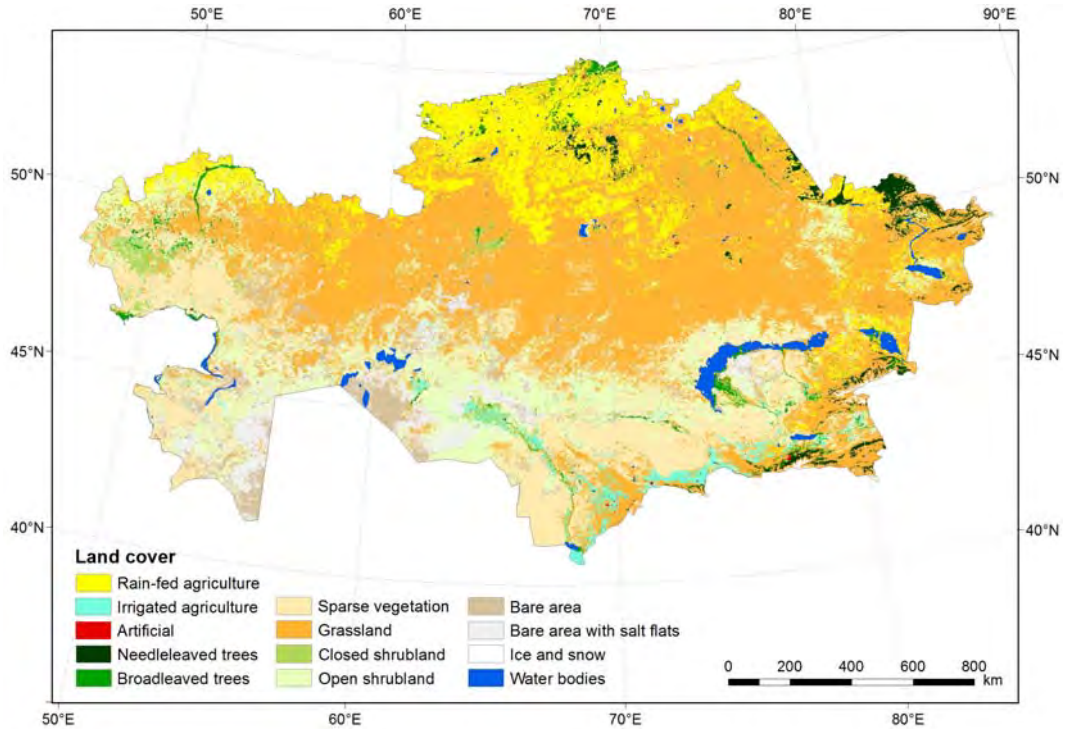

Figure 4-10: Central Asia land cover and land use map for Kazakhstan for the year 2009 (Klein et al. 2012).

4.1.4 SRTM Digital Elevation Model

Height information of the Earth was collected during the Shuttle Radar Topography Mission (SRTM). The data were used to produce a digital elevation model (DEM). SRTM was a joint mission of the National Aeronautics and Space Administration (NASA), the National Geospatial-Intelligence Agency (NGA), the German Aersopace Center (DLR) and the Agenzia Spaziale Italiana (ASI). Data collection by SRTM was produced by two radar systems, which were installed on the Space Shuttle Endeavour. The mission was realized during 11 days in February 2000.

The innovative data collection technique contained radar antennas on the shuttle and two additional antennas that were installed on a 60 m long mast. Both antennas, on the shuttle and on the mast, received the radar impulses that were scattered back from the Earth. This so called 'single pass interferometry' method was used to collect height information of the Earth's surface from the 233 km high orbit of the Endeavour.

Two different radar antennas were installed on the shuttle. One was a C-band radar (SIR-C) that was developed by NASA. This radar was used to generate data with a horizontal resolution of 90 m and a height accuracy of about 10 m. The Earth surface was scanned with 225 km wide stripes. The whole land surface between 60°N and 58°S was covered. The second radar antenna, the X-SAR, developed by DLR and ASI collected data stripes of 50 km width and reached a coverage of about 40% of the land surface (Rabus et al. 2003). The horizontal resolution of the X-SAR DEM is 25 m and the relative height accuracy reaches 6 m. Within this study, the DEM derived based on C-band data was used as input for the RBM. The data were projected to UTM projection, subsetted, and rescaled to 928 m.

4.2 Non-Remote-Sensing based Raster Input Data

Additional raster data that were used as input for the NPP models comprise the GTOPO30 DEM, which provides elevation information for BETHY/DLR, and a soil map, which is needed for both models. A short description of these two datasets is given in the following sections.

4.2.1 GTOPO30 Digital Elevation Model

The Global 30 Arc-Second Elevation Data Set (GTOPO30) provides digital elevation data of the whole Earth land surface with a spatial resolution of about 1 km. The dataset was developed by the USGS Center for Earth Resources Observation and Science (EROS) and several collaborators and was completed in 1996. The global elevation dataset is based on eight topographic information sources including raster and vector datasets. The area of Kazakhstan was completely derived from Digital Terrain Elevation Data (DTED), which is the major data source, used for 50% of the land surface area within GTOPO30. DTED is a raster elevation dataset with about 90 m spatial resolution produced by the National Imagery and Mapping Agency (USGS 1996).

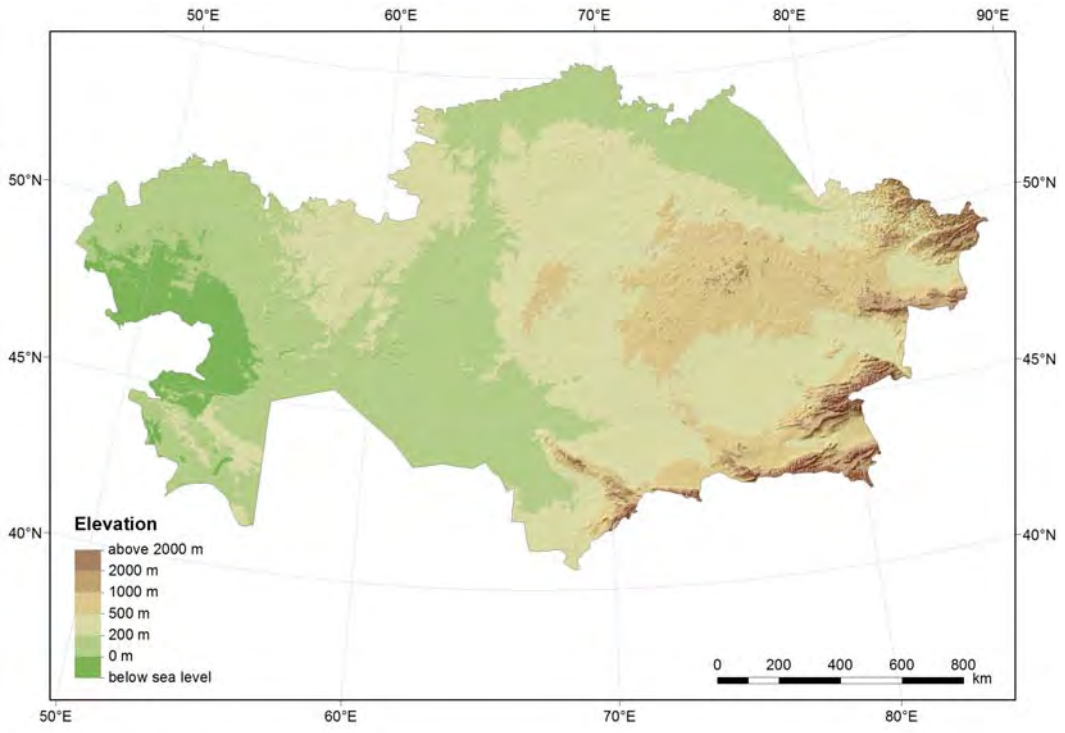

Figure 4-11: Terrain heights for Kazakhstan from the GTOPO30 digital elevation model.

The terrain heights from the GTOPO30 digital elevation model for Kazakhstan are shown in figure 4-11. The data is available in geographic coordinates and WGS84 projection and can be accessed via FTP from the USGS EROS Data Center at no cost. Within this study, the GTOPO30 was used as input for the vegetation model BETHY/DLR and for rescaling of the ECMWF temperature data.

4.2.2 HWSD Soil Map

The soil classification needed as model input is taken from the Harmonized World Soil Database (HWSD, FAO et al. 2009). It was produced by the Food and Agriculture Organization of the United Nations (FAO) and the International Institute for Applied Systems Analysis (IIASA) in cooperation with the ISRIC-World Soil Information, the European Soil Bureau Network and the Chinese Academy of Sciences. The HWSD is a combination of the information already contained within the FAO-UNESCO Digital Soil Map of the World and most recent regional and national updates of soil information. The updated soil information was compiled from the European Soil Database (ESDB), the 1:1 million soil map of China and various regional SOTER databases (SOTWIS Database).

The main aims of this digitized and online accessible soil information system were to be of practical use to modelers and to serve perspective studies in agro-ecological zoning, food security and climate change impacts. The HWSD was produced at a resolution of about 1 km (30 arc seconds). A total of 16,000 different soil mapping units are recognized in the global map (FAO et al. 2009).

Reliability of the soil information is variable. According to FAO et al. (2009) the map is less reliable for parts that make use of the Soil Map of the World such as North America, Australia, West Africa and South Asia. Areas covered by SOTER databases are considered to have the highest reliability, such as Southern and Eastern Africa, Latin America and the Caribbean, Central and Eastern Europe. For more information on the HWSD please refer to FAO et al. (2009).

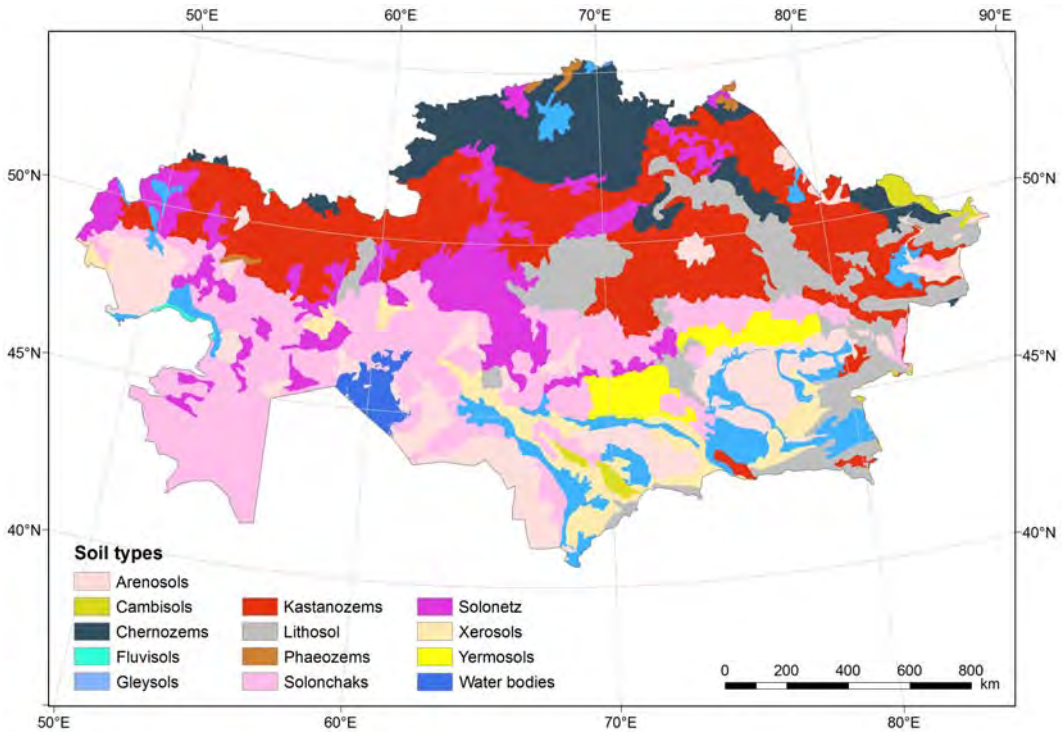

Figure 4-12: Soil types in Kazakhstan from the HWSD (FAO et al. 2009).

For Kazakhstan, the soil unit information in the HWSD is provided in the revised FAO90 classification system. In other regions of the world, different classification systems are used. Therefore, the soil information of the HWSD was harmonized before the map was used within BETHY/DLR. In this harmonization step, the FAO90 classification was reclassified to the FAO74 classification. Only main soils are needed for BETHY/DLR, which are described by 26 main soil classes. In Kazakhstan, 12 main soils are present in the HWSD, as displayed in figure 4-12. To be used as input for the RBM, the soil data were projected to UTM, subsetted, and rescaled to 928 m.

4.3 Collected Field Data

Ground-based measurements are essential for validation of the estimates obtained with BETHY/DLR and RBM. In the following sections, some general aspects on field estimation of biomass are provided, and the approach for field data collection within this study is described, including the choice of test sites and the method for biomass field data collection.

4.3.1 Issues in Field Estimation of Biomass in Semi-arid Areas

For validation of remote-sensing-based biomass estimation, *in situ* field measurements of biomass are essential. Moreover, even most recent methods need ground data for calibration to be able to accurately estimate biomass (e.g. Aranha et al. 2008, Baccini et al. 2008, Mutanga and Rugege 2006, Nijland et al. 2009).

The applied biomass field measurements can be divided into destructive and non-destructive estimations. In most research studies, a combination of both is applied. Destructive biomass measurements entail harvesting of plants, drying them, and weighing the biomass (cf. figure 4-13). The BGB can be estimated using entire harvesting and applying the root/shoot ratio (Harris 1992). Within semi-arid zones, direct AGB harvesting can usually be applied, because of generally low vegetation densities. For grass cover, clipping sub-plots sized about 0.5–1 m² is common. These methods are often combined with visual estimates (e.g. Diallo et al. 1991) or the use of a calibrated rising disc pasture meter (DPM, e.g. Sannier et al. 2002, Samimi and Kraus 2004, Mutanga and Rugege 2006, Wessels et al. 2006). Destructive biomass estimation is the most direct and accurate method for quantifying biomass, but can only be applied to a small area due to high cost, time consumption and impact on the environment (e.g. García et al. 2010).

Non-destructive biomass estimation is based on measurements of physical variables, such as height, stem diameter (DBH, diameter at breast height), crown area, number of stems (individual biomass) or number of plants, vegetation cover and stand height (plot biomass) (e.g. Etienne 1989, Radloff and Mucina 2007). These variables are converted to biomass values and extrapolated to unit ground area. Non-destructive biomass estimation is common especially for woody plants. Several studies have established allometric relationships for total or green biomass of woody plants within semi-arid regions around the world (e.g. Buras et al. 2012, Cissé 1980, Franklin and Hiernaux 1991, Henry et al. 2009, Thenkabail et al. 2004, Tietema 1993). A general overview of the major steps and methods applied in field biomass estimation is given in figure 4-13.

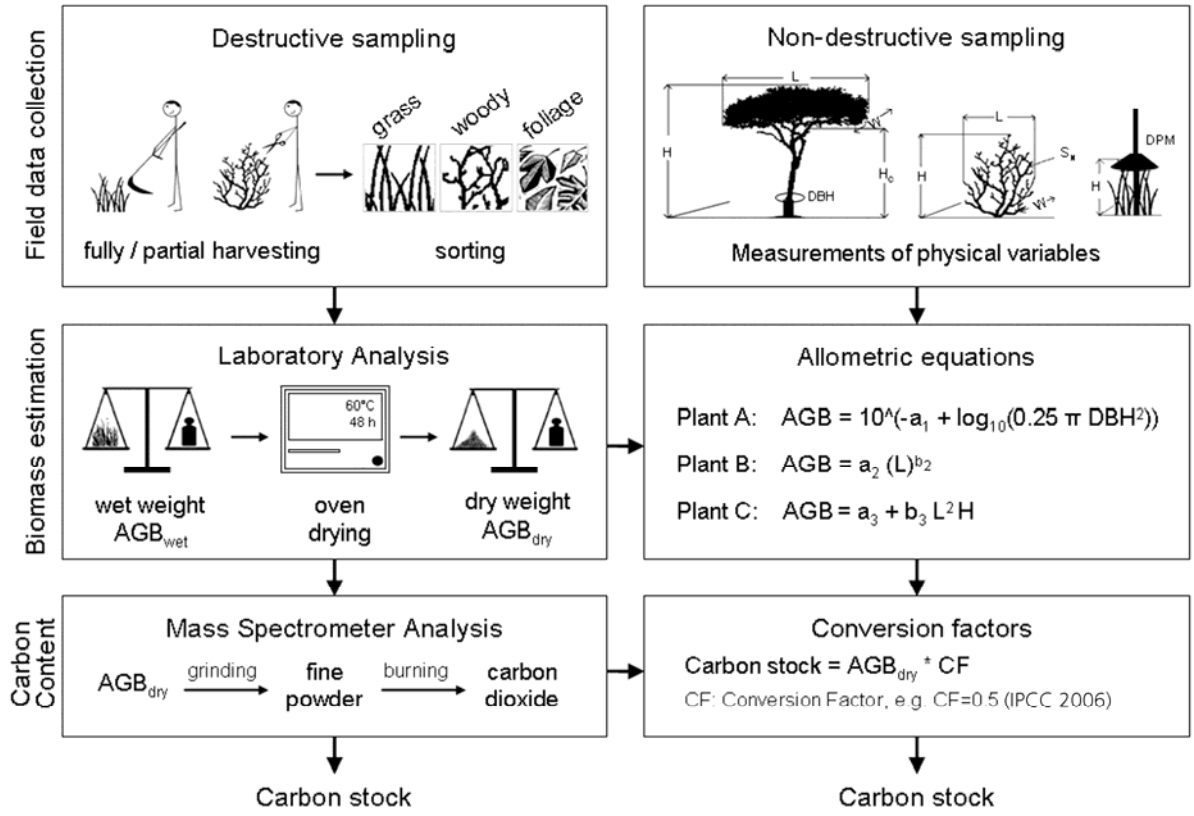

Figure 4-13: The way from field data collection to biomass estimation: typical above-ground biomass field measurements applied within studies in semi-arid regions (*H*: height, *L*: length, *W*: width, DBH: diameter at breast height, H_C: height to the base of the crown, S_N: number of stems, DPM: disc pasture meter; a, b: scalars; CF: conversion factor, for example CF=0.5 (IPCC 2006).

A common problem for validation of remote-sensing-based biomass estimates is the mismatch between the spatial resolution of satellite data and the field plot size. According to Justice and Townshend (1981), the minimum size of a field plot should be $a = p(1+2L)$, where a is the size of the field plot, p the pixel size and L the geometric accuracy.

Assuming an accuracy of 0.5 pixels, the sampling plot for Advanced Very High Resolution Radiometer (AVHRR) data should, hence, be at least 2.2 km. Such large sample plots are generally not feasible and smaller plots are used instead. To reduce the effects of registration errors, it is common to place the field plots in homogeneous areas (e.g. Frison et al. 1998, Sannier et al. 2002, Wessels et al. 2006) or to use a minimum number of field plots within each pixel (Baccini et al. 2008). The spatial scaling from plot to pixel size might be further improved by the use of additional high-resolution data.

Biomass sampling within the sample sites may follow different sampling strategies, including the establishment of transects (e.g. Mutanga and Rugege 2006, Samimi and Kraus 2004, Sannier et al. 2002, Wessels et al. 2006), nested sampling schemes (e.g. Addink et al. 2007, Sulieman 2007, Sulieman and Buchroithner 2006, Nijland et al. 2009) and clustered measurement plots (e.g. Wylie et al. 1991, Sannier et al. 2002).

4.3.2 Field Data Collection

For the independent validation of the NPP and biomass estimates, field data were collected at two field campaigns. The first campaign was realized in December 2010, before the beginning of the growing season, in the study area Central Kazakhstan. The second campaign in June

2011, in the mid of the growing season, covered all three study areas: Central, West and South Kazakhstan. Field data collection for both campaigns was standardized.

4.3.2.1 Choice of Test Sites

Three study areas were selected in Kazakhstan, as described in section 3.1. Within the study areas vegetation cover and biomass vary considerably. For the study areas in Central Kazakhstan and West Kazakhstan the biomass distribution shows a gradient from North to South, following soil and vegetation characteristics (cf. section 3.2). Therefore, test sites within these study areas were selected along a North-South transect. In South Kazakhstan vegetation does not show a distinct gradient.

The test sites for all study areas were selected according to the following criteria: 1) they represent all major soil and natural vegetation types (ecological communities) that are representative for larger parts of the study area, 2) they span a wide range of typical biomass amounts that occur within the representative vegetation in the study area, 3) they are located in relatively homogeneous regions so that the vegetation biomass in the surrounding area is not significantly different to that of the test site.

The choice of individual test site locations was partly based on an analysis of GIS and satellite data and partly of *in situ* observations during the field campaign. For the location of test sites in Central Kazakhstan it was also taken into account that these had to be accessible during winter conditions. Therefore, they are located near main roads and within reach of bigger settlements due to logistic requirements.

4.3.2.2 Method for Biomass Field Data Collection

The approach selected for biomass field data collection is a stratified random sampling design, which is adapted from Hiernaux et al. (2009). This approach was chosen for this study, because it is especially suitable for obtaining ground measurements for comparison with data at a spatial resolution of about 1 km². It combines destructive measurements with non-destructive stratification along transects. This allows to upscale the destructive measurements, which, of course, can only be realised at a limited number of small sample plots, to a larger test site, based on the records taken along the transect.

The procedure for the combined destructive measurements and non-destructive stratification, can be described by the following steps: First, four vegetation strata are defined for each test site based on the apparent bulk of vegetation. These strata describe typical biomass amounts from bare, low and medium to high biomass and are empirically defined relative to the status of the vegetation at the date of observation (Hiernaux et al. 2009).

Second, a representative transect is defined that runs orthogonal to any vegetation or landscape facieses (cf. figure 4-14). Along this transect the vegetation stratification is performed by classifying each square metre as one of the four vegetation strata, as illustrated in figure 4-14.

The vegetation strata are then sampled separately to derive mean aboveground biomass per strata. The biomass of the test site is finally described by the frequency of the vegetation strata and the weighted mean of the strata mean biomass (Hiernaux et al. 2009).

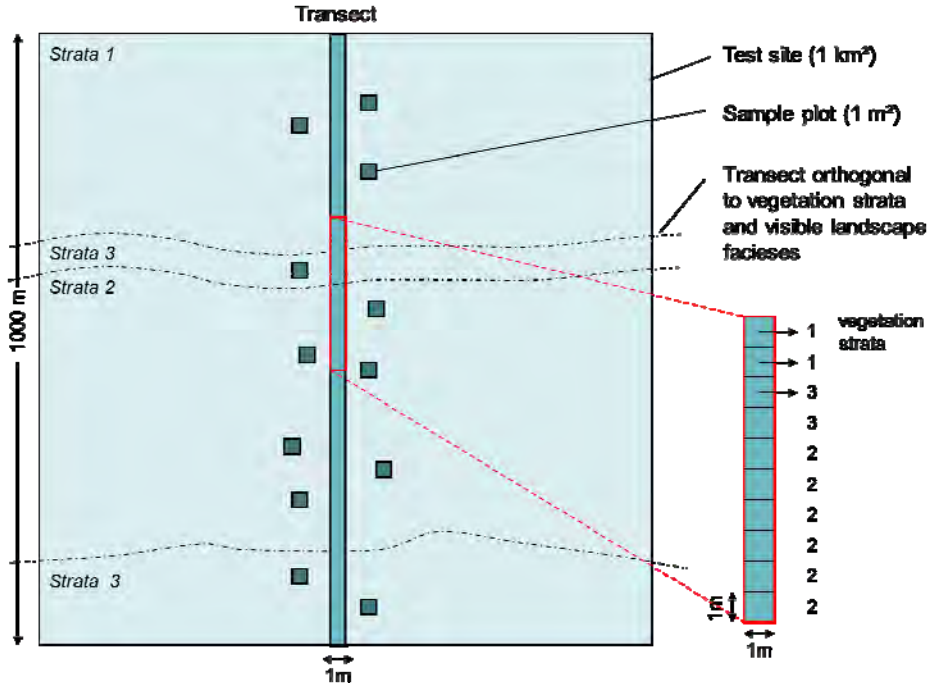

Figure 4-14: Schematic visualisation of the sampling design. For each test site the vegetation is stratified according to apparent vegetation bulks in four strata: 0=bare, 1=low, 2=medium, 3=high. A minimum of 12 sample plots (three for strata 1 and 3, six for strata 2) are randomly selected along the 1000 m transect (adapted from Hiernaux et al. 2009).

Following Hiernaux et al. (2009), the weighted mean biomass $\overline{M}$ is calculated according to equation 4-5. The weighted standard deviation of the sample $\overline{S}$ is calculated following equation 4-6, with k number of strata, p_k the absolute frequency of strata k recorded along the transect, $\overline{m}_k$ the arithmetic mean of sample items in strata k, x_{ki} the observed values of the sample items in strata k and n_k the absolute number of samples for strata k.

$$\overline{M} = \sum_{1}^{k}\left(\frac{p_k \overline{m}_k}{\sum p_k}\right) \tag{4-5}$$

$$\overline{S} = \sum_{1}^{k}\left(\frac{p_k}{\sum_{1}^{k} p_k} \cdot \sqrt{\frac{\sum_{i=1}^{n}\left(x_{ki} - \overline{m}_k\right)^2}{n_k}}\right) \tag{4-6}$$

For the test sites in Kazakhstan the length of the transect was typically 1000 m. Start and end coordinates were recorded using a GPS device, standardized photographs from start and end point taken, and the track recorded using a standardized protocol (cf. appendix E: Field protocol – Biomass Transects).

For each of the vegetation strata, except 'bare', sample plots for destructive measurements of 1 × 1 m were randomly defined along the transect. The minimum number of sample plots for the 'low' strata was three, for the 'medium' strata six, and for the 'high' strata three, resulting in a minimum of 12 sample plots per test site. This unequal number of plots per strata allows optimisation of the error on weighted mean biomass (Hiernaux et al. 2009).

For each sample plot the following attributes were recorded in a standardized manner using a standardized field protocol (cf. appendix E: Field protocol – Biomass Sub-Plots): Coordinates, photographs (GPS, nadir view of plot, two side views of plot, view to four directions: N, E, S, W), soil moisture, snow cover (only in December), topography, ground cover for individual classes, and species (only in June). The individual classes were defined according to a combination of cover/vegetation type (grass, herbs, shrubs, trees, bare, litter), vitality (green, medium, dry), and vegetation height (3–15 cm, 15–30 cm, 30–50 cm, 50–80 cm, 80–120 cm, 120–200 cm, >200 cm). Figure 4-15 shows exemplarily the standardized photographs of one sample plot.

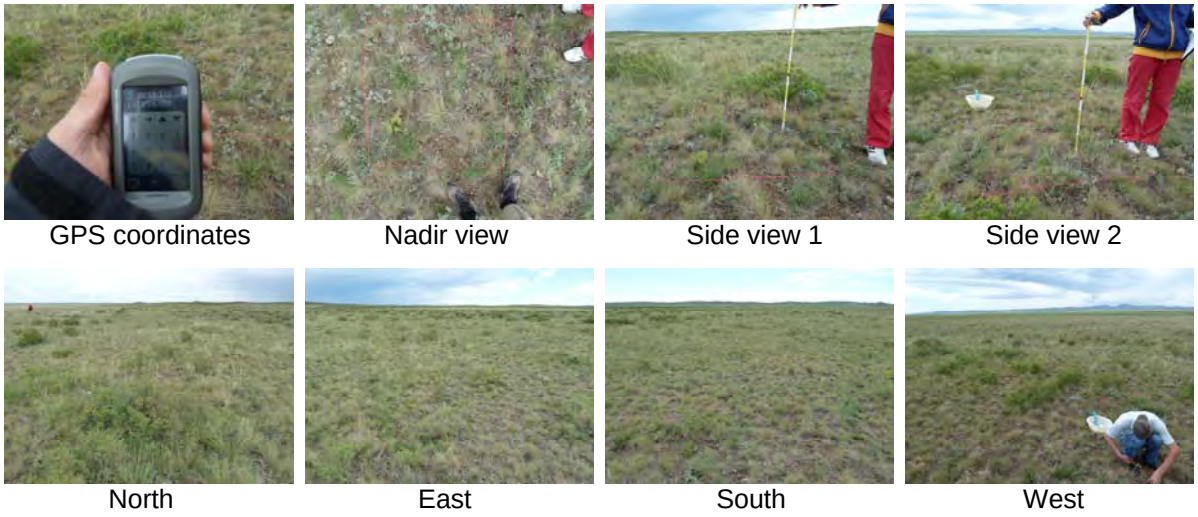

Figure 4-15: Photographic documentation of sample plot 10-1, recorded in June 2011. For each sample plot eight standardized pictures were taken.

After recording of attributes, the aboveground vegetation within the 1 m² sample plots was harvested to ground level, as shown in figure 4-16, and separated according to vegetation type (grass/herbs, shrubs) and vitality (green, dry). The samples were weighed to obtain fresh weight. Additionally, litter was collected and weighed. Depending on the size of the sample the whole or a representative part of it was chosen for estimation of dry weight. Dry weight was obtained after oven drying for 48 hours at 60°C.

Based on the ground cover recordings, mean fractional vegetation cover ($\overline{F}_i$) for grass and shrubs was calculated for each test site. The formula is shown in equation 4-7, with k number of strata, p_k the absolute frequency of strata k recorded along the transect, and $\overline{m}_{i,k}$ the arithmetic mean of ground cover of plant life-form i (grasses/herbs or shrubs) in strata k. Additionally, relative cover ($r\overline{F}_i$) of grass and shrubs was derived with equation 4-8, with $\overline{F}_i$ mean fractional cover of the vegetation type i and $\overline{F}_j$ mean fractional cover of the other plant life-form.

$$\overline{F}_i = \sum_{1}^{k} \left(\frac{p_k \overline{m}_{i,k}}{\sum p_k} \right) \tag{4-7}$$

$$r\overline{F}_i = \frac{\overline{F}_i \cdot 100}{\overline{F}_i + \overline{F}_j} \tag{4-8}$$

For some test sites the sampling design was expanded in order to account for heterogeneous or exceptional vegetation distribution. In some cases two orthogonal transects were laid out or additional vegetation strata were separated for which additional sample plots were recorded.

Figure 4-16: Pictures of sample plot 1-2 before (left) and after (right) harvest of the above-ground biomass. The right picture was taken after harvest of standing biomass but before collection of litter.

At some test sites large saxaul (*Haloxylon aphyllum*) shrubs occurred that could not be harvested (cf. figure 4-17). In this case, size parameters were measured that allow for allometric estimation of biomass with equations published in the literature. The following attributes and measurements were recorded for each individual plant: species, height, 1st crown diameter (maximum diameter), 2nd crown diameter (orthogonal to 1st crown diameter), number of stems, and sum of stem diameters at 5 cm above the ground.

Figure 4-17: Pictures of *Haloxylon aphyllum* shrubs at test site 17 in South Kazakhstan for which above-ground dry weight biomass was calculated based on physical parameters measured in the field.

In June 2011 a total of 30 test sites were sampled in Central (11), South (9), and West Kazakhstan (10) with a total of 364 sample plots. In the field campaign in December 2010, 12 test sites in Central Kazakhstan were visited with a total of 144 sample plots.

The field data collection was standardized for both campaigns. At seven test sites the identical transects were visited and destructive measurements taken close to those of the other field campaign. Drying and weighing of the biomass samples were also carried out by the same institute and staff with the same equipment according to a standardized procedure for both field campaigns.

4.3.3 Preparation of Field Data for Validation of NPP

For the validation of the NPP estimates, field data were collected at two field campaigns in the study area in Central Kazakhstan. Seven test sites were available for the validation of the model results, which were sampled at both field campaigns.

The difference between the biomass amounts obtained in June 2011 and December 2010 gives information about the vegetation growth in the meantime. This information can be applied for validation of the NPP estimates from the models RBM and BETHY/DLR (cf. section 5.2.2 and 7.3.2). To make the field data and model results comparable some conversions have to be applied to obtain data of the same quantity.

The field data measured in June 2011 and December 2010 contained above-ground biomass as dry weight. To make these data comparable to the model results, where NPP is defined as carbon uptake, the carbon content was calculated using conversion factors published by the IPCC (2006). The carbon fractions for herbaceous and woody biomass were taken as 0.47 t C (t DM)$^{-1}$ and 0.50 t C (t DM)$^{-1}$ respectively and for litter 0.40 t C (t DM)$^{-1}$. The carbon conversion factors from the IPCC are well established. Other studies also indicated that carbon comprises 45–50 % of dry matter of plant biomass (e.g. Lamlom and Savidge 2003, Schlesinger 1991).

Further, for some test sites in December 2010, a snow correction had to be applied because grass biomass was recorded above snow level by the field team. No correction was necessary for shrubs. Snow heights were also measured during the field campaign and varied between 2.5 and 13.5 cm for different test sites. A uniform distribution of plant mass from the soil to the measured plant height was assumed. The snow heights were then applied to derive the fraction of grass/herb vegetation above and below the snow. With this information the biomass below snow level was estimated.

4.3.4 Preparation of Field Data for Validation of Biomass

For validation of the above-ground biomass estimates (cf section 7.4.3), field data from 30 test sites were collected in June 2011. The conversion from dry matter biomass to carbon content, which is described in section 4.3.3, was also applied to the field data for validation of above-ground biomass estimates.

The preparation for validation of biomass estimates further included conversion from fresh to dry weight biomass for the samples from the study area in West Kazakhstan. This procedure is described in the section 4.3.4.1. For two test sites in South Kazakhstan also allometric equations were applied for calculation of above-ground biomass, as described in section 4.3.4.2.

4.3.4.1 Water Content

In the study area in West Kazakhstan no oven for drying of biomass samples was available. Therefore, mean conversion factors from fresh to dry biomass were derived based on fresh and dry weights measured in the study areas Central and South Kazakhstan in June 2011. The samples from these two study areas were oven dried at the Kazakh Research Institute for Plant

Protection and Quarantine in Almaty. This was done separately for grass/herbs and shrubs. For grass/herbs 192 individual sample plots were considered and a conversion factor of 54.6% (standard deviation: 18% absolute) derived. Shrub fresh and dry biomass were recorded at 85 sample plots and the dry weight was at average 61.8% (standard deviation: 16% absolute) of fresh weight. These conversion factors were applied to derive dry weight biomass for the test sites in West Kazakhstan (*BD*: dry weight above-ground biomass, *BF*: fresh weight above-ground biomass).

$$BD_{grass/herbs} = 0.546 \cdot BF_{grass/herbs} \quad (4\text{-}9)$$

$$BD_{shrubs} = 0.618 \cdot BF_{shrubs} \quad (4\text{-}10)$$

The water content in the vegetation varies between sample plots, test sites, and study areas. Therefore, oven drying should be favoured if possible. If drying of biomass samples is not possible and conversion factors have to be used instead, as for the study area in West Kazakhstan, it should be kept in mind that this adds a certain degree of uncertainty to the dry weights obtained.

Figure 4-18 shows fresh and dry weight biomass, as well as the water content for each test site. Additionally, the mean percental water content and its standard deviation are shown. Test site 18 from South Kazakhstan is disregarded because the reed grass observed at this site can not be compared to other test sites (cf. photo tables, Appendix D). For the test sites in the study areas Central Kazakhstan and South Kazakhstan, the water content in the grass/herb vegetation cover was at average 43.5% in June 2011. Minimum and maximum water content were 26.0% and 62.2% respectively, indicating a standard deviation of 11.1%.

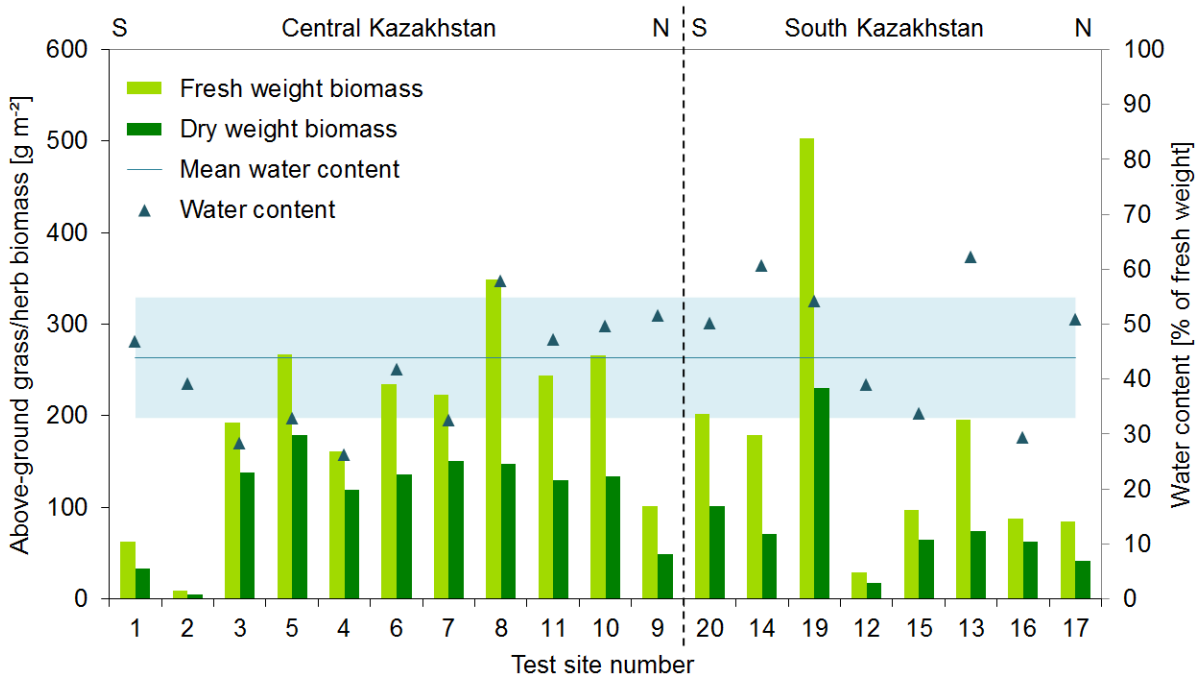

Figure 4-18: Mean fresh weight (light green bars) and dry weight (dark green bars) of above-ground grass/herb biomass for the test sites in Central and South Kazakhstan. The sites within the study areas are sorted from South to North. The blue triangles show the mean percental water content for each test site. The blue line shows the mean water content of all test sites. The light blue band shows the standard deviation of the mean water content.

4.3.4.2 Calculation of Shrub Biomass with Allometric Equations

At two test sites in South Kazakhstan large shrubs of black saxaul (*Haloxylon aphyllum*) were present that could not be harvested. Therefore, several physical variables were measured, as described above. The measured parameters were applied for calculation of above-ground biomass using a model developed for *Haloxylon aphyllum* by Buras et al. (2012). Following this equation the above-ground biomass *B* is calculated from height *H*, basal area *BA*, and crown area *CA* of individual shrubs as follows (Buras et al. 2012):

$$B = 1.997e^{-3} \cdot H^{0.93} \cdot BA^{0.68} \cdot CA^{0.025} \quad (4\text{-}11)$$

The parameter height was recorded directly in the field; crown area was calculated from the two crown diameters and basal area from the number of stems and the stem diameters 5 cm above the ground.
The equations were established by Buras et al. (2012) for *Haloxylon aphyllum* based on field data from six different regions within Central Asia that represent the range of ecosystem variability. Two sites at which harvests for the allometric relationships were carried out were situated in South-East Kazakhstan (Yany-Corgan and Karoi). The modelling accuracy was found to be very good with R^2 of 0.96 and a standard deviation of 0.01. The *Haloxylon aphyllum* shrubs in South Kazakhstan grow under similar environmental conditions as those sampled by Buras et al. (2012) so that these equations can be expected to result in reliable results for the test sites in South Kazakhstan.

4.4 Additional Data

Additional data that are used within this study comprise maps, vector data, as well as descriptive data. Remote-sensing based map products, which are not used as input data for the models, but provide background information, for example for study area selection, are also listed in this section.

Important information on distribution of vegetation communities within the three study areas was derived from the map “Vegetation” from the National Atlas of the Republic of Kazakhstan (Volkova et al. 2010). Details of the vegetation map for the three study areas are shown in figure B-1 (appendix B).

Other maps provide important base information for the selection of suitable study areas. Relevant maps were digitized, georeferenced, and vectorised – where necessary – before information was extracted. For this task, the following maps were used:

- Climate classification after Köppen-Geiger (Strahler and Strahler 1984)
- Climatic Regions (Philip’s 2003)
- Erde – Klima (Diercke 1992)
- Global map of irrigation areas (Siebert et al. 2007)
- GLOBCOVER 2006 (Bicheron et al. 2006)
- Central Asia in peril (UNEP/GRID-Arendal 2007)
- Radioactive, chemical and biological hazards in Central Asia (UNEP/GRID-Arendal 2005)

Vector data, which are applied in this thesis for the selection of study areas and for visualisation purposes, comprise cities, rivers, national borders, lakes, and nature reserves. These data were available from the Central-Asian Institute of Applied Geosciences (CAIAG) within the Regional Research Network Water in Central Asia (CAWa) project at DLR and from Esri (Esri World Topographic Map data, available at http://www.esri.com/data/free-data). Up to date maps of lakes were available at DLR (Klein et al. 2012).

Additionally, several descriptive data were gathered for this study from scientific sources. These include allometric equations (Buras et al. 2012), LUE parameters (Lagergren et al. 2005, Propastin et al. 2012, Richters 2005a), above-ground to below-ground NPP ratios (Propastin et al. 2012), as well as results from experimental studies on relative growth rates (cf. chapter 7). All sources of descriptive data are listed in the references.

5 Comparison of two Regional NPP Models for Central Kazakhstan

The results of this chapter have been accepted for publication in the IEEE Journal of Selected Topics in Applied Earth Observations and Remote Sensing (Eisfelder et al. in print).

5.1 Introduction

Modelling of NPP allows for quantification of CO_2 fluxes and provides valuable information on vegetation dynamics. NPP is a key variable for observing ecological functioning and has also been identified as a primary variable for observing degradation processes (CGER 2000). Therefore, NPP monitoring on a regional scale is important in arid and semi-arid regions.

NPP models are widely used on global scale. Several regional models have also been developed (cf. section 2.2.1). For global NPP models some comparison studies have been published (e.g. Adams et al. 2004, Cramer et al. 1999, 2001). Such intercomparisons do not exist for regional models and only few studies compared selected models, for example, for forest regions (Coops et al. 2007, 2009). The applicability and performance of models may vary largely for different ecosystems, especially on a regional scale. Regional remote-sensing based models lack comparative analyses, especially for ecosystems with variable climatic conditions, such as semi-arid environments.

In this study, the performance of a LUE model and a SVAT model for regional NPP estimation in a study area in semi-arid Kazakhstan is compared. The first model is the Regional Biomass Model (RBM, Richters 2005a), a LUE model that was designed for semi-arid environments and is driven by MODIS data. It is based on the theory of Monteith (1972). The second model is the Biosphere Energy Transfer Hydrology Model (BETHY/DLR, Wißkirchen 2005), which is a more complex SVAT model that calculates NPP on a regional scale. It is driven by remote sensing and meteorological data.

The models are based on well-known established global NPP models, but have been modified for regional analysis based on remote-sensing data. They have recently been applied for several studies (Dokupil 2008, Machwitz 2010, Niklaus et al. 2010a,b, 2012, Richters 2006, Tum et al. 2011, 2012, Tum and Günther 2011). Both models do not need any driving variables from ground observations, but retrieve this information from satellite data. Thus, they can relatively easily be applied to new regions and offer a good choice for possible future studies. Therefore, the investigation of these two models is especially interesting.

The study by Dokupil (2008) included a comparsion of the two models for a test site in Namibia. Input data from different sensors were used, which were additionally pre-processed with differing methods. The evaluation of Dokupil showed that the unharmonized input data strongly influenced the results and affected the comparability. A conclusion about the impact of model characteristics on the results was hardly possible.

As the previous study revealed, harmonization of input data is indispensable for a reliable comparison. Therefore, in this study, RBM and BETHY/DLR were compared with input

parameters that were harmonized as far as possible. Both models have not yet been applied to Kazakhstan or Central Asia, so the objectives of this study were to analyse (i) if the remote-sensing-based models can be applied for NPP estimation in the study area, (ii) how they differ with respect to quantitative results, as well as seasonal patterns of NPP, and (iii) in conclusion, what the advantages and shortcomings of the two models are and how their performance could possibly be improved.

5.2 Study Area for Model Comparison

The study area in Central Kazakhstan was chosen for the model comparison, because it contains a representative profile of typical natural vegetation types, soils, and climatic conditions for semi-arid Kazakhstan (cf. chapter 3). The study area stretches between 46°–50°N and 72°–76°E and covers about 130,000 km² (cf. figure 5-1).

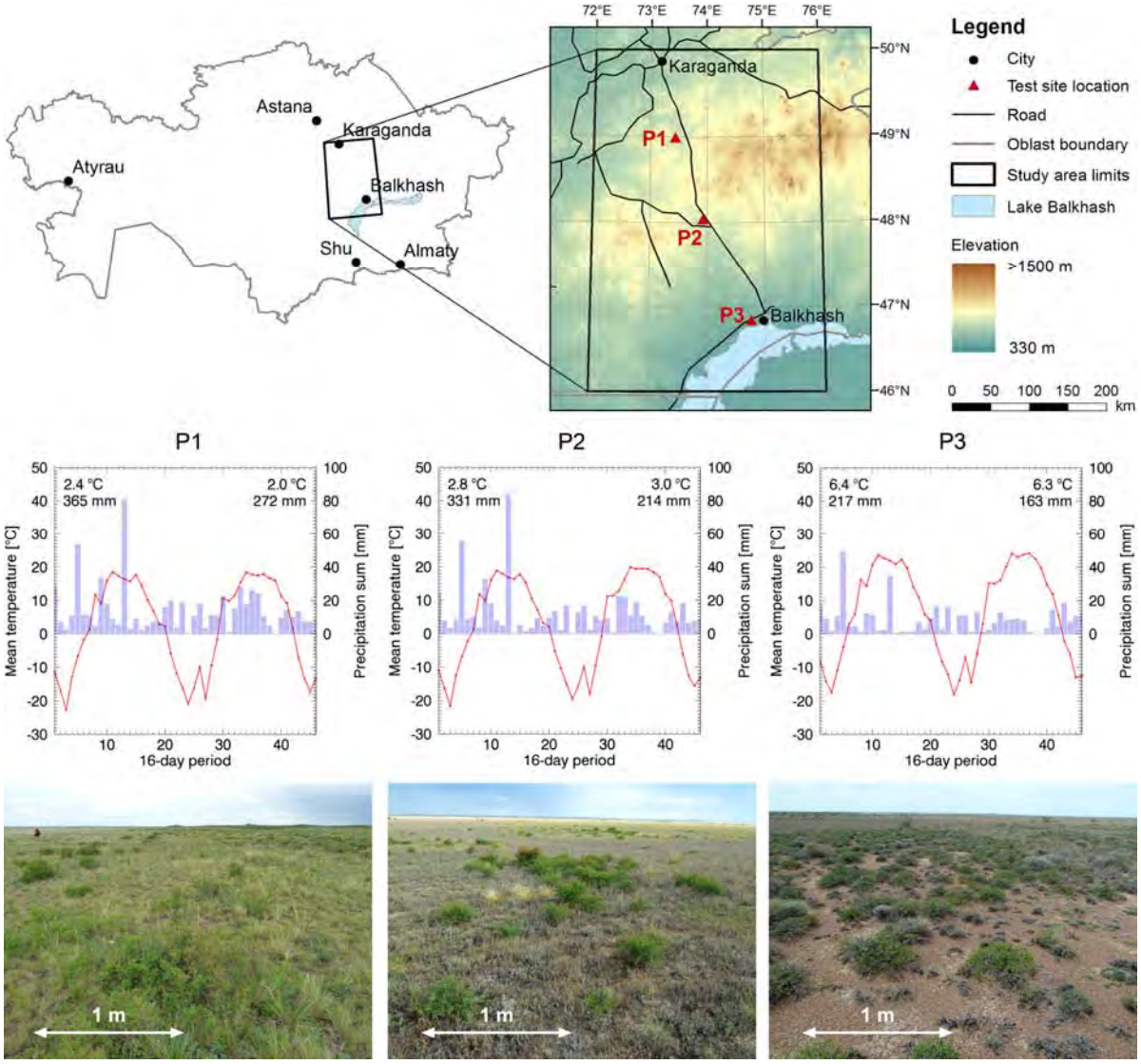

Figure 5-1: Location of the study area and the three exemplary test sites in Central Kazakhstan (above). Mean temperature and precipitation sum from ECMWF data for individual 16-day periods of 2010 and 2011 for the three test sites (mid); numbers in plots give the mean annual temperature and total annual precipitation for 2010 (left) and 2011 (right). Photographs of typical vegetation for the three test sites (below, photographs taken in June 2011).

The topography of the study area is described by large plains in the South and North-west. Hills and undulating terrain characterize the central eastern part. Dominant soil types are from North to South Kastanozem, Calcisol, and Gypsisol. Land cover gradually changes from steppe to semi desert vegetation. For comparison of intra-annual NPP patterns, three test sites were chosen (cf. figure 5-1) that represent different vegetation and climatic conditions. For more details on the study area, please refer to section 3.2.

5.3 Harmonization of Input Data

For a comparison of the two models, the following criteria are important:

- both models are run over the same study area and the same time period
- same spatial resolution for input data on LAI/LCC and FPAR
- same spatial resolution of model outputs
- same temporal resolution of model outputs
- for input data used within both models, same input data or derivatives from the same data source should be favoured.

Table 5-1: Input data, internal products and output products of the models RBM and BETHY/DLR.

Model	Variable input data (time series)	Annual or constant input data	Main intermediate products	Output
RBM	FPAR temperature water vapour cloud cover albedo emissivity	VCF soil type DEM	Potential PAR (PPAR) Actual PAR (APAR) PET Temperature stress Water stress Effective LUE	NPP
BETHY/DLR	LAI temperature precipitation cloud cover wind speed	LCC soil type DEM	PPAR APAR PET AET Stomatal conductance Water balance Soil respiration	GPP NPP NEP

Table 5-1 gives an overview of the input data needed for the two models, as well as intermediate products and output parameters. Both models need temperature data, so this dataset can be harmonized. From the daily ECMWF temperature data employed for BETHY/DLR, 16-day mean temperature datasets were calculated as input for the RBM. Further, cloud cover is used in both models to calculate actual PAR (APAR) from potential PAR (PPAR). To harmonize these parameters, first, another PAR calculation was introduced into RBM, which derives PAR according to the same approach used within BETHY/DLR. Second, the cloud-free APAR calculated within BETHY/DLR, based on ECMWF cloud data, was used as input for the RBM.

The LAI and FPAR data, which provide the vegetation phenology for BETHY/DLR and RBM respectively, were also harmonized. MODIS LAI was used as input dataset for BETHY/DLR for this study. The use of FPAR and LAI from the same sensor is expected to allow for a better comparability of the results, than if parameters derived from different sensors were used. The preprocessing of FPAR and LAI data was done completely identical, as described in section 4.1.2.1.

Moreover, the MODIS Land Cover Product was used as land cover information for BETHY/DLR instead of the GLC2000, to also base this information on MODIS data. Within BETHY/DLR, the land cover classes are translated to 33 model internal vegetation classes (cf. table 2-6). The model's parameterisation allows two vegetation types for each pixel. A weighting factor gives the relative importance of these vegetation classes. For the test site in Central Kazakhstan, five MODIS land cover classes are present. The BETHY/DLR internal classes used to translate these land cover classes are given in Table 5-2. The applied weighting factors were known based on fractional cover field estimations.

A modification of the parameterization was also necessary for the RBM. For this model, the most important parameter is the maximum LUE, a constant value applied for each vegetation type. For the study area in Central Kazakhstan, field-measured maximum LUE for grassland was available from Propastin et al. (2012). The observed maximum LUE of 0.72 g C MJ^{-1} was set as maximum LUE of herbaceous vegetation for this study. Maximum LUE for bare areas (0.15 g C MJ^{-1}) was taken from Richters (2005a) and for tree cover (0.962 g C MJ^{-1}) from Lagergren et al. 2005.

Table 5-2: Translation of MODIS land cover classes to BETHY/DLR vegetation types with weighting factors.

MODIS land cover class	BETHY/DLR vegetation types	Weighting factor
Grasses/Cereal crops	C_3 short grass Deciduous shrubs	0.7 0.3
Shrubs	Deciduous shrubs C_3 short grass	0.8 0.2
Savannah	Temperate broadleaved deciduous trees C_3 short grass	0.5 0.5
Evergreen needle leaf forest	Evergreen coniferous trees C_3 short grass	0.9 0.1
Non-vegetated	bare C_3 short grass	0.9 0.1

5.4 Results of the Model Comparison

5.4.1 Results of Comparison of Important Input Data and Intermediate Products

5.4.1.1 LAI and FPAR

LAI and FPAR are key input parameters and have a strong influence on the result. For BETHY/DLR, vegetation phenology is described by LAI, while RBM is based on FPAR. For a successful model comparison, these two datasets should be comparable in time and space, so that they do not produce major differences in NPP results.

To assess the temporal homogeneity, the behaviour of the two datasets over time was compared. The 16-day composite values for LAI and FPAR are displayed in figure 5-2. Both datasets show a similar behaviour over the year. In the northern and central test plots both feature peaks around composites 10 and 15 in 2010 and one major peak around composite 33 in 2011. In the last third of the year, the FPAR values show another peak, especially in the southern plot, which is not present in the LAI data. This, however, does not affect the NPP results significantly, because the growing season ends in September (around time-steps 17 and

40). Both datasets also equally picture the decreasing vegetation cover and density from the northern to the southern part of the study region.

The correlation between LAI and FPAR over the whole study area is also important, because the two datasets have to agree over space as well. For the individual 16-day composites, correlation coefficients vary between 0.68 and 0.95 (cf. figure 5-3). The mean correlation for the 46 composites of 2010 and 2011 is with R^2 of 0.86 very high. Because of the similar behaviour over time and the high correlation over the study area, it can be concluded, that these datasets are comparable and do not affect the comparability of the model results significantly.

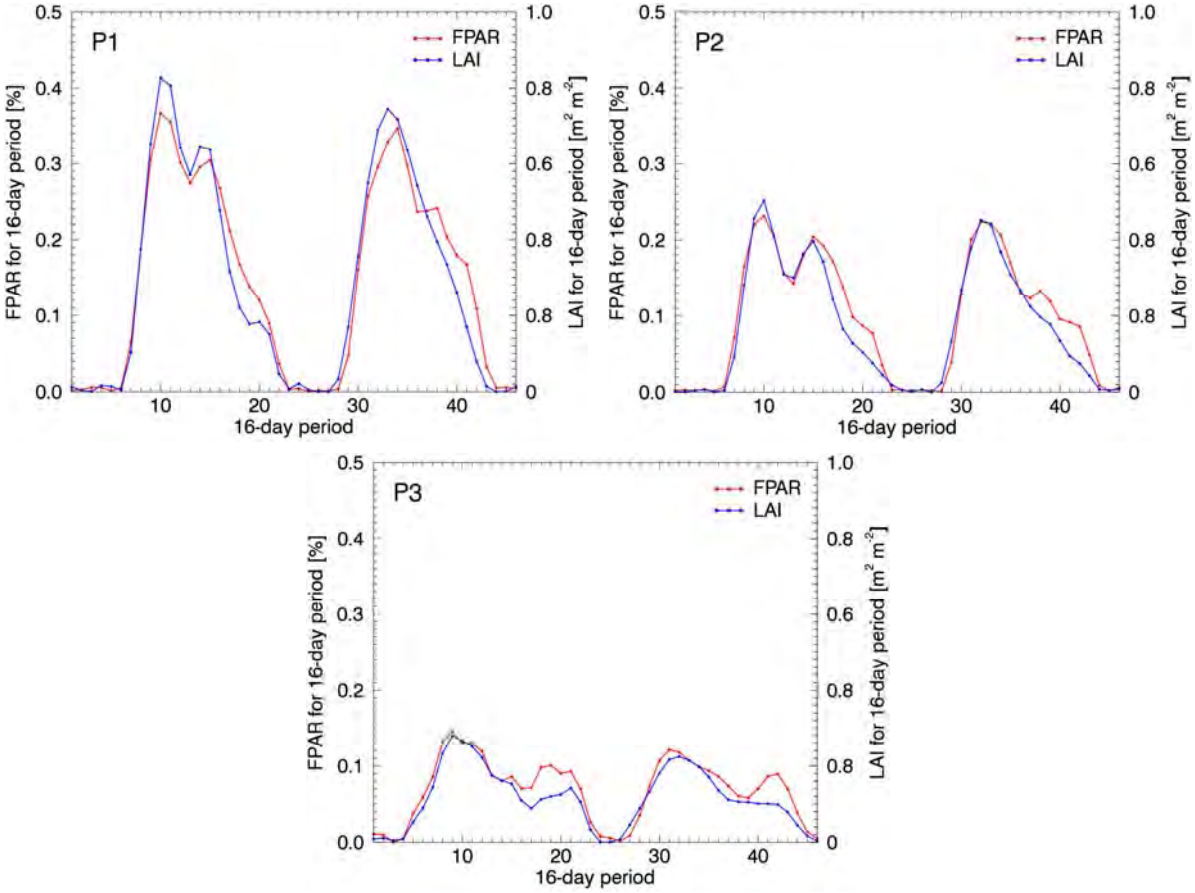

Figure 5-2: Comparison of the pre-processed input data of FPAR and LAI for the individual 16-day composites of 2010 and 2011 for the three test sites.

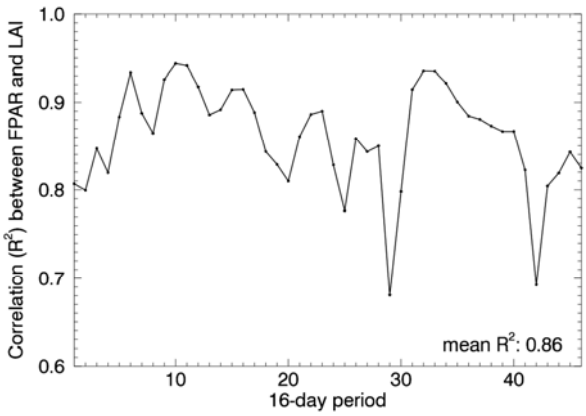

Figure 5-3: Correlation coefficients between the pre-processed input datasets of FPAR and LAI for the individual 16-day composites of 2010 and 2011. Each value gives the average correlation coefficient derived from all vegetated pixels within the study area for the given composite.

5.4.1.2 Potential and Actual PAR

Figure 5-4 displays mean daily sums of PPAR and APAR for 16-day periods of 2010 and 2011. The curves for PPAR are identical, because the formulations for PPAR calculation were harmonized. Differences in APAR mirror the differences in cloud coverage derived from MODIS data within RBM and from ECMWF data with BETHY/DLR. Generally, BETHY/DLR APAR is lower in the North than in the South of the test site. The opposite can be observed for RBM APAR. In the first two-thirds of the year, both for 2010 and for 2011, RBM APAR is higher than BETHY/DLR APAR. In the middle of the growing season, differences are especially significant for the northern and central test site at time steps 11 and 13 in 2010 and 34 and 36 in 2011. In the last third of the year, the resulting APAR is relatively similar with higher values for RBM APAR towards the end of each year. As the differences in APAR are quite significant, especially during the growing season, APAR has also been harmonized for the model comparison by using BETHY/DLR APAR as input for the RBM.

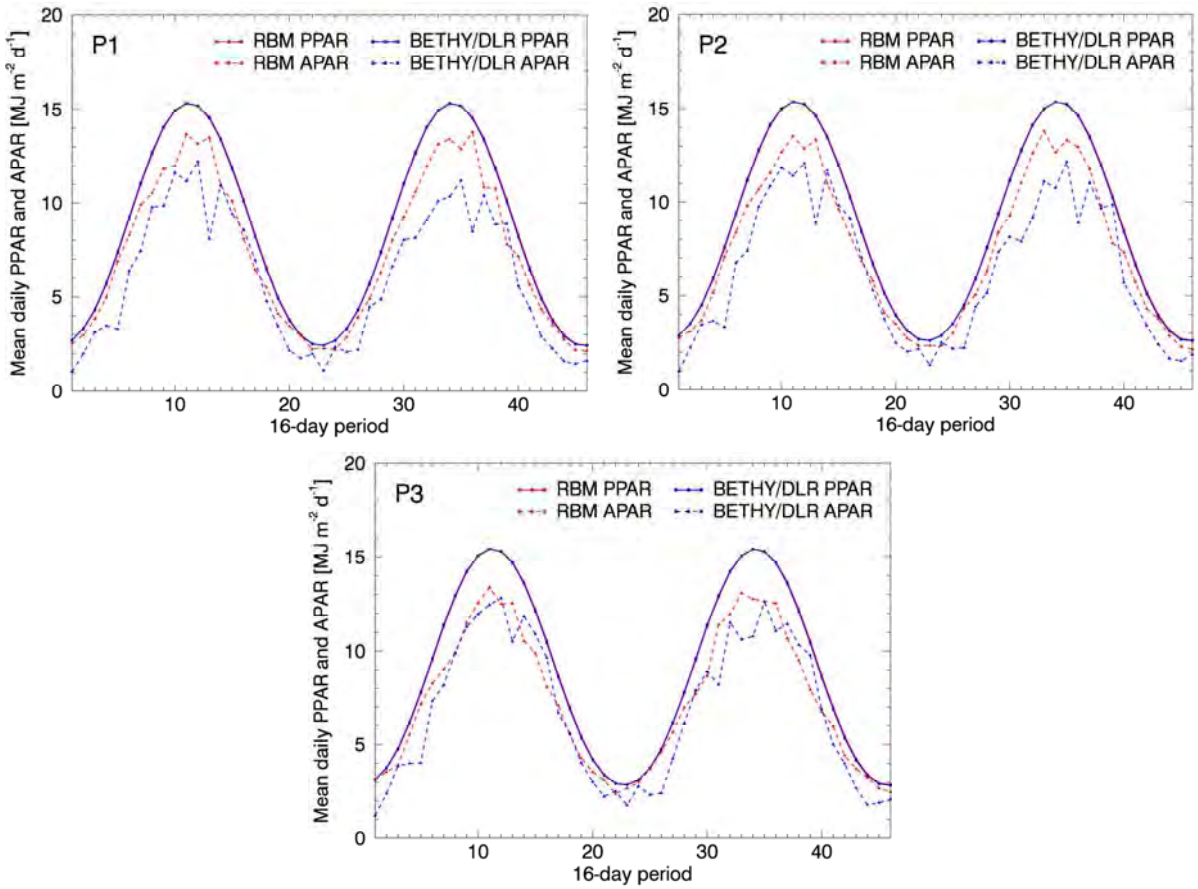

Figure 5-4: Comparison of mean daily PPAR and APAR calculated with RBM based on MODIS cloud cover and BETHY/DLR based on ECMWF data for the individual 16-day periods of 2010 and 2011 for the three test sites.

5.4.1.3 Potential and Actual Evapotranspiration

PET and AET have a strong influence on water stress in RBM and water balance in BETHY/DLR. Figure 5-5 shows PET and AET, calculated within the two models. Both PETs are similar for the beginning and very end of the growing season. For the mid to end of the growing season, BETHY/DLR PET is significantly higher. At time steps 13 in 2010 and 36 in

2011, BETHY/DLR PET features a significant depression. RBM PET rises and declines earlier in the year and does not change very much for the three test sites, while BETHY/DLR PET is significantly higher in the South than in the North of the study area. Consequently, also the PET difference between the two models gets bigger towards the South.

BETHY/DLR AET is higher than RBM AET for the whole growing season. Only in winter, RBM AET exceeds BETHY/DLR AET. Maximum daily AET rates reach between 1.6 mm and 2 mm for RBM (based on MODIS water vapour product). Maximum daily AET calculated within BETHY/DLR is higher with maximum rates in between 3.7 mm and 2.8 mm.

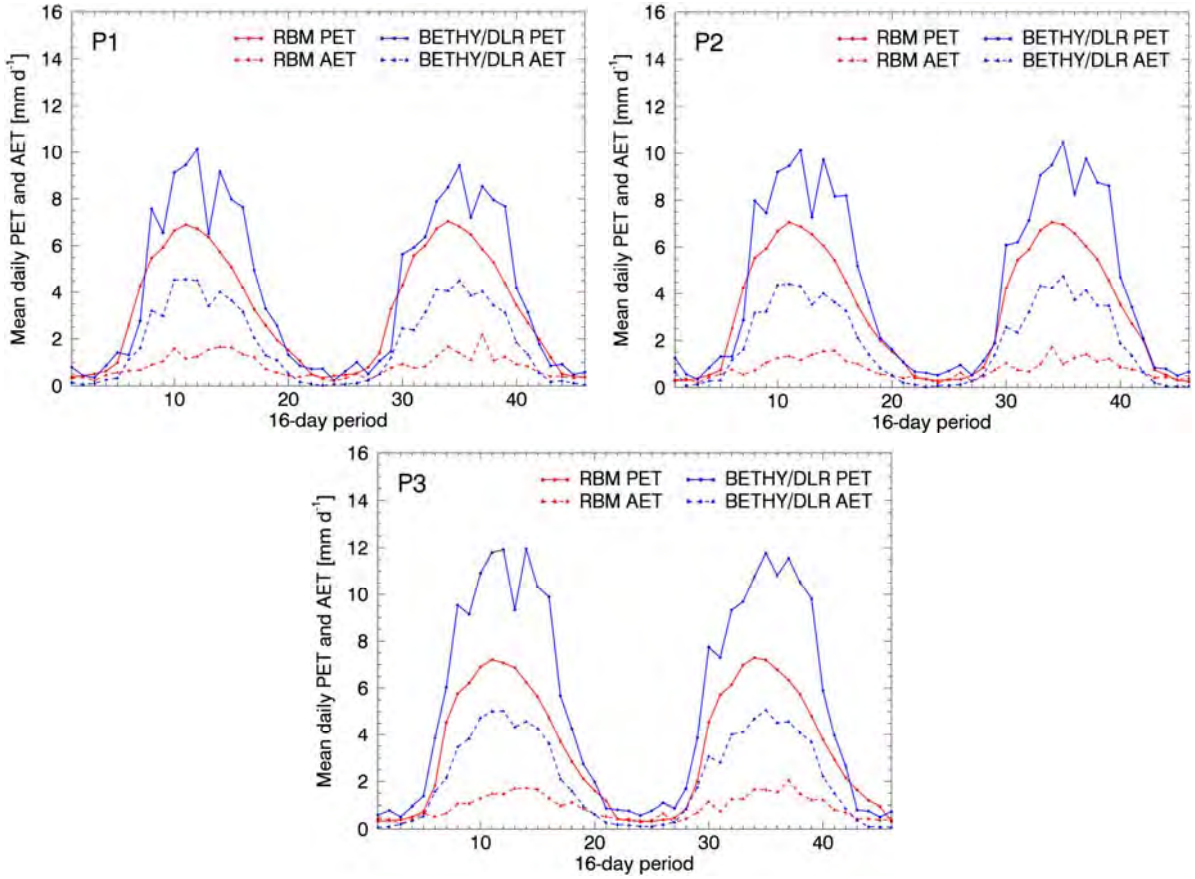

Figure 5-5: Comparison of mean daily PET and AET calculated with RBM (for AET MODIS water vapour data are used) and BETHY/DLR for the individual 16-day periods of 2010 and 2011 for the three test sites.

5.4.2 Results of Comparison of NPP Estimates

Both models were applied to calculate NPP from the harmonized input data at a spatial resolution of 928 m and ~0.00833° respectively. With RBM, NPP is calculated in 16-day intervals and summed up to annual NPP. BETHY/DLR calculates NPP on a daily basis. The daily data were summed up to 16-day composites for comparison with RBM and to annual NPP.

The results of NPP modelling for 2011 are shown in figure 5-6. This figure presents the annual sum of NPP of the two models calculated with the harmonized input data. Though results from BETHY/DLR are considerably higher, both results agree regarding the spatial distribution of biomass production. Both models calculate very high NPP for the small forest in the North-east of the study region, with NPP values greater than 250 g C m^{-2}. High NPP values can also be observed for the hilly regions in the North and North-east, south of Lake Balkhash,

and in river valleys, such as along River Tokrau in the central eastern part of the study area. A gradient from higher NPP in the North to lower NPP in the South is visible for both models. This gradient is also illustrated in figure 5-7, which shows the NPP values along a transect line that follows the 74°E longitude from North to South. BETHY/DLR models NPP values around 145 g C m^{-2} in the North and 70 g C m^{-2} in the South, while RBM models about 95 g C m^{-2} in the North and 10-20 g C m^{-2} in the South. The values along the transect also show that major peaks are present in both results. These peaks correspond to the relatively darker areas in figure 5-6, which clearly show a similar pattern.

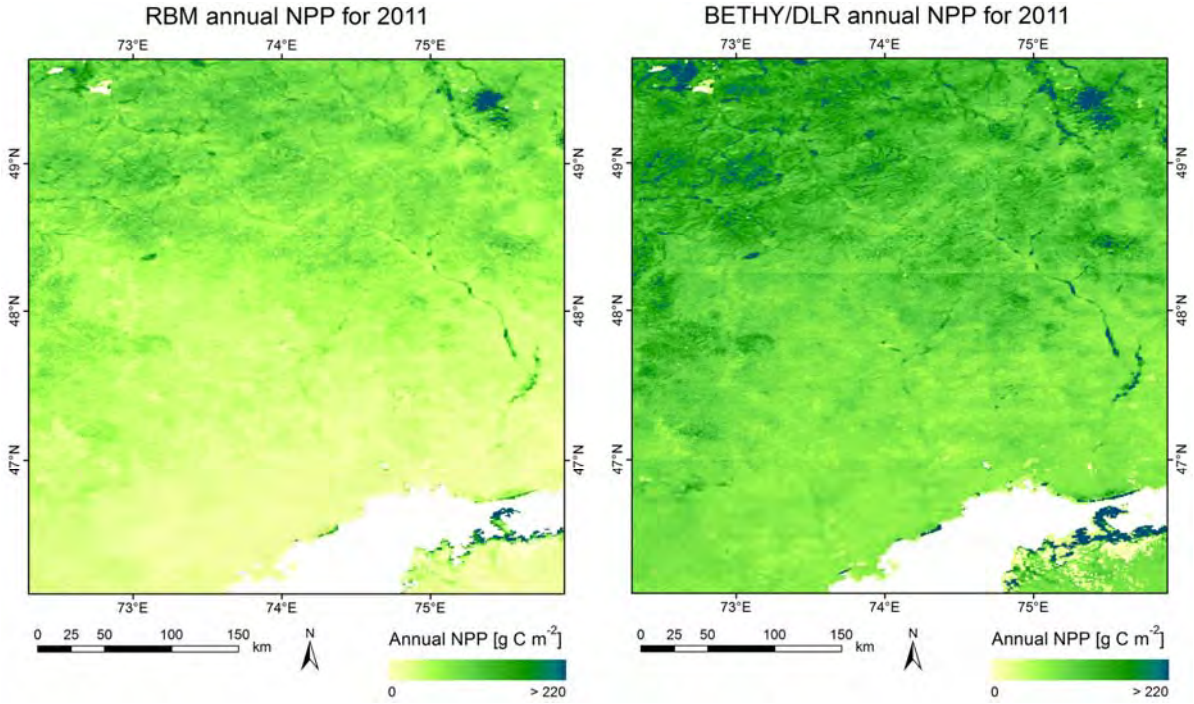

Figure 5-6: Annual NPP [g C m^{-2}] for 2011 for the study area in Central Kazakhstan modelled with the RBM (left) and BETHY/DLR (right).

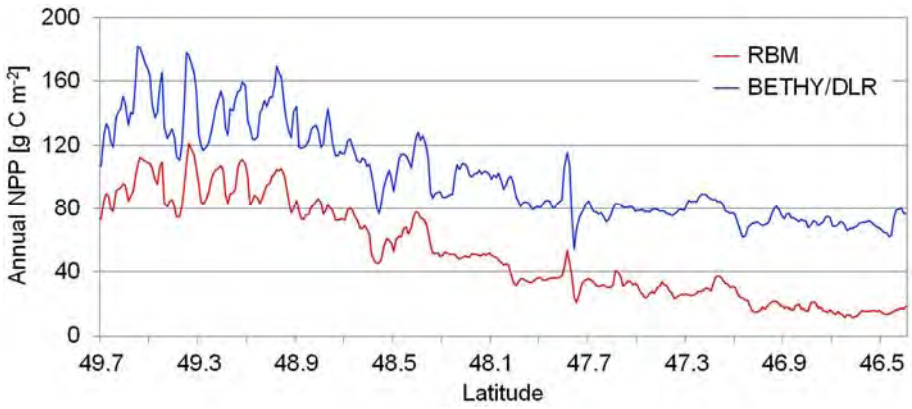

Figure 5-7: Annual NPP values [g C m^{-2}] modelled with the RBM (red) and BETHY/DLR (blue) for 2011 along the transect line at 74°E from North to South between 49.7°N and 46.4°N.

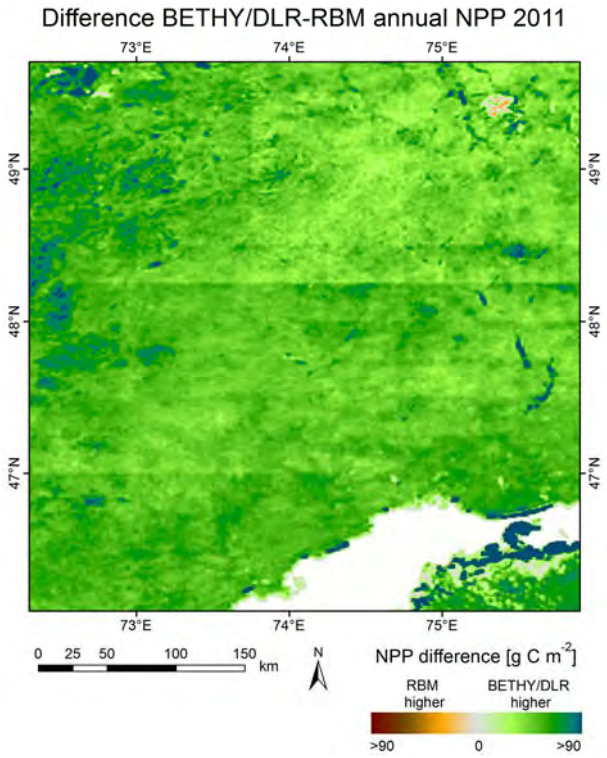

Figure 5-8: Difference between the annual NPP [g C m^{-2}] calculated with BETHY/DLR and RBM for 2011 for the study area in Central Kazakhstan.

Figure 5-8 presents the difference image for the annual NPP for 2011 from BETHY/DLR and RBM. Annual NPP from BETHY/DLR is higher than NPP from RBM for almost the entire study area. At average, this difference is about 52 g C m^{-2} for the study region. Figure 5-8 shows that the difference between the results is not constant, but reaches, for example, higher values in the north-eastern part of the study region. Relatively high differences, of about 60–70 g C m^{-2} are also noticeable within patches north of Lake Balkhash. These areas coincide with patches of low herbaceous vegetation cover in the VCF dataset. Strongest differences can be observed south of Lake Balkhash, where BETHY/DLR models much higher NPP than RBM. This area is mainly classified as forest in the land cover dataset used for BETHY, but contains only low tree cover in the VCF dataset. For the small forest area in the North-east of the study region, annual NPP from both models is similar and partly RBM results are even higher.

Figure 5-9 (left) displays the scatterplot of modelled annual NPP for 2011. All pixels within the study area with annual NPP>0 for both models are shown. Thus, water bodies and pixels, for which one model did not calculate NPP, are excluded. The frequency distribution of NPP values further helps to analyse the model results. Figure 5-9 (right) displays the frequency distribution of annual NPP in intervals of 1 g C m^{-2} computed over the study area for 2011.

The results of the two models show a high correlation with R=0.83. The slope of the linear correlation is almost 1, but the intercept is 52 g C m^{-2}. A change in slope is visible towards higher NPP. For RBM NPP values <50, the slope is 0.73 with an intercept of 62 g C m^{-2}, for RBM NPP values >50 slope and intercept are 1.2 and 38 g C m^{-2} respectively. RBM calculates a large number of pixels with annual NPP lower than 40 g C m^{-2}, while BETHY/DLR models only few pixels lower than 40 g C m^{-2}. On the other hand, BETHY/DLR results in significantly more pixels with annual NPP greater than 100 g C m^{-2}. Both frequency distributions feature a non-normal distribution. A peak at the beginning of each respective range of values is especially noticeable.

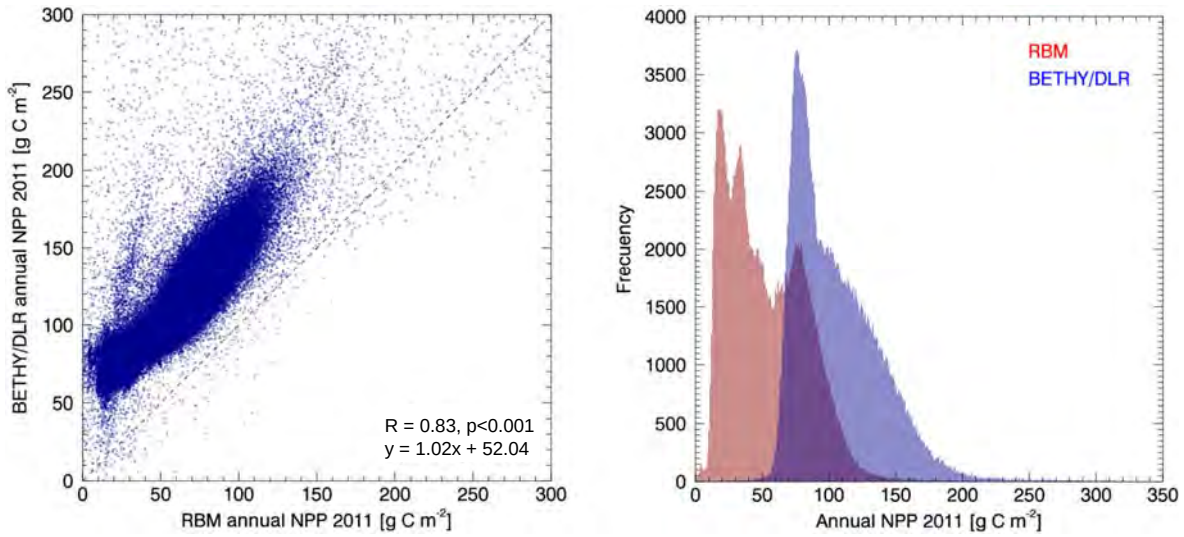

Figure 5-9: Comparison of annual NPP for 2011 (left) modelled with RBM (x-axis) and BETHY/DLR (y-axis). All pixels within the study area for which both results were >0 were considered. Frequency distribution of annual NPP values calculated with RBM and BETHY/DLR for 2011 (right).

Figure 5-10 shows the development of calculated NPP for the 16-day periods of 2010 and 2011. The vegetation period is clearly visible in both results and the beginning of biomass production agrees very well. The onset of biomass production lies between time steps 6 and 7 at the northern plot, between time steps 5 and 7 at the middle plot and between 5 and 6 at the southern plot.

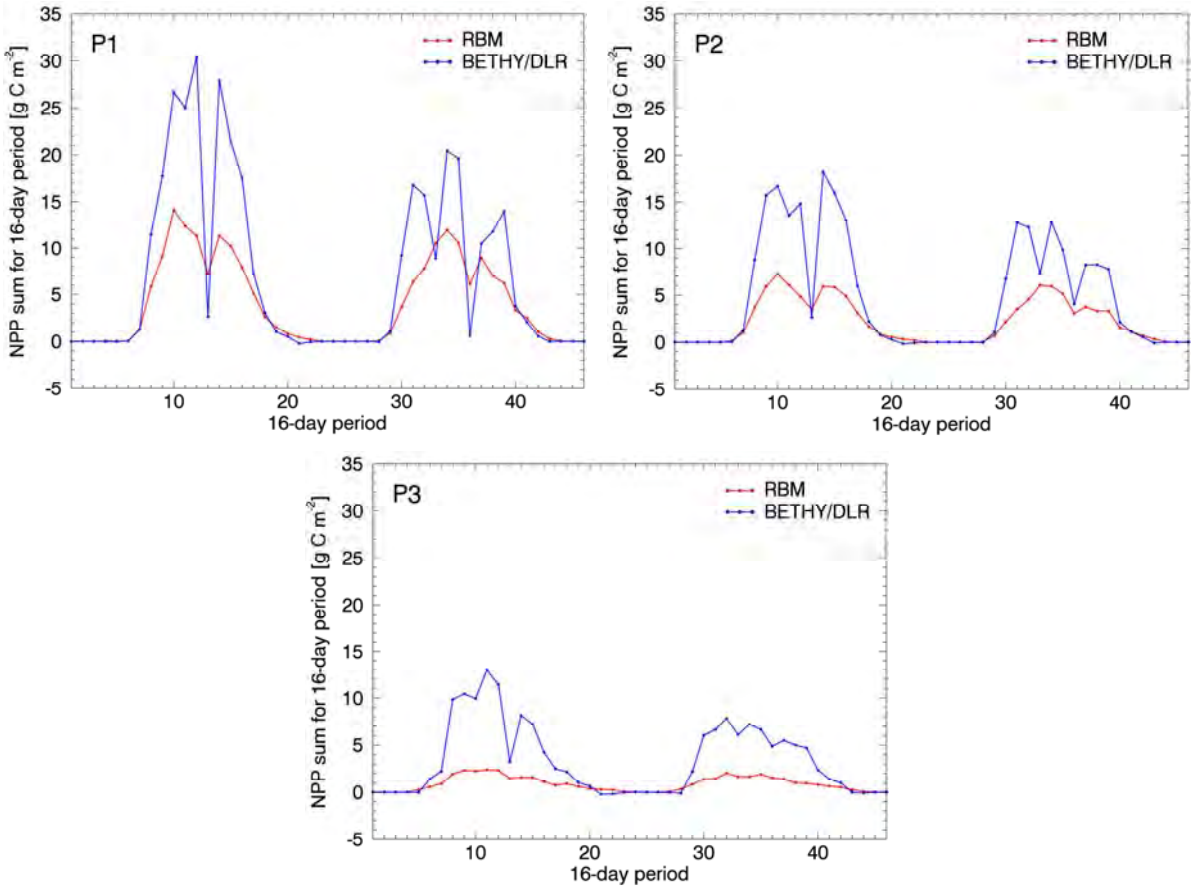

Figure 5-10: Comparison of the NPP results of RBM and BETHY/DLR for the individual 16-day periods of 2010 and 2011 for the three test sites.

The modelled NPP is in general higher for BETHY/DLR. Recessions in the vegetation period occur at time steps 13 (July 12–28) in 2010, 33 (May 25 – June 9) and 36 (July 12–28) in 2011. The two major recessions are present in both model results (cf. figure 5-10), but are stronger for BETHY/DLR. The minor recession (time step 33) is only present in BETHY/DLR results. RBM still calculates positive biomass production in November and December (time steps 20–23). BETHY/DLR does not calculate biomass production in this period, but slightly negative NPP. The difference between the two years is not very strong for RBM, but NPP in 2010 is clearly higher than in 2011 for BETHY/DLR.

5.5 Results of Evaluation and Validation with Field Data

To analyse how well the two models performed, it is desirable to give a quantitative evaluation of the results. Unfortunately, validation with flux tower measurements is not possible as no flux tower is available in the study area. Therefore, the outcomes of the two models are first compared with NPP estimates from other studies. Second, they are validated against field measurements from the study area collected in 2010 and 2011.

5.5.1 Comparison with NPP Estimates from Other Studies

A first evaluation of the results can be approached via comparison with NPP estimates from other studies. Propastin et al. (2012) estimated annual NPP in Central Kazakhstan for 2004 using a LUE model based on remote sensing, field data and meteorological data. Their study region (48°20'–49°30' N and 72°–74°10' E) covers the north-western part of our study area. Mean annual NPP retrieved from a Sea-viewing Wide Field-of-view Sensor (SeaWiFS) simulation was 168 g C m^{-2}. Field measured NPP in 2004 was at average 152 g C m^{-2} (Propastin et al. 2012).

For the comparison with the estimates from Propastin et al. (2012), mean annual NPP is calculated for all valid pixels (i.e. NPP>0 for both models) within the study area, as well as for four latitudinal zones from North to South. The mean annual NPP values calculated for RBM and BETHY/DLR are given in table 5-3. The NPP values derived for the two zones north of 48°N can be compared to the estimates from (Propastin et al. 2012). The results from BETHY/DLR (113.3–176.5 g C m^{-2}) are in the same range, while the RBM results (62.5–94.3 g C m^{-2}) are significantly lower.

Table 5-3: Mean annual NPP from RBM and BETHY/DLR for 2010 and 2011 as well as the corresponding standard deviations for the whole study area and four latitudinal zones.

	RBM				**BETHY/DLR**			
Area	Mean annual NPP [g C m^{-2}]		Standard deviation [g C m^{-2}]		Mean annual NPP [g C m^{-2}]		Standard deviation [g C m^{-2}]	
	2010	2011	2010	2011	2010	2011	2010	2011
Whole study area	62.14	54.61	33.34	32.69	136.87	106.69	50.25	41.80
49°N – 50°N	94.30	90.54	26.49	25.74	176.54	139.89	44.53	36.10
48°N – 49°N	76.13	62.50	18.77	18.22	157.85	113.27	35.41	26.01
47°N – 48°N	43.49	34.23	16.20	13.73	110.79	85.06	24.71	19.60
46°N – 47°N	26.93	25.89	24.66	27.40	92.42	85.22	46.97	56.81

A further study from Central Asia, in which annual NPP was estimated, obtained values in the range 126–326 g C m^{-2} for dry steppe and 90–310 g C m^{-2} for semi-desert (Propastin et al. 2012). Other studies from similar environments report comparable amounts. Yu et al. (2009), for example, estimated mean annual NPP values of 144.14 g C m^{-2} for open shrubland, 228.14 g C m^{-2} for grassland and 26.20 g C m^{-2} for sparse vegetation within East Asia, including eastern Kazakhstan. Feng et al. (2007) derived NPP over China and reported annual NPP values of 252.8 g C m^{-2} for deciduous shrubland, 122.6 g C m^{-2} for grassland and 14.3 g C m^{-2} for barren areas. These values are consistent with the results obtained with BETHY/DLR. The results from RBM are lower and reach only amounts comparable to the lowest values observed for dry steppe.

5.5.2 Validation with Field Data

For the validation of the NPP estimates, field data are available from seven test sites in Central Kazakhstan (cf. section 4.3.3). To make the model results comparable to the field data some conversions have to be applied to obtain data of the same quantity.

First, cumulative NPP is calculated from beginning of 2011 until the period of field data collection. The field data in the study area Central Kazakhstan were sampled between 8th June and 13th June 2011. As the smallest time step for RBM is 16 days, NPP sums for the period 1st January (DOY 1) to 9th June 2011 (DOY 160) were calculated for comparison with the field data.

The modelled NPP so far describes the whole biomass production. Therefore, the below-ground part has to be subtracted to obtain above-ground NPP. In a previous study by Propastin et al. (2012), the belowground NPP in the study area Central Kazakhstan was observed to be 23% of total NPP. As the measurements from Propastin et al. (2012) were taken from a region within the study area for model comparison of this study, the value reported by them was applied here to derive above-ground NPP.

One further conversion is necessary, because the MODIS land cover product as well as the MODIS fractional cover product do not distinguish between herbaceous and shrub cover but classify all vegetation in the test sites in Central Kazakhstan as herbaceous (grass/herb) vegetation. Based on these data the models cannot model shrub NPP. Therefore, only grass/herb biomass was considered for the comparison between field data and model results. The field data were sampled separately for shrubs and grass/herbs and also fractional cover was recorded. This fractional cover information was applied to scale down the modelled NPP to the fraction that was actually covered by grass/herbs.

The results of the modelled NPP and field measured carbon gains for the test sites in Central Kazakhstan are given in figure 5-11. Ground-based NPP amounts were higher for northern plots and lower for southern plots, representing the vegetation cover transition from steppe to semi-desert. In the South of the study area the growth of grass/herb biomass observed in the field reaches amounts of 8.7 to 15.2 g C m^{-2}, while in the North 43.5 to 54.6 g C m^{-2} were measured. For all test sites, modelled NPP from RBM is significantly lower than the carbon gain calculated from field data. BETHY/DLR results are closer to the field observations, with best results for the southern plots and higher differences for the northern plots. The results of both models are highly correlated to the field data with R^2 of 0.98 for RBM and R^2 of 0.95 for BETHY/DLR, but the slope of the regression line is closer to 1 and the average RMSE significantly lower for BETHY/DLR (cf. figure 5-11).

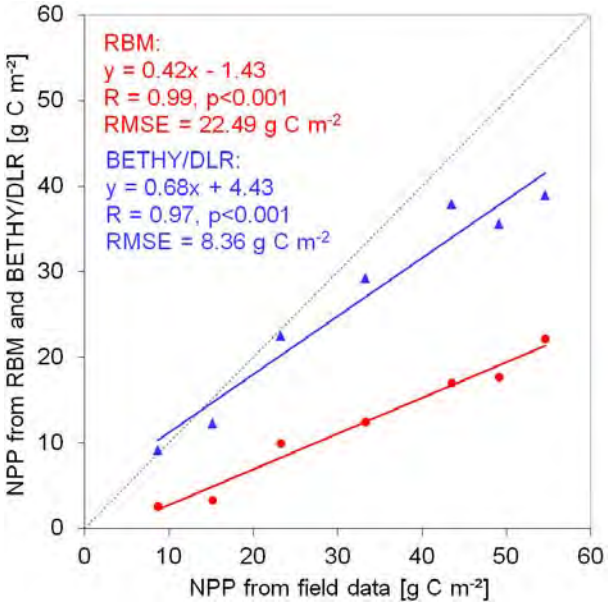

Figure 5-11: Correlation between the NPP of above-ground grass/herb vegetation derived from field data and the results of above-ground grass NPP from RBM and BETHY/DLR for DOY 1–160 in 2011 for seven test sites in Central Kazakhstan.

5.6 Discussion

In the previous section, the results of the comparison between NPP derived with RBM and BETHY/DLR were described as well as validation results presented. Major results and observed differences as well as possible explanations are discussed in the following.

For this comparison study, input data were made as similar as possible. FPAR and LAI, which cannot be substituted and provide important phenological information, were separately analysed and found to be comparable, so that they do not affect the comparability of the model results. This input data harmonization and analysis is an essential prerequisite for the comparison of the models' characteristics.

In general, the phenological development is well presented by both models. Both describe an earlier onset of biomass production in the South than in the North (figure 5-10). This is reasonable, as the onset of vegetation growth is strongly influenced by temperature that rises earlier in the southern part of the test site (cf. figure 5-1).

The recessions that were observed in the mid of the growing season (figure 5-10) can be explained by a combination of input parameters for these time-steps, such as low APAR (cf. figure 5-4) and decreased LAI and FPAR (figure 5-2). In BETHY/DLR the reduction is enhanced by factors dependent on temperature and available soil water. The less pronounced decrease for RBM might be caused by a lower influence of the reducing parameters due to model setup. Further, not all of the parameters lowering BETHY/DLR results are considered in the RBM. Most important, precipitation is no input parameter and water vapour used to define AET might not originate from the study area. MODIS water vapour data might also not fully represent precipitation, as precipitation in Central Asia is associated with both convective rainfall and westerly cyclones (Lioubimtseva et al. 2005, Tarasov et al. 1997). Additionally, the use of 16-day composites is likely to result in an attenuation of extreme events, for example lowering maximum temperatures. The vegetation growth can be expected to show a period of semi-dormancy due to drought and high temperatures in mid-summer. A decrease in vegetation

growth during July and early August is common in the study area and was also observed by Propastin and Kappas (2009).

The calculation of positive biomass production with RBM in November and December is not reasonable, due to temperatures below zero and common snow cover at this time of year. The positive NPP in early winter from RBM is caused by non-zero FPAR values. This could be compensated for by a modification of the temperature stress calculation for temperatures below zero in the RBM. The slightly negative values derived with BETHY/DLR result from plant respiration. Negative NPP is common at the end of the vegetation period and during drought periods. RBM is not able to calculate negative NPP due to the approach of NPP calculation by scaling the product of APAR and PAR. BETHY/DLR, however, calculates NPP as the difference between GPP and autotrophic respiration and can thus also capture periods of carbon release from vegetation.

The differences between the two years under investigation were stronger for BETHY/DLR that indicated a reduction in NPP of 22% for 2011 compared to 2010 (table 5-3). A reduction can be expected due to much lower precipitation amounts (cf. figure 5-1). RBM results showed a reduction of only 12% (table 5-3). This leads to the conclusion that BETHY/DLR seems to react more strongly to inter-annual variations in climatic conditions than RBM. The lower difference for RBM might be caused by the limited influence of temperature and water stress on NPP (cf. equations 2-9 and 2-10). The NPP time-series calculated with RBM also follows mainly the FPAR input data, while BETHY/DLR results differ considerably for single time-steps (figures 5-2 and 5-10). This responses indicate that meteorological conditions have a stronger influence on NPP calculation in BETHY/DLR than in RBM. For RBM, FPAR is the main driving parameter for NPP prediction and might lower the response to interannual variability and drought periods, as light could be absorbed but not used in photosynthesis, such as with senescent leaves (Zhang et al. 2005).

For the validation field data collection, a stratified sampling approach with two sampling periods was applied. The additional measurements taken before the start of the growing season enable the calculation of the amount of biomass that has grown in the current vegetation period until the date of the second field measurements. This double-sampling approach was used, because the two models under investigation do not include senescence and biomass carried over from the previous year. The suggested approach is an improvement with regard to the commonly applied peak biomass measurements with assumed complete plant mortality (Scurlock et al. 2002). It allows consideration of both perennial and ephemeral vegetation, which are typically present in natural arid and semi-arid environments.

The deviations between modelled NPP and field derived NPP might be caused by uncertainties of the input data. Uncertainties in the meteorological input data, for example, may influence estimated NPP (Zhao et al. 2006). For Kazakhstan, the ECWMF data were validated with available climate station data from the National Climatic Data Center (NCDC) of the National Oceanic and Atmospheric Administration (NOAA, see section 4.1.1.2). For the maximum temperature a mean correlation coefficient r of 0.97 was found. For precipitation the accuracy was lower with a correlation coefficient of 0.64 (cf. section 4.1.1.2). The temperature data, which were used for both models are thus very accurate, the precipitation data applied for BETHY/DLR, however, might add some uncertainty.

Another possible source of underestimated NPP is underestimated MODIS LAI and FPAR data. One reason for underestimated FPAR/LAI data might be cloud contamination, which is, however, not so strong for dryland regions (Zhao et al. 2005). MODIS LAI data have been validated for a grassland region in Central Kazakhstan by Kappas and Propastin (2012) and

their results showed an overestimation of LAI during the growing season by 10–15%. Thus, the FPAR/LAI data are probably not the cause for the low NPP results partly observed in this study.

The necessary MODIS parameters (e.g. albedo) for RBM are only available as 16-day composites. Without special pre-processing this limits the temporal resolution of modelled NPP with the current version of the model based on MODIS data. Meteorological input data for BETHY/DLR are available at a high temporal resolution. This high temporal resolution is a major advantage as different user demands can be satisfied and the effect of short-term weather conditions is considered. RBM based 16-day time steps might be too long to capture variable climatic conditions.

The validation with field data showed good results for BETHY/DLR, but comparatively low NPP values for the RBM. As all major input data were harmonized, this might be caused by model internal parameterizations. The major parameter that influences the results of the RBM is the LUE. The maximum LUE for herbaceous vegetation applied for this study was taken from Propastin et al. (2012), who estimated the maximum LUE based on field data from the study area in Central Kazakhstan. The value of 0.72 g C MJ^{-1} is well within the range of LUE values applied for grassland biomes in Central Asia and dryland regions (Propastin et al. 2012). The LUE from Propastin et al. (2012) is thus assumed to be a reliable source and to provide an optimum value for the study area.

The low NPP results might be caused by an additional scaling of the maximum LUE based on relief and soil parameters within the RBM, or by the fractional cover scaling. This, however, would indicate, that a higher maximum LUE had to be defined in the beginning, so that maximum LUE values published for Central Asian grassland biomes might not be suitable as input for the RBM.

Another important parameter within the RBM is water stress, which is calculated from AET and PET. For some time steps, AET from RBM is higher than PET (cf. figure 5-5). This may occur due to the independent derivation of these parameters, i.e. model internal calculation of PET and use of remote sensing based water vapour for AET. In the RBM, the resulting ratio between AET and PET, however, is limited to values between 0 and 1. The water stress factor is further limited to a range from 0.5 to 1 (cf. equation 2-10), so that the term takes 0.5, even when no water is available for evapotranspiration. This parameterization is identical to the water stress calculation in the original CASA model and reflects the observation that water stress already affects intercepted PAR (Potter et al. 1993).

The results from BETHY/DLR matched quite well the field data, but tended to underestimate higher NPP amounts. This might be caused by an insufficient representation of different vegetation cover in the MODIS land cover map, in which almost the entire study area is classified as grassland. In the current model version, BETHY/DLR assigns fixed fractional covers to each land cover class, so that the heterogeneity within land cover classes is not accounted for. A differentiation between closer vegetation cover in the North and more open vegetation in the South, as from a regional land cover product, would result in a regression line with a gradient closer to 1.

5.7 Conclusions

Two remote sensing based models for NPP calculation were applied in this study for a test site in Central Kazakhstan: RBM, a LUE model based on the theory of Monteith (1972), and BETHY/DLR, a SVAT model with a more complex description of the interactions between soil, vegetation and atmosphere. Both calculate NPP with a spatial resolution of about 1 km^2.

For this comparison study, the models were run with harmonized input data, which is an essential prerequisite for a sound model comparison. Additionally, not only NPP results but also intermediate products were included in the model comparison to have a complete basis for the analysis and interpretation of the results.

The field data for validation were derived using an approach that includes two sampling measurements, one before and one in the mid of the growing season. This approach is suitable for validation of models, which do not calculate senescence and biomass carried over from the previous year. It is further especially suggested for arid and semi-arid environments as it also captures perennial and ephemeral vegetation biomass.

The phenological development and spatial differences in NPP are presented well by both models, but BETHY/DLR predicts considerably higher NPP than RBM. Correlation coefficients obtained from comparison with field data were also very high for both models. The validation, however, showed that the RBM strongly underestimated the NPP. The parameterization of the LUE is most critical for the RBM, as it has a strong effect on model results. A higher LUE for herbaceous vegetation would countervail the underestimation, but disagree with published LUE values. For future application of the RBM in semi-arid Kazakhstan a special emphasis should be put on converting the available LUE data, under consideration of vegetation cover and soil aspects, to values applicable for the RBM. A modification of the temperature stress calculation within the RBM would help to deal with non-zero FPAR values in winter. A greenness index might additionally improve results at the end of season and during drought periods.

Further improvements of the RBM might be achieved by a higher temporal resolution of the meteorological input data. BETHY/DLR calculates NPP daily, while RBM is based on MODIS data with 16-day intervals. As this study indicated, 16-day time steps might be too long to capture the variable climatic conditions that are typical for semi-arid regions and attenuate extreme events. The higher temporal resolution of BETHY/DLR allows considering short-term climatic conditions. BETHY/DLR also reacts more strongly to inter-annual variations.

For BETHY/DLR the 8-day LAI time-series should also be favoured as input data. The results from BETHY/DLR further indicate that a more detailed land cover map is needed for regional studies. Global maps, such as the MODIS land cover map applied in this study, do not differentiate enough land cover types within the semi-arid environment. A land cover map that distinguishes more classes, or provides additional fractional cover information, would improve the results.

6 Spatio-temporal NPP Patterns for Kazakhstan and their Relation to Meteorological Parameters

The results of this chapter have been submitted for publication to the Journal of Arid Environments (Eisfelder et al. under review).

6.1 Introduction

Kazakhstan is a large country and faces extreme continental climatic conditions. The arid and semi-arid environments have experienced strong human impacts with dramatic ecological consequences (cf. section 1.2). Moreover, the vegetation is influenced by a changing climate and has to cope with increased annual and winter temperatures (Lioubimtseva et al. 2005). A shift to an earlier season has already been observed (de Beurs and Henebry 2004). Temperatures are expected to further increase 1–2°C by 2030–2050 (Lioubimtseva et al. 2005) and trends in precipitation are variable, but indicate an overall decrease. Consequently, aridity is expected to intensify (Lioubimtseva et al. 2009).

To understand possible effects of changing climatic conditions on the Kazakh environments, it is of great interest to observe spatial and temporal patterns of vegetation dynamics. Remote-sensing based modelling of NPP allows for analysing vegetation productivity of large areas. NPP time-series can additionally provide base information for analysing possible effects of changing meteorology on the vegetation in Kazakhstan. This information is valuable for identification of regions that are vulnerable to a possible climate change. It may also substantially support a sustainable land management.

In the previous chapter, the applicability of two remote-sensing based NPP models for Kazakhstan was analysed for a study area in Central Kazakhstan. The model BETHY/DLR proved to provide good results, but the usage of a more detailed land cover map was recommended. Therefore, in this chapter, the model BETHY/DLR was applied with a regional land cover map for NPP calculation for entire Kazakhstan.

The objectives of this study are (i) to present the results of mean annual and monthly NPP calculated with BETHY/DLR for Kazakhstan for the period 2003–2011, (ii) to locate areas with frequent NPP anomalies within the time period of interest, as well as areas of low and high NPP variability, and (iii) to analyse temporal correlation between NPP and meteorological parameters, and to compare deviations from mean NPP values with deviations in meteorological parameters.

6.2 BETHY/DLR Model Run and Data Used

The analyses performed for the study area in Central Kazakhstan (cf. chapter 5) showed that the MODIS land cover product, which was used to drive BETHY/DLR, did not differentiate sufficient vegetation classes within the semi-arid environment typical for Kazakhstan. Therefore, the Central Asia land cover and land use map was used as model input for the derivation of the 9-year NPP dynamics of Kazakhstan. This is a regional land cover map, which was derived by Klein et al. (2012, cf. section 4.1.3). Additionally, the MODIS LAI data were used with their highest temporal resolution to drive the model, i.e. as 8-day composites (cf. section 4.1.2.1). The other input data for BETHY/DLR were identical to the input data used for the test site in Central Kazakhstan as described in section 5.3.

As the NPP calculation with BETHY/DLR is based on specific biochemical parameters, the classes of the Central Asia land cover and land use map have to be translated to the model internal vegetation types (cf. table 2-6, section 2.2.2). The classes applied for translation as well as the weighting factors for the two complementing inherent vegetation classes are given in table 6-1. The classes and weighting factors were estimated based on the definitions of the land cover and land use classes, field observations, as well as – in the case of forests – from the fractional cover information of the MODIS VCF product. The weighting factors sum up to 1 because they describe the relative fraction of the two vegetation types. The actual vegetation coverage within a pixel is indirectly controlled by the LAI input data. For areas classified as artificial, ice and snow, and water bodies no NPP is calculated.

Table 6-1: Translation of land cover and land use classes from the the Central Asia land cover and land use map (Klein et al. 2012) to BETHY/DLR vegetation types with weighting factors.

Land cover and land use class	BETHY/DLR vegetation classes	Weighting factor	Number of BETHY/DLR class
Rain-fed agriculture	Arable crops	1.0	15
Irrigated agriculture	Arable crops	1.0	15
Needleleaved trees	Evergreen coniferous trees C_3 short grass	0.8 0.2	5 9
Broadleaved trees	Temperate broadleaved deciduous trees C_3 short grass	0.8 0.2	4 9
Sparse vegetation	Deciduous shrubs C_3 long grass	0.5 0.5	8 10
Grassland	C_3 long grass Deciduous shrubs	0.95 0.05	10 8
Closed shrubland	Deciduous shrubs C_3 short grass	0.8 0.2	8 9
Open shrubland	Deciduous shrubs C_3 short grass	0.65 0.35	8 9
Bare area	C_3 short grass Deciduous shrubs	0.5 0.5	9 8
Bare area with salt flats	C_3 short grass Deciduous shrubs	0.5 0.5	9 8
Artificial	-	-	-
Ice and snow	-	-	-
Water bodies	-	-	-

6.3 Calculation of Means, Deviations, Anomalies, and Variability

With BETHY/DLR, daily, monthly, and annual NPP for the period 2003 to 2011 was calculated. The NPP results as well as the meteorological data (temperature, PAR, precipitation) were used to calculate derivative datasets on monthly and annual basis, as common for analyses of time-series (e.g. Dietz et al. submitted, Gessner et al. 2012, Kuenzer et al. 2008, 2009).

6.3.1 Mean Monthly NPP and Mean Annual NPP

Mean monthly NPP was calculated from the monthly NPP data based on the 2003–2011 time-series. For every spatial location the monthly 9-year arithmetic mean ($\overline{NPP}_{x,y}$) was calculated using equation 6-1 with n being the number of years and $NPP_{x,y}$ the monthly NPP data of pixel x,y. Mean annual NPP was calculated similarly from the annual sums of NPP. Mean monthly climatic parameters (mean temperature, mean PAR, precipitation sum) were calculated respectively.

$$\overline{NPP}_{x,y} = \frac{1}{n}\sum_{1}^{n} NPP_{x,y} \tag{6-1}$$

6.3.2 Deviation from Mean Monthly NPP

The deviation of NPP ($DNPP_{x,y}$) for an individual month from the 2003–2011 mean monthly NPP is the basis for calculation of monthly anomalies. In comparison with the deviations of meteorological parameters, this information also allows to investigate the influence of meteorology on the calculated NPP. $DNPP_{x,y}$ at a given spatial location for a certain month is calculated according to equation 6-2.

$$DNPP_{x,y} = NPP_{x,y} - \overline{NPP}_{x,y} \tag{6-2}$$

Furthermore, the relative monthly NPP deviation ($rDNPP_{x,y}$) was derived, which describes the deviation as a percentage from the mean monthly NPP following equation 6-3. Areas for which $\overline{NPP}_{x,y}$ =0, for example water bodies, were excluded from the analysis. Monthly deviations of the climatic parameters were calculated respectively.

$$rDNPP_{x,y} = \frac{DNPP_{x,y} \cdot 100}{\overline{NPP}_{x,y}} \tag{6-3}$$

6.3.3 Monthly NPP Anomalies

In addition to NPP means and deviations, monthly NPP anomalies were derived. The term anomaly refers to the percentage deviation of monthly NPP ($rDNPP_{x,y}$) with respect to the 2003–2011 mean of all NPP values for that month. The case of an anomaly ($ANPP_{x,y}$) is defined when the NPP deviation is at least twice the mean standard deviation ($\overline{\sigma}$) for that month above or below the 9-year mean. The mean plus or minus two standard deviations corresponds to a 95% confidence interval. This is common for definition of significant anomalies (Schweiger 2008, Shackleton 1986, Vellinga and Wood 2002). The standard deviation of NPP deviations for each spatial location ($\sigma_{x,y}$), the mean standard deviation ($\overline{\sigma}$), and finally the anomaly of

NPP ($ANPP_{x,y}$) are calculated as given in equations 6-4 to 6-6, with n being the number of years and m the number of pixels.

$$\sigma_{x,y} = \sqrt{\frac{1}{n}\sum_{1}^{n}\left(rDNPP_{x,y}\right)^2} \tag{6-4}$$

$$\overline{\sigma} = \frac{1}{m}\sum_{1}^{m}\sigma_{x,y} \tag{6-5}$$

$$ANPP_{x,y} = \begin{cases} rDNPP_{x,y}, & \left|rDNPP_{x,y}\right| > 2\overline{\sigma} \\ 0, & otherwise \end{cases} \tag{6-6}$$

6.3.4 Mean NPP per Land Cover Class

Average mean annual NPP ($\overline{NPP}_{LC}$) of individual land cover classes and the standard deviation of mean annual NPP within these land cover classes were calculated according to equations 6-7 and 6-8 with m being the number of pixels for each land cover class and $\overline{NPP}$ being mean annual NPP.

$$\overline{NPP}_{LC} = \frac{1}{m}\sum_{1}^{m}\overline{NPP} \tag{6-7}$$

$$\sigma_{NPP,LC} = \sqrt{\frac{1}{m}\sum_{i=1}^{m}\left(NPP_i - \overline{NPP}\right)^2} \tag{6-8}$$

6.3.5 Annual NPP Variability

Mean annual NPP variability ($\overline{VNPP}$) is derived according to equation 6-9. It is based on relative annual NPP deviations ($rDNPP_{x,y}$), which are calculated from annual NPP sums and mean annual NPP, with n being the number of years as given in equations 6-1 to 6-3.

$$\overline{VNPP}_{x,y} = \frac{1}{n}\sum_{1}^{n}\left|rDNPP_{x,y}\right| \tag{6-9}$$

6.4 Results and Discussion

6.4.1 Spatial NPP Patterns

The mean annual NPP for Kazakhstan for 2003–2011 is illustrated in figure 6-1. Table 6-2 gives the average mean annual NPP values for individual land cover classes. The overall mean annual NPP for Kazakhstan was 143 g C m^{-2}. Highest mean annual NPP can be observed for irrigated agriculture (338 g C m^{-2}) located in southern Kazakhstan, for example along the Syr-Darya River and near the border to Kyrgyzstan (cf. figure 4-10). This is followed by forests (264 g C m^{-2}), which are mainly located in mountainous areas in the very East and South-east of Kazakhstan or along rivers. The rain-fed agricultural areas in the northern parts of Kazakhstan also show high mean annual NPP (225 g C m^{-2}). The natural and semi-natural vegetation classes

of closed shrubland, grassland, sparse vegetation, and open shrubland show lower average NPP values of 205 g C m^{-2}, 140 g C m^{-2}, 120 g C m^{-2}, and 112 g C m^{-2} respectively. Lowest NPP can be observed in the deserts in southern Kazakhstan, for example at the Tupyaraghan and Ustyurt Plateaus in the South-west, north and south of the lower reaches of the Syr-Darya River, and east of Almaty. These areas are mainly classified as bare area and have a very low vegetation cover (cf. section 4.1.3). Annual NPP over Kazakhstan sums up to a total of 543 Mt per year at average for 2003–2011.

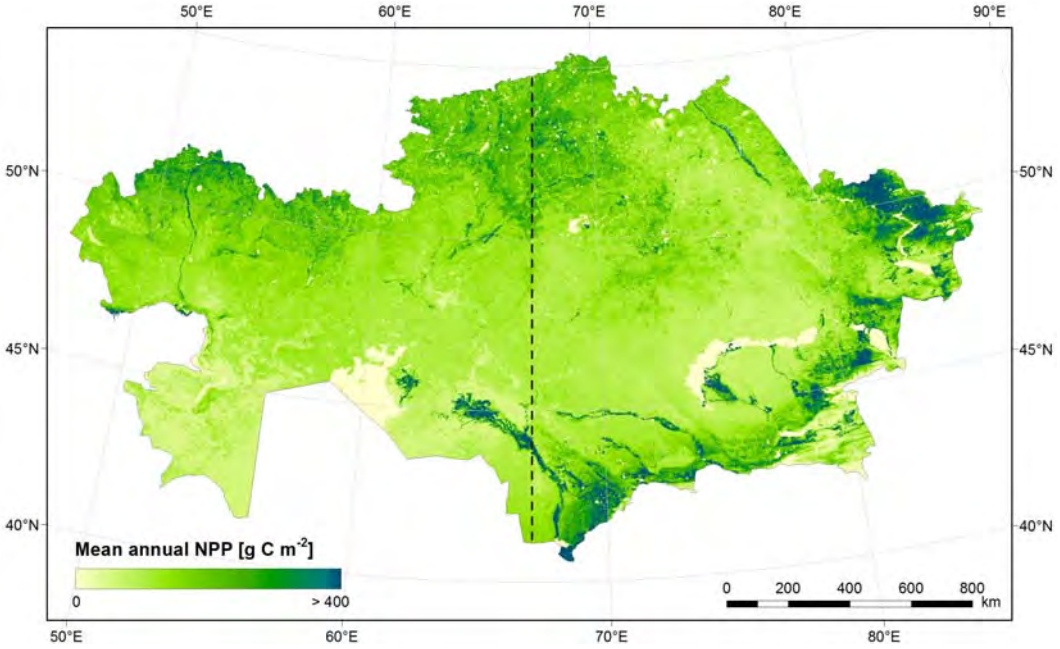

Figure 6-1: Mean annual NPP for Kazakhstan for 2003–2011. The dashed line shows the transect line along the 67°E longitude. For this transect line a profile of mean annual NPP for 2003–2011 is presented in figure 6-2 and dominant land cover classes in table 6-3.

Table 6-2: Average mean annual NPP for different land cover types for 2003–2011 and the standard deviation of mean annual NPP within the land cover classes. The percentages of the area of Kazakhstan were derived from the Central Asia land cover and land use map (Klein et al. 2012).

Class Name	% of area of Kazakhstan	Average mean annual NPP [g C m^{-2}]	σ [g C m^{-2}]	σ [%]
Irrigated agriculture	1.6	337.9	165.8	49.1
Broadleaved trees	1.3	264.1	164.1	62.1
Needleleaved trees	1.5	263.8	127.4	48.4
Rain-fed agriculture	10.7	224.5	72.6	32.3
Closed shrubland	1.5	205.1	115.2	56.2
Grassland	43.7	140.0	66.1	47.2
Sparse vegetation	13.8	119.9	44.5	37.1
Open shrubland	11.8	112.0	50.9	45.5
Bare area	4.2	73.0	43.7	59.9
Bare area with salt flats	4.0	65.4	25.9	39.6
Artificial, Ice and snow, Water	6.0	-	-	-

The standard deviation of mean annual NPP within the land cover classes are relatively high (table 6-2). This can be explained by the widespread distribution of the land cover classes over

Kazakhstan, which implies differences in conditions necessary for growth. Especially broadleaved trees and closed shrubland occur only in small spots at distant locations, which are characterized by significantly different climatic conditions (cf. figure 4-10 and section 3.2.2).

The most important natural land cover classes in Kazakhstan are grassland, sparse vegetation, and open shrubland. These three classes together cover 69.3% of the country. The NPP values calculated with BETHY/DLR for these classes correspond well to productivities published in other studies. Propastin et al. (2012), for example, estimated annual NPP in Central Kazakhstan with a light use efficiency model for 2004. The mean annual NPP obtained for the steppe grassland area was 168 g C m^{-2}. Field measured NPP was 131 g C m^{-2} for short grassland and 145 g C m^{-2} for dry steppe (Propastin et al. 2012). This is very close to our result of 140 g C m^{-2}. Further studies from Central Asia (Fartuschina 1986, Makarowa 1971, Perschina and Yakovlewa 1960, Robinson et al. 2002, Tyurmenco 1975), as summarized by Propastin et al. (2012), reported annual NPP values in the range 126–326 g C m^{-2} for dry steppe and 90–310 g C m^{-2} for semi-desert. In comparison, the results from this study are within the the lower part of these ranges.

Further studies from similar environments also report comparable amounts. Yu et al. (2009), for example, estimated mean annual NPP values of 144.1 g C m^{-2} for open shrubland, 228.1 g C m^{-2} for grassland, and 26.2 g C m^{-2} for sparse vegetation within East Asia, including eastern Kazakhstan. The result for open shrubland is very close to our result of 112 g C m^{-2}. For sparse vegetation, their results are lower. This can be explained by the different land cover map used in their study, which did not separate bare areas. NPP values obtained by Yu et al. (2009) for needleleaved forest (298–330 g C m^{-2}) and closed shrubland (266 g C m^{-2}) are also close to our results. For broadleaved forest (568 g C m^{-2}) and cropland (524.7 g C m^{-2}) they obtained higher values, which may be caused by different species and agricultural systems in East Asia. Feng et al. (2007) derived NPP for China and reported annual NPP values of 252.8 g C m^{-2} for deciduous shrubland, 122.6 g C m^{-2} for grassland and 14.3 g C m^{-2} for barren areas. These values are also consistent with the results obtained in this study (table 6-2).

As the vegetation in Kazakhstan is characterized by a typical north-south gradient (cf. figure 4-10 and section 3.2.4), a transect line along the 67°E longitude (shown in figure 6-1) was chosen to illustrate typical NPP for selected latitudinal zones. The mean annual NPP along the transect line is shown in figure 6-2. Additional information on dominant land cover classes for the latitudinal zones is provided in table 6-3.

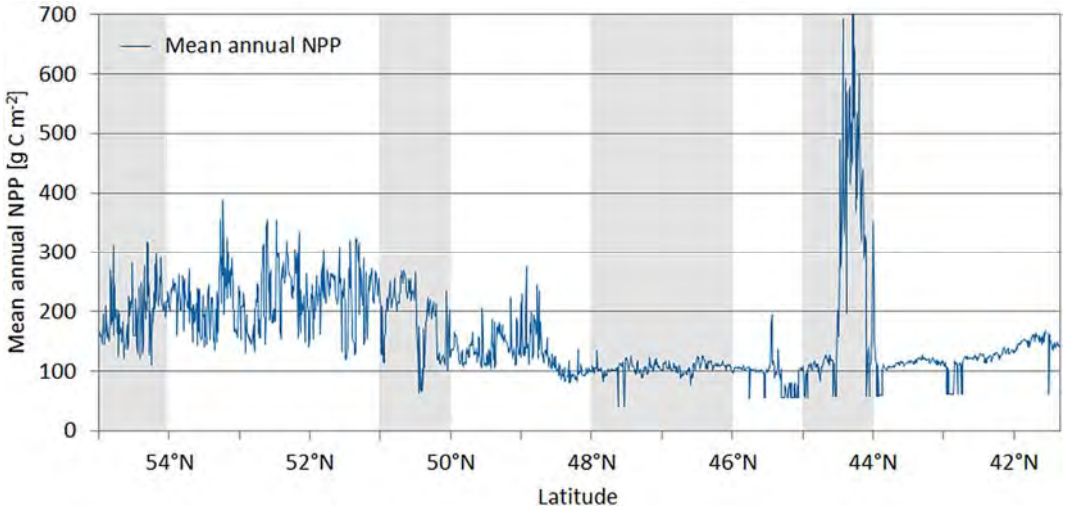

Figure 6-2: Profile of mean annual NPP for 2003–2011 along the 67°E longitude transect from North to South. The highlighted latitudinal zones correspond to the highlighted columns in table 6-3.

Table 6-3: Dominant land cover along the 67°E longitude transect within latitudinal zones from North to South. 1: primary vegetation class (>45% of pixels); 2: secondary vegetation class (> 25% but < 45% of pixels); 3: secondary vegetation class (>10%, but <25% of pixels); +: scarce minor vegetation class (<10% of pixels).

Class Name	> 54°	54°–51°	51°–50°	50°–48°	48°–46°	46°–45°	45°–44°	44°–<42°
Rain-fed agriculture	1	1	1	3				
Irrigated agriculture							2	+
Broadleaved trees	+							
Sparse vegetation			+		3	+	1	1
Grassland	1	2	3	1	1	3	+	+
Closed shrubland	+							
Open shrubland					3	1		+
Bare area (with salt flats)					+	+	3	+

The northern part of the transect line is characterized by a mixture of rain-fed agriculture and grassland (cf. table 6-3). These two land cover classes are highly intermixed (cf. also de Beurs and Henebry 2004), which causes the strong oscillation of mean annual NPP north of 48°N (cf. figure 6-2). The higher NPP values (around 300 g C m^{-2}) correspond to agricultural areas, while grassland has lower NPP values (about 160 g C m^{-2}). In the zone between 48°N and 46°N, the NPP values are lower (about 100 g C m^{-2}) and show a rather smooth behaviour. This region is characterized by a homogeneous land cover of mainly grassland with small strips of sparse vegetation and open shrubland. The NPP of grassland between 48°N and 46°N is considerably lower than that of grassland between 54°N and 51°N. After crossing a transitional zone with open shrubland and grassland, the transect line reaches the Syr-Darya River. In this zone, north of 44°N, very high NPP values with maxima up to 700 g C m^{-2} can be observed, which show the high productivity of the irrigated agricultural areas along the Syr-Darya River. The abrupt rise and decline clearly show the sudden change in land cover. South of the Syr-Darya region, land cover turns to sparse vegetation with relatively low NPP values (figure 6-2).

6.4.2 Intra-annual NPP Patterns

Figure 6-3 depicts the mean monthly NPP for the relevant months of vegetation growth from March to October. The monthly NPP indicates the beginning of vegetation activity in March in South Kazakhstan. Especially irrigated agriculture starts to grow early, with an average NPP of 8 g C m^{-2} in March and already 30 g C m^{-2} in April. Further North, vegetation growth begins later, mainly in April or May. The growth of forests in the Altay Mountains in eastern Kazakhstan is also hindered by low temperature before May. The rain-fed agricultural areas in North Kazakhstan do not show a strong vegetation activity before June. Natural steppe vegetation at the same latitude has already reached about 80% of its maximum productivity in May (cf. table 6-4). These findings correspond to observations by Doraiswamy et al. (2002), who found a difference in NDVI during April and May between rangeland and cropped areas in northern Kazakhstan. They state that crops are planted in late May and crop growth can be observed from June on in this region.

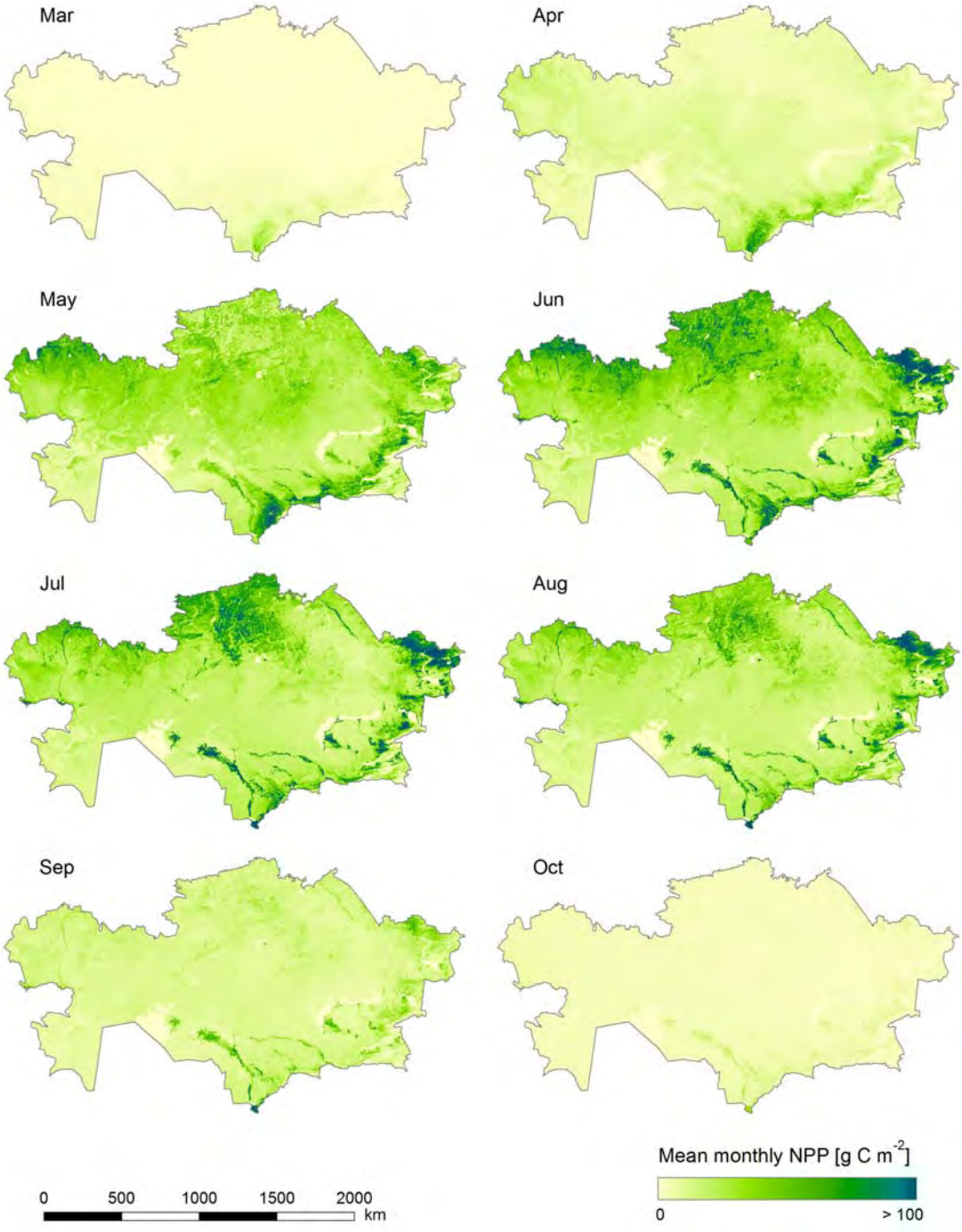

Figure 6-3: Mean monthly NPP for Kazakhstan (March to October for the time period 2003–2011).

Table 6-4: Mean monthly NPP values for 2003–2011 for individual vegetated land cover classes within Kazakhstan.

Class Name	Mean monthly NPP [g C m^{-2}]							
	Mar	Apr	May	Jun	Jul	Aug	Sep	Oct
Rain-fed agriculture	0.4	7.7	37.4	61.1	52.7	43.0	16.2	3.8
Irrigated agriculture	8.2	29.8	63.1	66.6	55.9	57.9	35.4	11.5
Needleleaved trees	0.6	6.9	37.2	69.1	61.6	59.6	26.1	4.9
Broadleaved trees	1.1	6.9	35.8	68.6	64.7	54.4	24.5	5.6
Sparse vegetation	3.5	12.7	23.6	23.1	20.8	18.5	11.9	4.6
Grassland	0.9	8.2	29.8	36.0	27.0	23.1	11.9	3.4
Closed shrubland	1.8	9.9	33.9	48.4	44.2	38.5	20.8	6.3
Open shrubland	1.9	9.3	23.2	24.5	20.3	17.9	10.8	3.9
Bare area	1.6	6.5	14.0	14.9	13.3	11.5	7.6	3.2
Bare area with salt flats	1.8	5.7	10.9	12.7	12.6	10.7	7.4	3.4
All land areas in Kazakhstan	0.9	8.3	24.4	34.6	31.4	27.9	13.5	3.5

The maximum vegetation productivity is reached in June throughout the country for all vegetation classes except sparse vegetation, for which NPP is slightly higher in May (cf. table 6-4). Vegetation productivity for agricultural areas and woody vegetation classes stays high in July (>50 g C m^{-2} for agriculture and >60 g C m^{-2} for forests), while the productivity of steppes and semi-deserts already decreases. In July and August, the agricultural areas are clearly identifiable with high NPP values in figure 6-3: rain-fed cultivation in northern Kazakhstan and irrigated agriculture along the rivers in southern Kazakhstan. Especially irrigated agriculture shows a high mean NPP through all months from May on as temperature conditions in southern Kazakhstan are convenient and water availability is not a limiting factor due to water management (de Beurs and Henebry 2004). In September, the vegetation activity drops throughout the country and in October, only minor NPP can be observed in the Syr-Darya valley and other irrigated areas.

6.4.3 Inter-annual NPP Patterns

NPP anomalies were calculated for each individual month between March and October for 2003–2011 (cf. figures F-4 to F-12 in appendix F). The anomalies are based on monthly NPP means and deviations, as described in section 6.3.3. From the monthly anomalies, the number of months showing anomalies for each year was derived. Two datasets were separately calculated, one for positive anomalies and one for negative anomalies, as presented in figures 6-4 and 6-5. The mean monthly standard deviations of NPP are provided in table 6-6 for reference.

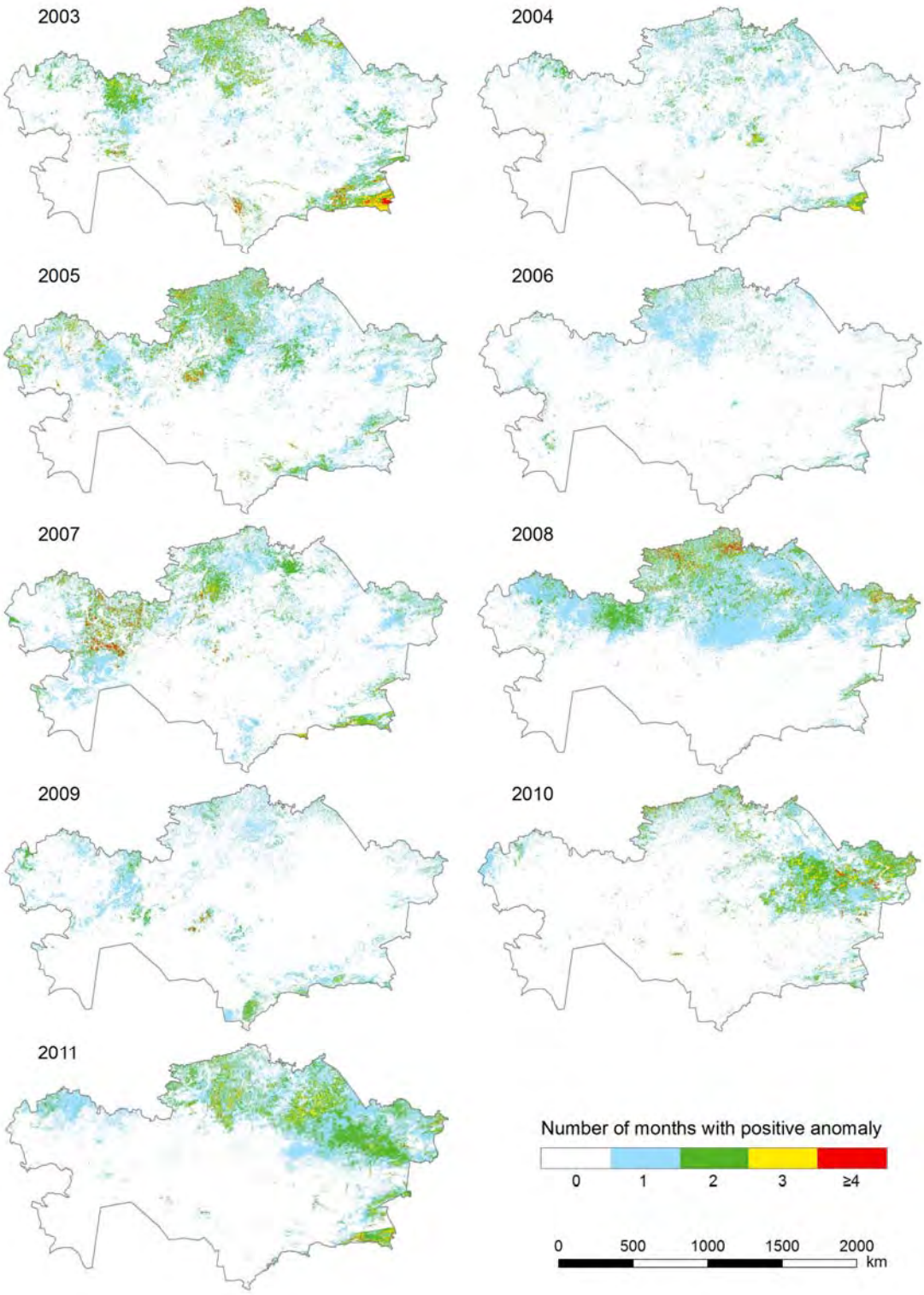

Figure 6-4: Number of months per year with positive NPP anomalies (March–October considered). A positive anomaly is defined if the monthly NPP is higher than the 2003–2011 mean NPP for that month plus two standard deviations.

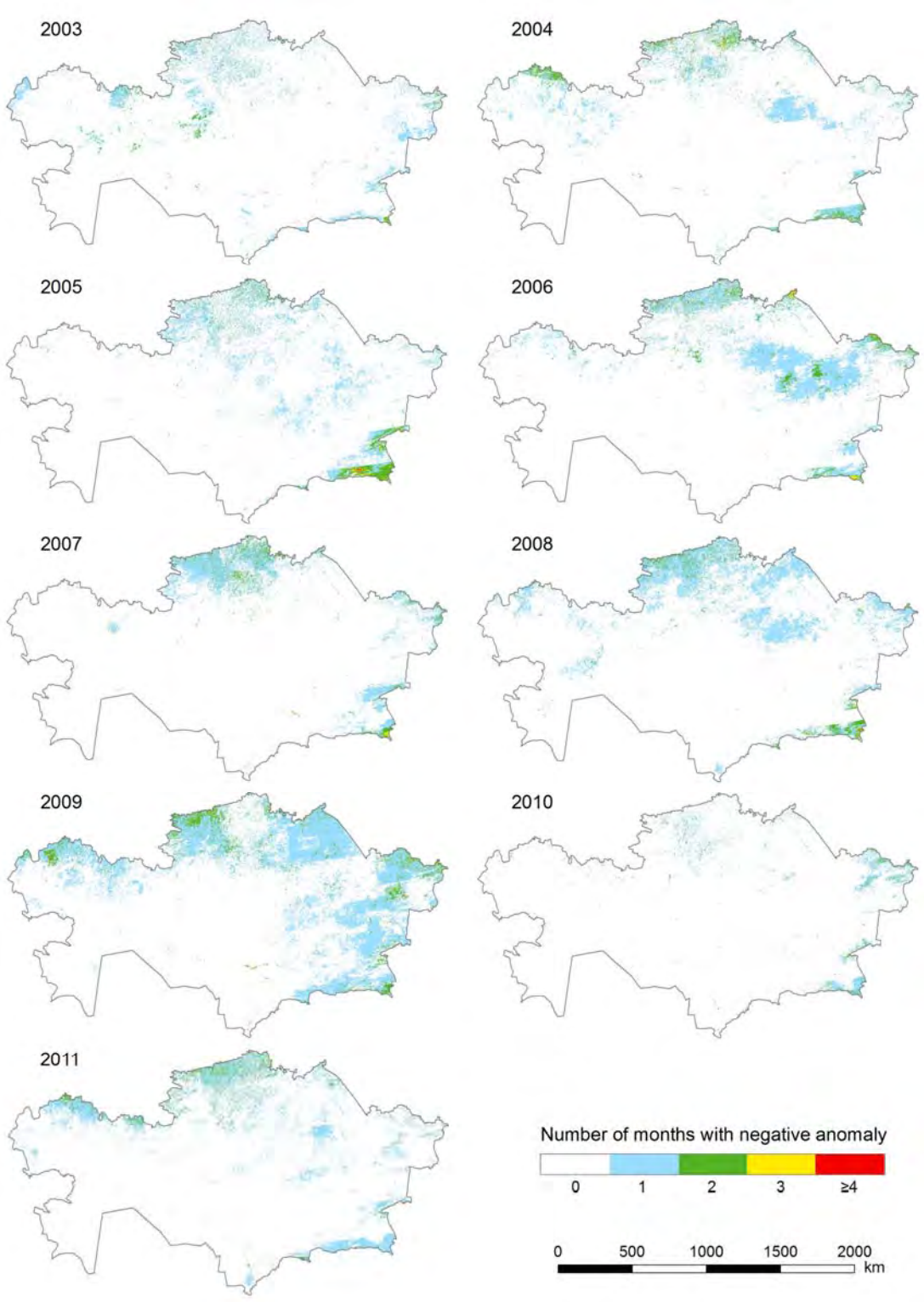

Figure 6-5: Number of months per year with negative NPP anomalies (March–October considered). A negative anomaly is defined if the monthly NPP is lower than the 2003-2011 mean NPP for that month minus two standard deviations.

The region with most positive anomalies is located in central northern Kazakhstan. In this region, NPP was especially high in 2003, 2005, 2008, and 2011 (figure 6-4). In north-eastern Kazakhstan, positive anomalies occurred in in 2008, 2010, and 2011, and in the north-western part of the province Aktobe positive anomalies can be observed for 2003, 2007, and 2008. The percentages of the land area of Kazakhstan for the individual years that experienced ≥2 positive or negative anomalous months are summarized in table 6-5.

Table 6-5: Percentages of the land area of Kazakhstan for the individual years that experienced ≥2 positive or negative anomalous months within the period March–October.

Percentage of land area of Kazakhstan with ≥2 anomalous months	2003	2004	2005	2006	2007	2008	2009	2010	2011
Positive anomalies	9	3	7	1	8	8	2	7	11
Negative anomalies	1	2	2	2	1	2	4	2	1

The number of months with negative NPP anomalies during 2003–2011 is lower than for positive anomalies, but the regions, in which most months with negative anomalies occurred are located in similar regions: the most northern parts of central and western Kazakhstan (mainly 2004 and 2009), and north-eastern Kazakhstan (2006 and 2009). The high mountainous regions of the Tian Shan also show positive or negative anomalies in some years (cf. figure 6-6).

Anomalies within the period 2003–2011 in Kazakhstan have not been analysed in other studies so far. However, Propastin et al. (2008a) observed significant upward trends of NDVI in the period 1982–2003 in northern Kazakhstan. Though their study covered a different time-period and focused on a different phenomenon, their findings indicate stronger changes in vegetation activity in northern Kazakhstan than in other regions of the country. This supports our findings, because strongest anomalies are observed for the same region in this study. High variability in vegetation activity for northern Kazakhstan was also reported by Lioubimtseva et al. (2005), de Beurs and Henebry (2004), and Doraiswamy et al. (2002).

Table 6-6: Mean monthly standard deviation of NPP values for the time-period 2003–2011 for the months March to October for all land pixels within Kazakhstan.

Month	Mean monthly NPP [g C m^{-2}]	Mean standard deviation [g C m^{-2}]	Mean standard deviation [%] (=$\bar{\sigma}$)
March	0.9	1.3	140.2
April	8.3	4.0	48.0
May	24.4	8.0	32.8
June	34.6	9.9	28.6
July	31.4	9.0	28.7
August	27.9	7.5	26.9
September	13.5	3.7	27.5
October	3.5	1.6	45.2

The numbers of months with positive or negative anomalies in the period March to October in 2003–2011 were further summed for all years. Four anomalous months correspond to >5% and eight months to >10% of all 72 months (9 years of observation and 8 months per year analysed) considered for the analysis. The resulting anomaly maps (figure 6-6) show the regions that were most strongly affected by anomalous conditions in the 9-year period.

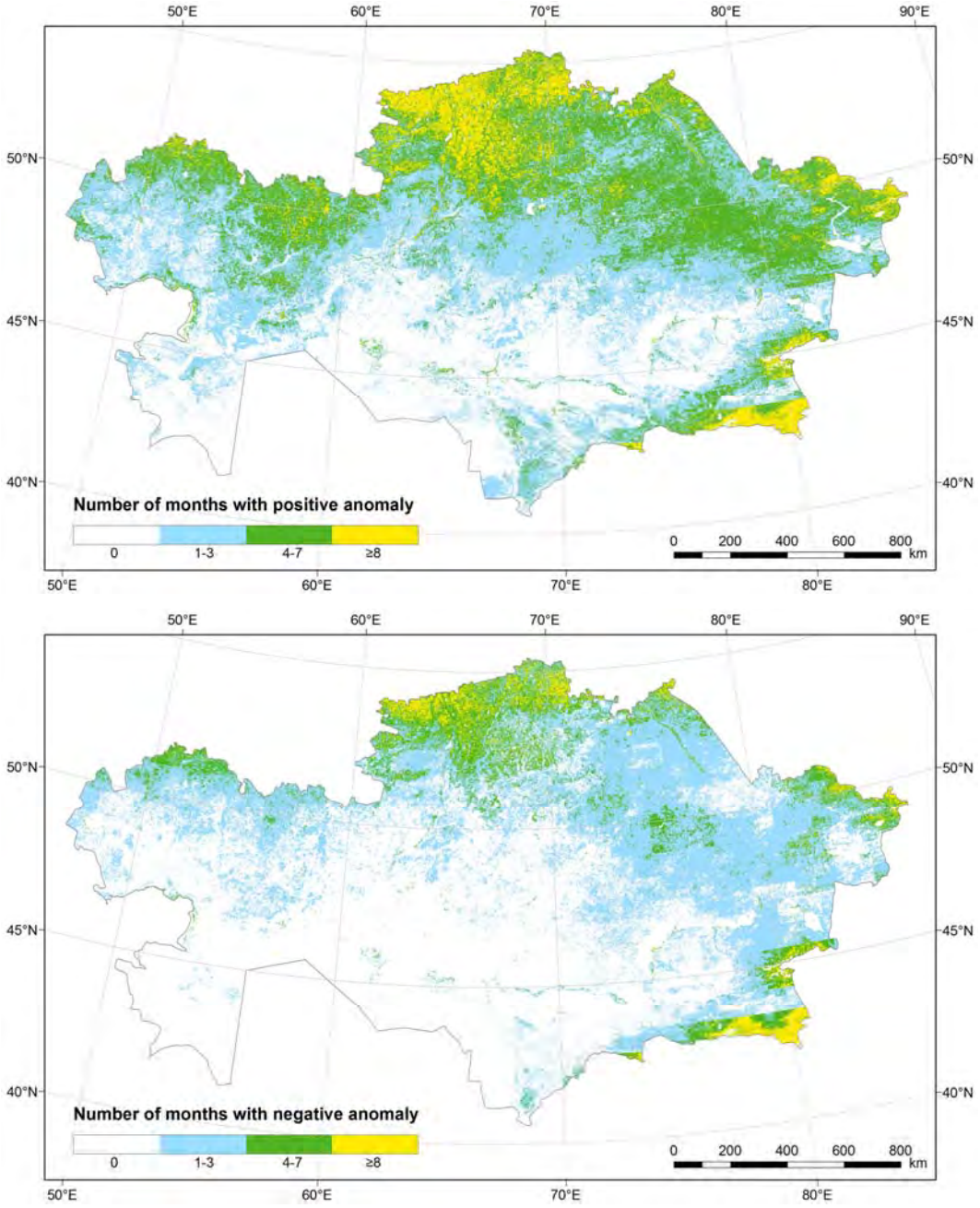

Figure 6-6: Total number of months with positive (above) and negative (below) NPP anomalies (March–October considered) within the 2003–2011 time period.

Regarding positive anomalies, 30% of the area of Kazakhstan was affected in ≥4 months and 9% in ≥8 months. For negative anomalies the corresponding area is 12% for ≥4 months and 4% for ≥8 months. Most anomalies occurred in the northern part of Kazakhstan, while the southern part was rarely affected. The areas with many anomalous months in the East and South-East are all located in mountainous regions, for example in the Altay Mountains, the Zhungar Alatau Mountains and the northern Tian Shan. The low mountain ranges of the Kazakh Highlands and the Mugodschar Mountains (Aktobe oblast) show more anomalous months than their surrounding regions.

The areas in North Kazakhstan, for which positive anomalies were observed, agree with findings of other studies. Lioubimtseva et al. (2005), for example, observed higher NDVI values at the beginning of growing season for northern Kazakhstan. They suggest that this change

might be explained by increase of fallow area and thus fewer herbicides controlling weeds (Lioubimtseva et al. 2005). De Beurs and Henebry (2004) also observed a high variability in NDVI phenologies in dryland cultivation areas in North Kazakhstan. This study shows a high number of monthly anomalies for the same region.

6.4.4 Annual NPP Variability

The mean annual NPP variability for the 2003–2011 period is displayed in figure 6-7. It gives information on how strong NPP varies from year to year. It is derived from relative annual NPP deviations (figure F-3, appendix F), which are based on annual NPP sums (figure F-1) and mean annual NPP, as described in section 6.3.5. The results indicate that 39% of the area of Kazakhstan have low annual NPP variability below 10%, 61% of the area have a variability higher than 10%, 11% show a variability higher than 20%, and for only 2% of the area NPP varies more than 30%.

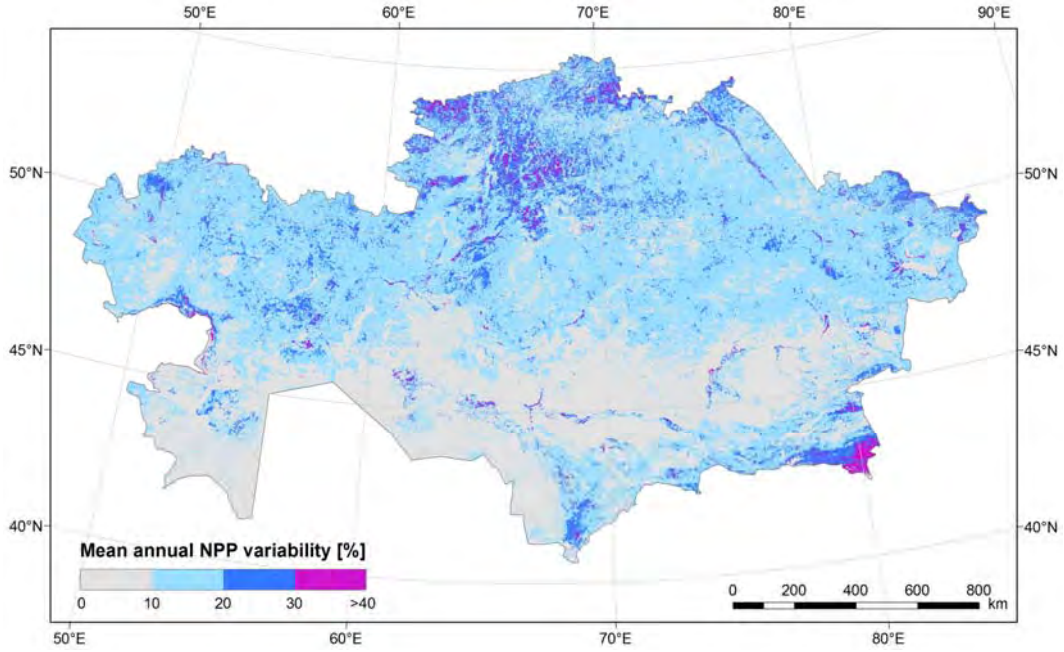

Figure 6-7: Mean annual NPP variability for Kazakhstan for 2003–2011. Mean percentage variability is calculated from absolute annual values of percentage deviation from the 2003–2011 mean per year.

Highest NPP variability can be observed in some agricultural areas in North Kazakhstan, which are likely to be caused by changing crop cultivation. This has also been reported by de Beurs and Henebry (2004). In the mountainous areas of the Altay, the Zhungar Alatau, and the Tian Shan also high NPP variability occurs, which might be due to strong variability of meteorology in mountainous environments (von Wehrden et al. 2010) and variability of snow cover duration (Dietz et al. submitted). The exceptionally high variability in the very South-East is an artifact caused by errors in meteorological input data in this high mountainous area.

Further, high NPP variability was detected along rivers and next to water bodies, such as along the Irtysh River, the southern shore of Lake Balkhash, and at the Caspian Sea. This can be attributed to differing water discharge in rivers (Propastin at al. 2008a), but might also be caused by imprecise geolocation of LAI time-series from MODIS.

The zones with semi-arid to arid conditions show very stable mean annual NPP within the observed time period. This leads to the conclusion that differences in annual meteorology are

lower in these areas, or that variation in climate parameters does not affect natural vegetation as strong as land use classes such as rain-fed agriculture.

Figure 6-8 (right) provides a more detailed view of a part of the area with high mean annual NPP variability in North Kazakhstan. In comparison to the Central Asia land cover and land use classification (figure 6-8 left) it becomes obvious, that high NPP variability higher than 20% (dark blue and violet areas) is mainly located in regions classified as agricultural land (yellow area). Grasslands (orange area) show a relatively low mean annual NPP variability, which not exceeds 20% (grey and light blue areas).

For areas with low variability, the NPP values of individual years are predicted quite well by the 9-year mean. Thus, NPP modelling provides valuable information for ecosystem and rangeland management in terms of prediction of possible carbon sequestration and available biomass for livestock for the large semi-arid and arid regions in Kazakhstan. Our finding of high variability in rain-fed agriculture in northern Kazakhstan is supported by de Beurs and Henebry (2004), who observed high inter-annual variability in crop yields in northern Kazakhstan. According to Doraiswamy et al. (2002), frequent droughts in northern Kazakhstan might explain the high variability in this region.

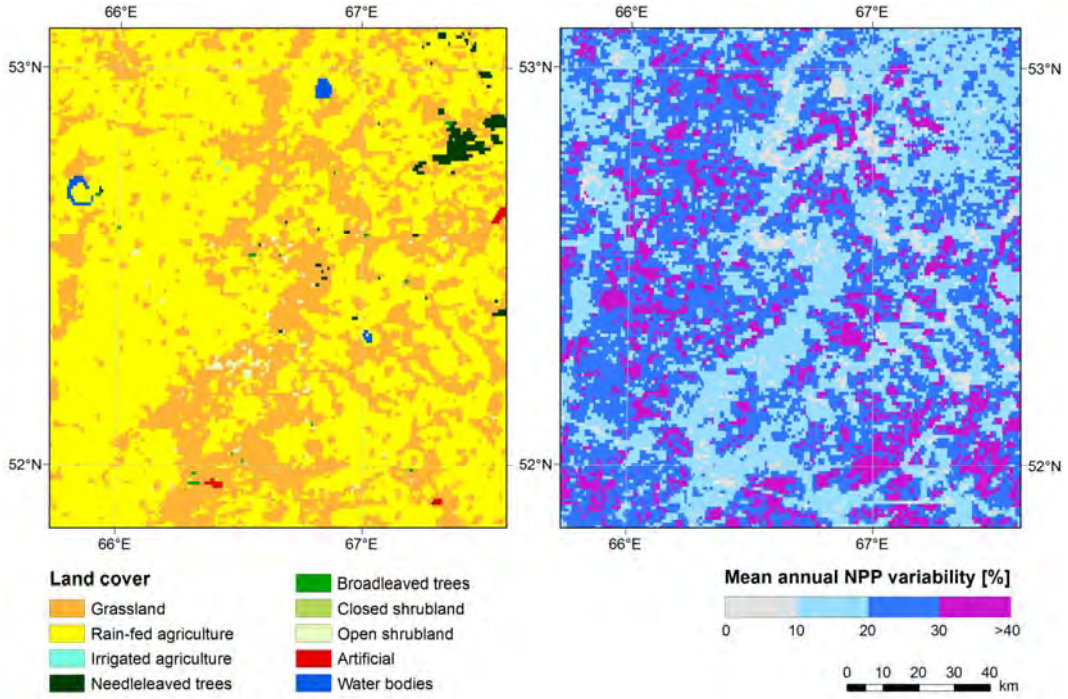

Figure 6-8: Land cover classification from the Central Asia land cover and land use map (Klein et al. 2012) and mean annual NPP variability for the period 2003–2011 for a region with high mean annual NPP variability in North Kazakhstan.

6.4.5 Relation between NPP and Meteorological Parameters

To analyse the relation between NPP and the meteorological parameters temperature, PAR, and precipitation, the correlation (linear Pearson correlation coefficient) between monthly NPP and monthly meteorological parameters for March–October for 2003–2011 was calculated. The results are shown in figure 6-9 and figure 6-10.

For temperature and PAR, a relatively strong positive correlation ($r>0.6$ for 90% of the land area) can be observed to NPP of the same month for large areas. The correlation between NPP

and precipitation of the same month was poor. Therefore, correlation to cumulative precipitation including previous months was analysed. The best overall correlation over Kazakhstan was found when NPP was correlated to precipitation sums of the two previous months. The time lag can be explained by the fact that precipitation does not directly condition vegetation growth, but first infiltrates into the soil and is then available to plants as soil water (Tum and Borg submitted). The observation of a time delay between precipitation and NDVI anomalies in Central Asia has also been observed by Gessner et al. (2012). They observed a temporal lag of 1–3 months between precipitation anomalies and vegetation response, particularly in semi-arid and arid regions with 100 to 400 mm of annual precipitation. Propastin et al. (2008b) also point out that cumulative precipitation has to be considered for analysing correlation between vegetation activity and precipitation, and that the optimum correlation period may vary for different vegetation communities.

Regarding the spatial distribution of the correlations, one can observe that the correlation between NPP and temperature is highest in southern Kazakhstan (cf. figure 6-9). For 90% of the land area, the correlation coefficient r is higher than 0.6. Lower values are only found in the most south-eastern part at the border to Kyrgyzstan and in some agricultural areas. For 38% of the land area of Kazakhstan the correlation coefficient between NPP and temperature is even higher than 0.8. Correlation to PAR is very high (r>0.8) for 66% of the land area, and high (r>0.6) for 93%. Exceptions are again in the very South-east and some agricultural areas in the North, where correlations are lower. Significant correlation between NPP and precipitation sum of the two previous months can be observed in the north-western part of the country, in the Kazakh Highland, and the mountainous regions in the East and South-east. Furthermore, correlation to precipitation is relatively high (r of 0.4–0.8) in the South-east, where correlation to temperature and PAR is lowest. From all land areas, 23% show a correlation coefficient higher than 0.4 for NPP and precipitation.

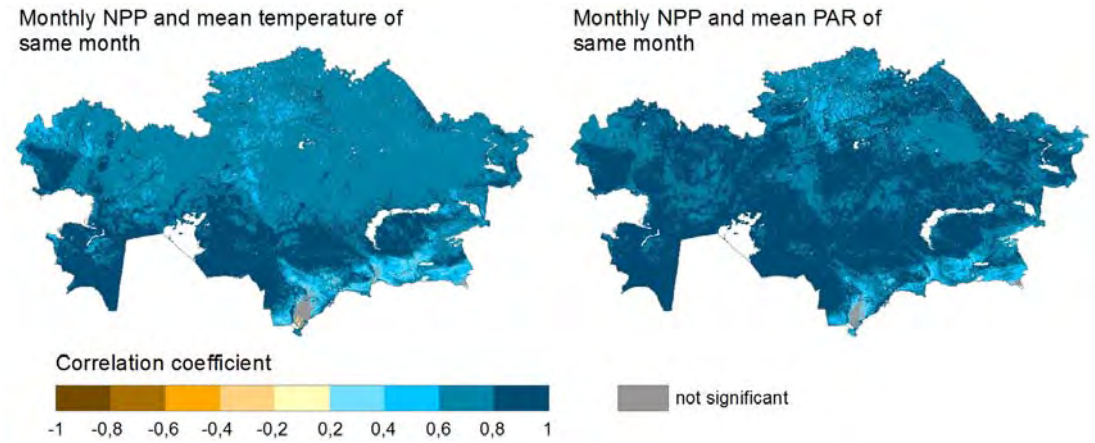

Figure 6-9: Linear Pearson correlation coefficients between monthly NPP and monthly meteorological parameters for 2003–2011. Left: NPP and temperature of same month, Right: NPP and PAR of same month.

Large areas of Kazakhstan show no significant correlation to precipitation (figure 6-10). This was also reported by Robinson et al. (2002), who found poor rainfall-biomass relationships for Kazakhstan in general and no significant rainfall-biomass relationship at all for semi-desert regions. The very most southern part of Kazakhstan even shows a negative correlation to precipitation in our study (figure 6-10). This area is irrigated agriculture for which no appreciable influence by precipitation can be expected (de Beurs and Henebry 2004). A

substantial dependency of vegetation growth on soil moisture and thus precipitation for arid grassland in north-western Kazakhstan was also observed by de Beurs and Henebry (2004). For agricultural areas they report a strong influence of precipitation and temperature on crop productivity. Dependency on PAR was not analysed in their study. Propastin et al. (2008a) also found that correlation between NDVI trends and precipitation was strongest in cropland and grassland areas in northern Kazakhstan.

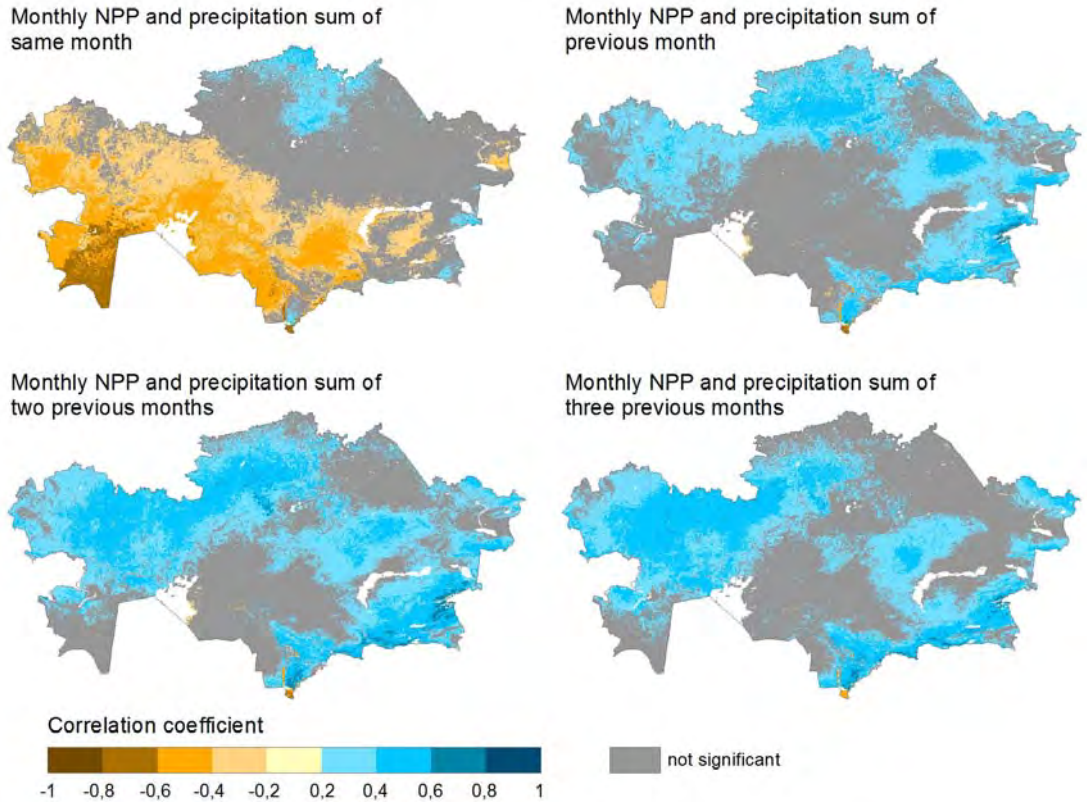

Figure 6-10: Linear Pearson correlation coefficients between monthly NPP and monthly meteorological parameters for 2003–2011. Upper left: NPP and precipitation of same month, upper right: NPP and precipitation of previous month, lower left: NPP and precipitation of two previous months, lower right: NPP and precipitation of three previous months.

As the relations between NPP and the meteorological parameters show a significant positive correlation, it was further analysed, whether the deviations from the mean monthly values are also correlated. Therefore, monthly deviations from the mean monthly values for 2003–2011 were calculated for NPP and the three meteorological parameters. The comparison of monthly NPP deviations and deviations of the climatic input parameters allows investigation of the influence of the climatic characteristics on the calculated NPP.

The diagrams in figure 6-11 show the percentage of pixels with a positive or negative NPP deviation, which also had a positive or negative deviation in the meteorological parameters. The percentages above or below 50% are plotted, as >50% indicates a mainly positive correlation and <50% a mainly negative correlation. The analysis was done on a monthly basis to enable differentiation of intra-annual differences in the dependency. For precipitation, sums of the two previous months were considered. For each month, all land pixels of entire Kazakhstan from 2003–2011, which show relative NPP deviations higher than 10% were included in the analysis. Thus, pixels that feature a very low monthly deviation were exluded. At average, 71% of the land area of Kazakhstan was considered for the analysis.

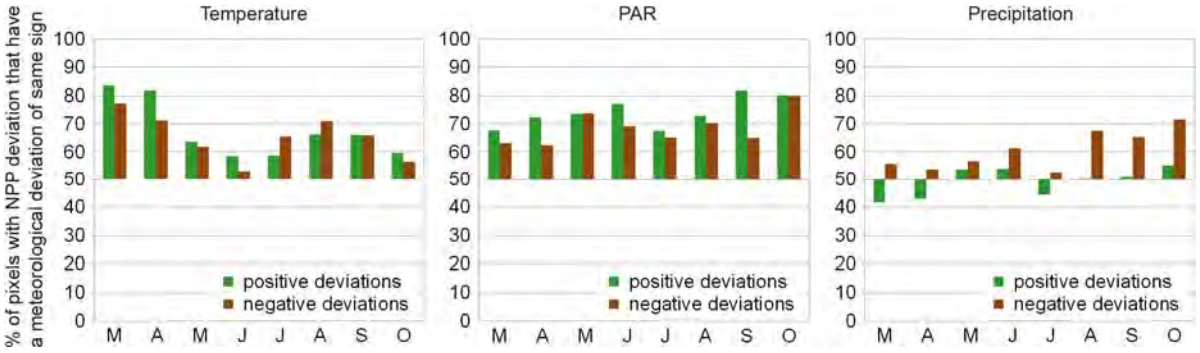

Figure 6-11: Agreement between deviations in NPP and deviations in the meteorological parameters for March to October: temperature (left), PAR (mid), and precipitation (right). The green bars refer to pixels with a positive monthly NPP deviation >10% that also have a positive deviation in the meteorological parameter. The brown bars refer to pixels with a negative monthly NPP deviation >10% that also have a negative deviation in the meteorological parameter. The bars show the percentage of pixels for which both deviations have the same sign as difference to 50% of the relevant pixels. For precipitation, the sum of two previous months was used. The years 2003–2011 were considered.

For more than 80% of the pixels with higher NPP in March and April, the temperature was also higher than the mean temperature for these months. For negative NPP deviations in March and April, lower temperatures explain for 77% and 71% of pixels (figure 6-11). The results indicate that differences in vegetation productivity at the beginning of vegetation growth are most likely to be caused by varying temperature in different years. Figure 6-12 shows, exemplary, deviations in NPP and temperature for April 2010 and 2011. The regions with positive NPP deviation correspond well to regions with positive temperature deviation. The same is the case for negative deviations. Thus, April temperature seems to influence the vegetation growth significantly almost for entire Kazakhstan.

During the summer months, deviations in NPP and temperature show a lower correlation. This can be explained by the temperature that is close to the optimum temperature for vegetation growth of 25°C (Knorr and Heimann 2001, Lioubimtseva at al. 2005). In a study by Propastin et al. (2008a) even negative correlations to temperature were found in summer for some land cover classes in Kazakhstan. The overall correlation between NDVI and temperature was not significant for summer, but strong for spring (Propastin et al. 2008a). The trend in the correlation regarding the difference between spring and summer agrees with the results of this study.

In August and September, temperature deviation explains again for 65% to 70% of NPP deviation. As this study presents mean values for entire Kazakhstan, a large country with distinct climatic conditions, it has to be pointed out that the meteorological parameters might explain better the NPP deviations on a regional basis.

The combination of NPP and PAR deviations reveals a more stable relation over the year than for NPP and temperature (figure 6-11). PAR deviation explains between 65% (March) and 80% (October) of the NPP deviation, with an average value of 71% (74% for positive and 69% for negative NPP deviations). This reflects the high importance of PAR, which is an essential driver for photosynthesis on vegetation growth throughout the year.

The spatial distribution of positive and negative NPP and PAR deviations also shows this strong dependency, for example in June and July 2009, as illustrated in figure 6-13. A large overlap of area with positive or negative deviations in NPP and PAR over Kazakhstan is obvious, though locally, exceptions can be observed, for example for irrigated agriculture in southern Kazakhstan.

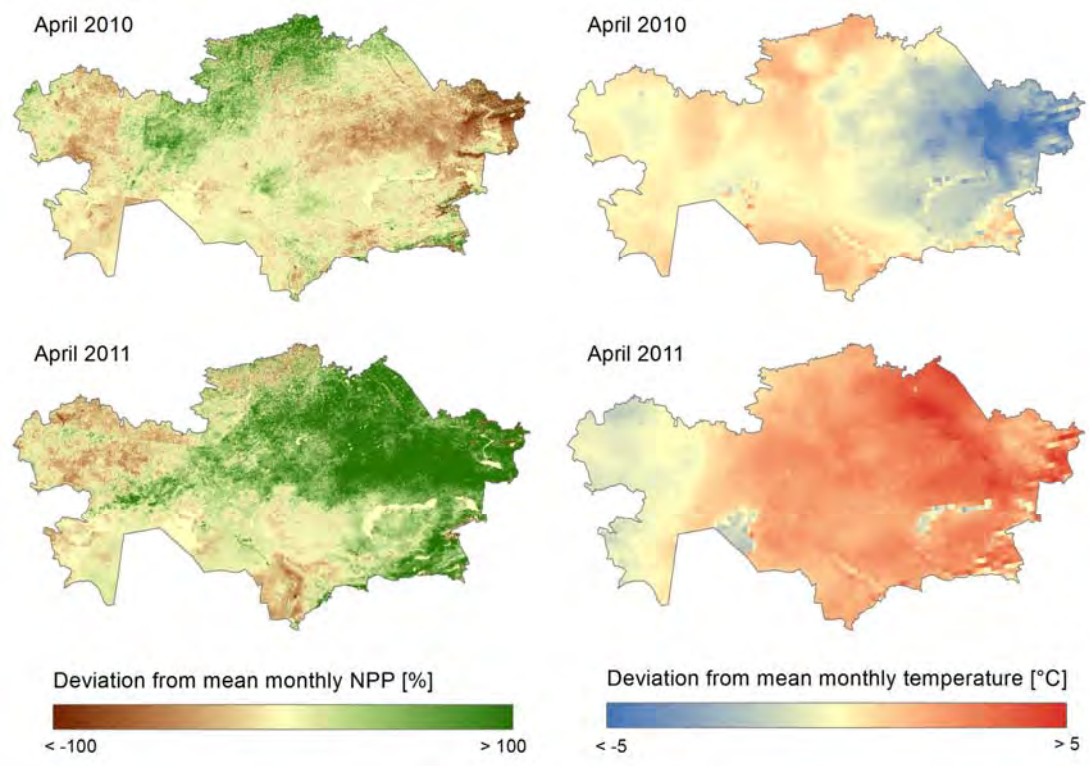

Figure 6-12: Comparison of monthly NPP deviations (left) and monthly temperature deviations (right) for Kazakhstan for April 2010 and 2011.

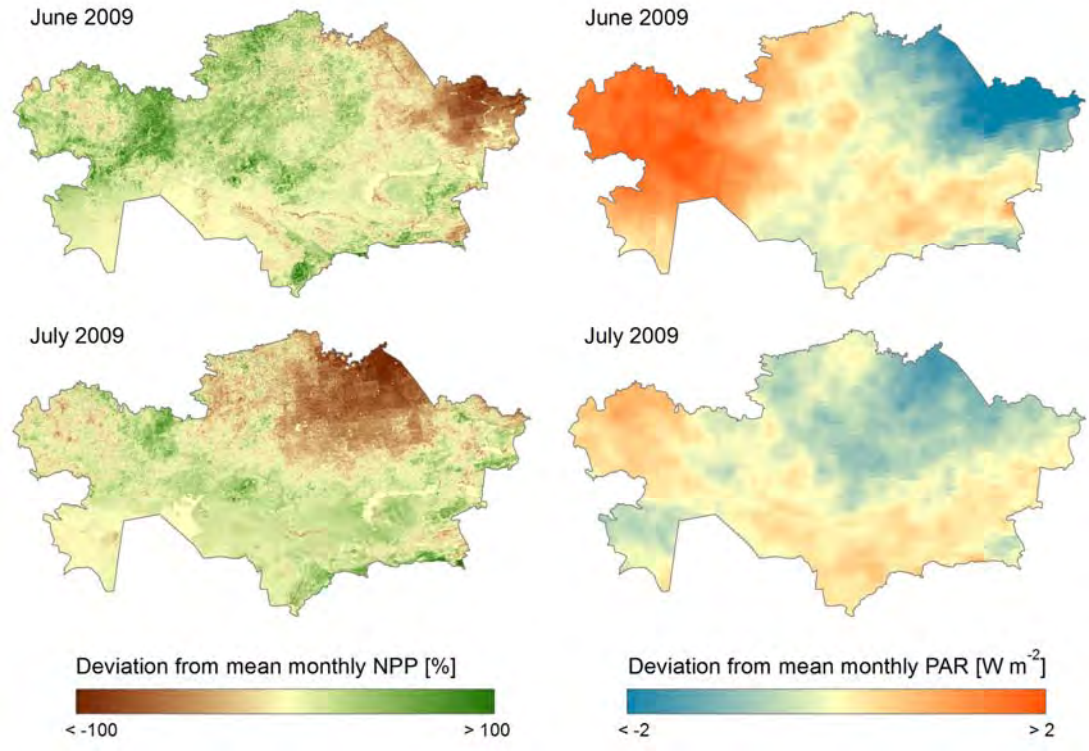

Figure 6-13: Comparison of monthly NPP deviations (left) and monthly PAR deviations (right) for Kazakhstan for June and July 2009.

The relation between NPP deviation and deviation of the sum of precipitation from the two previous months is not as obvious as for temperature and PAR. Especially positive NPP deviation does not seem to be caused by higher precipitation (cf. figure 6-11). However, in the months August to October, a clear relation can be observed between negative NPP and precipitation deviations. About 70% of the area with low NPP also shows low precipitation.

This observation indicates that low precipitation in early summer causes low vegetation productivity in the months August to October. This may be explained by the drying out of the soil during summer when precipitation is low. The relation between negative NPP and precipitation deviations is weaker at the beginning of the growing period, which is likely, because melting snow adds to the available soil water content (Dietz et al. submitted).

Overall, NPP deviations seem to be more strongly influenced by temperature and PAR than by precipitation. This corresponds to findings by Propastin et al. (2008a), who report that for most vegetation types precipitation played a minor role than temperature as explanatory factor for NDVI trends in Kazakhstan. For spring, their analyses even indicated that NDVI trends were only controlled by temperature. Xiao and Moody (2004) also reported that temperature was the leading factor controlling greening patterns in similar ecosystems in China, and that correlation to precipitation was low. The results of this study support those findings.

6.5 Conclusions

In this study, the model BETHY/DLR was applied for Kazakhstan for the period 2003–2011. The NPP results were analysed regarding spatial, monthly, and inter-annual variations. The mean annual NPP for Kazakhstan was 143 g C m^{-2}. The four most important land cover classes in Kazakhstan and their mean annual NPP are grasslands with 140 g C m^{-2}, sparse vegetation with 120 g C m^{-2}, open shrubland with 112 g C m^{-2}, and rain-fed agriculture with 225 g C m^{-2} (cf. table 6-2). The maximum vegetation productivity is reached in June throughout the country with an average monthly NPP of 35 g C m^{-2}.

The regions that experienced the greatest number of months with anomalous NPP in the period 2003–2011 were mainly located in the North of Kazakhstan. NPP variability showed a similar spatial pattern, with 11% of the area of Kazakhstan experiencing annual NPP variability above 20%. Percentage variability was lowest in the semi-arid and arid regions covered by open shrubland and grassland. For these regions, NPP modelling may allow prediction of possible carbon sequestration and available biomass for livestock. The regions in the North of the country seem to be most strongly affected by changing meteorological conditions or human impact. Longer time-series of NPP would be desirable for further analyses, especially regarding trends.

Comparison of monthly NPP and meteorological parameters revealed differing influences of temperature, PAR, and precipitation on the productivity. The correlation coefficients between NPP and temperature as well as between NPP and PAR were higher than 0.6 for 90% of the land area of Kazakhstan.

The comparison of monthly NPP and precipitation of the same month showed no clear relationship. However, the sum of precipitation of two previous months showed a significant correlation to NPP for large parts of Kazakhstan. The correlation between NPP and precipitation was lower than for temperature and PAR. 23% of the land area show a correlation coefficient above 0.4, mainly north-western Kazakhstan, the Kazakh Highlands, and the south-eastern part of the country.

Deviations from mean monthly temperature most strongly influenced deviations in vegetation productivity in spring. Up to 84% of NPP deviations in March and April could be explained by temperature deviations. Regarding possible effects of climate change, this leads to the conclusion that possible changes in temperature at the beginning of vegetation growth will strongly affect NPP in Kazakhstan.

If Central Asia is becoming warmer during the coming decades as projected (Lioubimtseva and Henebry 2009), this might lead to an increase in productivity at the beginning of vegetation growth. Higher temperatures in summer might result in a decrease of NPP and in a longer period of semi-dormancy. A further shift to an earlier season would also be likely, as already observed in the past (e.g. de Beurs and Henebry 2004, Propastin et al. 2008a).

Incoming PAR showed to be of importance for NPP during the whole period of vegetation growth. The monthly analysis of NPP and precipitation deviations indicated that vegetation growth is especially sensitive to lower precipitation in summer and autumn. Thus, the projected decrease in precipitation for summer and autumn (Lioubimtseva and Henebry 2009) will probably lead to a decrease in productivity in the period August to October.

7 Derivation of Above-Ground Biomass Estimates from NPP Time-Series

7.1 Introduction

Previous studies on biomass estimation revealed several challenges for remote-sensing based biomass estimation in semi-arid regions (cf. section 2.1). Most important for repeatable application and coverage of large areas is the transferability of biomass estimation approaches, which is a major challenge. Modelling approaches are among the methods that obtained most promising results. Nevertheless, modelling approaches have not been extensively analysed in the context of biomass estimation yet (cf. section 2.1.6).

On the other hand, NPP models are commonly applied for large areas. They are suitable for obtaining NPP time-series for several years. Remote-sensing based NPP models allow for regional NPP calculation (cf. section 2.2). This information may be of value for the estimation of standing biomass, because NPP is closely related to AGB (e.g. Fensholt et al. 2006). If modelled NPP data may be converted to biomass information, this will allow the development of an approach to biomass estimation that is potentially transferable. This would be a big step forward for several applications that need large-scale biomass estimates on a regular basis (cf. section 1.2).

For annual crops, cumulative NPP may provide information about the standing biomass, because start and end of the plants' life cycle are known. For perennial vegetation, however, biomass at the beginning of the growth period cannot be assumed to be zero. Thus, cumulative NPP can not be used as proxy for standing biomass for natural vegetation. Moreover, the presence of ephemeral vegetation, which is typical for semi-arid environments, is a problem for cumulative approaches. Thus, for natural vegetation in semi-arid regions the estimation of biomass from NPP is especially challenging.

Vegetation productivity models have been successfully used for crop yield estimation (e.g. Lobell et al. 2009, Mo et al. 2005, Pan et al. 2009, Wang et al. 2005). Some ecosystem models also include calculation of assimilation, senescence and decomposition (e.g. Jarlan et al. 2008, Woodward and Lomas 2004). These models are able to calculate the total standing biomass as a function of cumulative NPP minus biomass losses from senescence (Gough 2012). Most remote sensing-based NPP models, however, do not consider mortality and are not able to calculate biomass assimilation over several years.

This study aims at developing a methodological approach for direct biomass estimation for natural vegetation based on NPP time-series. The focus is on analysing the suitability of combining NPP data with plants' relative growth rates (RGRs). RGRs are widely used for plant physiological analyses, but no research combining NPP and RGR to estimate standing biomass in semi-arid environments has been reported previously.

The most relevant time for biomass estimation is at peak biomass or at maximum productivity (e.g. Hobbs 1995, Mangiarotti et al. 2008). For Kazakhstan, the period of maximum vegetation productivity is in June (cf. section 6.4.2). The available field data for

validation were also collected in June 2011 (cf. section 4.3). The aim of this study is, thus, to develop a method for estimation of standing biomass for the period of maximum vegetation growth.

In section 7.2 the methodological concept for derivation of biomass from NPP is developed and described. Possible errors of the input data for biomass estimation are discussed (section 7.3). The developed approach is then applied to the three study areas in semi-arid Kazakhstan. For this, NPP time-series calculated with BETHY/DLR (cf. chapter 6) are used. The biomass estimates for the three study areas are validated with field measurements of above-ground biomass (section 7.4). In the last section of this chapter the results are discussed (section 7.5).

7.2 Methodological Concept for Derivation of Biomass Estimates from NPP Time-Series for Natural Vegetation

7.2.1 Relative Growth Rates

A plant's absolute growth rate depends on both the amount of plant biomass and its relative growth rate (RGR) (Oesterheld 1992). Since NPP describes the absolute growth rate (e.g. in g d^{-1}), knowledge about the plant's relative growth rate can be used to derive the plant's standing biomass from NPP. As Titlyanova et al. (1999), for example, formulated, *NPP* can be described as the product of the relative rate of dry matter production per day *RGR* (e.g. in g g^{-1} d^{-1}), and the standing dry matter biomass *B* (e.g. in g), as presented in equation 7-1.

$$NPP = RGR \cdot B \tag{7-1}$$

Relative growth rates of plants have been widely studied in plant physiology. They provide information on the speed of plant growth. The RGR of a plant is defined as the mass increase per standing biomass per unit of time, for example as g g^{-1} d^{-1}. Some studies consider total plant biomass (*TPB*), while others relate the increase only to the above-ground biomass present, as shown in equations 7-2 and 7-3 (e.g. Levang-Brilz and Biondini 2002).

$$RGR_{TPB} = \frac{1}{TPB}\frac{dTPB}{dt} \tag{7-2}$$

$$RGR_{AGB} = \frac{1}{AGB}\frac{dTPB}{dt} \tag{7-3}$$

The above equations define the per gram rate of biomass production, i.e. RGR, with units of g g^{-1} d^{-1} of a species. TPB and AGB are commonly defined as dry weight biomass of an individual species at the time of investigation (Shipley and Keddy 1988). In many plant physiological studies, RGR is derived as the slope of a linear regression of the natural logarithm of dry weight biomass on time (cf. equation 7-4). These so called harvest-interval calculations are the classical approach for growth analyses measurements. The experimental approach is illustrated schematically in figure 7-1. Equation 7-4 shows that the slope of the regression, which is applied in physiological studies to derive RGR, describes the same RGR as defined by equation 7-2 (combined from Schönbach et al. 2011 and Shipley and Keddy 1988), with *B*, dry weight biomass (in g) of an individual species, and *RGR* (in g g^{-1} $time^{-1}$).

$$RGR = \frac{\ln \frac{B_2}{B_1}}{t_2 - t_1} = \frac{\ln B_2 - \ln B_1}{t_2 - t_1} = \frac{d \ln B}{dt} = \frac{1}{B}\frac{dB}{dt} \quad (7\text{-}4)$$

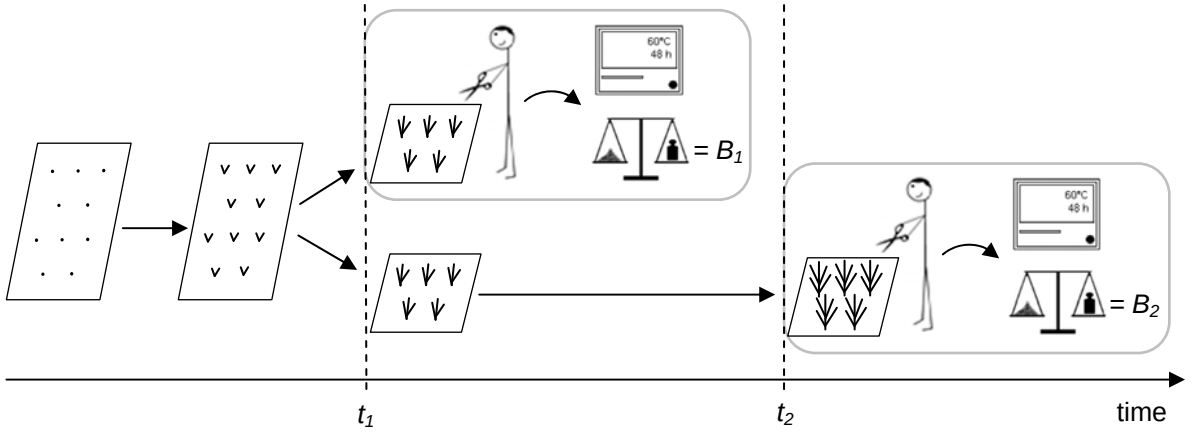

Figure 7-1: Schematic illustration of the common approach for experimental determination of the RGR of a species. B_1 and B_2 are the mean dry weight biomass of the harvest at t_1 and t_2 respectively.

RGR is often measured for plant seedlings under controlled conditions, but some studies also investigated RGR values of mature plants in natural environments (e.g. Pugnaire and Haase 1996). Maximum growth rates are often derived (e.g. Levang-Brilz and Biondini 2002, Shipley and Keddy 1988, Vile et al. 2006), which define the dry weight increase per unit of biomass and per unit of time under optimum conditions (Poorter and Remkes 1990). RGR is the most useful single comparator of innate growth potential (Hunt and Cornelissen 1997), but has not yet been applied in the context of estimation of biomass from NPP data.

7.2.2 Methodological Approach

Equation 7-1 establishes the relationship between NPP, biomass *B*, and RGR. This equation can be transposed, so that it defines how biomass can be derived from NPP and RGR. The transposition results in equation 7-5. This equation specifies that biomass information can be estimated from the quotient of NPP and RGR, provided that the reference periods of NPP and RGR match.

$$B = \frac{NPP}{RGR} \quad (7\text{-}5)$$

The aim of this study is to estimate the biomass for the period of maximum vegetation growth, i.e. June for Kazakhstan. Two approaches can be applied for calculation of biomass for this period: Either mean RGR values for the period of maximum growth are combined with mean NPP for this period (equation 7-6), or maximum daily relative growth rates are combined with the maximum daily NPP for this period (equation 7-7).

$$B_{June} = \frac{NPP_{June,mean}}{RGR_{June,mean}} \quad (7\text{-}6)$$

$$B_{June} = \frac{NPP_{June,max}}{RGR_{June,max}} \tag{7-7}$$

Figure 7-2 schematically illustrates the difference between mean NPP and maximum NPP for the month with maximum vegetation growth. These two values may differ significantly. This demonstrates the importance of applying maximum RGR to maximum daily NPP and mean RGR to mean NPP.

The decision on which to take is determined by the availability of measured RGR values. Maximum RGRs are available for several species of genera typical for the study areas in Kazakhstan (cf. section 7.2.4). Thus, maximum daily NPP from June is chosen as base information for biomass estimation.

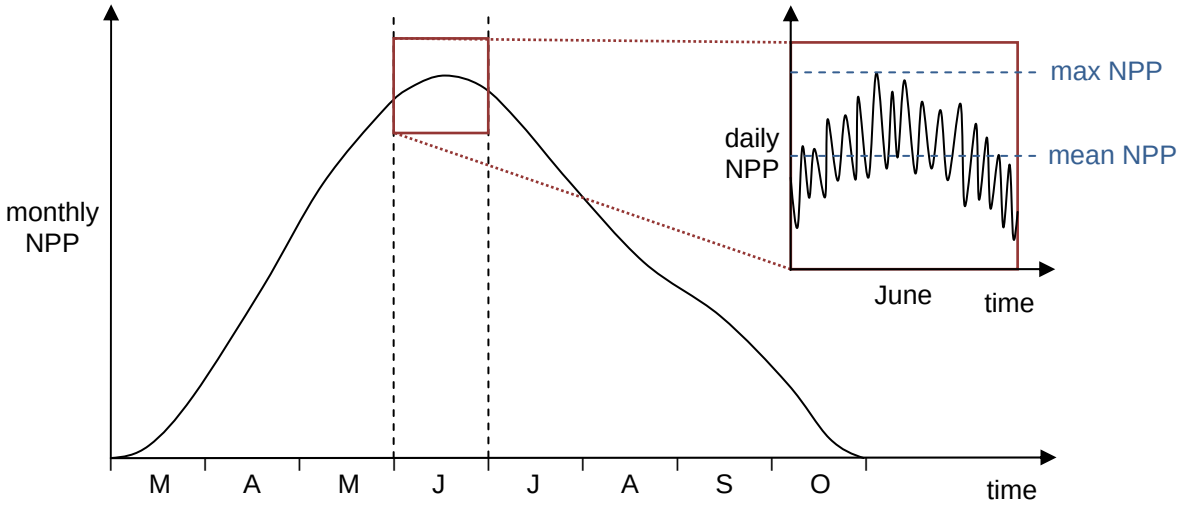

Figure 7-2: Schematic illustration showing the difference between mean NPP and maximum NPP for the month of maximum vegetation growth.

The calculation of NPP with BETHY/DLR was based on the Central Asia land cover and land use map (Klein et al. 2012). This classification is used to define the vegetation types for each pixel (cf. sections 4.1.3 and 6.2). For most natural vegetation classes (sparse vegetation, grassland, closed shrubland, open shrubland, and bare areas) the same two vegetation types were applied for NPP calculation. These are C_3 grass and deciduous shrubs (cf. section 6.2).

The natural vegetation classes listed above cover together 79% percent of the area of Kazakhstan. Therefore, the methodological development focuses on derivation of grass and shrub biomass estimates.

NPP for grass and shrubs was modelled separately for each pixel with BETHY/DLR. Thus, it is possible to apply RGR values separately for these two vegetation types to derive grass and shrub biomass. Distinction between grass and shrub RGRs is necessary, because several studies report that RGR is generally lower for woody species than for herbaceous species (e.g. Grime and Hunt 1975, Hunt and Cornelissen 1997).

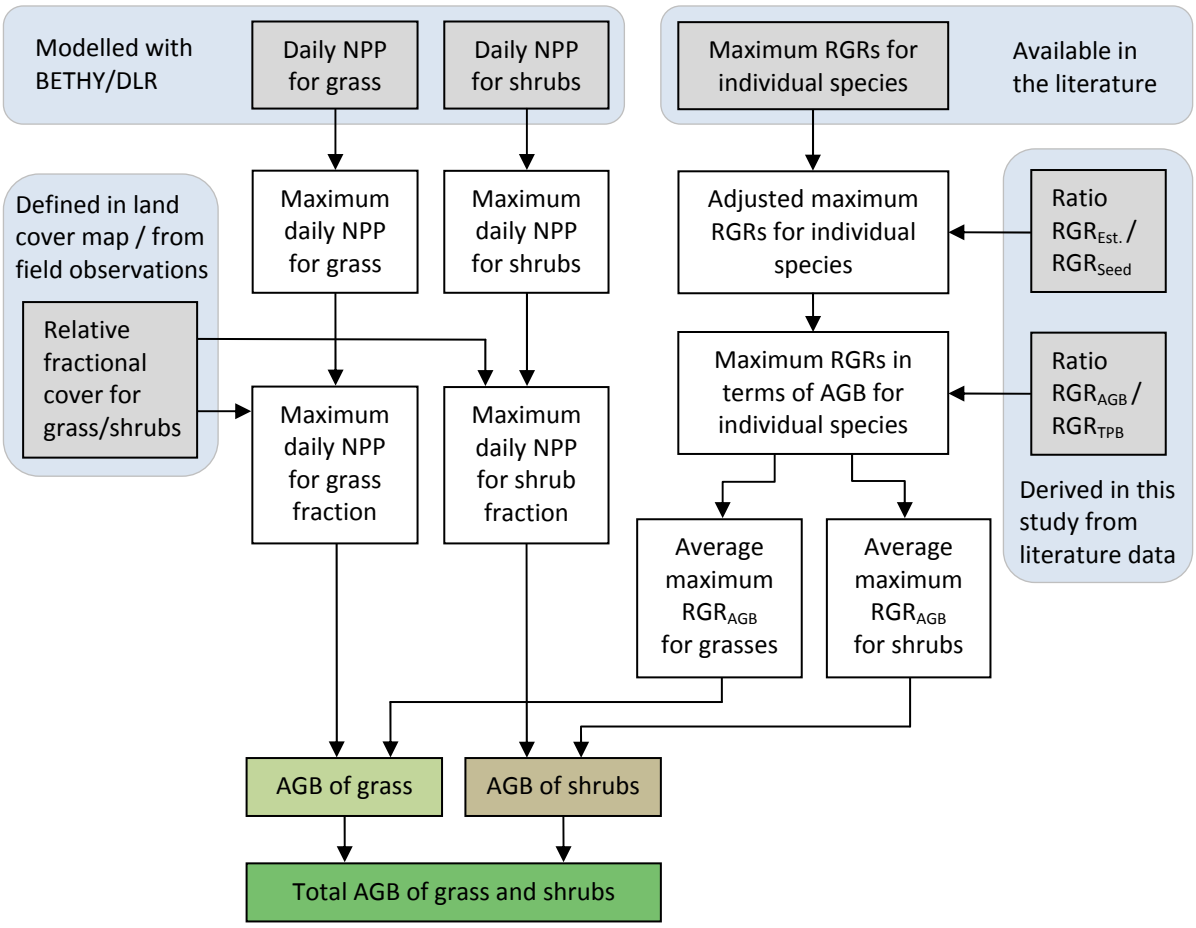

Figure 7-3: Flowchart showing the approach for derivation of above-ground biomass estimates from NPP data and RGR values for grass and shrub biomass.

Figure 7-3 shows a flowchart of the methodological approach for estimation of AGB from NPP. The upper left part of the diagram shows the derivation of the required NPP values. Input data are daily grass NPP and daily shrub NPP. These data are available from the model BETHY/DLR (cf. chapter 6). From the daily NPP time-series, the maximum daily NPP values for grass and shrubs for the period of maximum vegetation productivity (e.g. June 2011 in Kazakhstan) are extracted.

The maximum daily NPP values are then combined with information about relative fractional cover of grass and shrubs. This information is used to scale the NPP of grass and shrubs according to their relative fractional cover. This results in maximum daily NPP values for the grass fraction and the shrub fraction within a pixel.

The left part of the diagram illustrates the steps for derivation of suitable RGR values. The main input parameters are maximum RGRs for individual species. These are available in the literature (e.g. references provided in tables 7-2 and 7-3). The RGRs are often derived from seedling experiments. Thus, an adjustment has to be applied, which converts RGR_{max} of seedlings to RGR_{max} of established plants. For this, an adjustment factor with respect to the ratio between these two RGR_{max} values has been derived in this study based on data available in the literature. The adjustment step is explained in detail in section 7.2.4.

A second conversion of the RGR values is necessary, because most experimental studies aim at deriving RGR_{TPB} (as defined in equation 7-2). For this study, however, RGR_{AGB} (equation 7-3) is needed. The necessary conversion factor regarding the ratio between RGR_{AGB} and RGR_{TPB}

has been derived in this study based on information available in the literature. Details on the conversion step are provided in section 7.2.4.

The adjustment and conversion are applied to the RGR values of individual species. The next step is the calculation of average maximum RGR_{AGB} values for the two plant life-forms of grasses and shrubs (cf. figure 7-3).

Finally, the maximum NPP values and the maximum RGR_{AGB} values are combined to estimate the AGB. Following equation 7-7, the maximum NPP values for the grass and shrub fractions are divided by the mean $RGR_{AGB,max}$ of grass and shrubs, respectively. This results in estimates of grass and shrub AGB. These two values are finally summed to obtain the total standing AGB of grass and shrubs.

7.2.3 Conditions for the Applicability of Constant RGR Values

Within the developed approach, constant maximum RGR_{AGB} values are applied to derive AGB from maximum NPP. The application of constant RGR values is valid, if RGRs can be assumed to be constant for varying amounts of standing biomass.

The biomass estimation approach in this study is based on NPP data from BETHY/DLR. This data has a spatial resolution of ~0.00833° (ca. 925 m × 650 m for Kazakhstan). Thus, the RGR values are not applied to individual plants. The pixels represent the NPP of an area of about 0.6 km². Each pixel thus defines one "site" and the vegetation within each site is made up of many individual plants.

A higher standing biomass within a site can be caused by larger individual plants or by a higher number of individual plants. These two possible causes for varying standing biomass show a different behaviour with respect to RGR. This is illustrated schematically in figure 7-4.

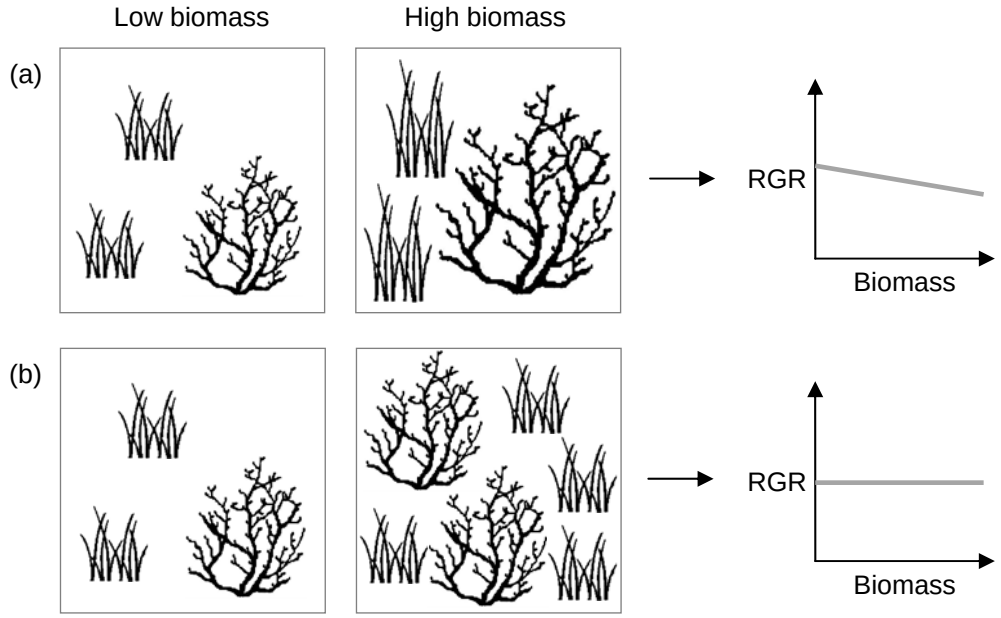

Figure 7-4: Different causes for varying standing biomass and their effect on the relation between biomass and maximum RGR: (a) higher biomass caused by older plants; (b) higher biomass caused by a higher number of individual plants of same age. The diagrams on the right show the trend for the relationship for medium aged plants, neither including exponential growth at seedling stadium nor dying of senescent plants.

Case (a) assumes that higher biomass is caused by the same number, but larger, i.e. older, individual plants (cf. figure 7-4). For an individual plant, RGR usually declines as biomass

increases, i.e. the plant becomes older (e.g. Eissenstat and Caldwell 1987, Vile et al. 2006). This is illustrated in figure 7-4 (a). Case (b), on the other hand, assumes that higher biomass is caused by more plants of the same size, i.e. age. In this case, RGR is constant for different biomass amounts.

For both cases, it should be noted that any effect from shading or self-shading is ignored. This is reasonable, because shading does not play a significant role in the open semi-arid environments with mainly low fractional cover and only one vertical vegetation layer (i.e. no trees with understory, for example) considered in this study.

As the examples illustrate, maximum RGRs can be assumed to be constant for varying amounts of biomass when the age structure is similar for different sites. For natural environments without anthropogenic influence, the following assumptions can be made for the vegetation within a site:

- The vegetation within a site in a natural environment consists of many individual plants.
- The individual plants have different age and cover the whole age spectrum.
- All plants within a site together form a quasi-natural age distribution.
- This results in a "medium" mean age for the vegetation within a site.

Additionally, the following assumptions can be made for different sites with similar plant species composition in natural environments:

- The age distribution and, thus, the mean age of the natural vegetation are similar for different sites.
- Differences in biomass between sites are, therefore, not caused by a differing age structure, but primarily by a different number of plants within the sites.

For the natural environments in the sparsely populated study areas in Kazakhstan (cf. section 3.2.5), the assumptions of natural age distribution within test sites and similar age structure between test sites are valid. This leads to the conclusion that the application of constant maximum RGR values for a whole study area with varying amounts of standing biomass is feasible. Therefore, constant maximum RGR_{AGB} values can be applied to derive AGB from maximum NPP for the natural vegetation in semi-arid Kazakhstan.

7.2.4 Derivation of Suitable RGR Values

RGR values for several individual species are available in the literature. The genera of characteristic plant species for the study areas in Kazakhstan are listed in table 7-1. Species occurrence was derived from field observations and a detailed map of vegetation communities' distribution (Volkova et al. 2010, cf. figure B-1, appendix B). Main grass and herbaceous genera are *Agropyron, Artemisia, Festuca, Poa*, and *Stipa*. Most of these genera are present in at least two of the three study areas. Main shrub genera are *Anabasis, Calligonum, Caragana, Haloxylon, Salsola*, and *Tamarix*. The presence of shrub genera differs more strongly.

For the genera listed in table 7-1, RGR values were taken from the literature. RGRs for species that grow in semi-arid regions, especially from Central Asia and similar environments, were preferred. As maximum RGRs are needed, only studies which derived maximum RGR were considered. Tables 7-2 and 7-3 summarize the available RGRs from the individual studies for grass and shrub species.

Table 7-1: Main plant genera that are characteristic for the three study areas in Central, South, and West Kazakhstan; plant life-form (G: Grass, H: Herb, S: Shrub) and occurrence (X: Genus is typical for study area).

Genus	Plant life-form (grass, herb or shrub)	Central Kazakhstan	South Kazakhstan	West Kazakhstan
Agropyron	G			X
Anabasis	S		X	X
Artemisia	H	X	X	X
Calligonum	S		X	X
Caragana	S	X		
Festuca	G	X		X
Haloxylon	S		X	
Poa	G		X	X
Salsola	S	X	X	
Stipa	G	X	X	X
Tamarix	S			X

For some species only RGRs from seedling experiments were available. As described in section 7.2.2, the RGR values for seedlings have to be adjusted to obtain RGR values that are valid for established plants. This is because experiments show that during the first few weeks following germination RGRs are at maximum (e.g. Dunn et al. 1987, Eissenstat and Caldwell 1987, Hunt and Cornelissen 1997, Meziane and Shipley 1999).

Therefore, data from Eissenstat and Caldwell (1987) were used to derive information on how strong RGRs recess and which fraction of seedling RGRs can be applied for older plants. The experiment from Eissenstat and Caldwell (1987) included two *Agropyron* species. Initial seedling RGRs were very high (129 mg g^{-1} d^{-1} and 172 mg g^{-1} d^{-1} respectively). After eight weeks, when plants were established, the two *Agropyron* species had RGRs of about 80 and 90 mg $g^{-1}d^{-1}$. The relation between the RGRs for seedlings and established plants indicates a reduction of RGR to about 57% of the initial value. Estimates of both initial and later maximum RGR were not available for other relevant species. Therefore, the percentage of 57% was assumed to be applicable to both grass and shrub species.

An additional conversion is necessary, because the available RGRs were derived from total plant harvests. Thus, they describe total plant growth in terms of total biomass. For this study, however, RGR in terms of AGB is needed. Therefore, a conversion factor has to be applied, as described in section 7.2.2.

Levang-Brilz and Biondini (2002) experimentally estimated both maximum RGR_{TPB} (equation 7-2), and maximum RGR_{AGB} (equation 7-3). 55 plant species (including 38 shrubs and 9 C_3 grasses) from the Great Plains were investigated. Several of the investigated genera are also present in semi-arid Kazakhstan (e.g. *Artemisia, Agropyron, Poa*, and *Stipa*). Thus, their observations were used to obtain the relation between these two values for this study.

The relation between RGR_{TPB} and RGR_{AGB} was calculated separately for C_3 grass and shrub species. This is important, because the two plant life-forms feature significantly different root-shoot ratios (C_3 grasses: 0.9, shrubs: 1.4; Levang-Brilz and Biondini 2002). A different ratio of biomass stored in roots and shoots, of course, alters the ratio between TPB and AGB.

The obtained ratios indicate that RGR_{AGB} was at average 150.2% of RGR_{TPB} for shrub species (relative standard deviation: 17.5%). For grass species, RGR_{AGB} was at average 166.1% of RGR_{TPB} (relative standard deviation: 18.9%). These percentages are applied to the available RGRs of grasses and shrubs to derive RGRs in terms of AGB. The resulting final RGR_{AGB} values

for the individual species from genera typical for the three study areas in Kazakhstan are presented in tables 7-2 and 7-3.

Table 7-2: RGRs for grass/herbaceous species and conversion to final RGR_{AGB} values. X: adjustment/conversion was applied, –: no adjustment was applied.

Species	RGR_{TPB} [mg g^{-1} d^{-1}]	Source study	Comment	Seedling adjustment	TPB to AGB conversion	Final RGR_{AGB} [mg g^{-1} d^{-1}]
Agropyron desertorum	40	Eissenstat and Caldwell 1987	RGR from glasshouse experiment with older seedlings, second experiment, low nutrient treatment	–	X	66.4
Agropyron repens	86	Reich et al. 2003	Species from plain grassland and savannah of central North America, growth of seedlings, total biomass harvested	X	X	81.4
Agropyron smithii	93	Reich et al. 2003	[See *Agropyron repens*, Reich et al. 2003]	X	X	88.0
Agropyron spicatum	50	Eissenstat and Caldwell 1987	[See *A. desertorum*, Eissenstat and Caldwell 1987]	–	X	83.1
Artemisia ordosica	28	Zheng et al. 2008	Species from Inner Mongolia, seedlings experiment, total biomass harvested, precipitation: 37.5 mm/month, temperature: 15°C/25°C (night/day)	X	X	26.5
Artemisia sphaerocephala	28	Zheng et al. 2008	[See *Artemisia ordosica*, Zheng et al. 2008]	X	X	26.5
Stipa bavioensis	34.5	Oesterheld 1992	Species from Argentina, experiment with plants of at least 2 years age, total plant growth per total biomass calculated	–	X	57.3
Stipa comate	80	Reich et al. 2003	[See *Agropyron repens*, Reich et al. 2003]	X	X	75.7
Festuca arundinacea	23.5	Wilhelm and Nelson 1978	Experiment with established plants of at least 2.5 months age, RGR calculated when dry-weight accumulation was nearly linear, total plants harvested	–	X	39.0

Table 7-3: RGRs for shrub species and conversion to final RGR_{AGB} values. X: adjustment/conversion was applied, (X): 'half' (78.5%) adjustment was applied.

Species	RGR_{TPB} [mg g^{-1} d^{-1}]	Source study	Comment	Seedling adjustment	TPB to AGB conversion	Final RGR_{AGB} [mg g^{-1} d^{-1}]
Caragana korshinskii	13	Zheng et al. 2008	Species from Inner Mongolia, seedlings experiment, total biomass harvested, precipitation: 37.5 mm/month, temperature: 15°C/25°C (night/day)	X	X	11.1
Haloxylon persicum	22.9	Song et al. 2006	Seeds from sandy desert, Xinjiang province, northwestern China, seedlings experiment, total biomass harvested, RGR value for control salinity level and low NO_3^--N (similar to conditions in the region where *H. persicum* occurs)	X	X	19.6
Tamarix aphylla + Tamarix ramosissima	24	Hayes et al. 2009	Stem cuttings planted in nursery, RGR calculated after 19 weeks, total biomass harvested, RGR of *T. aphylla*: 23 mg g^{-1} d^{-1}, RGR of *T. ramosissima* 25 mg g^{-1} d^{-1})	(X)	X	28.3

Finally, average RGR_{AGB} values for the plant life-forms of grasses and shrubs are needed. RGR values are available for several grass species from four different genera. First, mean RGR_{AGB} values for these four genera were calculated (cf. table 7-4). Second, average RGR_{AGB} values were derived from the characteristic species for the three study areas. Final RGR_{AGB} values derived were 44 mg g^{-1} d^{-1} for Central Kazakhstan, 46.5 mg g^{-1} d^{-1} for South Kazakhstan, and 53 mg g^{-1} d^{-1} for West Kazakhstan.

For the characteristic shrub genera for the study areas in Kazakhstan, only three maximum RGRs were available for three different genera (table 7-3). Each of these genera occurs in one of the three study areas (cf. table 7-1). Thus, no mean RGRs were calculated for shrubs, but the three RGR_{AGB} values were directly applied for the study area with major occurrence of the corresponding shrub genus. The final RGR_{AGB} values to be applied for the three study areas are 11.1 mg g^{-1} d^{-1} for Central Kazakhstan, 19.6 mg g^{-1} d^{-1} for South Kazakhstan, and 28.3 mg g^{-1} d^{-1} for West Kazakhstan.

Table 7-4: Mean RGR_{AGB} values for grass genera and resulting average RGR_{AGB} for the three study areas in Central, South, and West Kazakhstan. X: Genus is typical for study area.

Genus	Mean RGR_{AGB} [mg g^{-1} d^{-1}]	Central Kazakhstan	South Kazakhstan	West Kazakhstan
Agropyron	79.7			X
Artemisia	26.5	X	X	X
Festuca	39.0	X		X
Stipa	66.5	X	X	X
Average RGR_{AGB}	53.0	44.0	46.5	53.0

7.3 Possible Error Sources from Input Data and the Resulting Potential Error of the Biomass Estimate

The developed approach for biomass estimation is based on five input parameters: NPP, fractional cover, $RGR_{TPB,max}$, and the two conversion factors $r_{Est./Seed}$ (ratio between RGR of established plants and RGR of seedlings) and $r_{AGB/TPB}$ (ratio between RGR in terms of AGB and RGR in terms of TPB). These parameters are subject to errors. In this section, possible errors associated with these input data are discussed and quantified as far as possible. This information in then used in section 7.3.5 to assess the potential error associated with the resulting biomass estimate.

7.3.1 Possible Error Sources of the NPP Input

The NPP calculation with BETHY/DLR is based on several input data and defined biochemical parameters (cf. section 2.2.2). The complexity of the model makes it hardly possible to define the impact of each parameter on the NPP result. Extensive Monte Carlo experiments would be needed, which have not been performed so far. However, sensitivity analyses are available, as well as results from validation of the modelled NPP.

Regarding the input data, sensitivity analyses performed by Wißkirchen (2005) showed that NPP results from BETHY/DLR are most strongly affected by CO_2 concentration, LAI, the vegetation classification, and precipitation. Niklaus (in preparation) also performed a detailed sensitivity study for test sites in southern Africa. Several input parameters of BETHY/DLR were varied by ±5, ±10, ±20, ±25, ±50, ±75, and ±100 per cent. Results showed that NPP was linearly related to temperature. However, at very high temperatures, which result in vegetation canopy temperatures >55°C, NPP decreased due to a limitation of the photosynthesis rate. Regarding varying precipitation, the sensitivity tests showed that the effect on NPP strongly depends on soil characteristics. A rise in precipitation only leads to higher productivity, when the soil dries out at lower precipitation amounts (Niklaus, in preparation). PAR proved to strongly influence the productivity with an almost linear relationship. However, very high PAR results in a high canopy temperature that may limit the photosynthesis rate. Strong influences on NPP were also observed for LAI with an almost linear relationship, and for the land cover classification (Niklaus, in preparation).

In this study, an accuracy assessment of the meteorological input data from ECMWF has been performed (cf. section 4.1.1.2). Comparison to climate station data showed high correlation coefficients of R>0.96 for temperature. For monthly precipitation, the correlation coefficient was R=0.64. An error thus inheres in the precipitation data from the ECMWF, but the effect on NPP might be low. The temperature data seem to have a very small error.

Previously, also validations of BETHY/DLR have been performed for forests and agriculture. For example, Wißkirchen (2005) compared modelled NEP with measured NEP from CARBOEUROPE stations for forests. The model was driven by station data. The observed correlation coefficient was R=0.93 and the mean relative deviation +20.4%. Tum and Günther (2011) recently validated BETHY/DLR results for agricultural areas in Germany and Austria with statistical data. For German districts BETHY/DLR underestimated the NPP by 17% (R^2: 0.58–0.96); for Austrian districts NPP was overestimated by 8% (R^2: 0.74–0.78).

In this study, BETHY/DLR is applied to a region with very different land cover and climatic conditions, compared to the previous studies. Thus, an independent validation is needed to reliably estimate the error of the modelled NPP for Kazakhstan. In the following section, results from the validation of NPP for grassland in Central Kazakhstan are presented.

7.3.2 Validation of Modelled NPP Data for Central Kazakhstan

As input data for the biomass estimation approach, the NPP estimates derived with BETHY/DLR for Kazakhstan (cf. section 6.2) are used in this study. For the validation of the NPP estimates, field data from Central Kazakhstan were collected (cf. section 4.3). These data were already used for the validation of results from BETHY/DLR and RBM for the model comparison. The NPP estimates derived with BETHY/DLR for Kazakhstan, however, are based on a different land cover classification. The MODIS land cover product (cf. section 4.1.2.6) was used for the model comparison. The Central Asia land cover and land use map (cf. section 4.1.3) was applied for modelling of the NPP for entire Kazakhstan (cf. section 6.2). Therefore, the NPP results are again validated with ground-based data.

BETHY/DLR calculates NPP of the grass and shrub fraction within each grid cell separately. For the validation, cumulative grass NPP is calculated from beginning of 2011 until the period of field data collection (DOY 1–160). Previous measurements of below-ground NPP (23% of total NPP, Propastin et al. 2012) are then applied to obtain above-ground grass NPP (cf. section 5.5.2).

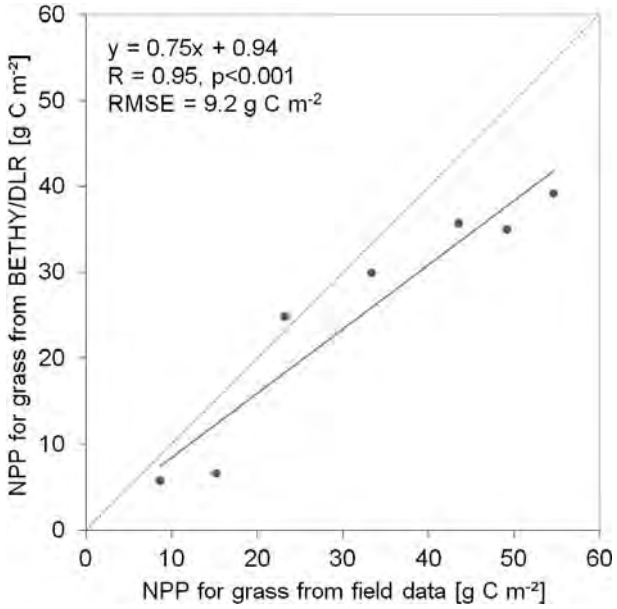

Figure 7-5: Correlation between the NPP of above-ground grass/herb vegetation derived from field data and the results of above-ground grass NPP calculated with BETHY/DLR for seven test sites in Central Kazakhstan in 2011. The NPP calculation with BETHY/DLR was based on the Central Asia land cover and land use map. Daily NPP was summed for DOY 1–160.

The results of the modelled NPP and corresponding field-based NPP for the test sites in Central Kazakhstan are shown in figure 7-5. Ground-based above-ground grass NPP for the validation test sites ranges from 9 to 55 g C m^{-2}. Results from BETHY/DLR for above-ground grass NPP are between 8 and 45 g C m^{-2}. The slope of the regression line is 0.75 and the correlation is high with R=0.95. The RMSE is 9.2 g C m^{-2}. At six of the seven test sites available for validation NPP is underestimated by BETHY/DLR (cf. figure 7-5). The percentage absolute error is 26%. A reliable validation of the shrub NPP was not feasible, because the available field data for shrubs were not sufficient. Therefore, the relative error of 26% is also used to represent the error associated with the NPP for shrubs.

7.3.3 Error Associated with the Fractional Cover Input

A second major parameter that strongly affects the accuracy of the biomass estimate is the percentage fractional cover assumed for grass and shrubs. For regional biomass estimation in this study, the fractional cover is defined by the classification of the Central Asia land cover and land use map (cf. table 4-2, section 4.1.3). The land cover map, of course, defines constant fractions for individual classes. Thus, the heterogeneity in fractional cover observed in the field within land cover classes cannot be taken into account.

Table 7-5: Relative fractional grass and shrub cover based on the classification of the Central Asia land cover and land use map (Klein et al. 2012), as well as fractional cover from field observations, and the difference between the two fractional cover values.

Study area	Test site	Grass fractional cover [%]			Shrub fractional cover [%]		
		Land cover map (LC)	Field data	Difference LC – field	Land cover map (LC)	Field data	Difference LC – field
Central Kazakhstan	1	50	17	33	50	83	-33
	2	35	11	24	65	89	-24
	3	35	29	6	65	71	-6
	4	95	92	3	5	8	-3
	5	95	97	-2	5	3	2
	6	95	89	6	5	11	-6
	7	95	74	21	5	26	-21
	8	95	98	-3	5	2	3
	9	95	74	21	5	26	-21
	10	50	96	-46	50	4	46
	11	95	87	8	5	13	-8
South Kazakhstan	12	50	46	4	50	54	-4
	13	50	98	-48	50	2	48
	14	50	98	-48	50	2	48
	15	50	84	-34	50	16	34
	16	50	100	-50	50	0	50
	17	50	26	24	50	74	-24
	18	95	100	-5	5	0	5
	19	50	100	-50	50	0	50
	20	95	100	-5	5	0	5
West Kazakhstan	21	50	30	20	50	70	-20
	22	50	99	-49	50	1	49
	23	95	100	-5	5	0	5
	24	35	100	-65	65	0	65
	25	95	97	-2	5	3	2
	26	95	100	-5	5	0	5
	27	50	100	-50	50	0	50
	28	50	87	-37	50	13	37
	29	50	100	-50	50	0	50
	30	50	88	-38	50	12	38
Ø fractional cover		**66**	**81**		**34**	**19**	
Ø |difference|				**25**			**25**
absolute σ of Ø |difference|				**20**			**20**

Comparison of the fractional cover definitions from the Central Asia land use and land cover map with the relative fractional cover estimates from field observation allows for quantification of the error of the defined fractions (cf. figure 7-6). The comparison indicates that the defined fractions differ at average 25% (absolute difference between the fractional cover values) from the field-based grass and shrub fractions.

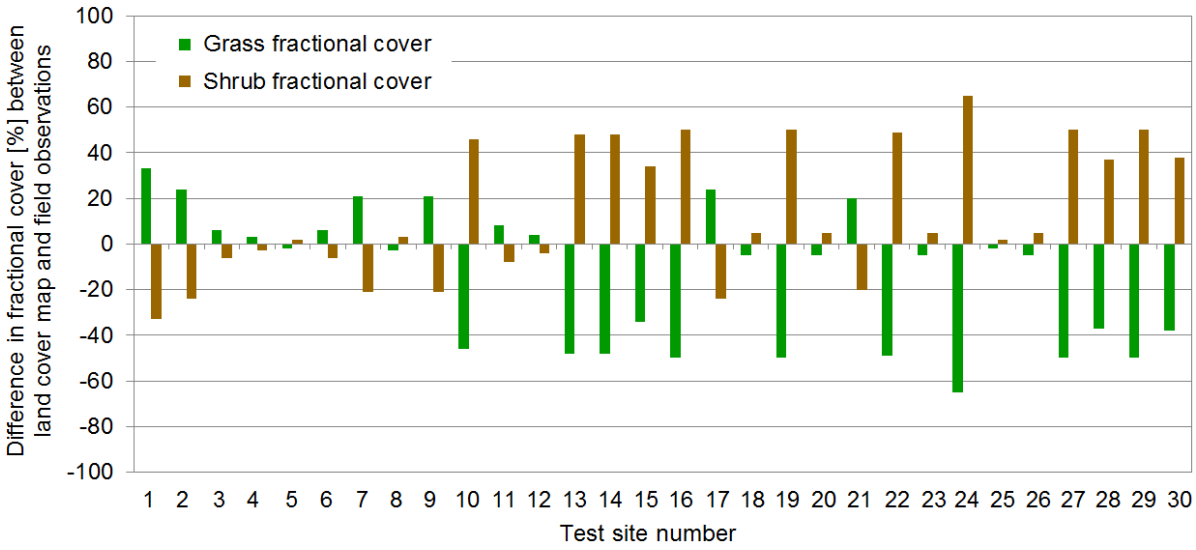

Figure 7-6: Difference between the relative fractional cover definitions based on the Central Asia land cover and land use map (Klein et al. 2012) and the relative fractional cover estimates from field observations.

For demonstration of the methodological approach for derivation of biomass estimates from NPP, therefore, two biomass estimates were calculated for the test sites. First, with fractional cover defined based on the Central Asia land cover and land use map. Additionally, a second estimate was derived for which the percentage cover fraction of grass and shrubs was defined according to the fractional cover estimates observed during the field campaign in June 2011 (cf. section 4.3.2).

7.3.4 Errors Associated with the RGRs and Conversion Factors

Actual RGR varies with differing ecological conditions, i.e. temperature, water availability, light, and fertilization. The influences of these parameters on the RGR have been widely investigated. However, results from different studies and for different species are not always coherent.

For example, higher temperatures were found to reduce RGR in some species (*Artemisia*), but had no impact on others (*Caragana*, Zheng et al. 2008). An increase in water stress was found to decrease RGR for *Artemisia, Caragana*, and *Stipa*, but with different magnitudes (Shimizu et al. 2010, van Staalduinen and Anten 2005, Zheng et al. 2008). In another study, no effect was observed from different water supplies on growth of arid shrubs (Padilla et al. 2009). Nutrient regimes, e.g. phosphorus and nitrogen levels may also influence RGR, as well as soil temperature (Eissenstat and Caldwell 1987), PAR (Hunt and Cornelissen 1997), and grazing intensities (Oesterheld 1992, van Staalduinen and Anten 2005).

Because of these diverse possible influences, maximum RGRs, which are derived under optimum conditions, have to be used in order to minimize the error inherent in the RGR value. Maximum RGRs are commonly used to compare the speed of growth of different species (e.g. Levang-Brilz and Biondini 2002, Poorter and Remkes 1990).

Within this study, also maximum RGRs were used. These are combined with the maximum daily NPP from the period of maximum productivity. Thus, it can be assumed that the conditions at the time of investigation were favourable for plant growth. Consequently, the maximum RGR can be combined with the maximum NPP value for biomass estimation (cf. equation 7-7).

7.3.4.1 Assumed Error of the RGR Values

For the individual RGR values derived from experimental studies, errors were not provided. Nevertheless, an error can be estimated for the averaged RGRs that are calculated for grasses and shrubs within this study.

As observed in many studies, RGRs between species may vary considerably (e.g. Grime and Hunt 1975, Hunt and Cornelissen 1997). The variation is especially strong between species classified as ruderals or competitors (high RGR_{max}) and stress-tolerators (low RGR_{max}). In the semi-arid environments of Kazakhstan only stress-tolerators, i.e. species adapted to growth-limiting conditions, are common. Thus, the variability in RGRs can be assumed to be lower than if species from different ecosystems had to be considered. RGRs, however, still differ between species. Thus, the averaged RGR value contains an error, because the actual species composition of individual pixels is not known.

The mean RGR for the four grass genera available within this study is 51.7 mg g^{-1} d^{-1}. The standard deviation is 19.7 mg g^{-1} d^{-1}, which corresponds to 38% of the RGR. This value is used as estimate of the error associated with the averaged grass RGRs. For shrubs no average RGR was calculated. Nevertheless, the applied RGR values cannot be assumed to have no error. Thus the error estimate obtained for grass RGRs is also used as error estimate for shrub RGRs.

7.3.4.2 Assumed Error of the RGR Adjustment Factor

The two conversions applied to the RGRs, of course, add an error to the RGR values. The first adjustment is made to convert RGRs for seedlings to RGRs for established plants.

The adjustment factor was derived from RGRs observed for two species (cf. section 7.2.4). The difference between the reduction for the two species investigated by Eissenstat and Caldwell (1987) is used as an estimate for the error of the reduction value. Other information concerning the error is unfortunately not available.

For the two species, a reduction to 52% and 62% of initial RGR was observed respectively. These two values differ relatively 8.8% from the average. The actual error can be assumed to be higher, because other species from other genera are also present in the study areas. This error cannot be quantified due to limited data availability.

7.3.4.3 Assumed Error of the RGR Conversion Factor

The second conversion relates RGR_{TPB} to RGR_{AGB}. The relation between these two values was derived from results of a study by Levang-Brilz and Biondini (2002). Their study included 55 plant species (cf. section 7.2.4).

For C_3 grasses, RGR_{AGB} was at average 166.1% of RGR_{TPB} with a standard deviation of 18.9%. For the investigated shrub species, the relation was 150.2% with a standard deviation of 17.5%. As no other information is available, these values are used as estimates of the error associated with the conversion factors applied to grass RGRs and shrub RGRs.

7.3.5 Potential Error of the Biomass Estimate Resulting from Error Propagation

The developed approach for biomass estimation from NPP, as described in section 7.2, can be summarized in the following equation:

$$Biomass = \frac{NPP_{max} \cdot FC}{RGR_{TPB,max} \cdot r_{Est./Seed} \cdot r_{AGB/TPB}} \tag{7-8}$$

The accuracy of the final biomass estimate thus directly depends on the accuracy of five parameters: NPP_{max}, fractional cover (FC), $RGR_{TPB,max}$, and the two conversion factors $r_{Est./Seed}$ and $r_{AGB/TPB}$. The possible errors associated with these input parameters have been discussed in the previous sections. For the RGR values and their conversion factors only assumptions could be made with respect to the actual error. Thus, only a rough estimate of the potential error of the biomass estimate can be provided in this section.

The error of the final biomass estimate m_F can be calculated based on the law of error propagation for standard errors. The equation for calculation of the error of the biomass result is provided in equation 7-9, with F being the biomass function (i.e. equation 7-8), x_i being the individual parameters from the biomass function (i.e. NPP_{max}, FC, $RGR_{TPB,max}$, $r_{Est./Seed}$, and $r_{AGB/TPB)}$), and m_i being the mean error of parameter x_i.

$$m_F = \sqrt{\sum_{i=1}^{n} \left(\frac{\partial F}{\partial x_i} \right)^2 m_i^2} \tag{7-9}$$

The mean errors of the input parameters have been obtained in the previous sections. The NPP data have been validated with field data from Central Kazakhstan (cf. section 7.3.2). The validation results for grass NPP indicated a percentage error of 26%. For the fractional cover definitions based on the Central Asia land cover and land use map an absolute error of 25% was observed (cf. section 7.3.3). The assumed relative error for the RGR values is 38% and the relative error for the adjustment factor $r_{Est./Seed}$ is 8.8%. The relative errors assumed for conversion from RGR_{TPB} to RGR_{AGB} are 18.9% for grass and 17.5% for shrubs (cf. section 7.3.4).

Based on these input parameter errors, the mean error of the final biomass estimate m_F is calculated with equation 7-9. The error associated with the biomass estimate is determined separately for grass biomass and shrub biomass. Table 7-6 gives an overview of the parameter values and errors used for error calculation. For NPP and FC typical values for the study areas in semi-arid Kazakhstan are chosen.

The calculated absolute error is finally set in relation to the biomass estimate to obtain the relative error of the biomass estimate. The biomass estimate is therefore calculated with equation 7-8 based on the values given in table 7-6.

The potential errors of the NPP-based biomass estimates amount to about 117%. This is mainly caused by the high errors of the fractional cover input and the RGR values. It has to be pointed out that these results are only rough estimates of the error. A detailed analysis of the actual errors of all input parameters for the biomass estimation would be necessary for profound error estimation.

Table 7-6: Overview of typical parameter values and associated errors used for the calculation of the potential error of the biomass estimate. The error for the fractional cover input is related to the definitions based on the Central Asia land cover and land use map.

	Grass			Shrub		
	Value	Absolute error	Relative error	Value	Absolute error	Relative error
NPP_{max} [g C d^{-1}]	2.5	0.65	26.0	1.5	0.39	26.0
FC [%]	0.66	0.25	37.9	0.34	0.25	73.5
$RGR_{TBP,max}$ [mg g^{-1} d^{-1}]	54.6	20.8	38.0	22.9	8.7	38.0
$r_{Est./Seed}$	0.57	0.05	8.8	0.57	0.05	8.8
$r_{AGB/TPB}$	1.66	0.31	18.9	1.50	0.26	17.5
Biomass estimate [g C]	**32.4**	**37.9**	**117.0**	**26.0**	**30.6**	**117.7**

Because of the uncertainties in the errors associated with the input data, it is of special interest to validate the NPP-based biomass estimates with field data. In the following chapter, results of the application of the developed approach to the three study areas as well as the validation with biomass field data are described.

7.4 Results of Biomass Estimation for the Study Areas and Validation with Field Data

7.4.1 Biomass Results for the Three Study Areas

The developed methodology is applied to the NPP data derived with BETHY/DLR for the three study areas in Central, South, and West Kazakhstan. For demonstration and validation of the approach, two biomass estimates are derived based on different fractional cover definitions. For application to the entire study areas, the coverage definitions from the Central Asia land cover and land use map (cf. section 4.1.3) are used. For the test sites, additionally, biomass estimates based on fractional cover information from the field are obtained.

The spatial resolution of the resulting biomass estimate is ~0.00833° (ca. 925 m × 650 m for Kazakhstan), the same as for NPP data. For pixels that are classified as agriculture in the land cover and land use classification no biomass is calculated. For forest areas only biomass of the secondary class 'C_3 short grass' is obtained (cf. table 6-1). Finally, estimated biomass amounts for grass and shrubs are summed to obtain a map of total AGB for the three study areas.

The results of the above-ground biomass estimation for grass and shrub biomass are presented in figures 7-7 and 7-8 respectively. Additionally, figure 7-9 shows the result of the sum of grass and shrub biomass. The obtained above-ground grass biomass for Central Kazakhstan shows higher biomass in the North of the study area. South of Akshatau grass AGB is typically between 5 and 30 g C m^{-2}, north of Akshatau between 30 and 100 g C m^{-2}.

In West Kazakhstan also high grass biomass can be observed for large areas in the North, where grass AGB is typically 40–80 g C m^{-2}. In the southern part grass biomass is mainly between 10 and 20 g C m^{-2}. Above-ground grass biomass estimates for the study area in South Kazakhstan show high biomass values along the valley of the Shu River. Highest grass biomass with up to >200 g C m^{-2} can be observed in the South-East of the study area. This is a mountainous grassland region with Kastanozem soil and relatively high precipitation (cf. chapter 3). For other parts of the study area in South Kazakhstan only low grass biomass, mainly between 10 and 20 g C m^{-2} is obtained.

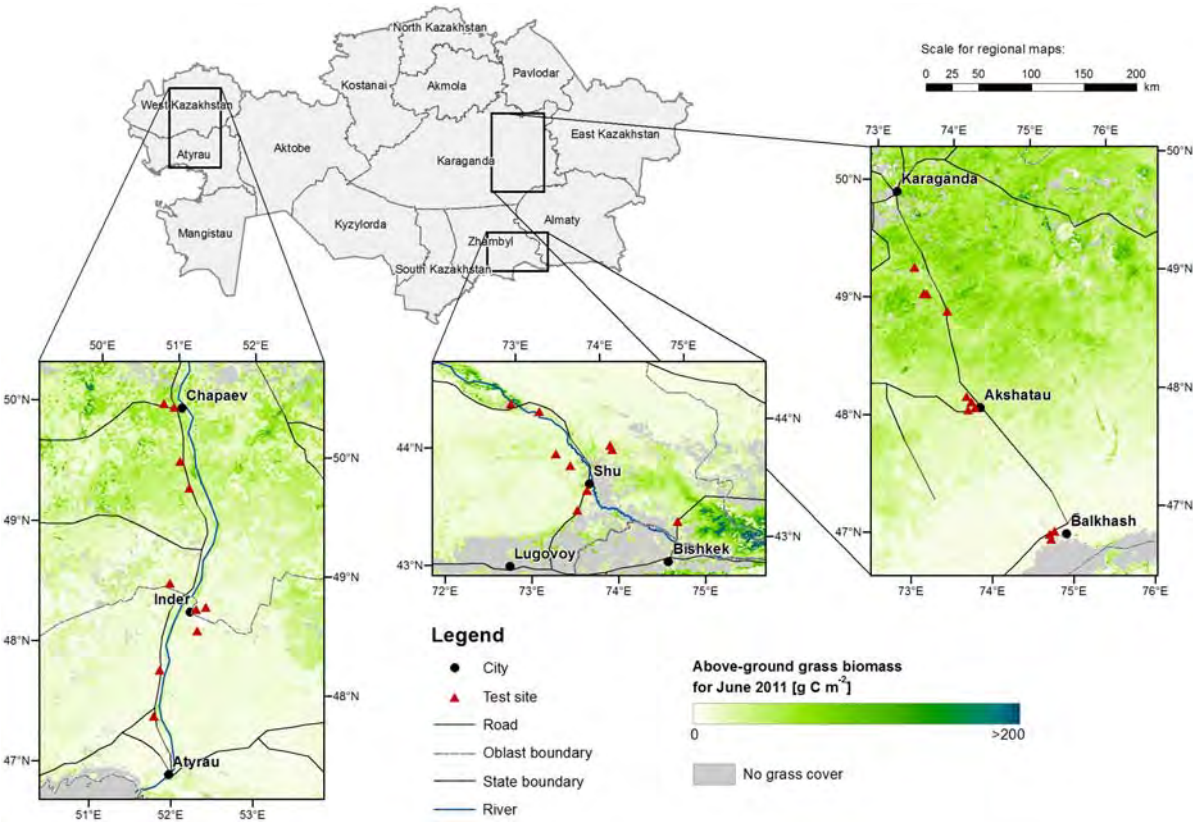

Figure 7-7: Result of above-ground grass biomass for June 2011 derived with the developed approach for the three study areas in Central, South, and West Kazakhstan.

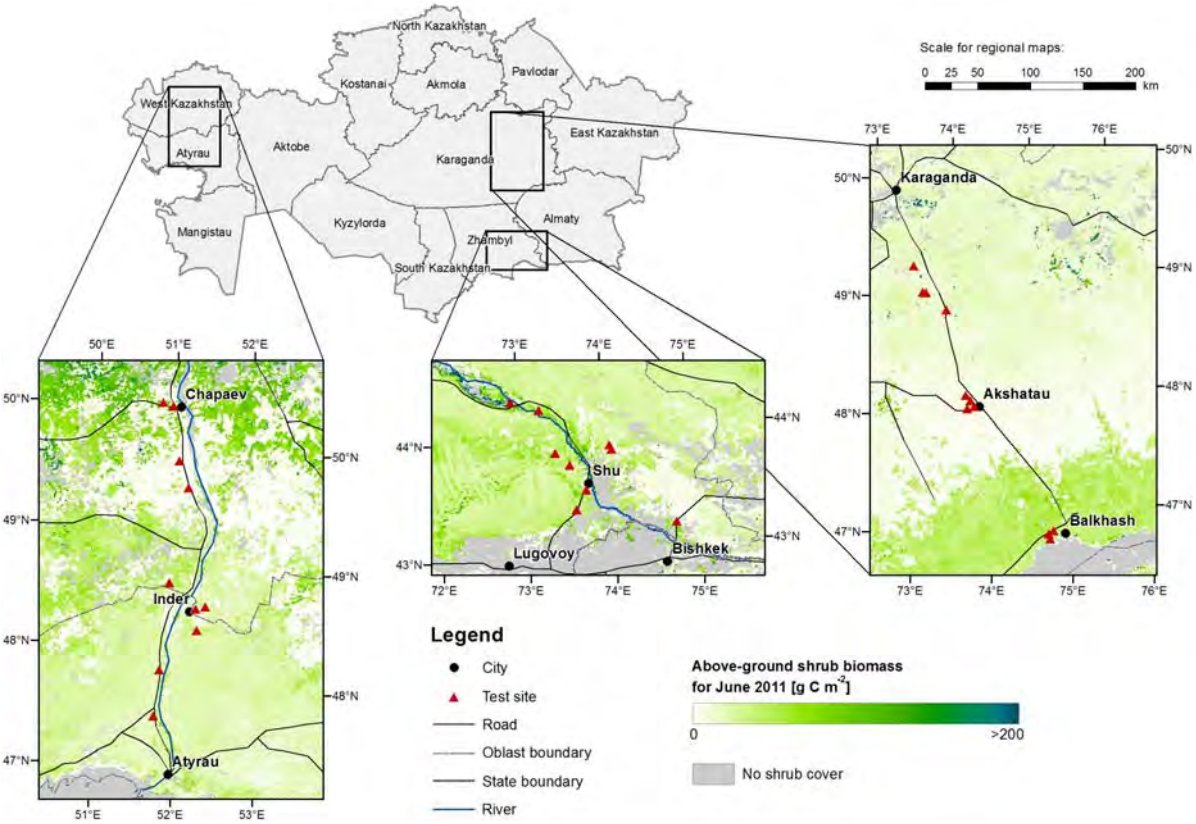

Figure 7-8: Result of above-ground shrub biomass for June 2011 derived with the developed approach for the three study areas in Central, South, and West Kazakhstan.

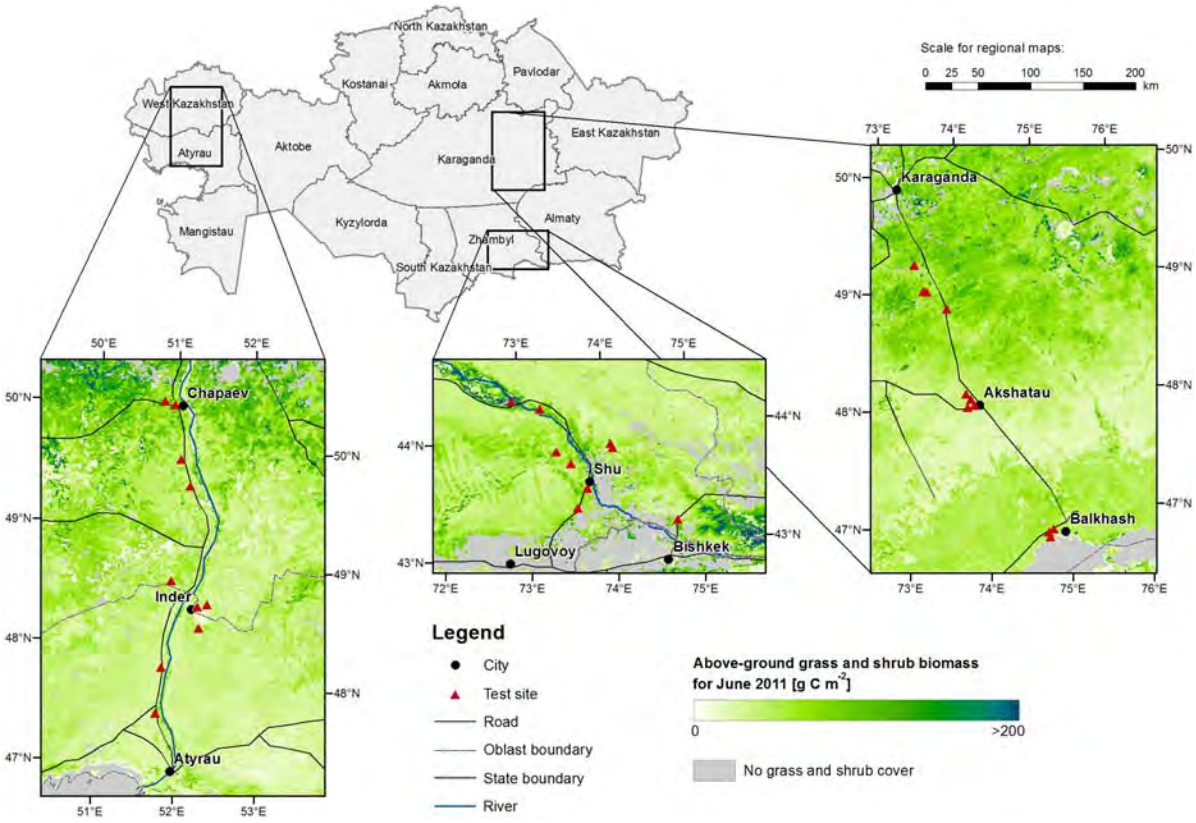

Figure 7-9: Result of above-ground grass and shrub biomass for June 2011 derived with the developed approach for the three study areas in Central, South, and West Kazakhstan. This map shows the sum of the above-ground grass and shrub biomass.

The results of above-ground shrub biomass show a different pattern. In Central Kazakhstan high shrub biomass is estimated in the South, within a strip north of Lake Balkhash. Above-ground shrub biomass in this zone is between 30 and 60 g C m^{-2}. For most other parts of Central Kazakhstan above-ground shrub biomass between 5 and 25 g C m^{-2} is obtained. In West Kazakhstan low shrub biomass with typically 15–30 g C m^{-2} covers the southern part of the study area. Highest shrub biomass occurs in the very northern part with up to 100–150 g C m^{-2}. Between these two regions a strip with low shrub biomass can be observed especially in the eastern part. In the study area in South Kazakhstan large areas show above-ground shrub biomass between 20 and 40 g C m^{-2}. The grassland region in the South-East shows very low shrub biomass. Along the Shu River and south-west of the Shu River valley some areas with shrub biomass of up to 80–150 g C m^{-2} can be found.

7.4.2 Observations from Field Data

The above-ground dry matter (DM) biomass measured at the test sites in Central Kazakhstan varies largely especially regarding the shrub biomass (cf. figure 7-10). The three southernmost sites are covered by desert shrubland, the central and northern sites are steppe grassland. For the shrubland sites grass/herb biomass ranges from 5.2 to 138.1 g DM m^{-2} while shrub biomass ranges from 243.8 to 792.7 g DM m^{-2}. Mean grass/herb and shrub biomass are 58.8 and 445.3 g DM m^{-2} respectively. For the central and northern part of the study area grass/herb above-ground biomass in the range 49.0–179.0 g DM m^{-2} with a mean of 130.5 g DM m^{-2} was observed. Shrub biomass at these sites reaches values of 7.1 to 88.8 g DM m^{-2} with a mean value of 34.7 g DM m^{-2}.

In the study area in South Kazakhstan biomass amounts vary from site to site due to changing water availability, differences in soils, and plant species distribution. Above-ground DM biomass is lower than in Central Kazakhstan. Biomass amounts are generally below 100 g DM m^{-2} except for three test sites that show significantly higher biomass. The highest biomass is observed in a reed grass community (test site 18) and in an ephemeroid – grass – sagebrush desert with high *Artemisia* cover of 50–80 cm plant height (test site 19). The third test site (test site 17) with high biomass amounts contains an extraordinary high shrub cover due to large *Haloxylon aphyllum* shrubs. Significant shrub biomass was only present at this and one other test site (test site 12) in South Kazakhstan. Considering all test sites in South Kazakhstan, grass/herb biomass ranges from 17.6 g DM m^{-2} to 299.0 g DM m^{-2} with a mean of 106.7 g DM m^{-2}. Shrubs grow only in few test sites and reach a maximum of 127.6 g DM m^{-2} for the test site with high *Haloxylon aphyllum* cover. Mean shrub DM biomass over the Southern Kazakhstan test sites is 23.3 g DM m^{-2}.

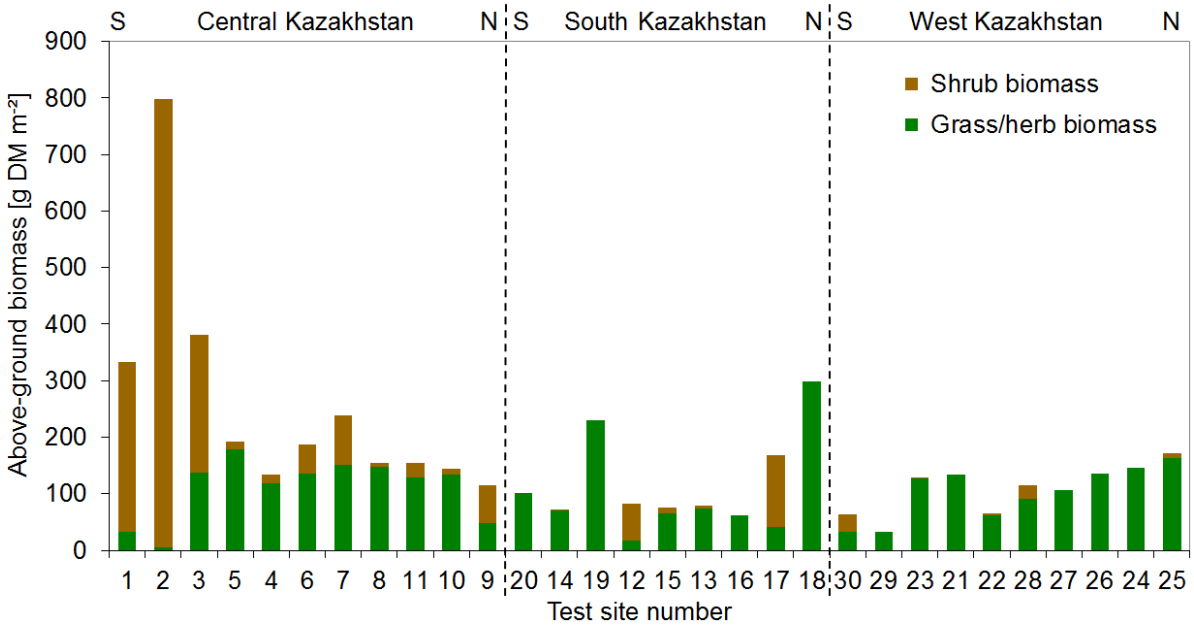

Figure 7-10: Field measurements of mean above-ground dry weight biomass for the test sites in Central, South, and West Kazakhstan in June 2011. The sites within the study areas are sorted from South to North.

In West Kazakhstan the grass/herbs biomass is in the range 32.0–163.4 g DM m^{-2} with a mean of 102.8 g DM m^{-2}. Shrub biomass was only present at few test sites in this study area with a maximum of 30.9 g DM m^{-2} and a mean of 6.6 g DM m^{-2} over all test sites. For this study area a gradient from lower biomass in the South to higher biomass in the North is apparent, except for two test sites (test sites 21 and 23) where higher biomass is observed (cf. also photo tables in Appendix D). Similar biomass amounts to those observed in this study were reported from field measurements in other semi-arid regions of Central Asia and China (table 7-7) as well as in other semi-arid environments around the world (table 7-8).

Table 7-7: Reported field measured vegetation biomass for semi-arid regions in Central Asia and China.

Ecosystem/vegetation	Location	Above-ground biomass [g DM m^{-2}]	Source
Grasslands: typical steppe, desert steppe, steppe desert	Inner Mongolia, China	88 (desert steppe) – 177 (meadow steppe)	Fan et al. 2009
Desert shrubland of *Artemisia ordosica*	Ordos Plateau, Inner Mongolia, China	ca. 480 – 1090 (annual + old branch biomass)	Jin et al. 2007
Xilingol steppe: mean plant biomass	Inner Mongolia, China	118.9	Kawamura et al. 2005
Haloxylon persicum	Kyzylkum desert, Kazakhstan	100 – 300	Kurochkina 1966
Artemisia ordosica: stand total biomass	Mu Us desert, Northern China	Fixed dunes: 339.9, semi-fixed dunes: 178.8, shifting dunes: 25.0	Li and Xiao 2007
Stipa grandis and *Leymus chinensis steppe*	Inner Mongolia, China	140 – 190	Xiao et al. 1995
Grasslands: dry grass yield	China	For individual provinces: 32.6 – 295.5; Mean over all plots: 83.0	Xu et al. 2008

Table 7-8: Reported field measured vegetation biomass for semi-arid regions around the world.

Ecosystem/vegetation	Location	Above-ground biomass [g DM m^{-2}]	Source
Semi-arid vegetation: standing crop	Morocco	Desert: 33.1 – 43.7 Steppe: 53.1 – 214.6 Woodsteppe: 11.7 – 251.8 Shrubs: 107.5 – 878.6	Baumann 2009
Mixed-grass prairie	Northern Great Plains, USA	total: 539.4 standing live: 239.8	Beeri et al. 2007
Grazing ecosystem: herbaceous biomass	Sahel, Burkina Faso	22 – 235	Bénié et al. 2005
Semi-arid rangelands	South-east Botswana	18.5 – 170	Dancy et al. 1986
Range of vegetation types from short grass plains to dense mopane savannah	Etosha, Namibia	29 – 420	Du Plessis 1999
Saharo-sahelian transition: maximum herbaceous biomass	Gourma region, Mali	24 – 105	Frison et al. 1998
Semi-arid rangelands: peak total biomass (herbage and shrubs)	South Australia	50 – 150	Graetz et al. 1988
Rangeland, herbaceous vegetation	Gourma region, Mali	93.8	Hiernaux et al. 2009
Arid rangelands: herbage peak biomass	Central Australia	14 (*Acacia* shrubland) – 172 (floodplain site)	Hobbs 1995
Rangeland vegetation (herbaceous and sparse woody): peak biomass	Gourma region, Mali	30 – 300	Mangiarotti et al. 2008
Semi-arid ecosystems: mean above-ground carbon storage including leaf litter	South Africa	Xeric shrubland: 150 – 1290 Grassland: 200 Karoo: 170	Mills et al. 2005
Semi-arid grassland, steppe, and savannah	Etosha, Namibia	Grass: 19.6 – 101.6 Woody: 35.9 – 97.9 Total: 104.7 – 137.5	Sannier et al. 2002
Semi-arid natural herbaceous vegetation	Israel	50 – 300	Svoray and Shoshany 2002
Rangelands: end-of-season herbaceous biomass	Sahel, Niger	20 – 170	Wylie et al. 1995

7.4.3 Validation of Above-Ground Biomass Estimates with Field Data

As described in section 7.4.1, two biomass estimates were obtained for the test sites in Kazakhstan. The first estimate is calculated with fractional cover values based on the land cover and land use map. The second estimate is calculated with fractional cover estimates derived from field observations. The estimated above-ground biomass of grass and shrubs are compared to field-measured above-ground biomass. Results of comparison for grass biomass are presented in figures 7-11 and 7-12 and results for shrub biomass are presented in figures 7-13 and 7-14.

For the validation of grass biomass, a total of 28 test sites is available. Two sites from the study area in South Kazakhstan have to be excluded from the analysis. Test site 18 from South Kazakhstan is disregarded because the corresponding location is classified as irrigated agriculture in the Central Asia land cover and land use map and thus no grass NPP was calculated with BETHY/DLR. Second, test site 19 is excluded because the vegetation of this site is very special and not made up of a typical combination of herbaceous species. It is densely covered by *Artemisia* and can not be compared to the other test sites in the study area South Kazakhstan (cf. photo tables, Appendix D).

As the results of the comparison show, ground-based biomass observations are higher than biomass estimates from NPP data for most test sites (cf. figure 7-11). The underestimation is especially strong for the biomass estimates derived with fractional cover definitions based on the land cover map. Table 7-9 provides an overview of the number of grass biomass estimates that fall within the error ranges of ±10 g C m^{-2}, –10 to –20 g C m^{-2}, and lower than –20 g C m^{-2} compared to the field observations. The overall RMSE is 28.5 g C m^{-2} and the correlation coefficient R is 0.68.

The biomass results obtained with fractional cover information from the field show better results (figure 7-11, right). The estimated biomass for the individual test sites becomes mainly closer to the field observations (cf. also table 7-9). This results in an overall RMSE of about 25.4 g C m^{-2}. The correlation coefficient R is 0.64.

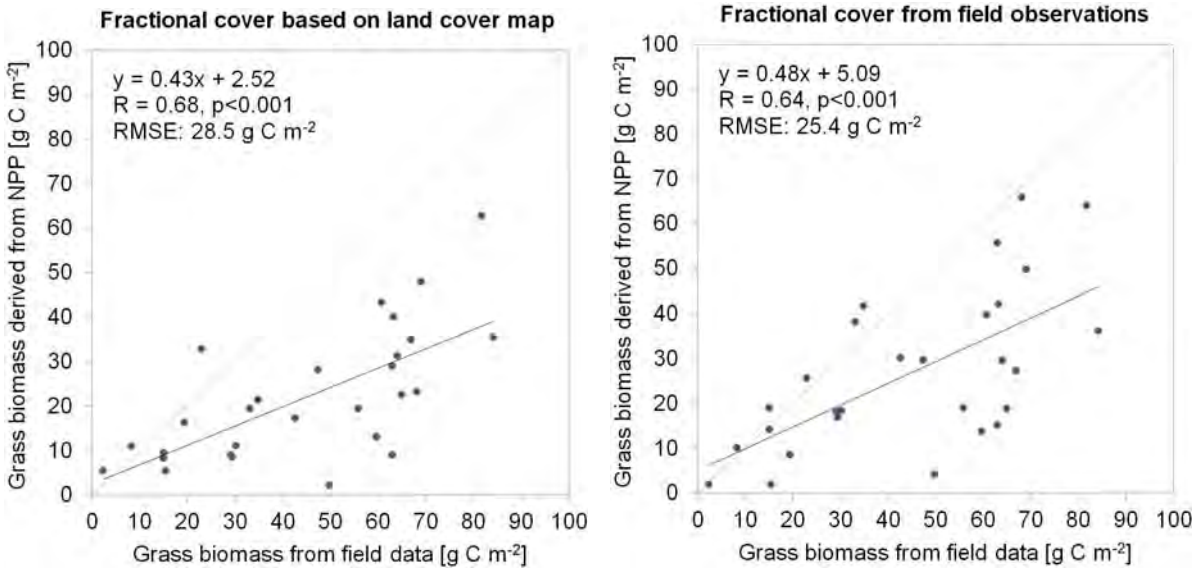

Figure 7-11: Correlation between grass biomass derived from NPP data and grass biomass from field observation. Left: Biomass from NPP data derived with fractional cover based on land cover classes. Right: Biomass from NPP data derived with fractional cover from field observation.

Table 7-9: Number of grass biomass estimates within given error ranges for the 28 available validation sites in Kazakhstan.

Basis for fractional cover information	Number of biomass estimates in the error range		
	±10 g C m^{-2}	–10 to –20 g C m^{-2}	<–20 g C m^{-2}
Land cover map	6	7	15
Field observations	9	9	10

Figure 7-12 shows scatter plots of grass biomass derived from NPP data with fractional cover from field observation and ground-based grass biomass for the three study areas Central, South, and West Kazakhstan. The correlation coefficient varies between 0.61 and 0.72. The results for Central Kazakhstan indicate an underestimation for higher biomass values. This is not obvious for the other two study areas. In West Kazakhstan three test sites show a high grass biomass in the field (50–63 g C m^{-2}), but low NPP-based biomass estimates (4–15 g C m^{-2}). These are test sites 21, 27 (classified as sparse vegetation), and 23 (grassland).

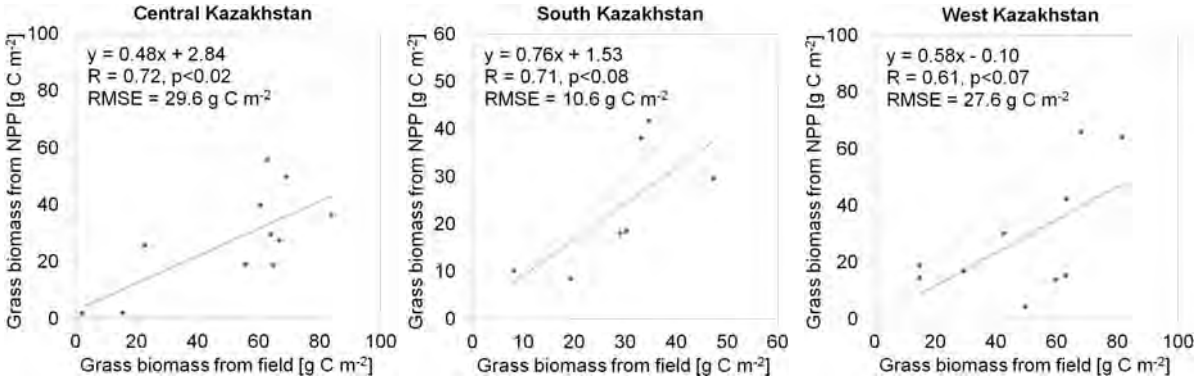

Figure 7-12: Correlation between grass biomass derived from NPP data with fractional cover from field observation and grass biomass from field data for the test sites within the three study areas Central, South, and West Kazakhstan.

For the validation of shrub biomass, a total of 20 test sites is available. The number is lower than for grass biomass, because shrubs are not present at all test sites. At nine test sites no shrub cover was observed during the field campaign (cf. table 7-5 and figure 7-10). Additionally, test site 2 from the study area Central Kazakhstan is excluded. This is because field data show exceptional high shrub biomass of almost 800 g DM m^{-2} which is far beyond the range of other sites from this study area, which do not reach more than 300 g DM m^{-2} shrub biomass (cf. figure 7-10). The cause for this high biomass measurement is unclear, because fractional cover, vegetation height, and species do not differ significantly from the other sites. Therefore, this site was not used for validation.

Above-ground shrub biomass estimates calculated from NPP with fractional cover definitions based on the land cover map show a low correlation to the field-based biomass data with R of 0.33 (cf. figure 7-13, left). The RMSE of 56 g C m^2 is also high. The relationship is significantly better when fractional cover information from field observations is used (cf. figure 7-13, right).

For the biomass estimates based on fractional cover information from field observations, the correlation coefficient R reaches 0.83. The slope of the regression line is 0.51. This slope is strongly influenced by two sites with very high field-based biomass. For these two sites the results indicate an underestimation of 50%. For all other test sites the above-ground shrub biomass estimates based on field fractional cover ratios are closer to the field observations. The

overall RMSE is 24.4 g C m^{-2} and only three test sites show an error higher than ±20 g C m^{-2} compared to field biomass observations.

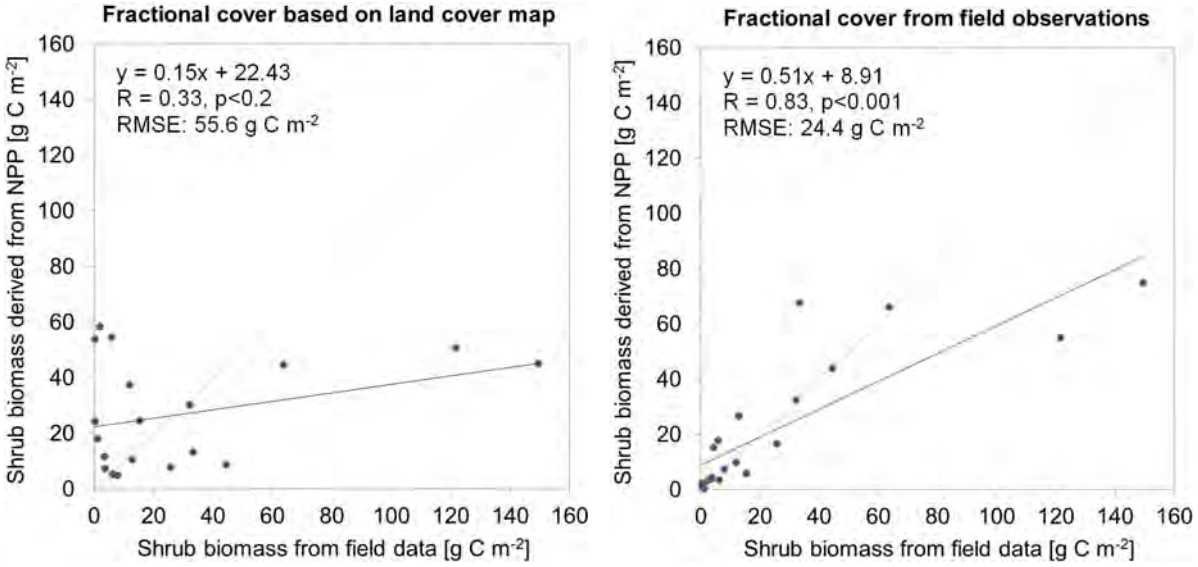

Figure 7-13: Correlation between shrub biomass derived from NPP data and shrub biomass from field observation. Left: Biomass from NPP data derived with fractional cover based on land cover classes. Right: Biomass from NPP data derived with fractional cover from field observation.

Figure 7-14 shows scatter plots between above-ground shrub biomass derived from NPP data with fractional cover from field observation and ground-based shrub biomass observations for the three study areas Central, South, and West Kazakhstan. The coefficient of determination is similar for Central and West Kazakhstan with R about 0.8. For the study area South Kazakhstan the correlation between the NPP-based shrub biomass estimates and the field observation is very high. The correlation coefficient R is 0.98 and the slope of the regression line is close to 1 (cf. figure 7-14).

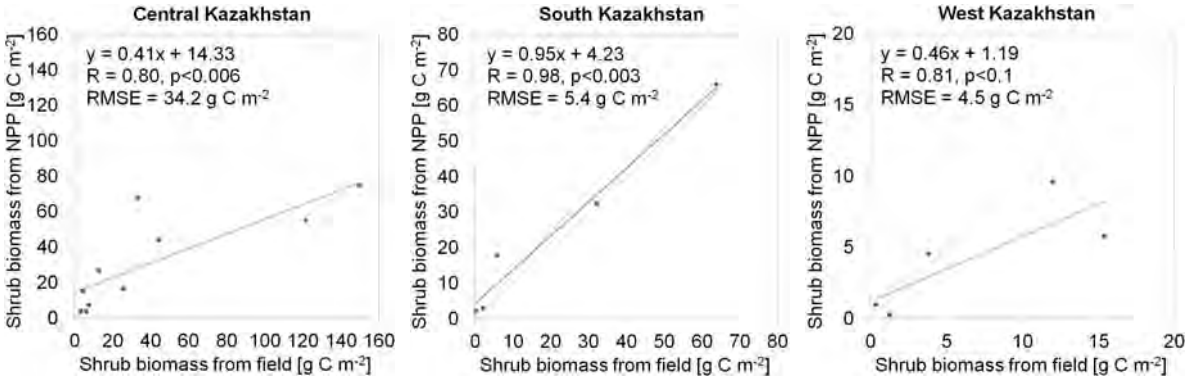

Figure 7-14: Correlation between shrub biomass derived from NPP data with fractional cover from field observation and shrub biomass from field data for the test sites within the three study areas Central, South, and West Kazakhstan.

7.5 Discussion

In this chapter, an approach for derivation of AGB estimates for natural environments based on NPP data has been developed. The methodological concept has been presented and the application has been demonstrated for three study areas in semi-arid Kazakhstan.

The biomass estimation approach is based on NPP data, RGRs, and fractional cover information. It is designed to derive the standing biomass for the period of maximum vegetation growth. Application of maximum RGRs for another period would not be feasible, because unfavourable conditions for vegetation growth reduce the RGR (cf. section 7.2.2).

The validation with field data showed that the NPP-based above-ground grass biomass estimates are lower than the field-observed grass biomass for most test sites (cf. section 7.4.3). This is the case both for estimates derived with fractional cover from the field and for estimates derived with fractional cover based on the land cover map. This indicates that the NPP input is too low and/or that the applied RGRs for grass are too high.

The validation of the grass NPP input data, which were calculated with BETHY/DLR, indicated that the modelled NPP results underestimate the NPP (cf. section 7.3.2). The accuracies of the applied RGR values are not exactly known. However, the assumed errors and their influence on the biomass estimates are high (cf. sections 7.3.4 and 7.3.5).

To reduce the error associated with the RGR values, more experimental studies with plants typical for the study areas in Kazakhstan are needed. Particularly, measurements of maximum RGRs of mature plants are required. Furthermore, availability of additional RGRs in terms of AGB would be desirable.

The moderate overall correlation between modelled grass biomass and field-observed grass biomass (R=0.64, cf. section 7.4.3) might be caused by a high variation of herbaceous species present within the test sites. The applied RGR values do not differentiate between different herbaceous vegetation types within a study area. For NPP calculation with BETHY/DLR based on the Central Asia land cover and land use map, only two grass types are distinguished (cf. section 6.2). A map that provides information on the spatial distribution of different vegetation types and the separate modelling of additional vegetation types with BETHY/DLR would be needed to improve the grass biomass results.

The ground-data might also impose an error on the validation. The method applied for biomass field data collection in this study is especially designed for obtaining measurements that are suitable for comparison at approximately 1 km² spatial resolution (cf. section 4.3.2). Nevertheless, a mismatch between the vegetation composition within the footprint of the input data for NPP calculation and within the test sites for field observation cannot be ruled out.

The validation of the shrub biomass estimates showed a large difference between the results obtained with fractional cover information based on the land cover map and the estimates obtained with fractional cover from field observations. The shrub biomass estimates that are based on fractional cover from land cover class definitions showed a weak correlation to field data (R=0.33). The shrub biomass calculated with fractional cover from field observations showed a high correlation to the ground-based biomass data (R=0.83, cf. section 7.4.3).

The results obtained in this study reveal the high importance of accurate fractional cover information for shrub biomass estimation. The fractional cover definitions based on the land cover map have a mean absolute error of 25% (cf. section 7.3.3). The accuracy for individual sites is obviously not sufficient for reliable shrub biomass estimation. Unfortunately, a suitable fractional cover dataset currently does not exists for Kazakhstan. Such information can, however, be derived from remote sensing (e.g. Geßner 2011). Provided that accurate shrub

fractional cover is available, the developed approach seems to yield good estimates of above-ground shrub biomass.

The focus of this study was on biomass estimation for natural vegetation in semi-arid environments in Kazakhstan. The methodological development therefore focused on derivation of grass and shrub biomass, which are the two main vegetation types in these areas. The developed approach could also be applied to other natural grasslands and shrublands, but the RGR values would have to be adapted.

The developed approach could also be applied to other NPP data, providing that these are available on a daily basis. This is necessary for the combination with maximum RGRs. The availability of separate NPP data for different vegetation types within a pixel is also essential. As a precondition for the applicability of constant RGR values, the individual NPP values have to represent a characteristic mixture of species and plants (cf. section 7.2.3). Thus, the NPP data should be based on spatially explicit remote sensing datasets. The pixel size should be at minimum approximately 250 m × 250 m to ensure sufficient plant and species variability within each pixel.

8 Conclusions and Outlook

In the past years, rising concerns regarding the future evolution of the global climate and its impact on and interactions with the Earth's ecosystems, have led to an increased interest in biomass estimation and NPP modelling. Semi-arid regions, such as most of Kazakhstan, are expected to be especially affected by the global change. Vegetation in these regions already faces extreme climatic conditions. Degradation and desertification are the major threats. Remote-sensing based mapping of spatial biomass distribution for large areas is needed, along with the analysis of vegetation dynamics for several years, to identify and monitor areas that are potentially affected.

The first objective of this thesis was to perform a sound review on methods for remote-sensing based biomass estimation for semi-arid regions. This had not been available before. The review revealed that the majority of studies were based on optical or radar data with low to medium spatial resolution. The sensors NOAA AVHRR and Landsat TM/ETM+, as well as ERS-1/2 data, have been most intensively used. Synergetic approaches based on optical and radar data were rarely investigated, but showed an improvement compared to the usage of solely optical or radar data.

Empirical relationships between remote-sensing-derived indices and biomass field data were used throughout the majority of the previous studies. These regression approaches are hardly transferable in time or space. More complex approaches, such as radiative transfer models or the usage of ecosystem models, have a much higher potential for transferability. Nevertheless, modelling approaches have been poorly investigated so far for biomass estimation in semi-arid environments.

Regarding the usage of sensors, future investigation of synergetic approaches using a combination of optical and SAR data is recommended. From the methodological point of view, future research should focus more on complex modelling approaches. Robust and transferable models need to be developed, which will be a big challenge. Limited transferability is the major constraint hindering the operational application of remote-sensing-based biomass estimation in semi-arid environments so far.

The second objective of this dissertation was to compare two selected regional remote-sensing-based NPP models. The two models are the RBM and BETHY/DLR. Both models calculate NPP with a spatial resolution of approximately 1 km². In this study they have been applied to Kazakhstan for the first time. The models were applied with harmonized input data to calculate NPP for 2010 and 2011 for a study area in Central Kazakhstan.

The results showed that the phenological development was presented well by both models and that the resulting spatial NPP distribution within the study area was similar. Results from the model BETHY/DLR were considerably higher than those from the RBM and closer to the NPP estimates from field data. The correlation to field data was high for both models ($R \geq 0.97$), but the RBM strongly underestimated the NPP. The published LUE values for Kazakhstan seem to be not applicable with the RBM.

The results also indicate, that the 16-day time steps of the MODIS-data-based RBM might be too long, to capture the variable climatic conditions that are typical for semi-arid regions.

They might not account for extreme events. The daily NPP data from BETHY/DLR is advantageous for semi-arid environments and additionally allows application for topics that need a daily time-series.

For a possible future application of the RBM in semi-arid Kazakhstan it is recommended to analyse ways to convert the available LUE values to values applicable for the RBM. Vegetation cover and soil aspects must be considered. A modification of the temperature stress calculation is recommended to deal with non-zero FPAR values in winter. Research towards the possible benefits of using a greenness index would also be interesting and might improve NPP results especially at the end of season and during drought periods.

For BETHY/DLR, the analysis indicated that the MODIS land cover map does not differentiate enough between different land cover types. A land cover map that shows more classes within the semi-arid environment is needed, along with additional fractional cover information for representation of regional differences.

The third objective of this thesis included the application of one model for NPP modelling in Kazakhstan and the analysis of the results regarding spatial, monthly, and inter-annual characteristics. Due to the good results obtained from the study area in Central Kazakhstan, the model BETHY/DLR was chosen for NPP modelling in Kazakhstan. Input data was obtained from a new regional land cover map for Central Asia along with 8-day MODIS LAI composites.

The results showed that the mean annual NPP for the period 2003–2011 for Kazakhstan was 143 g C m^{-2}. For the four most important land cover classes in Kazakhstan mean annual NPP was as follows: grassland: 140 g C m^{-2}, sparse vegetation: 120 g C m^{-2}, open shrubland: 112 g C m^{-2}, and rain-fed agriculture: 225 g C m^{-2}. The maximum monthly vegetation productivity was reached in June with an average NPP of 35 g C m^{-2}.

The highest NPP variability and the greatest number of months with anomalous NPP were located mainly in the North of Kazakhstan. The comparison between agricultural areas and grassland in this region indicated that the high variability is most likely caused by variations in crop types. The lowest variability was observed in semi-arid and arid grassland and open shrubland. This indicates that NPP modelling may allow prediction of possible carbon sequestration and available biomass for livestock in these areas.

Additionally, the correlation between NPP and meteorological parameters was analysed. The comparisons between monthly NPP and monthly temperature as well as between NPP and PAR showed correlation coefficients higher than 0.6 for 90% of the land area of Kazakhstan. The analyses of the correlation between NPP and precipitation revealed that the highest positive correlation is observed when monthly NPP is compared to the sum of precipitation of the two previous months.

Furthermore, seasonal dependencies between NPP and the meteorological parameters were analysed. The results showed that up to 84% of NPP deviations in March and April can be explained by temperature deviations. The sensitivity of NPP to precipitation was found to be strongest in summer and autumn. From the results of the analyses, the following conclusions can be drawn regarding the possible effects of climate change on vegetation productivity in Kazakhstan: (i) If temperature rises in the coming decades, as projected for Central Asia, this will lead to an increase in productivity at the beginning of vegetation growth. (ii) A further shift to an earlier season is also likely. (iii) Higher temperatures in summer might lead to longer drought periods and a decrease in productivity. (iv) The projected decrease in precipitation for summer and autumn would result in lower vegetation productivity in the period August to October.

The investigations in this dissertation show that valuable information can be derived from NPP time-series. Such detailed analyses of NPP data for Kazakhstan have not been published

before. The analysed time period of nine years is relatively short. A longer timespan would be more useful and provide a better basis for the analyses. It is recommended to carry out similar research analyses in the future, based on a longer time frame.

The meteorological input data for BETHY/DLR is continuously available since 1979. Temporally consistent LAI time-series since 1981 could be derived from AVHRR and MODIS data (e.g. Liu et al. 2012). For future application, the usage of Sentinel-3 OLCI data may be considered (launch currently planned for 2014). The availability of an NPP time-series of 30 years or longer would additionally allow for trend analyses. The investigation of anomalies, for example, could then provide information on a possible intensification of extreme events. Based on the daily NPP data, trends regarding the duration of the vegetation growth period and the frequency of droughts could be derived.

The final objective of this dissertation was the development of a methodological approach for derivation of biomass estimates from NPP data for natural environments. This approach could then be applied to the study areas in Kazakhstan. The developed approach is based on modelled NPP time-series, relative growth rates (RGRs) of plants, and fractional cover information. It has been the first time that these parameters are combined for biomass estimation in semi-arid environments. The developed methodology aims at derivation of the AGB of grass and shrubs for the period of maximum vegetation growth.

The validation with field data showed that biomass information can be estimated based on NPP and RGRs. However, accurate fractional cover information is essentially needed, especially for shrub biomass derivation. Validation with field data showed a strong linear relationship (R=0.83) between modelled and field-measured shrub biomass when accurate information on the fractional cover of shrubs was used. For grass biomass a moderate correlation between modelled and field-based data was observed (R=0.64). A differentiation between major grass and herbaceous communities seems to be necessary to obtain reliable biomass estimates.

For the comprehensive validation of the biomass results, it would be desirable to have more field data available. The coverage of different time periods and data from several years would be desirable for the validation of the modelled NPP. For the validation of NPP time-series also eddy covariance flux tower measurements would be useful. Such measurements are unfortunately not available for the study areas in Kazakhstan.

For a future improvement of the developed approach the differentiation of a higher number of vegetation types is recommended. This would require the modelling of additional vegetation types with BETHY/DLR and the availability of a map that provides information on the spatial distribution of these vegetation types. The RGR values would also have to be adapted. Additionally, accurate fractional cover information is essential. For Kazakhstan, suitable fractional cover datasets currently do not exist. However, such information can be derived from remote sensing (e.g. Geßner 2011).

The developed methodology for NPP-based biomass estimation is potentially transferable. Providing the necessary data regarding vegetation cover is available, this method will allow for repeated and large-area biomass estimations of natural vegetation in Kazakhstan and other semi-arid environments. The combination of annual estimations of biomass with continuous NPP time-series analyses might allow for the set-up of an operational monitoring system in the future. This would be a big step forward for observing and understanding the changes in biomass in semi-arid areas. It would also provide essential base information for sustainable land management, the derivation of possible climate change related trends or value-added carbon storage products.

9 References

ADAM, H.E. (2010). Integration of Remote Sensing and GIS in Studying Vegetation Trends and Conditions in the Gum Arabic Belt in North Kordofan, Sudan. Dissertation, Faculty of Forest, Geo and Hydro Sciences, Technische Universität Dresden, 165 pp.

ADAMS, B., WHITE, A. and LENTON, T.M. (2004). An analysis of some diverse approaches to modelling terrestrial net primary productivity. *Ecological Modelling,* 177(3-4), pp. 353–391.

ADB, Asian Development Bank (2010). Central Asia Atlas of Natural Resources, Central Asian Countries Initiative for Land Management, Asian Development Bank: Manila, Philippines, ISBN 979-971-561-886-1.

ADDINK, E.A., DE JONG S.M. and PEBESMA, E.J. (2007). Object definition for aboveground biomass and leaf area index estimation. In: *5th EARSeL Workshop on Imaging Spectroscopy*, 23–25 April 2007, Bruges, Belgium, 14 pp. Available online at: http://5thearselsigis.vgt.vito.be/CD/Fullpapers/Addink_final.pdf (accessed 18 March 2010).

ANDERSON, G.L., HANSON, J.D. and HAAS, R.H. (1993). Evaluating Landsat Thematic Mapper derived Vegetation Indices for estimating above-ground Biomass on semiarid rangelands. *Remote Sensing of Environment*, 45(2), pp. 165–175.

ARANHA, J.T., VIANA, H.F. and RODRIGUEZ, R. (2008). Vegetation classification and quantification by satellite image processing. A case study in north Portugal. In: *Bioenergy: Challenges and Opportunities*, International Conference and Exhibition on Bioenergy, 6–9 April 2008, Universidad de Minho, Guimaraes, Portugal, 7 pp.

AWAYA, Y., KODANI, E., TANAKA, K., LIU, J., ZHUANG, D. and MENG, Y. (2004). Estimation of the global net primary productivity using NOAA images and meteorological data: changes between 1988 and 1993. *International Journal of Remote Sensing,* 25(9), 1597–1613.

BABAN, S.M.J. (2005). Accomplishing Sustainable Development in Southern Kurdistan Using Geoinformatics: An Overview. *Kurdish Scientific and Medical eJournal*, 1, pp. 31–43.

BACCINI, A., LAPORTE, N.T., GOETZ, S.J., SUN, M. and HUANG, D. (2008). A first map of tropical Africa's above-ground biomass derived from satellite imagery. *Environmental Research Letters*, 3, 9 pp.

BALSAMO, G., BOUSSETTA, S., LOPEZ, P. and FERRANTI, L. (2010). Evaluation of ERA-Interim and ERA-Interim-GPCP-rescaled precipitation over the U.S.A. In: *ERA report series*, No. 5, ECMWF: Reading, UK, 10 pp.

BARET, F. and BUIS, S. (2008). Estimating Canopy Characteristics from Remote Sensing Observations: Review of Methods and Associated Problems. In: *Advances in Land Remote Sensing*, S. Liang (Ed.), pp. 173–201, ISBN 978-1-4020-6449-4 (Dordrecht: Springer).

BARET, F., HAGOLLE, O., GEIGER, B., BICHERON, P., MIRAS, B., HUC, M., BERTHELOT, B., NINO, F., WEISS, M., SAMAIN, O., ROUJEAN, J.L. and LEROY, M. (2007). LAI, FAPAR, and FCover CYCLOPES global products derived from Vegetation. Part 1: principles of the algorithm. *Remote Sensing of Environment,* 110(3), pp. 275–286.

BARTHOLOMÉ, E., BELWARD A.S. and ACHARD F. (2002). GLC 2000: Global Land Cover mapping for the year 2000. EUR 20524 EN. Luxemburg: European Commission.

BAUMANN, G. (2009). How to assess rangeland condition in semiarid ecosystems? The indicative value of vegetation in the High Atlas Mountains, Morocco. Dissertation, Mathematisch-Naturwissenschaftliche Fakultät, Universität Köln, 195 pp.

BAYRAMOV, E. and MAMEDOV, R. (2008). Modeling Method for the Prediction of the Caspian Sea Level Fluctuation Impacts on the Azerbaijan Coastal Zones Landscape Based on GIS. *Ekoloji*, 17(67), pp. 46–51.

BAYRAMOV, E., BUCHROITHNER, M.F. and MCGURTY, E. (2012a). Determination of main climate and ground factors controlling vegetation cover regrowth along oil and gas pipelines using multiple, spatial and geographically weighted regression procedures. *Environmental Earth Sciences*, 66(7), pp. 2047–2062.

BAYRAMOV, E., BUCHROITHNER, M.F. and MCGURTY, E. (2012b). Quantitative assessment of vegetation cover and soil degradation factors within terrain units for planning, monitoring and assessment of renaturation along oil and gas pipelines. *Geocarto International*, 27(7), pp. 535–555.

BAZILEVISCH, N.I. and YE RODIN, L. (1967). Maps of productivity and the biological cycle in the Earth's principal terrestrial vegetation types. *Izvestiya Vsesoyuznogo Geograficheskogo Obschestva*, 99, pp. 190–194.

BEERI, O., PHILLIPS, R., HENDRICKSON, J., FRANK, A.B. and KRONBERG, S. (2007). Estimating forage quantity and quality using aerial hyperspectral imagery for northern mixed-grass prairie. *Remote Sensing of Environment*, 110(2), pp. 216–225.

BÉNIÉ, G.B., KABORÉ, S.S., GOÏTA, K. and COUREL, M.-F. (2005). Remote sensing-based spatio-temporal modeling to predict biomass in Sahelian grazing ecosystem. *Ecological Modelling*, 184(2-4), pp. 341–354.

BERG, L.S. (1959). Die geographischen Zonen der Sowjetunion. Band 2. B.G. Teubner: Leipzig [in German].

BERRISFORD, P., DEE, D., POLI, P., BRUGGE, R., FIELDING, K., FUENTES, M., KALLBERG, P. KOBAYASHA, S., UPPALA, S. and SIMMONS, A. (2011). The ERA-Interim archive. In: *ERA report series*, No. 1, Version 2.0, ECMWF: Reading, UK.

BICHERON, P., LEROY, M., BROCKMANN, C., KRÄMER, U., MIRAS, B., HUC, M., NINŐ, F., DEFOURNY, P., VANCUTSEM, C., ARINO, O., RANÉRA, F., PETIT, D., AMBERG, V., VERTHELOT, B. and GROSS, D. (2006). GLOBCOVER: a 300m global land cover product for 2005 using ENVISAT/MERIS time series. In: *Proceedings of the Recent Advances in Quantitative Remote Sensing Symposium*, Valencia, September 2006.

BIRO, K. (2011). Development of a Multi-Temporal Satellite Data for Landuse/Landcover Change Analysis and its Impacts on Soil Properties in Gadarif Region, Sudan. Dissertation, Faculty of Forest, Geo and Hydro Sciences, Technische Universität Dresden, 237 pp.

BIRO, K., PRADHAN, B., BUCHROITHNER, M. and MAKESCHIN, F. (2010). Use of Multi-temporal Satellite Data for Land-Use/Land-Cover Change Analyses and its Impacts on Soil Properties in the Northern Part of Gadarif Region, Sudan. In: *30th EARSeL Symposium*, 31 May–03 June 2010, Paris, France, pp. 305–311.

BIRO, K., PRADHAN, B., BUCHROITHNER, M. and MAKESCHIN, F. (2011). Land use/land cover change analysis and its impact on soil properties in the Northern Part of Gadarif Region, Sudan. *Land Degradation & Development*, DOI: 10.1002/ldr.1116.

BOLIN, B., DEGENS, E.T., KEMPE, S. and KETNER, P. (1979). The Global Carbon Cycle, SCOPE 13 (New York: John Wiley & Sons).

BONDEAU, A., SMITH, P.C., ZAEHLE, S., SCHAPHOFF, S., LUCHT, W., CRAMER, W., GERTEN, D., LOTZE-CAMPEN, H., MÜLLER, C., REICHSTEIN, M. and SMITH, B. (2007). Modelling the role of agriculture for the 20th century global terrestrial carbon balance. *Global Change Biology*, 13(3), pp. 679–706.

BOYD, D.S., FOODY, G.M., CURRAN, P.J., LUCAS, R.M. and HONZAK, M. (1996). An assessment of radiance in Landsat TM middle and thermal infrared wavebands for the detection of tropical forest regeneration. *International Journal of Remote Sensing*, 17(2), pp. 249–261.

BREIMAN, L. (2001). Random Forests. *Machine Learning*, 45, pp. 5–32.

BROWN, S. (2002). Measuring carbon in forests: current status and future challenges. *Environmental Pollution*, 116(3), pp. 363–372.

BUCHROITHNER, M.F. (2009). Veränderung von Landnutzung und Vegetationsbedeckung in der östlichen Sahelzone von 1972 bis 2003. *Wissenschaftliche Zeitschrift der Technischen Universität Dresden*, 58(3-4), pp. 61–67 [in German].

BURAS, A., WUCHERER, W., ZERBE, S., NIVISKIY, Z., MUCHITDINOV, N., SHIMSHIKOV, B., ZVEREV, N., SCHMIDT, S., WILMKING, M. and THEVS, N. (2012). Allometric variability of *Haloxylon* species in Central Asia. *Forest Ecology and Management,* 274, pp. 1–9.

BURRIDGE, D.M. and GADD, A.J. (1974). The Meteorological Office Operational 10 Level Numerical Weather Prediction Model. Technical report, British Met. Office Tech. Notes Nos. 12 and 48, England.

CALVÃO, T. and PALMEIRIM, J.M. (2004). Mapping Mediterranean scrub with satellite imagery: biomass estimation and spectral behaviour. *International Journal of Remote Sensing*, 25(16), pp. 3113–3126.

CESBIO (2010). Biomass monitoring mission for Carbon Assessment (BIOMASS). Available online at: http://www.cesbio.ups-tlse.fr/us/indexbiomass.html (accessed 16 March 2010).

CGER (2000). Ecological Indicators for the Nation. National Academy Press, Washington, D.C. Available online at: http://www.nap.edu/openbook.php?record_id=9720&page=66 (accessed 27 September 2012).

CHEN, W., BLAIN, D., LI, J., KOEHLER, K., FRASER, R., ZHANG, Y., LEBLANC, S., OLTHOF, I., WANG, J. and MCGOVERN, M. (2009). Biomass measurements and relationships with Landsat-7/ETM+ and JERS-1/SAR data over Canada's western sub-arctic and low arctic. *International Journal of Remote Sensing*, 30(9), pp. 2355–2376.

CHO, M.A. and SKIDMORE, A.K. (2009). Hyperspectral predictors for monitoring biomass production in Mediterranean mountain grasslands: Majella National Park, Italy. *International Journal of Remote Sensing*, 30(2), pp. 499–515.

CHOPPING, M., SU, L., RANGO, A., MARTONCHIK, J.V., PETERS, D.P.C. and LALIBERTE, A. (2008). Remote sensing of woody shrub cover in desert grasslands using MISR with a geometric-optical canopy reflectance model. *Remote Sensing of Environment*, 112(1), pp. 19–34.

CISSÉ, M.I. (1980). The browse production of some trees in the Sahel: Relationships between maximum foliage biomass and various physical parameters. In: *Browse in Africa, the current state of knowledge*, H.N. Le Houérou (Ed.), pp. 205–210 (Addis Ababa: International Livestock Centre for Africa).

COLLATZ, G.J., RIBAS-CARBO, M. and BERRY, J.A. (1992). Coupled Photosynthesis–stomatal conductance model for leaves of C_4 plants. *Australian Journal of Plant Physiology,* 19(5), pp. 519–538.

COLLINS, J.N., HUTLEY, L.B., WILLIAMS, R.J., BOGGS, G., BELL, D. and BARTOLO, R. (2009). Estimating landscape-scale vegetation carbon stocks using airborne multi-frequency polarimetric

synthetic aperture radar (SAR) in the savannahs of north Australia. *International Journal of Remote Sensing*, 30(5), pp. 1141–1159.

COSTANZA, R., D'ARGE, R., DE GROOT, R., FARBER, S., GRASSO, M., HANNON, B., LIMBURG, K., NAEEM, S., O'NEILL, R.V., PARUELO, J., RASKIN, R.G., SUTTON, P. and VAN DEN BELT, M. (1997). The value of the world's ecosystem services and natural capital, *Nature*, 387, pp. 253–260.

COOPS, N.C., BLACK, T.A., JASSAL, R.J., TROFYMOW, J.A. and MORGENSTERN, K. (2007). Comparison of MODIS, eddy covariance determined and physiologically modelled gross primary production (GPP) in a Douglas-fir forest stand. *Remote Sensing of Environment,* 107(3), pp. 385–401.

COOPS, N.C., FERSTER, C.J., WARING, R.H. and NIGHTINGALE, J. (2009). Comparison of three models for predicting gross primary production across and within forested ecoregions in the contiguous United States, *Remote Sensing of Environment,* 113(3), pp. 680–690.

CRABTREE, R., POTTER, C., MULLEN, R., SHELDON, J., HUANG, S., HARMSEN, J., RODMAN, A. and JEAN, C. (2009). A modeling and spatio-temporal analysis framework for monitoring environmental change using NPP as an ecosystem indicator. *Remote Sensing of Environment*, 113(7), pp. 1486–1496.

CRAMER, W., KICKLIGHTER, D.W., BONDEAU, A., MOORE, B., CHURKINA, G., NEMRY, B., RUIMY, A., SCHLOSS, A.L. and the participants of the Potsdam NPP Model Intercomparison (1999). Comparing global models of terrestrial net primary productivity (NPP): overview and key results. *Global Change Biology,* 5(S1), pp. 1–15.

CRAMER, W., BONDEAU, A., WOODWARD, F.I., PRENTICE, I.C., BETTS, R.A., BROVKIN, V., COX, P.M., FISHER, V., FOLEY, J.A., FRIEND, A.D., KUCHARIK, C., LOMAS, M.R., RAMANKUTTY, N., SITCH, S., SMITH, B., WHITE, A. and YOUNG-MOLLING, C. (2001). Global response of terrestrial ecosystem structure and function to CO_2 and climate change: Results from six dynamic global vegetation models. *Global Change Biology,* 7(4), pp. 357–373.

CRONIN, N.L.R. (2004). The potential of airborne polarimetric synthetic aperture radar data for quantifying and mapping the biomass and structural diversity of woodlands in semi-arid Australia. PhD thesis, School of Biological, Earth and Environmental Sciences. University of New South Wales, 517 pp.

DAI, Y., ZENG, X., DICKINSON, R.E., BAKER, I., BONAN, G.B., BOSILOVICH, M.G., DENNING, A.S., DIRMEYER, P.A., HOUSER, P.R., NIU, G., OLESON, K.W., SCHLOSSER, C.A. and YANG, Z.-L. (2003). The Common Land Model. *Bulletin of the American Meteorological Society*, 84(8), pp. 1013–1023.

DANCY, K.J., WEBSTER, R. and ABEL, N.O.J. (1986). Estimating and mapping grass cover and biomass from low-level photographic sampling. *International Journal of Remote Sensing*, 7(12), pp. 1679–1704.

DE BEURS, K.M. and HENEBRY, G.M. (2004). Land surface phenology, climatic variation, and institutional change: analyzing agricultural land cover change in Kazakhstan. *Remote Sensing of Environment*, 89(4), pp. 423–433.

DECH, S., GÜNTHER, K. and STRUNZ, G. (2001). Möglichkeiten der Fernerkundung zur Bilanzierung des terrestrischen Kohlenstoffbudgets. In: *Wissenschaftlich-Technische Jahrestagung der DGPF,* Band 10, E. Seyfert (Ed.), pp. 23–32 (Berlin: Deutsche Gesellschaft für Photogrammetrie und Fernerkundung), [in German].

DECH, S., BACHMANN, M. and MÜLLER, A. (2003). New Remote Sensing Approaches in Support of Sustainable Land Use Management in Semi-Arid Environments. In: *30th International Symposium on Remote Sensing of Environment*, 10–14 November 2003, Honolulu, Hawaii.

DEE, D.P., UPPALA, S.M., SIMMONS, A.J., BERRISFORD, P., POLI, P., KOBAYASHI, S., ANDRAE, U., BALMASEDA, M.A., BALSAMO, G., BAUER, P., BECHTOLD, P., BELJAARS, A.C.M., VAN DE BERG, L., BIDLOT, J., BORMANN, N., DELSOL, C., DRAGANI, R., FUENTES, M., GEER, A.J., HAIMBERGER, L., HEALY, S.B., HERSBACH, H., HÓLM, E.V., ISAKSEN, L., KÅLLBERG, P., KÖHLER, M., MATRICARDI, M., MCNALLY, A.P., MONGE-SANZ, B.M., MORCRETTE, J.-J., PARK, B.-K., PEUBEY, C., DE ROSNAY, P., TAVOLATO, C., THÉPAUT, J.-N. and VITART, F. (2011). The ERA-Interim reanalysis: configuration and performance of the data assimilation system. *Quarterly Journal of the Royal Meteorological Society,* 137(656), pp. 553–597. DOI: 10.1002/qj.828.

DEFRIES, D.S., HANSEN, M.C., TOWNSHEND, J.R.G., JANETOS, A.C. and LOVELAND, T.R. (2000). A new global 1-km dataset of percentage tree cover derived from remote sensing. *Global Change Biology,* 6(2), pp. 247–254.

DIALLO, O., DIOUF, A., HANAN, N.P., NDIAYE, A. and PRÉVOST, Y. (1991). AVHRR monitoring of savanna primary production in Senegal, West Africa: 1987–88. *International Journal of Remote Sensing*, 12(6), pp. 1259–1279.

DIERCKE (1992). *Diercke Weltatlas*, Klima. 3rd ed., pp. 220–221 (Braunschweig: Westermann Schulbuchverlag GmbH) [in German].

DIETZ, A., KUENZER, C. and CONRAD, C. (submitted). Snow cover variability in Central Asia between 2000 and 2011 derived from improved MODIS daily snow cover products. *International Journal of Remote Sensing.*

DI GREGORIO, A. and JANSEN, L.J.M. (2001). Land Cover Classification System (LCCS): Classification Concepts and User Manual for Software Version 1.0. Rome: United Nations Food and Agricultural Organization.

DIOUF, A. and LAMBIN, E. (2001). Monitoring land-cover changes in semi-arid regions: remote sensing data and field observations in the Ferlo, Senegal. *Journal of Arid Environments*, 48(2), pp. 129–148.

DOKUPIL, A. (2008). Regionale Biomasse-Modellierung im südlichen Afrika: Vergleich der Biomasse-Modelle BETHY/DLR und RBM. Unpublished. Diploma thesis, Universität Bonn.

DONG, J., KAUFMANN, R.K., MYNENI, R.B., TUCKER, C.J., KAUPPI, P.E., LISKI, J., BUERMANN, W., ALEXEYEV, V. and HUGHES, M.K. (2003). Remote sensing estimates of boreal and temperate forest woody biomass: carbon pools, sources, and sinks. *Remote Sensing of Environment*, 84(3), pp. 393–410.

DORAISWAMY, P., MURATOVA, N., SINCLAIR, T., STERN, A. and AKHMEDOV, B. (2002). Evaluation of MODIS data for assessment of regional spring wheat yield in Kazakhstan. In: *Proceedings of the International Geoscience and Remote Sensing Symposium 2002*, (IGARSS 2002), 24-28 June 2002, Toronto, Canada, pp. 487–490.

DU PLESSIS, W.P. (1999). Linear regression relationship between NDVI, vegetation and rainfall in Etosha National Park, Namibia. *Journal of Arid Environments*, 42(4), pp. 235–260.

DUNCAN, J., STOW, D., FRANKLIN, J. and HOPE, A. (1993). Assessing the relationship between spectral vegetation indices and shrub cover in the Jornada Basin, New Mexico. *International Journal of Remote Sensing*, 14(18), pp. 3395–3416.

DUNN, R., THOMAS, S.M., KEYS, A.J. and LONG, S.P. (1987). A Comparison of the Growth of the C4 Grass Spartina anglica with the C_3 Grass Lolium perenne at Different Temperatures. *Journal of Experimental Botany*, 38(188), pp. 433–441.

EISSENSTAT, D.M. and CALDWELL, M.M. (1987). Characteristics of successful competitors: An evaluation of potential growth rate in two cold desert tussock grasses. *Oecologia*, 71(2), pp. 167–173.

EISFELDER, C., KUENZER, C. and DECH, S. (2012). Derivation of biomass information for semi-arid areas using remote sensing data. *International Journal of Remote Sensing*, 33(9), pp. 2937–2984.

EISFELDER, C., KUENZER, C., DECH, S. and BUCHROITHNER, M.F. (in print). Comparison of two remote sensing based models for regional net primary productivity estimation – a case study in semi-arid Central Kazakhstan. *IEEE Journal of Selected Topics in Applied Earth Observation and Remote Sensing,* DOI: 10.1109/JSTARS.2012.2226707.

EISFELDER, C., KLEIN, I., NIKLAUS, M. and KUENZER, C. (under review). Net primary productivity in Kazakhstan, its spatio-temporal patterns and relation to meteorological variables. *Journal of Arid Environments*.

ELVIDGE, C.D. and LYON, R.J.P. (1985). Influence of rock-soil spectral variation on the assessment of green biomass. *Remote Sensing of Environment*, 17(3), pp. 265–279.

ESWARAN, H., LAL, R. and REICH, P.F. (2001). Land degradation: an overview. In: *Responses to Land Degradation.* In: E.M. Bridges, I.D. Hannam, L.R. Oldeman, F.W.T. Pening de Vries, S.J. Scherr and S. Sompatpanit (Eds.). In: *Proceedings of the 2nd International Conference on Land Degradation and Desertification*, Khon Kaen, Thailand, pp. 20–35 (New Delhi, India: Oxford Press).

ETIENNE, M. (1989). Non destructive methods for evaluating shrub biomass: a review. *Acta Oecologica - International Journal of Ecology*, 10(2), pp. 115–128.

FABRICIUS, C., BURGER, M. and HOCKEY, P.A.R. (2003). Comparing biodiversity between protected areas and adjacent rangeland in xeric succulent thicket, South Africa: arthropods and reptiles. *Journal of Applied Ecology*, 40(2), pp. 392–403.

FAN, J.W., WANG, K., HARRIS, W., ZHONG, H.P., HU, Z.M., HAN, B., ZHANG, W.Y. and WANG, J.B. (2009). Allocation of vegetation biomass across a climate-related gradient in the grasslands of Inner Mongolia. *Journal of Arid Environments*, 73(4-5), pp. 521–528.

FAO (1989). Arid zone forestry: a guide for field technicians. Available online at: http://www.fao.org/docrep/T0122E/t0122e03.htm (accessed 17 September 2012).

FAO (2006). Global Forest Resources Assessment 2005: progress towards sustainable forest management (Rome: Food and Agriculture Organization of the United Nations). Available online at: ftp://ftp.fao.org/docrep/fao/008/A0400E/A0400E00.pdf (accessed 16 March 2010).

FAO/IIASA/ISRIC/ISSCAS/JRC (2009). Harmonized World Soil Database (version 1.1). FAO, Rome, Italy and IIASA, Laxenburg, Austria.

FAO (2010). Available online at: http://www.fao.org/docrep/T0122E/t0122e03.htm (accessed 16 March 2010).

FARQUHAR, G.D., CAEMMERER, S. and BERRY, J.A. (1980). A biochemical model of photosynthesis in leaves of C_3 species. *Planta,* 149(1), pp. 78–90.

FARTUSCHINA, M.M. (1986). Produktivnost Senokosov I Pastbistch, pp. 74–77 (Novosibirsk: Nauka) [in Russian].

FENG, X., LIU, Y. and ZHAO, Y. (2005). Remote sensing linked modelling of the aboveground biomass of semiarid grasslands in Inner Mongolia. In: *Proceedings of International Geoscience and Remote Sensing Symposium 2005*, (IGARSS 2005), 29 July 2005, Seoul, Korea, 5, pp. 3047–3050.

FENG, X., LIU, G., CHEN, J.M., CHEN, M., LIU, J., JU, W.M., SUN, R. and ZHOU, W. (2007). Net primary productivity of China's terrestrial ecosystems from a process model driven by remote sensing. *Journal of Environmental Management,* 85(3), pp. 563–573.

FENSHOLT, R., SANDHOLT, I., SCHULTZ RASMUSSEN, M., STISEN, S. and DIOUF, A. (2006). Evaluation of satellite based primary production modelling in the semi-arid Sahel. *Remote Sensing of Environment*, 105(3), pp. 173–188.

FIELD, C.B., RANDERSON, J.T. and MALMSTRÖM, C.M. (1995). Global net primary production: combining ecology and remote sensing. *Remote Sensing of Environment,* 51(1), pp. 74–88.

FIELD, C.B., CAMPBELL, J.E. and LOBELL, D.B. (2008). Biomass energy: the scale of the potential resource. *Trends in Ecology & Evolution*, 23(2), pp. 65–72.

FILELLA, I. and PEÑUELAS, J. (1994). The red edge position and shape as indicators of plant chlorophyll content, biomass and hydric status. *International Journal of Remote Sensing*, 15(7), pp. 1459–1470.

FILELLA, I., PEÑUELAS, J., LLORENS, L. and ESTIARTE, M. (2004). Reflectance assessment of seasonal and annual changes in biomass and CO_2 uptake of a Mediterranean shrubland submitted to experimental warming and drought. *Remote Sensing of Environment*, 90(3), pp. 308–318.

FRANKLIN, J. and HIERNAUX, P.H.Y. (1991). Estimating foliage and woody biomass in Sahelian and Sudanian woodlands using a remote sensing model. *International Journal of Remote Sensing*, 12(6), pp. 1387–1404.

FREY, C.M., KUENZER, C. and DECH, S. (2012). Quantitative comparison of the operational NOAA AVHRR LST product of DLR and the MODIS LST product V005. *International Journal of Remote Sensing*, 33(22), pp. 7165–7183.

FRIEND, A.D., STEVENS, A.K., KNOX, R.G. and CANNELL, M.G.R. (1997). A process-based, biogeochemical, terrestrial biosphere model of ecosystem dynamics (Hybrid v3.0). *Ecological Modelling*, 95(2-3), pp. 249–287.

FRISON, P.L. and MOUGIN, E. (1996). Monitoring global vegetation dynamics with ERS-1 wind scatterometer data. *International Journal of Remote Sensing*, 17(16), pp. 3201–3218.

FRISON, P.L., MOUGIN, E. and HIERNAUX, P. (1998). Observations and interpretation of seasonal ERS-1 wind scatterometer data over Northern Sahel (Mali). *Remote Sensing of Environment*, 63(3), pp. 233−242.

FRISON, P.L., MOUGIN, E., JARLAN, L., KARAM, M.A. and HIERNAUX, P. (2000). Comparison of ERS wind-scatterometer and SSM/I data for Sahelian vegetation monitoring. *IEEE Transactions on Geoscience and Remote Sensing*, 38(4), pp. 1794–1803.

FROLKING, S., PALACE, M.W., CLARK, D.B., CHAMBERS, J.Q., SHUGART, H.H. and HURTT, G.C. (2009). Forest disturbance and recovery: A general review in the context of spaceborne remote sensing of impacts on aboveground biomass and canopy structure. *Journal of Geophysical Research-Biogeosciences*, 114, G00E02, 27 pp.

GAO, B.-C. and KAUFMAN, Y.J. (1998). The MODIS Near-IR Water Vapor Algorithm. Algorithm Technical Background Document. Product ID: MOD05 – Total Precipitable water. ATBD Reference Number: ATBD-MOD-03. Available online at: http://modis-atmos.gsfc.nasa.gov/_docs/atbd_mod03.pdf (accessed 2 May 2012).

GARCÍA, M., RIAÑO, D., CHIVIECO, E. and DANSON, F.M. (2010). Estimating biomass carbon stocks for a Mediterranean forest in central Spain using LiDAR height and intensity data. *Remote Sensing of Environment*, 114(4), pp. 816–830.

GARCÍA-HARO, F.J., GILABERT, M.A. and MELIÁ, J. (1996). Linear spectral mixture modelling to estimate vegetation amount from optical spectral data. *International Journal of Remote Sensing*, 17(17), pp. 3373–3400.

GARRAT, J.R. (1992). The atmospheric boundary layer. Cambridge University Press, Cambridge, ISBN 0-521-38052-9.

GCOS (2003). The Second Report on Adequacy of Global Observation Systems for Climate in Support of the UNFCCC. Global Climate Observing System, World Meteorological Organisation, Report GCOS–82. Available online at: http://www.fao.org/gtos/doc/ECVs/T12/ECV-T12-biomass-ref04-GCOS-2nd-Adequacy-Report.pdf (accessed 16 March 2010).

GCOS (2005). GCOS Regional Action Plan for Eastern and Central Europe, December 2005. Available online at: http://www.wmo.int/pages/prog/gcos/documents/GCOS_ECE_RAP_Dec05.pdf (accessed 16 March 2010).

GCOS (2006). Systematic observation requirements for satellite-based products for climate. Supplemental details to the satellite-based component of the "Implementation Plan for the Global Observing System for Climate in Support of the UNFCCC". GCOS–107, WMO/TD No. 1338. Available online at: http://www.wmo.int/pages/prog/gcos/Publications/gcos-107.pdf (accessed 16 March 2010).

GEßNER, U. (2011). Räumliche und zeitliche Muster der Vegetationsstruktur in Savannen des südlichen Afrika. Dissertation, Lehrstuhl für Fernerkundung, Julius-Maximilians-Universität Würzburg, 242 pp. [in German].

GESSNER, U., NAEIMI, V., KLEIN, I., KUENZER, C., KLEIN, D. and DECH, S. (2012). The relationship between precipitation anomalies and satellite-derived vegetation activity in Central Asia. *Global and Planetary Change.*

GIBBS, H.K., BROWN, S., NILES, J.O. and FOLEY, J.A. (2007). Monitoring and estimating tropical forest carbon stocks: making REDD a reality. *Environmental Research Letters*, 2(4), 045023, 13 pp.

GLCF (2012). MODIS Vegetation Continuous Fields. Global Land Cover Facility. Available online at: http://glcf.umiacs.umd.edu/data/vcf/index.shtml (accessed 17 October 2012).

GOETZ, S., BACCINI, A., LAPORTE, N.T., JOHNS, T., WALKER, W., KELLNDORFER, J., HOUGHTON, R. and SUN, M. (2009). Mapping and monitoring carbon stocks with satellite observations: a comparison of methods. *Carbon Balance and Management*, 4(2), 7 pp. Available online at: http://www.cbmjournal.com/content/4/1/2 (accessed 19 March 2010).

GÖTTLICHER, D., OBREGÓN, A., HOMEIER, J., ROLLENBECK, R., NAUSS, T. and BENDIX, J. (2009). Land-cover classification in the Andes of southern Ecuador using Landsat ETM+ data as a basis for SVAT modelling. *International Journal of Remote Sensing*, 30(8), pp. 1867–1886.

GOUGH, C.M. (2012). Terrestrial Primary Production: Fuel for Life. *Nature Education Knowledge*, 3(10), 28 pp.

GRAETZ, R.D. and GENTLE, M.R. (1982). The relationships between reflectance in the Landsat wavebands and the composition of an Australian semi-arid shrub rangeland. *Photogrammetric Engineering and Remote Sensing*, 48, pp. 1721–1730.

GRAETZ, R.D., PECH, R.P. and DAVIS, A.W. (1988). The assessment and monitoring of sparsely vegetated rangelands using calibrated Landsat data. *International Journal of Remote Sensing*, 9(7), pp. 1201–1222.

GRASSI, G., MONNI, S., FEDERICI, S., ACHARD, F. and MOLLICONE, D. (2008). Applying the conservativeness principle to REDD to deal with the uncertainties of the estimates. *Environmental Research Letters*, 3(3), 035005, 12 pp.

GRIME, J.P. and HUNT, R. (1975). Relative growth-rate: its range and adaptive significance in a local flora. *Journal of Ecology*, 63(2), pp. 393–422.

GRIPPA, M. and WOODHOUSE, I.H. (2002). Retrieval of bare soil and vegetation parameters from wind scatterometer measurements over three different climatic regions. *Remote Sensing of Environment*, 84(1), pp. 16–24.

GTOS (2009). Biomass. Assessment of the status of the sevelopment of the standards for the Terrestrial Essential Climate Variables. GTOS 67. Available online at: http://www.fao.org/gtos/doc/ECVs/T12/T12.pdf (accessed 16 March 2010).

HAASE, P., PUGNAIRE, F.I., CLARK, S.C. and INCOLL, L.D. (1999). Environmental control of canopy dynamics and photosynthetic rate in the evergreen tussock grass Stipa tenacissima. *Plant Ecology*, 145(2), pp. 327–339.

HANSEN, M.C., DEFRIES, R.S., TOWNSHEND, J.R.G., MARUFU, L. and SOHLBERG, R. (2002a). Development of a MODIS tree cover validation data set for Western Province, Zambia. *Remote Sensing of Environment,* 83(1-2), pp. 320–335.

HANSEN, M.C., DEFRIES, R.S., TOWNSHEND, J.R.G., SOHLBERG, R., DIMICELI, C. and CARROLL, M. (2002b). Towards an operational MODIS continuous field of percent tree cover algorithm: examples using AVHRR and MODIS data. *Remote Sensing of Environment,* 83(1-2), pp. 303–319.

HANSEN, M.C., DEFRIES, R.S., TOWNSHEND, J.R.G., CARROL, M., DIMICELI, C. and SOHLBERG, R.A. (2003). Global Percent Tree Cover at a Spatial Resolution of 500 Meters: First Results of the MODIS Vegetation Continuous Fields Algorithm. *Earth Interactions,* 7(10), pp. 1–15.

HARRIS, R.W. (1992). Root-Shoot ratios. *Journal of Arboriculture*, 18(1), pp. 39–42.

HAXELTINE, A. and PRENTICE, I.C. (1996). BIOME3: An equilibrium terrestrial biosphere model based on ecophysiological constraints, resource availability, and competition among plant functional types. *Global Biogeochemical Cycles*, 10(4), pp. 693–709, doi: 10.1029/96GB02344.

HAYES II, W.E., WALKER, L.R. and POWELL, E.A. (2009). Competitive abilities of Tamarix aphylla in southern Nevada. *Plant Ecology*, 202(1), pp. 159–167.

HEINSCH, F.A., REEVES, M., VOTAVA, P., KANG, S., MILESI, C., ZHAO, M., GLASSY, J., JOLLY, W.M., LOEHMAN, R., BOWKER, C.F., KIMBALL, J.S., NEMANI, R.R. and RUNNING, S.W. (2003). User's Guide, GPP and NPP (MOD 17A2/A3) Products, NASA MODIS Land Algorithm. Version 2.0, December 2, 2003. 57 pp.

HENRY, M., TITTONELL, P., MANLAY, R.J., BERNOUX, M., ALBRECHT, A. and VANLAUWE, B. (2009). Biodiversity, carbon stocks and sequestration potential in aboveground biomass in smallholder farming systems of western Kenya. *Agriculture, Ecosystems & Environment*, 129(1-3), pp. 238–252.

HIERNAUX, P., MOUGIN, E., DIARRA, L., SOUMAGUEL, N., LAVENU, F., TRACOL, Y. and DIAWARA, M. (2009). Sahelian rangeland response to changes in rainfall over two decades in the Grouma region, Mali. *Journal of Hydrology*, 375(1-2), pp. 114–127.

HIJMANS, R.J., CAMERON, S.E., PARRA, J.L., JONES, P.G. AND JARVIS, A. (2005). Very high resolution interpolated climate surfaces for global land areas. *International Journal of Climatology,* 25(15), pp. 1965–1978.

HILKER, T., COOPS, N.C., WULDER, M.A., BLACK, T.A. and GUY, R.D. (2008). The use of remote sensing in light use efficiency based models of gross primary production: A review of current status and future requirements. *Science of The Total Environment*, 404(2-3), pp. 411–423.

HIRATA, M., KOGAB, N., SHINJO, H., FUJITA, H., GINTZBURGER, G. and MIYAZAKI, A. (2001). Vegetation classification by satellite image processing in a dry area of northeastern Syria. *International Journal of Remote Sensing*, 22(4), pp. 507–516.

HOBBS, T.J. (1995). The use of NOAA-AVHRR NDVI data to assess herbage production in the arid rangelands of Central Australia. *International Journal of Remote Sensing*, 16(7), pp. 1289–1302.

HOLDRIDGE, L.R. (1967). Life Zone Ecology (San Jose, Costa Rica: Tropical Science Center).

HOLM, A.M., CRIDLAND, S.W. and RODERICK, M.L. (2003). The use of time-integrated NOAA NDVI data and rainfall to assess landscape degradation in the arid shrubland of Western Australia. *Remote Sensing of Environment*, 85(2), pp. 145–158.

HOUGHTON, R.A. (1991). Tropical deforestation and atmospheric carbon dioxide. *Climate Change*, 19(1-2), pp. 99–118.

HUETE, A.R., JACKSON, R.D. and POST, D.F. (1985). Spectral response of a plant canopy with different soil backgrounds. *Remote Sensing of Environment*, 17(1), pp. 37–53.

HUETE, A., JUSTICE, C. and VAN LEEUWEN, W. (1999). MODIS Vegetation Index (MOD13) Algorithm Theoretical Basis Document. Version 3. Available online at: http://modis.gsfc.nasa.gov/data/atbd/atbd_mod13.pdf (accessed 2 May 2012).

HUNT, R. and CORNELISSEN, J.H.C. (1997). Components of relative growth rate and their interrelations in 59 temperate plant species. *New Phytologist*, 135(3), pp. 395–417.

HUTH, J., KUENZER, C., WEHRMANN, T., GEBHARDT, S. and DECH, S. (2012). Land cover and land use classification with TWOPAC: towards automated processing for pixel- and object-based image classification. *Remote Sensing,* 4(9), pp. 2530–2553, doi: 10.3390/rs4092530.

IGCOS (2004). Integrated Global Carbon Observation Theme. A Strategy to Realize a Coordinated System of Integrated Global Carbon Cycle Observations. Available online at: http://www.fao.org/gtos/doc/ECVs/T12/ECV-T12-biomass-ref19-IGCO-carbon-theme.pdf (accessed 16 March 2010).

IPCC (1997). The Regional Impacts of Climate Change: An Assessment of Vulnerability. Watson, R.T., Zinyowera, M.C. and Moss, R.H. (Eds). Cambridge University Press, UK. pp. 517. Available online at: http://www.ipcc.ch/ipccreports/sres/regional/158.htm (accessed 25 October 2012).

IPCC (2003). Good Practice Guidance for Land-Use, Land-Use Change and Forestry. Institute for Global Environmental Strategies, Kanagawa, Japan. Available online at: http://www.ipcc-nggip.iges.or.jp/public/gpglulucf/gpglulucf.html (accessed 16 March 2010).

IPCC (2006). 2006 IPCC Guidelines for National Greenhouse Gas Inventories. Prepared by the National Greenhouse Gas Inventories Programme, Eggleston, H.S., Buendia, L., Miwa, K., Ngara, T. and Tanabe, K. (Eds.), published: IGES, Japan. Available online: http://www.ipcc-nggip.iges.or.jp/public/2006gl/index.html (accessed 10 May 2012).

IUSS Working Group WRB (2006). World reference base for soil resources 2006. World Soil Resources Reports No. 103. FAO, Rome.

JAKUBAUSKAS, M., KINDSCHER, K. and DEBINSKI, D. (2001). Spectral and biophysical relationships of montane sagebrush communities in multi-temporal SPOT XS data. *International Journal of Remote Sensing*, 22(9), pp. 1767–1778.

JARLAN, L., MAZZEGA, P. and MOUGIN, E. (2002). Retrieval of land surface parameters in the Sahel from ERS wind scatterometer data: a "brute force" method. *IEEE Transactions on Geoscience and Remote Sensing*, 40(9), pp. 2056–2062.

JARLAN, L., MAZZEGA, P., MOUGIN, E., LAVENU, F., MARTY, G., FRISON, P.L. and HIERNAUX, P. (2003). Mapping of sahelian vegetation parameters from ERS scatterometer data with an evolution strategies algorithm. *Remote Sensing of Environment*, 87(1), pp. 72−84.

JARLAN, L., MANGIAROTTI, S., MOUGIN, E., MAZZEGA, P., HIERNAUX, P. and LE DANTEC, V. (2008). Assimilation of SPOT/VEGETATION NDVI data into a sahelian vegetation growth model. *Remote Sensing of Environment*, 112(4), pp. 1381−1394.

JIN, Z., QI, Y.-C. and DONG, Y.-S. (2007). Storage of biomass and net primary productivity in desert shrubland of Artemisia ordosica on Ordos Plateau of Inner Mongolia, China. *Journal of Forestry Research*, 18(4), pp. 298–300.

JUSTICE, C.O. and TOWNSHEND, J.R.G. (1981). Integrating ground data with remote sensing. In: *Terrain Analysis and Remote Sensing,* J.R.G. Townshend (Ed.), pp. 38–58, (London: George Allen & Unwin).

JUSTICE, C.O., VERMOTE, E., TOWNSHEND, J.R.G., DEFRIES, R., ROY, D.P., HALL, D.K., SALOMONSON, V.V., PRIVETTE, J.L., RIGGS, G., STRAHLER, A., LUCHT, W., MYNENI, R.B., KNJAZIKHIN, Y., RUNNING, S.W., NEMANI, R.R., WAN, Z., HUETE, A.R., VAN LEEUWEN, W., WOLFE, R.E., GIGLIO, L., MULLER, J.-P., LEWIS, P. and BARNSLEY, M.J. (1998). The Moderate Resolution Imaging Spectroradiometer (MODIS): Land remote sensing for global change research. *IEEE Transactions on Geoscience and Remote Sensing*, 36(4), pp. 1228–1249.

KAPPAS, M.W. and PROPASTIN, P.A. (2012). Review of Available Products of Leaf Area Index and Their Suitability over the Formerly Soviet Central Asia. *Journal of Sensors*, 2012, Article ID 582159, pp. 1–11, doi: 10.1155/2012/582159.

KASISCHKE, E.S., MELACK, J.M. and DOBSON, M.C. (1997). The use of imaging radars for ecological applications - A review. *Remote Sensing of Environment*, 59(2), pp. 141–156.

KAWAMURA, K., AKIYAMA, T., YOKOTA, H., TSUTSUMI, M., YASUDA, T., WATANABE, O. and WANG, S.P. (2005). Quantifying grazing intensities using geographic information systems and satellite remote sensing in the Xilingol steppe region, Inner Mongolia, China. *Agriculture Ecosystems & Environment*, 107(1), pp. 83–93.

KING, M.D., KAUFMAN, Y.J., MENZEL, W.P. and TANRÉ, D. (1992). Remote Sensing of Cloud, Aerosol, and Water Vapor Properties from the Moderate Resolution Imaging Spectrometer (MODIS). *IEEE Transactions on Geoscience and Remote Sensing*, 30(1), pp. 2–27.

KLEIN, I., GESSNER, U. and KUENZER, C. (2012). Regional land cover mapping and change detection in Central Asia using MODIS time series. *Applied Geography,* 35(1-2), pp. 219–234.

KNORR, W. (1997). Satellite Remote Sensing and Modelling of the Global CO_2 Exchange of Land Vegetation: A Synthesis Study. PhD thesis. Max-Planck-Institut für Meteorologie, Hamburg.

KNORR, W. (2000). Annual and interannual CO_2 exchanges of the terrestrial biosphere: process-based simulations and uncertainties. *Global Ecology and Biogeography,* 9(3), pp. 225–252.

KNORR, W. and HEIMANN, M. (2001). Uncertainties in global terrestrial biosphere modeling 1. A comprehensive sensitivity analysis with a new photosynthesis and energy balance scheme. *Global Biogeochemical Cycles,* 15(1), pp. 207–255.

KNYAZIKHIN, Y., GLASSY, J., PRIVETTE, J.L., TIAN, Y., LOTSCH, A., ZHANG, Y., WANG, Y., MORISETTE, J.T., VOTAVA, P., MYNENI, R.B., NEMANI, R.R. and RUNNING, S.W. (1999). MODIS Leaf Area Index (LAI) and Fraction of Photosynthetically Active Radiation Absorbed by Vegetation (FPAR) Product (MOD15). Algorithm Theoretical Basis Document. Version 4.0. Available online at: http://modis.gsfc.nasa.gov/data/atbd/atbd_mod15.pdf (accessed 2 May 2012).

KÖCHY, M., MATHAJ, M., JELTSCH, F. and MALKINSON, D. (2008). Resilience of stocking capacity to changing climate in arid to Mediterranean landscapes. *Regional Environmental Change*, 8(2), pp. 73–87.

KOGAN, F., STARK, R., GITELSON, A., JARGALSAIKHAN, L., DUGRAJAV, C. and TSOOJ, S. (2004). Derivation of pasture biomass in Mongolia from AVHRR-based vegetation health indices. *International Journal of Remote Sensing*, 25(14), pp. 2889–2896.

KOTTEK, M., GRIESER, J., BECK, C., RUDOLF, B. and RUBEL, F. (2006). World Map of the Köppen-Geiger climate classification updated. *Meteorologische Zeitschrift*, 15(3), pp. 259–263.

KRAUS, T. and SAMIMI, C. (2002). Biomass estimation for land use management and fire management using Landsat-TM and -ETM+. *Erdkunde*, 56(2), pp. 130–143.

KRINNER, G., VIOVY, N., DE NOBLET-DUCOUDRÉ, N., OGÉE, J., POLCHER, J., FRIEDLINGSTEIN, P., CIAIS, P., SITCH, S. and PRENTICE, I.C. (2005). A dynamic global vegetation model for studies of the coupled atmosphere-biosphere system. *Global Biogeochemical Cycles*, 19, GB1015, doi: 10.1029/2003GB002199.

KUENZER, C., BARTALIS, Z., SCHMIDT, M., ZHAO, D. and WAGNER, W. (2008). Trend analyses of a global soil moisture time series derived from ERS-1/-2 scatterometer data: floods, droughts and long term changes. *The International Archives of Photogrammetry, Remote Sensing and Spatial Information Sciences*, 37, pp. 1363–1368.

KUENZER, C., ZHAO, D., SCIPAL, K., SABEL, D., NAEIMI, V., BARTALIS, Z., HASENAUER, S., MEHL, H., DECH, S. and WAGNER, W. (2009). El Niño southern oscillation influences represented in ERS scatterometer-derived soil moisture data. *Applied Geography*, 29(4), pp. 463–477.

KUROCHKINA, L.J. (1966). Vegetation of the Sand Deserts of Kazakhstan. In: *Vegetation of Kazakhstan*. B.A. Bykov (Ed.), pp. 191–592. (Alma-Ata, Kazakhstan: Nauka) [in Russian].

LAGERGREN, F., EKLUNDH, L., GRELLE, A., LUNDBLAD, M., MÖLDER, M., LANKREIJER, H. and LINDROTH, A. (2005). Net primary production and light use efficiency in a mixed coniferous forest in Sweden. *Plant, Cell & Environment*, 28(3), pp. 412–423.

LAMLOM, S.H. and SAVIDGE, R.A. (2003). A reassessment of carbon content in wood: variation within and between 41 North American species. *Biomass and Bioenergy*, 25(4), pp. 381–388.

LAPITAN, R.L. and PARTON, W.J. (1996). Seasonal variabilities in the distribution of the microclimatic factors and evapotranspiration in a shortgrass steppe. *Agricultural and Forest Meteorology,* 79(1), pp. 113–130.

LEINENKUGEL, P., KUENZER, C. and DECH, S. (submitted). Comparison and Enhancement of MODIS Cloud Mask Products for South East Asia. *International Journal of Remote Sensing*.

LE MAIRE, G., FRANÇOIS, C., SOUDANI, K., BERVEILLER, D., PONTAILLER, J.-Y., BRÉDA, N., GENET, H., DAVI, H. and DUFRÊNE, E. (2008). Calibration and validation of hyperspectral indices for the estimation of broadleaved forest leaf chlorophyll content, leaf mass per area, leaf area index and leaf canopy biomass. *Remote Sensing of Environment*, 112(10), pp. 3846–3864.

LEVANG-BRILZ, N. and BIONDINI, M.E. (2002). Growth rate, root development and nutrient uptake of 55 plant species from the Great Plains Grasslands, USA. *Plant Ecology*, 165(1), pp. 117–144.

LI, S.-G., ASANUMA, J., KOTANI, A., DAVAA, G. and OYUNBAATAR, D. (2007). Evapotranspiration from a Mongolian steppe under grazing and its environmental constraints. *Journal of Hydrology,* 333(1), pp. 133–143.

LI, C.P. and XIAO, C.W. (2007). Above- and belowground biomass of Artemisia ordosica communities in three contrasting habitats of the Mu Us desert, northern China. *Journal of Arid Environments,* 70(2), pp. 195–207.

LIOUBIMTSEVA, E. and ADAMS, J.M. (2004). Possible implications of increased carbon dioxide levels and climate change for desert ecosystems. *Environmental Management*, 33(1), pp. 388–404.

LIOUBIMTSEVA, E., COLE, R., ADAMS, J.M. and KAPUSTIN, G. (2005). Impacts of climate and land-cover changes in arid lands of Central Asia. *Journal of Arid Environments,* 62(2), pp. 285–308.

LIOUBIMTSEVA, E. and HENEBRY, G. (2009). Climate and environmental change in arid Central Asia: Impacts, vulnerability, and adaptations. *Journal of Arid Environments,* 73(11), pp. 963–977.

LIU, A.X., LIU, Z.J., WANG, C.Y. and NIU, Z. (2003). Monitoring of desertification in central Asia and western China using long term NOAA-AVHRR NDVI time-series data. In: *Proceedings of International Geoscience and Remote Sensing Symposium 2003,* (IGARSS 2003), 21-25 July 2003, Proceedings, IEEE International, 4, pp. 2278–2280.

LIU, Y., YINGSHI, Z. and FENG, X. (2005). A remote sensing-based net primary productivity model for semi-arid grasslands: Model description and validation. In: *Proceedings of International Geoscience and Remote Sensing Symposium 2005*, (IGARSS 2005), 29 July 2005, Seoul, Korea, 1.

LIU, L. and CHENG, Z. (2010). Detection of Vegetation Light-Use Efficiency Based on Solar-Induced Chlorophyll Fluorescence Separated From Canopy Radiance Spectrum. *IEEE Journal of Selected Topics in Applied Earth Observations and Remote Sensing*, 3(3), pp. 306–312.

LIU, Y., LIU, R. and CHEN, J.M. (2012). Retrospective retrieval of long-term consistent global leaf area index (1981–2011) from combined AVHRR and MODIS data. *Journal of Geophysical Research*, 117, G04003, 14 pp., doi: 10.1029/2012JG002084.

LOBELL, D.B., CASSMAN, K.G. and FIELD, C.B. (2009). Crop Yield Gaps: Their Importance, Magnitudes, and Causes. *Annual Review of Environment and Resources*, 34, pp. 179–204.

LO SEEN, D., MOUGIN, E., RAMBAL, S., GASTON, A. and HIERNAUX, P. (1995). A regional Sahelian grassland model to be coupled with multispectral satellite data. II: Toward the control of its simulations by remotely sensed indices. *Remote Sensing of Environment*, 52(3), pp. 194–206.

LU, D. (2006). The potential and challenge of remote sensing-based biomass estimation. *International Journal of Remote Sensing*, 27(7), pp. 1297–1328.

MACHWITZ, M. (2010). Eine raum-zeitliche Modellierung der Kohlenstoffbilanz mit Fernerkundungsdaten auf regionaler Ebene in Westafrika. Dissertation, Lehrstuhl für Fernerkundung, Julius-Maximilians-Universität Würzburg, 201 pp. Available online at: http://opus.bibliothek.uniwuerzburg.de/frontdoor.php?source_opus=5513&la=de (accessed 24 October 2011) [in German].

MACHWITZ, M., FALK, U., RICHTERS, J., CONRAD, C. and DECH, S. (2009). Modelling the carbon budget at regional scale in West Africa using 250m MODIS data and ground observations. In: *33rd International Symposium on Remote Sensing of Environment*, (ISRSE 2009), 03–08 May 2009, Stresa, Italy.

MAKAROWA, L.I. (1971). Tyrsovaya formacia w basseyne ozera Tchelkar. In: *Materialy Po Flore I Rastitelnosti Severnogo Prikaspiya*, pp. 179–186 (Leningrad: Wsesojuz. geogr. obstch.) [in Russian].

MANGIAROTTI, S., MAZZEGA, P., JARLAN, L., MOUGIN, E., BAUP, F. and DEMARTY, J. (2008). Evolutionary bi-objective optimization of a semi-arid vegetation dynamics model with NDVI and σ^0 satellite data. *Remote Sensing of Environment,* 112(4), pp. 1365–1380.

MCKNIGHT, T.L. and HESS, D. (2000). Climate Zones and Types: The Köppen System. Physical Geography: A Landscape Appreciation, pp. 200–201. (Upper Saddle River, NJ: Prentice Hall).

MCVICAR, T.R. and JUPP, D.L.B. (1998). The Current and Potential Operational Uses of Remote Sensing to Aid Decisions on Drought Exceptional Circumstances in Australia: a Review. *Agricultural Systems*, 57(3), pp. 399–468.

MEAB (2005). Living Beyond Our Means. Natural Assets and Human Well-Being. Statement from the Board. Millenium Ecosystem Assessment Board. Available online at: http://www.millenniumassessment.org/documents/document.429.aspx.pdf (accessed 16 March 2010).

MEANS, J.E., ACKER, S.A., HARDING, D.J., BLAIR, J.B. LEFSKY, M.A., COHEN, W.B., HARMON, M.E. and MCKEE, W.A. (1999). Use of Large-Footprint Scanning Airborne Lidar To Estimate Forest Stand Characteristics in the Western Cascades of Oregon. *Remote Sensing of Environment*, 67(3), pp. 298–308.

MEZIANE, D. and SHIPLEY, B. (1999). Interacting components of interspecific relative growth rate: constancy and change under differing conditions of light and nutrient supply. *Functional Ecology*, 13(5), pp. 611–622.

MILLS, A.J., O'CONNER, T.G., DONALDSON, J.S., FEY, M.V., SKOWNO, A.L., SIGWELA, A.M., LECHMERE-OERTEL, R.G. and BOSENBERG, J.D. (2005). Ecosystem carbon storage under different land uses in three semi-arid shrublands and a mesic grassland in South Africa. *South African Journal of Plant and Soil,* 22(3), pp. 183–190.

MILLS, A.J., TURPIE, J.K., COWLING, R.M., MARAIS, C., KERLEY, G.I.H., LECHMERE-OERTEL, R.G., SIGWELA, A.M. and POWELL, M. (2007). Assessing Costs, Benefits, and Feasibility of Restoring Natural Capital in Subtropical Thicket in South Africa. In: *Restoring natural capital: science, business, and practice*, J. Aronson, S.J. Milton and J.N. Blignaut (Eds.), Chapter 21, pp. 179–187 (Washington: Island Press).

MITCHARD, E.T.A, SAATCHI, S.S, WOODHOUSE, I.H., NANGENDO, G., RIBEIRO, N.S., WILLIAMS, M., RYAN, C.M., LEWIS, S.L., FELDPAUSCH, T.R. and MEIR, P. (2009). Using satellite radar backscatter to predict above-ground woody biomass: A consistent relationship across four different African landscapes. *Geophysical Research Letters*, 36, L23401, 6 pp.

MO, X., LIU, S., LIN, Z., XU, Y., XIANG, Y. and MCVICAR, T.R. (2005). Prediction of crop yield, water consumption and water use efficiency with a SVAT-crop growth model using remotely sensed data on the North China Plain. *Ecological Modelling,* 183(2-3), pp. 301–322.

MOLEELE, N., RINGROSE, S., ARNBERG, W., LUNDEN, B. and VANDERPOST, C. (2001). Assessment of vegetation indexes useful for browse (forage) prediction in semi-arid rangelands. *International Journal of Remote Sensing*, 22(5), pp. 741–756.

MONTANDON, L.M. and SMALL, E.E. (2008). The impact of soil reflectance on the quantification of the green vegetation fraction from NDVI. *Remote Sensing of Environment*, 112(4), pp. 1835–1845.

MONTEITH, J.L. (1965a). Evaporation and Environment in the State and Movement of Water in Living Organisms. In: *Symposia of the Society for Experimental Biology*, 19, pp. 205–234.

MONTEITH, J.L. (1965b). Light distribution and photosynthesis in field crops. *Annals of Botany*, 29(1), pp. 17–37.

MONTEITH, J.L. (1972). Solar radiation and productivity in tropical ecosystems. *Journal of Applied Ecology,* 9(3), pp. 747–766.

MONTÈS, N., BERTAUDIERE-MONTES, V., BADRI, W., ZAOUI, E.H. and GAUQUELIN, T. (2002). Biomass and nutrient content of a semi-arid mountain ecosystem: the Juniperus thurifera L. woodland of Azzaden Valley (Morocco). *Forest Ecology and Management*, 166(1), pp. 35–43.

MOUGIN, E., LO SEEN, D., RAMBAL, S., GASTON, A. and HIERNAUX, P. (1995). A regional sahelian grassland model to be coupled with multispectral satellite data. I. Description and validation. *Remote Sensing of Environment*, 52(3), pp. 181−193.

MULLIGAN, M. (2009). Integrated environmental modelling to characterise processes of land degradation and desertification for policy support. In: *Recent Advances in Remote Sensing and Geoinformation Processing for Land Degradation Assessment*, A. Röder and J. Hill (Eds.), pp. 45–72, (London: Taylor & Francis Group).

MUSICK, H.B. (1984). Assessment of Landsat Multispectral Scanner spectral indices for monitoring arid rangeland. *IEEE Transactions on Geoscience and Remote Sensing*, 22, pp. 512–519.

MUTANGA, O. and SKIDMORE, A.K. (2004). Narrow band vegetation indices overcome the saturation problem in biomass estimation. *International Journal of Remote Sensing,* 25(19), pp. 3999–4014.

MUTANGA, O. and RUGEGE, D. (2006). Integrating remote sensing and spatial statistics to model herbaceous biomass distribution in a tropical savanna. *International Journal of Remote Sensing*, 27(16), pp. 3499–3514.

MYNENI, R.B., HOFFMAN, S., KNYAZIKHIN, Y., PRIVETTE, J.L., GLASSY, J., TIAN, Y., WANG, Y., SONG, X., ZHANG, Y., SMITH, G.R., LOTSCH, A., FRIEDL, M., MORISETTE, J.T., VOTAVA, P., NEMANI, R.R. and RUNNING, S.W. (2002). Global products of vegetation leaf area and fraction absorbed PAR from year one of MODIS data. *Remote Sensing of Environment,* 83(1-2), pp. 214–231.

NASA (2012a). MOD 15 – Leaf Area Index (LAI) and Fractional Photosynthetically Active Radiation (FPAR). Available online at: http://modis.gsfc.nasa.gov/data/dataprod/dataproducts.php?MOD_NUMBER=15 (accessed 17 October 2012).

NASA (2012b). Leaf Area Index. Information from the MODIS Land group. Available online at: http://modis-land.gsfc.nasa.gov/lai.html (accessed 17 October 2012).

NASA (2012c). Vegetation Continuous Fields. Information from the MODIS Land group. Available online at: http://modis-land.gsfc.nasa.gov/vcc.html (accessed 17 October 2012).

NÆSSET, E. and GOBAKKEN, T. (2008). Estimation of above- and below-ground biomass across regions of the boreal forest zone using airborne laser. *Remote Sensing of Environment*, 112(6), pp. 3079–3090.

NELSON, R.F., KIMES, D.S., SALAS, W.A. and ROUTHIER, M. (2000). Secondary forest age and tropical forest biomass estimation using Thematic Mapper imagery. *Bioscience*, 50(5), pp. 419–431.

NIEMEIJER, D. (2002). Developing indicators for environmental policy: Data-driven and theory-driven approaches examined by example. *Environmental Science and Policy,* 5(2), pp. 91–103.

NIJLAND, W., ADDINK, E.A., DE JONG, S.M. and VAN DER MEER, F.D. (2009). Optimizing spatial image support for quantitative mapping of natural vegetation. *Remote Sensing of Environment*, 113(4), pp. 771–780.

NIKLAUS, M., TUM, M. and GÜNTHER, K.P. (2010a). Modeling Carbon Sinks and Sources in semi-arid Environments for a Land Degradation Assessment Approach. In: *Greve, K. and Cremers, A.B. (Eds.). EnviroInfo 2010, Proceedings of the 24th International Conference on Informatics for Environmental Protection*, 6-8 October 2010, Cologne/Bonn, Germany, pp. 648–656.

NIKLAUS, M., TUM, M. and GÜNTHER, K.P. (2010b). Estimating the Carbon Cycle of South Africa with BETHY/DLR. In: *EGU General Assembly 2010*, 2-7 May 2010, Vienna, Austria.

NIKLAUS, M., EISFELDER, C., TUM, M. and GÜNTHER, K.P. (2012). A remote sensing model based land degradation index for the arid and semi-arid regions of southern Africa. In: *International Geoscience and Remote Sensing Symposium* 2012, (IGARSS 2012), 22-27 July 2012, Munich, Germany.

NIKLAUS, M., GÜNTHER, K.P., TUM, M. and BITTNER, M. (submitted). Generation of a global, gap-free SPOTVGT LAI dataset using spectral analysis techniques. *Computers and Geosciences*.

NIKLAUS, M. (in preparation). Modellierung der vegetativen Produktivität zur Bewertung der Landdegradation im ariden und semi-ariden südlichen Afrika. Dissertation, Mathematisch-Naturwissenschaftliche Fakultät, Universität Augsburg [in German].

NORI, W. (2012). Detection of land cover changes in El Rawashda forest, Sudan: A systematic comparison. Dissertation, Faculty of Forest, Geo and Hydro Sciences, Technische Universität Dresden, 123 pp.

NOUVELLON, Y., MORAN, M.S., SEEN, D.L., BRYANT, R., RAMBAL, S., NI, W., BÉGUÉ, A., CHEHBOUNI, A., EMMERICH, W.E., HEILMAN, P. and QI, J. (2001). Coupling a grassland ecosystem model with Landsat imagery for a 10-year simulation of carbon and water budgets. *Remote Sensing of Environment*, 78(1-2), pp. 131–149.

OESTERHELD, M. (1992). Effect of defoliation intensity on aboveground and belowground relative growth rates. *Oecologia*, 92(3), pp. 313–316.

OKIN, G.S., ROBERTS, D.A., MURRAY, B. and OKIN, W.J. (2001). Practical limits on hyperspectral vegetation discrimination in arid and semiarid environments. *Remote Sensing of Environment*, 77(2), pp. 212–225.

OLSON, D.M., DINERSTEIN, E., WIKRAMANAYAKE, E.D., BURGESS, N.D., POWELL, G.V.N., UNDERWOOD, E.C., D'AMICO, J.A., ITOUA, I., STRAND, H.E., MORRISON, J.C., LOUCKS, C.J., ALLNUTT, T.F., RICKETTS, T.H., KURA, Y., LAMOREUX, J.F., WETTENGEL, W.W., HEDAO, P. and KASSEM, K.R. (2001). Terrestrial Ecoregions of the World: A New Map of Life on Earth. *Bioscience*, 51(11), pp. 933–938.

OTTERMAN, J. (1996). Desert-scrub as the cause of reduced reflectances in protected versus impacted sandy arid areas. *International Journal of Remote Sensing*, 17(3), pp. 615–619.

OZDEMIR, I. (2008). Estimating stem volume by tree crown area and tree shadow area extracted from pan-sharpened Quickbird imagery in open Crimean juniper forests. *International Journal of Remote Sensing*, 29(19), pp. 5643–5655.

PADILLA, F.M., MIRANDA, J.D., JORQUERA, M.J. and PUGNAIRE, F.I. (2009). Variability in amount and frequency of water supply affects roots but not growth of arid shrubs. *Plant Ecology*, 204(2), pp. 261–270.

PAN, G., SUN, G.-J. and LI, F.M. (2009). Using QuickBird imagery and a production efficiency model to improve crop yield estimation in the semi-arid hilly Loess Plateau, China. *Environmental Modelling & Software*, 24(4), pp. 510–516.

PARKINSON, C.L. and GREENSTONE, R., Eds. (2000). EOS Data Products Handbook. Volume 2. Available online at: aqua.nasa.gov/doc/pubs/data_products_vol2.pdf (accessed 2 May 2012).

PARRESOL, B.R. (1999). Assessing tree and stand biomass: a review with examples and critical comparisons. *Forest Science*, 45(4), pp. 573–593.

PARTON, W.J. and RASMUSSEN, P.E. (1994). Long-Term Effects of Crop Management in Wheat-Fallow: II. CENTURY Model Simulations. *Soil Science Society of America Journal,* 58(2), pp. 530–536.

PATENAUDE, G., MILNE, R. and DAWSON, T.P. (2005). Synthesis of remote sensing approaches for forest carbon estimation: reporting to the Kyoto Protocol. *Environmental Science and Policy*, 8(2), pp. 161–178.

PEEL, M.C., FINLAYSON, B.L. and MCMAHON, T.A. (2007). Updated world map of the Köppen-Geiger climate classification. *Hydrology and Earth System Sciences,* 11(5), pp. 1633–1644.

PEREIRA, J.M.C., OLIVEIRA, T.M. and PAUL, J.C.P. (1995). Satellite-based estimation of Mediterranean shrubland structural parameters. *EARSeL Advances in Remote Sensing*, 4(3), pp. 14–20.

PERSCHINA, M.N. and YAKOVLEWA, M.E. (1960). Biologitcheskiy Krugovorot W Zone Sukhich Stepey SSSR. In: *Dokl. Sov. Potchwowedov K VII Mezschdunar. Kongr. Potchwowedov W USA*, pp. 116–123 (Moscow: AN SSSR) [in Russian].

PFAFF, A.S.P., KERR, S., HUGHES, R.F., LIU, S., SANCHEZ-AZOFEIFA, G.A., SCHIMEL, D., TOSI, J. and WATSON, V. (2000). The Kyoto protocol and payments for tropical forest: An interdisciplinary method for estimating carbon-offset supply and increasing the feasibility of a carbon market under the CDM. *Ecological Economics*, 35(2), pp. 203–221.

PHILIP's (2003). Philip's School Atlas, Climatic Regions. Chancellor Press, pp. 74–75 (London: George Philip Limited).

PICKUP, G. (1996). Estimating the Effects of Land Degradation and Rainfall Variation on Productivity in Rangelands: An Approach Using Remote Sensing and Models of Grazing and Herbage Dynamics. *Journal of Applied Ecology*, 33(4), pp. 819–832.

POORTER, H. and REMKES, C. (1990). Leaf area ratio and net assimilation rate of 24 wild species differing in relative growth rate. *Oecologia*, 83(4), pp. 553–559.

POTTER, C.S., RANDERSON J.T., FIELD, C.B., MATSON, P.A., VITOUSEK, P.M., MOONEY, H.A. and KLOOSTER, S.A. (1993). Terrestrial ecosystem production – a process model based on global satellite and surface data. *Global Biogeochemical Cycles,* 7(4), pp. 811–841.

POTTER, C., KLOOSTER, S., MYNENI, R., GENOVESE, V., TAN, P.-N. and KUMAR, V. (2003). Continental-scale comparisons of terrestrial carbon sinks estimated from satellite data and ecosystem modeling 1982–1998, *Global and Planetary Change,* 39(3-4), pp. 201–213.

PRIESTLEY, C.H.B. and R.J. TAYLOR (1972). On the assessment of surface heat fluxes and evaporation using large-scale parameters. *Monthly Weather Review,* 100(2), pp. 81–92.

PRINCE, S.D. and ASTLE, W.L. (1986). Satellite remote sensing of rangelands in Botswana. I: Landsat MSS and herbaceous vegetation. *International Journal of Remote Sensing*, 7(11), pp. 1533–1553.

PRINCE, S.D. and TUCKER, C.J. (1986). Satellite remote sensing of rangelands in Botswana II: NOAA AVHRR and herbaceous vegetation. *International Journal of Remote Sensing*, 7(11), pp. 1555–1570.

PRINCE, S.D. (1991). Satellite remote sensing of primary production: comparison of results for Sahelian grasslands 1981-1988. *International Journal of Remote Sensing*, 12(6), pp. 1301–1311.

PRINCE, S.D. and GOWARD, S.J. (1995). Global primary production: A remote sensing approach. *Journal of Biogeography*, 22(4-5), pp. 815–835.

PROPASTIN, P. (2006). Remote sensing based study on vegetation dynamics in drylands of Kazakhstan. Dissertation, Mathematisch-Naturwissenschaftliche Fakultät, Georg-August-Universität Göttingen, 176 pp.

PROPASTIN, P.A., KAPPAS, M. and MURATOVA, N.R. (2008a). Inter-annual changes in vegetation activities and their relationship to temperature and precipitation in Central Asia from 1982 to 2003. *Journal of Environmental Informatics,* 12(2), pp. 75–87.

PROPASTIN, P.A., KAPPAS, M. and MURATOVA, N.R. (2008b). A remote sensing based monitoring system for discrimination between climate and human-induced vegetation change in Central Asia. *Remote monitoring system,* 19(5), pp. 579–596.

PROPASTIN, P. and KAPPAS, M. (2009). Modeling Net Ecosystem Exchange for Grassland in Central Kazakhstan by Combining Remote Sensing and Field Data. *Remote Sensing,* 1(3), pp. 159–183, doi: 10.3390/rs1030159.

PROPASTIN, P.A., KAPPAS, M.W., HERRMANN, S.M. and TUCKER, C.J. (2012). Modified light use efficiency model for assessment of carbon sequestration in grasslands of Kazakhstan: combining

ground biomass data and remote-sensing. *International Journal of Remote Sensing,* 33(5), pp. 1465–1487.

PUGNAIRE, F.I. and HAASE, P. (1996). Comparative Physiology and Growth of Two Perennial Tussock Grass Species in a Semi-Arid Environment. *Annals of Botany*, 77(1), pp. 81–86.

QI, J., MARSETT, R.C. and HEILMAN, P. (2000). Rangeland vegetation cover estimation from remotely sensed data. In: *2nd International conference on Geospatial Information in Agriculture and Forestry*, 10-12 January 2000, Lake Buena Vista, Florida, pp. II–243–252.

QI, J. and WALLACE, O. (2002). Biophysical Attributes Estimation from Satellite Images in Arid Regions. In: *Proceedings of the International Geoscience and Remote Sensing Symposium 2002*, (IGARSS 2002), 24-28 Juni 2002, Toronto, Canada, 4, pp. 2000–2002.

RABUS, B., EINEDER, M., ROTH, A. and BAMLER, R. (2003). The shuttle radar topography mission – a new class of digital elevation models acquired by spaceborne radar. *ISPRS Journal of Photogrammetry and Remote Sensing,* 57(4), pp. 241–262.

RADLOFF, F.G.T. and MUCINA, L. (2007). A quick and robust method for biomass estimation in structurally diverse vegetation. *Journal of Vegetation Science*, 18(5), pp. 719–724.

RAHMAN, M.M., CSAPLOVICS, E. and KOCH, B. (2008). Satellite estimation of forest carbon using regression models. *International Journal of Remote Sensing*, 29(23), pp. 6917–6936.

REICH, P.B., BUSCHENA, C., TJOELKER, M.G., WRAGE, K., KNOPS, J., TILMAN, D. and MACHADO, J.L. (2003). Variation in growth rate and ecophysiology among 34 grassland and savanna species under contrasting N supply: a test of functional group differences. *New Phytologist*, 157(3), pp. 617–631.

RICHTERS, J. (2005a). Erfassung von pflanzlicher Biomasse im nordwestlichen Namibia – eine fernerkundungsgestützte Modellierung. Dissertation, Math.-Nat. Fakultät, Universität Bonn. 257 pp. Available online at: http://hss.ulb.unibonn.de/diss_online/math_nat_fak/2005/richters_jochen (accessed 24 October 2011) [in German].

RICHTERS, J. (2005b). Biomass changes in north-western Namibia: First results from a remote sensing modelling approach. *EARSeL eProceedings,* 4(2), pp. 157–170.

RICHTERS, J. (2006). Biomass production, pasture balance, and their ecologic consequences in NW Namibia. In: *Gao, W. and Ustin, S.L. (Eds.). Remote Sensing and Modeling of Ecosystems for Sustainability III. Proceedings of the SPIE*, Volume 6298, pp. 62980F.

RINGROSE, S., MATHESON, W., MATLALA, C.J.S.S., O'NEILL, T. and WERNER, P.A. (1994). Vegetation spectral reflectance along a north-south vegetation gradient in northern Australia. *Journal of Biogeography*, 21(1), pp. 33–47.

ROBINSON, S., MILNER-GULLAND, E.L. and ALIMAEV, I. (2002). Rangeland degradation in Kazakhstan during the Soviet-era: re-examining the evidence. *Journal of Arid Environments*, 53(3), pp. 419–439.

ROSEMA, A. (1993). Using METEOSAT for operational evapotranspiration and biomass monitoring in the Sahel region. *Remote Sensing of Environment*, 46(1), pp. 27–44.

ROSENQVIST, Å., MILNE, A., LUCAS, R., IMHOFF, M. and DOBSON, C. (2003). A review of remote sensing technology in support of the Kyoto Protocol. *Environmental Science & Policy*, 6(5), pp. 441–455.

RUDOLF, B., BECKER, A., SCHNEIDER, U., MEYER-CHRISTOFFER, A. and ZIESE, M. (2010). GPCC Status Report December 2010 (On the most recent gridded global data set issued in fall 2010 by the Global Precipitation Climatology Centre (GPCC)).

RUDOLF, B. and SCHNEIDER, U. (2005). Calculation of Gridded Precipitation Data for the Global Land-Surface using in-situ Gauge Observations. In: *Proceedings of the 2nd Workshop of the International Precipitation Working Group IPWG*, Monterey October 2004, EUMETSAT, ISBN 92-9110-070-6, ISSN 1727-432X, 231-247.

RUIMY, A., DEDIEU, G. and SAUGIER, B. (1996). TURC: A diagnostic model of continental gross primary productivity and net primary productivity. *Global Biogeochemical Cycles*, 10(2), pp. 269–285.

RUNNING, S.W., LOVELAND, T.R., PIERCE, L.L., NEMANI, R.R. and HUNT JR., E.R. (1995). A Remote Sensing Based Vegetation Classification Logic for Global Land Cover Analysis. *Remote Sensing of Environment*, 51(1), pp. 39–48.

RUNNING, S.W., BALDOCCHI, D.D., TURNER, D.P., GOWER, S.T., BAKWIN, P.S. and HIBBARD, K.A. (1999). A Global Terrestrial Monitoring Network Integrating Tower Fluxes, Flask Sampling, Ecosystem Modeling and EOS Satellite Data. *Remote Sensing of Environment,* 70(1), pp. 108–127.

RUNNING, S.W., THORNTON, P.E., NEMANI, R.R. and GLASSY, J.M. (2000). Global Terrestrial Gross and Net Primary Productivity from the Earth Observing System. In: *Methods in Ecosystem Science*, O.E. Sala, R.B. Jackson, H.A. Mooney and R.W. Howarth (Eds.), pp. 44–57, (New York: Springer).

RUNNING, S.W., NEMANI, R.R., HEINSCH, F.A., ZHAO, M., REEVES, M. and HASHIMOTO, H. (2004). A Continuous Satellite-Derived Measure of Global Terrestrial Primary Production. *BioScience,* 54(6), pp. 547–560.

SAMIMI, C. and KRAUS, T. (2004). Biomass estimation using Landsat-TM and -ETM+. Towards a regional model for Southern Africa? *GeoJournal*, 59(3), pp. 177–187.

SANNIER, C.A.D., TAYLOR, J.C. and PLESSIS, W.D. (2002). Real-time monitoring of vegetation biomass with NOAA-AVHRR in Etosha National Park, Namibia, for fire risk assessment. *International Journal of Remote Sensing*, 23(1), pp. 71–89.

SANTOS, J.R., PARDI LACRUZ, M.S., ARAUJO, L.S. and KEIL, M. (2002). Savanna and tropical rainforest biomass estimation and spatialization using JERS-1 data. *International Journal of Remote Sensing*, 23(7), pp. 1217–1229.

SCHIMEL, D.S. (1995). Terrestrial biogeochemical cycles: Global estimates with remote sensing. *Remote Sensing of Environment,* 51(1), pp. 49–56.

SCHLESINGER, W.H. (1991). Biogeochemistry: An analysis of global change. 113 pp. (San Diego, USA: Academic Press, Inc.).

SCHÖNBACH, P., WAN, H., GIERUS, M., BAI, Y., MÜLLER, K., LIN, L., SUSENBETH, A. and TAUBE, F. (2011). Grassland responses to grazing: effects of grazing intensity and management system in an Inner Mongolian steppe ecosystem. *Plant and Soil*, 340(1-2), pp. 103–115.

SCHWEIGER, A.J., ZHANG, J., LINDSAY, R.W. and STEELE, M. (2008). Did unusually sunny skies help drive the record sea ice minimum of 2007? *Geophysical Research Letters*, 35, L10503, doi: 10.1029/2008GL033463

SCURLOCK, J.M.O., JOHNSON, K. and OLSON, R.J. (2002). Estimating net primary productivity from grassland biomass dynamics measurements. *Global Change Biology*, 8(8), pp. 736–753.

SEGOLI, M., UNGAR, E.D. and SHACHAK, M. (2008). Shrubs enhance resilience of a semi-arid ecosystem by engineering and regrowth. *Ecohydrology*, 1(4), pp. 330–339.

SELLERS, P.J. (1985). Canopy reflectance, photosynthesis and transpiration. *International Journal of Remote Sensing*, 6(8), pp. 1335–1372.

SELLERS, P.J., RANDELL, D.A., COLLATZ, G.J., BERRY, J.A., FIELD, C.B., DAZLICH, D.A., ZHANG, C., COLLELO, G.D. and BOUNUA, L. (1996a). A revised land surface parameterization (SiB 2) for atmospheric GCMs. Part I: Model formulation. *Journal of Climate*, 9(4), pp. 676–705.

SELLERS, P.J., LOS, S.O., TUCKER, C.J., JUSTICE, C.O., DAZLICH, D.A., COLLATZ, G.J. and RANDELL, D.A. (1996b). A revised land surface parameterization (SiB 2) for atmospheric GCMs. Part II: The generation of global fields of terrestrial biophysical parameters from satellite data. *Journal of Climate*, 9(4), pp. 706–737.

SHACKLETON, W.G. (1986). Economic and Applied Geology: An Introduction. Croom Helm, New Hampshire, USA, 227 pp., ISBN 0-7099-3387-8.

SHIMIZU, H., ITO, S. and SASAKAWA, H. (2010). Responses to Water Stress and a Functional-structural Growth Model of Plant Species Growing in Semi-arid Desertified Areas of Northeast Asia. *Global Environmental Research*, 14(1), pp. 47–54.

SHIPLEY, B. and KEDDY, P.A. (1988). The Relationship Between Relative Growth Rate and Sensitivity to Nutrient Stress in Twenty-Eight Species of Emergent Macrophytes. *Journal of Ecology,* 76(4), pp. 1101–1110.

SHOSHANY, M. (2000). Satellite remote sensing of natural Mediterranean vegetation: A review within an ecological context. *Progress in Physical Geography*, 24(2), pp. 153–178.

SHUAI, Y., SCHAAF, C.B., STRAHLER, A.H., LIU, J. and JIAO, Z. (2008). Quality assessment of BRDF/albedo retrievals in MODIS operational system. *Geophysical Research Letters*, 35, L05407, 5 pp.

SIEBERT, S., DÖLL, P., FEICK, S., HOOGEVEEN, J. and FRENKEN, K. (2007). Global Map of Irrigation Areas version 4.0.1. Johann Wolfgang Goethe University, Frankfurt am Main, Germany / Food and Agriculture Organization of the United Nations, Rome, Italy.

SONG, J., DING, X., FENG, G. and ZHANG, F. (2006). Nutritional and osmotic roles of nitrate in a euhalophyte and a xerophyte in saline conditions. *New Phytologist*, 171(2), pp. 357–366.

STRAHLER, A.N. and STRAHLER, A.H. (1984). Elements of physical geography. 3rd ed., 538 pp. (New York: Wiley).

STRAHLER, A., MUCHONEY, D., BORAK, J., FRIEDL, M., GOPAL, S., LAMBIN, E. and MOODY, A. (1999a). MODIS Land Cover Product Algorithm Theoretical Basis Document (ATBD). MODIS Land Cover and Land-Cover Change. Version 5.0. Available online at: http://modis.gsfc.nasa.gov/data/atbd/atbd_mod12.pdf (accessed 2 May 2012).

STRAHLER, A.H., MULLER, J.-P. and the MODIS Science Team Members (1999b). MODIS BRDF/Albedo Product: Algorithm Theoretical Basis Document. Version 5.0. Available online at: http://modis.gsfc.nasa.gov/data/atbd/atbd_mod09.pdf (accessed 2 May 2012).

SUGANUMA, H., ABE, Y., TANIGUCHI, M., TANOUCHI, H., UTSUGI, H., KOJIMA, T. and YAMADA, K. (2006). Stand biomass estimation method by canopy coverage for application to remote sensing in an arid area of Western Australia. *Forest Ecology and Management,* 222(1-3), pp. 75–87.

SULIEMAN, H.M. (2007). Mapping and Modelling of Vegetation Changes in the Southern Gadarif Region, Sudan, Using Remote Sensing. Dissertation, Faculty of Forest, Geo and Hydro Sciences, Technische Universität Dresden, 176 pp.

SULIEMAN, H.M. and BUCHROITHNER, M.F. (2006). Assessment of Natural Vegetation Clearing and Re-Growth in Southern Gadarif (Sudan) Using Change Vector Analysis Based on Remote Sensing and Field Data. In: *ISPRS Commission VII Mid-term Symposium "Remote Sensing: From Pixels to Processes"*, 08-11 May 2006, Enschede, Netherlands, pp. 586–591.

SVORAY, T., SHOSHANY, M., CURRAN, P.J., FOODY, G.M. and PEREVOLOTSKY, A. (2001). Relationship between green leaf biomass volumetric density and ERS-2 SAR backscatter of four vegetation formations in the semi-arid zone of Israel. *International Journal of Remote Sensing*, 22(8), pp. 1601–1607.

SVORAY, T. and SHOSHANY, M. (2002). SAR-based estimation of areal aboveground biomass (AAB) of herbaceous vegetation in the semi-arid zone: a modification of the water-cloud model. *International Journal of Remote Sensing*, 23(19), pp. 4089–4100.

SVORAY, T. and SHOSHANY, M. (2003). Herbaceous biomass retrieval in habitats of complex composition: A model merging SAR images with unmixed Landsat TM data. *IEEE Transactions on Geoscience and Remote Sensing*, 41(7), pp. 1592–1601.

SWIFT, L.W., JR. (1976). Algorithm for Solar Radiation on Mountain Slopes. *Water Resources Research*, 12(1), pp. 108–112.

TARASOV, P.E., JOLLY, D. and KAPLAN, J.O. (1997). A continuous Late Glacial and Holocene record of vegetation changes in Kazakhstan. *Palaeogeography, Palaeoclimatology, Palaeoecology*, 136(1–4), pp. 281–292.

THENKABAIL, P.S., STUCKY, N., GRISCOM, B.W., ASHTON, M.S., DIELS, J., VAN DER MEER, B. and ENCLONA, E. (2004). Biomass estimations and carbon stock calculations in the oil palm plantations of African derived savannas using IKONOS data. *International Journal of Remote Sensing*, 25(23), pp. 5447–5472.

THORNTON, P.E., LAW, B.E., GHOLZ, H.L., CLARK, K.L., FALGE, E., ELLSWORTH, D.S., GOLDSTEIN, A.H., MONSON, R.K., HOLLINGER, D., FALK, M., CHEN, J. and SPARKS, J.P. (2002). Modeling and measuring the effects of disturbance history and climate on carbon and water budgets in evergreen needleleaf forests. *Agricultural and Forest Meteorology*, 113(1-4), pp. 185–222.

TIETEMA, T. (1993). Biomass determination of fuelwood trees and bushes of Botswana, Southern Africa. *Forest Ecology and Management*, 60(3-4), pp. 257–269.

TITLYANOVA, A.A., ROMANOVA, I.P., KOSYKH, N.P. and MIRONYCHEVA-TOKAREVA, N.P. (1999). Pattern and process in above-ground and below-ground components of grassland ecosystems. *Journal of Vegetation Science*, 10(3), pp. 307–320.

TODD, S.W., HOFFER, R.M. and MILCHUNAS, D.G. (1998). Biomass estimation on grazed and ungrazed rangelands using spectral indices. *International Journal of Remote Sensing*, 19(3), pp. 427–438.

TUCKER, C.J. (1980). A critical review of remote sensing and other methods for non-destructive estimation of standing crop biomass. *Grass and Forage Science*, 35(3), pp. 177–182.

TUCKER, C.J., VANPRAET, C.L., SHARMAN, M.J. and VAN ITTERSUM, G. (1985). Satellite remote sensing of total herbaceous biomass production in the Senegalese Sahel: 1980-1984. *Remote Sensing of Environment*, 17(3), pp. 233–249.

TUELLER, P.T. (1987). Remote sensing science applications in arid environments. *Remote Sensing of Environment*, 23(2), pp. 143–154.

TUM, M. (2008). Variabilitätsuntersuchungen der NPP von Energiepflanzen für das Gebiet Deutschland – Österreich. Unpublished. Diploma thesis, Fachgebiet Geographie, Universität Göttingen. 121 pp. [in German].

TUM, M., BUCHHORN, M., GÜNTHER, K.P. and HALLER, B.C. (2011). Validation of modelled forest biomass in Germany using BETHY/DLR. *Geoscientific Model Development,* 4, pp. 1019–1034.

TUM, M. and GÜNTHER, K.P. (2011). Validating modelled NPP using statistical yield data. *Biomass and Bioenergy,* 35(11), pp. 4665–4674.

TUM, M., STRAUSS, F., MCCALLUM, I., GÜNTHER, K.P. and SCHMID, E. (2012). How sensitive are estimates of carbon fixation in agricultural models to input data? *Carbon Balance and Management,* 7(3), pp. 1–13.

TUM, M. and BORG, E. (submitted). A conceptual remote sensing based interception-infiltration model for regional and global applications. *Hydrology and Earth System Sciences.*

TYURMENCO, A.N. (1975). Biologitcheskiy krugovorot zolnych elementov pod celinnoy i culturnoy rastitelnostyu w zone sukhich i polupustynnych stepey. In: *Genesis, Swoystwa I Plodorodiye Potchw*, pp. 135–176 (Kazan': Izd. Kazan. Universiteta) [in Russian].

UN (1994). Elaboration of an international Convention to Combat Desertification in Countries experiencing serious Drought and/or Desertification, particularly in Africa. UN General Assembly. A/AC.241/27. Available online at: http://www.unccd.int/convention/text/pdf/conv-eng.pdf (accessed 17 March 2010).

UN (2004). A more secure world: Our shared responsibility. Report of the Secretary-General's high-level Panel on Threats, Challenges and Change Published by the United Nations Department of public Information, DPI/2367, December 2004. Available online at: http://www.un.org/secureworld/report2.pdf (accessed 17 March 2010).

UNEP (1999). National Action Programme to Combat Desertification in Republic of Uzbekistan. Tashkent 1999. Available online at: http://www.unccd.int/actionprogrammes/asia/national/1999/uzbekistan-eng.pdf (accessed 17 March 2010).

UNEP/GRID-Arendal (2005). Radioactive, chemical and biological hazards in Central Asia. Available online at: http://www.grida.no/graphicslib/detail/radioactive-chemical-and-biological-hazards-in-central-asia_83a5 (accessed 25 October 2012).

UNEP/GRID-Arendal (2007). Central Asia in peril. Available online at: http://www.grida.no/graphicslib/detail/central-asia-in-peril_7371 (accessed 25 October 2012).

UNEP-WCMC (2008). Carbon in Drylands: Desertification, Climate Change and Carbon Finance. A UNEP-UNDP-UNCCD Technical Note for Discussions at CRIC 7, Istanbul, Turkey, 03–14 November, 2008. Available online at: http://www.unep-wcmc.org/pdfs/Carbon%20in%20drylands.pdf (accessed 17 March 2010).

UNSO/UNDP (1997). Aridity zones and dryland populations: an assessment of population levels in the World's drylands. United Nations Office to Combat Desertification and Drought / United Nations Development Programme. 23 pp., New York.

USGS (1996). GTOPO30, Global 30-Arc-Second Elevation Data Set. U.S. Geological Survey, EROS Data Center, Sioux Falls, South Dakota. Available online at: http://eros.usgs.gov/#/Find_Data/Products_and_Data_Available/GTOPO30 (accessed 1 October 2012).

VANAMBURG, L.K., TRLICA, M.J., HOFFER, R.M. and WELTZ, M.A. (2006). Ground based digital imagery for grassland biomass estimation. *International Journal of Remote Sensing*, 27(5), pp. 939–950.

VAN DER MEER, F., BAKKER, W., SCHOLTE, K., SKIDMORE, A., DE JONG, S., CLEVERS, J., ADDINK, E. and EPEMA, G. (2001). Spatial scale variations in vegetation indices and above-ground biomass estimates: implications for MERIS. *International Journal of Remote Sensing*, 22(17), pp. 3381–3396.

VAN STAALDUINEN, M.A. and ANTEN, N.P.R. (2005). Differences in the compensatory growth of two co-occurring grass species in relation to water availability. *Oecologia*, 146(2), pp. 190–199.

VELLINGA, M. and WOOD, R.A. (2002). Global climatic impacts of a collapse of the Atlantic thermohaline circulation. *Climatic Change*, 54(3), pp. 251–267.

VERBESSELT, J., SOMERS, B., VAN AARDT, J., JONCKHEERE, I. and COPPIN, P. (2006). Monitoring herbaceous biomass and water content with SPOT VEGETATION time-series to improve fire risk assessment in savanna ecosystems. *Remote Sensing of Environment*, 101(3), pp. 399–414.

VERÓN, S.R., PARUALO, J.M. and OESTERHELD, M. (2010). Grazing-induced losses of biodiversity affect the transpiration of an arid ecosystem. *Oecologia*, DOI: 10.1007/s00442-010-1780-4, 10 pp.

VEROUSTRAETE, F., PATYN, J. and MYNENI, R.B. (1994). Forcing of a simple ecosystem model with fAPAR and climate data to estimate regional scale photosynthetic assimilation. In: *Veroustraete F., et al. (Editors), VGT, Modelling and Climate Change Effects*. (The Hague, the Netherlands: Academic Publishing), pp. 151–177.

VERSTRAETE, M.M. (1986). Defining Desertification: A Review, *Climatic Change*, 9(1-2), pp. 5–18.

VERSTRAETE, M.M. and PINTY, B. (1991). The potential contribution of satellite remote sensing to the understanding of arid lands processes. *Vegetatio*, 91, pp. 59–72.

VERSTRAETEN, W.W., VEROUSTRAETE, F. and FEYEN, J. (2006). On temperature and water limitation of ecosystem productivity: Implementation in the C-Fix model. *Ecological Modelling,* 199(1), pp. 4–22.

VILE, D., SHIPLEY, B. and GARNIER, E. (2006). Ecosystem productivity can be predicted from potential relative growth rate and species abundance. *Ecology Letters*, 9(9), pp. 1061–1067.

VOLKOVA, E.A., OGAR, N.P., RACHKOVSKAYA, E.I., SADVOKASOV, P.E. and HRAMTSOV, V.N. (2010). The National Atlas of the Republic of Kazakhstan, Map: Vegetation, Volume 1, Almaty, 2010, pp. 110–113.

VON WEHRDEN, H., HANSPACH, J., RONNENBERG, K. and WESCHE, K. (2010). The interannual climatic variability in Central Asia - a contribution to the discussion on the importance of environmental stochasticity in drylands. *Journal of Arid Environments*, 74(10), pp. 1212–1215.

WALTER, H. and BRECKLE, S.-W. (1989). Ecological Systems of the Geobiosphere, Volume 3, Temperate and Polar Zonobiomes of Northern Eurasia. Springer-Verlag: Berlin, Heidelberg, New York, ISBN: 3-540-15029-3.

WAN, Z. (1999). MODIS Land-Surface Temperature Algorithm Theoretical Basis Document (LST ATBD). Version 3.3. Available online at: http://modis.gsfc.nasa.gov/data/atbd/atbd_mod11.pdf (accessed 2 May 2012).

WAN, Z. (2008). New refinements and validation of the MODIS land-surface temperature/emissivity products. *Remote Sensing of Environment*, 112(1), pp. 59–74.

WANG, J., RICH, P.M., PRICE, K.P. and KETTLE, W.D. (2005). Relations between NDVI, Grassland Production, and Crop Yield in the Central Great Plains. *Geocarto International*, 20(3), pp. 5–11.

WANG, C. and QI, J. (2008). Biophysical estimation in tropical forests using JERS-1 SAR and VNIR imagery. II. Aboveground woody biomass. *International Journal of Remote Sensing*, 29(23), pp. 6827–6849.

WEISS, M., BARET, F., GARRIGUES, S. and LACAZE, R. (2007). LAI and FAPAR CYCLOPES global products derived from Vegetation. Part 2: validation and comparison with MODIS C_4 products, *Remote Sensing of Environment,* 110(3), pp. 317–331.

WESSELS, K.J., PRINCE, S.D., ZAMBATIS, N., MASFADYEN, S., FROST, P.E. and VAN ZYL, D. (2006). Relationship between herbaceous biomass and 1-km² Advanced Very High Resolution Radiometer (AVHRR) NDVI in Kruger National Park, South Africa. *International Journal of Remote Sensing*, 27(5), pp. 951–973.

WHITE, M.A., THORNTON, P.E., RUNNING, S.W. and NEMANI, R.R. (2000). Parameterization and sensitivity analysis of the BIOME-BGC terrestrial ecosystem model: Net Primary Production controls. *Earth Interactions,* 2000, 4(3), pp. 1–85.

WILHELM, W.W. and NELSON, C.J. (1978). Growth Analysis of Tall Fescue Genotypes Differing in Yield and Leaf Photosynthesis. *Crop Science*, 18, pp. 951–954.

WISKERKE, W.T., DORNBURG, V., RUBANZA, C.D.K., MALIMBWI, R.E. and FAAIJ, A.P.C. (2010). Cost/benefit analysis of biomass energy supply options for rural smallholders in the semi-arid eastern part of Shinyanga Region in Tanzania. *Renewable and Sustainable Energy Reviews*, 14(1), pp. 148–165.

WIßKIRCHEN, K. (2005). Modellierung der regionalen CO_2-Aufnahme durch Vegetation. Dissertation, Meteorologisches Institut, Rhein. Friedrich–Wilhelms–Universität, Bonn. Available online at: http://hss.ulb.uni-bonn.de/2005/0765/0765.htm (accessed 24 October 2011) [in German].

WOODWARD, F.I. and LOMAS, M.R. (2004). Vegetation dynamics – simulating responses to climatic change. *Biological Reviews,* 79(3), pp. 643–670.

WRI (2003). Drylands, People, and Ecosystem Goods and Services: A Web-based Geospatial Analyis. World Resources Institute. Available online at: http://www.wri.org (accessed 17 March 2010).

WRI (2008). Ecosystem Services. A Guide for Decision Makers. Available online at: http://pdf.wri.org/ecosystem_services_guide_for_decisionmakers.pdf (accessed 17 March 2010).

WYLIE, B.K., HARRINGTON, J.A., PRINCE, S.D. and DENDA, I. (1991). Satellite and ground-based pasture production assessment in Niger: 1986-1988. *International Journal of Remote Sensing*, 12(6), pp. 1281–1300.

WYLIE, B.K., DENDA, I., PIEPER, R.D., HARRINGTON, J.A., REED, B.C. and SOUTHWARD, G.M. (1995). Satellite-based herbaceous biomass estimates in the pastoral zone of Niger. *Journal of Range Management*, 48(2), pp. 159–164.

WYLIE, B.K., MEYER, D.J., TIESZEN, L.L. and MANNEL, S. (2002). Satellite mapping of surface biophysical parameters at the biome scale over the North American grasslands: A case study. *Remote Sensing of Environment*, 79(2-3), pp. 266–278.

XIAO, J. and MOODY, A. (2004). Trends in vegetation activity and their climatic correlates: China 1982 to 1998. *International Journal of Remote Sensing*, 25(4), pp. 5669–5689.

XIAO, X. (2006). Light absorption by leaf chlorophyll and maximum light use efficiency. *IEEE Transactions on Geoscience and Remote Sensing*, 44(7), pp. 1933–1935.

XIAO, X.M., WAN, Y.F., JIANG, S., OJIMA, D.S. and BONHAM, C.D. (1995). Interannual variation in the climate and above-ground biomass of Leymus chinense steppe and Stipa grandis steppe in the Xilin river basin, Inner Mongolia, China. *Journal of Arid Environments,* 31(3), pp. 283–299.

XIAO, X., HOLLINGER, D., ABER, J., GOLTZ, M., DAVIDSON, E.A., ZHANG, Q. and MOORE III, B. (2004a). Satellite-based modeling of gross primary production in an evergreen needleleaf forest. *Remote Sensing of Environment*, 89(4), pp. 519–534.

XIAO, X., ZHANG, Q., BRASWELL, B., URBANSKI, S., BOLES, S., WOFSY, S., MOORE III, B. and OJIMA, D. (2004b). Modeling gross primary production of temperate deciduous broadleaf forest using satellite images and climate data. *Remote Sensing of Environment*, 91(2), pp. 256–270.

XU, B., YANG, X.C., TAO, W.G., QIN, Z.H., LIU, H.Q., MIAO, J.M. and BI, Y.Y. (2008). MODIS-based remote sensing monitoring of grass production in China. *International Journal of Remote Sensing*, 29(17-18), pp. 5313–5327.

YANG, F. and ZHOU, G. (2011). Characteristics and modeling of evapotranspiration over a temperate desert steppe in Inner Mongolia, China. *Journal of Hydrology,* 396(1-2), pp. 139–147.

YANG, W., HUANG, D., TAN, B., STROEVE, J.C., SHABANOV, N.V., KNYAZIKHIN, Y., NEMANI, R.R. and MYNENI, R.B. (2006). Analysis of Leaf Area Index and Fraction of PAR Absorbed by Vegetation Products from the Terra MODIS Sensor: 2000-2005. *IEEE Transactions on Geoscience and Remote Sensing*, 44(7), pp. 1829–1842.

YU, D., SHI, P., SHAO, H., ZHU, W. and PAN, Y. (2009). Modelling net primary productivity of terrestrial ecosystems in East Asia based on an improved CASA ecosystem model. *International Journal of Remote Sensing,* 30(18), pp. 4851–4866.

ZHANG, Y., XIAO, X., BRASWELL, B., LINDER, E., BARET, F. and MOORE, B (2005). Estimating light absorption by chlorophyll, leaf and canopy in a deciduous broadleaf forest using MODIS data and a radiative transfer model. *Remote Sensing of Environment*, 99(3), pp. 357–371.

ZHAO, M., HEINSCH, F.A., NEMANI, R.R. and RUNNING, S.W. (2005). Improvements of the MODIS terrestrial gross and net primary production global data set. *Remote Sensing of Environment*, 95(2), pp. 164–176.

ZHAO, M., RUNNING, S.W. and NEMANI, R.R. (2006). Sensitivity of Moderate Resolution Imaging Spectroradiometer (MODIS) terrestrial primary production to the accuracy of meteorological reanalyses. *Journal of Geophysical Research,* 111, G01002, pp. 1–13, doi: 10.1029/2004JG000004.

ZHENG, Y., RIMMINGTON, G.M., XIE, Z., ZHANG, L., AN, P., ZHOU, G., LI, X., YU, Y., CHEN, L. and SHIMIZU, H. (2008). Responses to air temperature and soil moisture of growth of four dominant species on sand dunes of central Inner Mongolia. *Journal of Plant Research*, 121(5), pp. 473–482.

ZINE, S., JARLAN, L., FRISON, P.L., MOUGIN, E., HIERNAUX, P. and RUDANT, J.P. (2005). Land surface parameter monitoring with ERS scatterometer data over the Sahel: A comparison between agro-pastoral and pastoral areas. *Remote Sensing of Environment*, 96(3-4), pp. 438–452.

10 Appendices

Appendix A: Summary Tables from Literature Review

Table A-1: Overview of studies for biomass estimation in semi-arid regions using low-resolution optical data.

Study	Data used	Approach	Variables used	Information derived	Landcover	Field data	Country/ Area	Repeatability/ Portability (R/P)	Time covered	Accuracy
Tucker et al. 1985	AVHRR (LAC, GAC)	empirical regression	I-NDVI, $NDVI_{max}$	end-of-growing-season dry AGB	herbaceous biomass	herbaceous AGB, grass height, cover, species, radiometer	Sahel (Senegal)	-	5 years	I-NDVI: R^2=0.69, $NDVI_{max}$: R^2=0.64
Prince and Tucker 1986	AVHRR	empirical regression – linear	NDVI, I-NDVI	herbaceous AGB	rangeland, woodland	3 sites (12 km × 12 km) with 20 plots (200 m × 200 m), each with 30 plots (0.5 m × 0.5 m): live and dead AGB	Botswana	-	1 year	NDVI – live herbaceous biomass: 0.56
Prince 1991	AVHRR (LAC, GAC)	empirical regression – linear	I-NDVI	seasonal maximum herbaceous AGB	semi-arid annual grassland, low bush/tree cover	number of sites varied between years and countries (between 11 and 95 sites, total: 363 sites	Sahel (Senegal, Mali, Niger)	R/P: Model used for analysis of several years and sites together	7 years	Several years and sites: R^2=0.73/0.80, confidence intervals between ±65 and ±163 kg ha^{-1} (for seasonal production 0–3000 kg ha^{-1})
Diallo et al. 1991	AVHRR	empirical regression – linear, also multiple regression (herbs, trees)	I-NDVI	primary production (herbaceous and tree)	savannah	18 sites (1st year) + 11 sites (2nd year): total AGB	Sahel	R/P: Atmospheric interference inhibits retrieval of comparable I-NDVI for different years/areas	2 years	Multiple regression: year 1: R^2=0.82, year 2: R^2=0.70
Wylie et al. 1991,	AVHRR (MVC)	empirical regression –	I-NDVI	pasture production/	rangeland	ground based peak standing	Sahel, Niger	R: considerable differences in	3 years, 5 years	R^2=0.68–0.91 (Wylie *et al.* 1991), R^2=0.25–0.80

1995		linear		biomass		biomass estimates		relationship for different years		(Wylie *et al.* 1995)
Rosema 1993	METEO-SAT	simulation of vegetation development from daily total evapo-transpiration	In/out radiation etc.	herbaceous biomass development	savannah grassland	Biomass field measurements from 25 plots	Sahel	-	1 year	No good correlation to field data. Comparison to NDVI: correlation coefficient r=0.86
Hobbs 1995	AVHRR	empirical regression – linear, exponential	$NDVI_{Max}$, $NDVI_{BAMax}$, $NDVI_{Cum}$, $NDVI_{CumRat}$	herbaceous production	arid rangelands	29 sites (1 km²), each with 50 plots (1 m²): dry herbage AGB	Australia	-	1 year	Exponential curve with $NDVI_{Max}$ was best: R^2 up to 0.91
Du Plessis 1999	AVHRR	empirical regression – linear	NDVI, 10-day MVC	AGB ranges, green vegetation cover (GVC)	grassland, steppe, savannah	19 sites (2 km × 2 km): biomass, green biomass	Namibia	-	3 years	NDVI–GVC raw data: R^2=0.52, smoothed data: R^2=0.86, without outliers: R^2=0.91; MVC better for prediction of dry season biomass
Diouf and Lambin 2001	AVHRR	empirical regression – linear	I-NDVI	Herbaceous production + green leaf production	steppe, savannah	12 sites (3 km × 3 km), annual measurements	Senegal	R: strong inter-annual variations in the regression parameters. I-NDVI not robust	10 years	Separate regressions for each year: R^2=0.53–0.81, average: 0.68
Van der Meer et al. 2001	Simulated MERIS data (from (DAIS)	empirical regression – with NDVI, best: exponential	Seven vegetation indices	AGB	garrigue, maquis, mixed forest, agriculture	120 transects of 30 m length: shrub and tree AGB	France	-	-	Correlations for spectral bands: 0.32–0.44

Sannier et al. 2002	AVHRR (7 images over 2 years)	empirical regression	NDVI	biomass	grassland, steppe, savannah	11 sites, of 1 km² - transect with 20 plots	Namibia (Etosha National Park)	P: different regressions for different vegetation types suggested	2 years	High correlation for single vegetation cover (R^2=0.77, 0.89), weaker relationship for all sites together: R^2=0.61
Holm et al. 2003	AVHRR time-series, rainfall data	empirical regression – linear	I-NDVI + rainfall (also maximum NDVI and maximum - minimum NDVI)	Total phytomass	shrubland	4 sites, each sized 25 km x 25 km, 97 plots	Australia	-	2 years	I-NDVI: R^2=0.82, maximum NDVI: R^2=0.50, maximum – minimum NDVI: R^2=0.45
Kogan et al. 2004	AVHRR (GVI)	empirical comparison of biomass anomalies to VH indices	NDVI-based VCI, BT-based TCI, combination: VH Index	pasture biomass	steppe	study site: 1 ha, 60 measurements of biomass, meteorological data	Mongolia	-	13 years	Vegetation Health (VH) Index: R^2=0.66, 10% estimation error (BT = brightness temperature)
Kawamura et al. 2005	MODIS	empirical regression - exponential	NDVI (cloud-free image from 5-day MVC)	Total plant biomass	grassland	12 sites, each with 5 plots of 1 m² size	Mongolia, China	-	1 year	R^2=0.45
Mutanga and Rugege 2006	MODIS	regression + ordinary kriging (OK), cokriging (CK); stepwise linear regression	spectral bands, VIs (NDVI, SR, TVI) and principle components	herbaceous biomass	tropical savannah	463 sites, each covering 50 m × 60 m, each with 100 sub-plots	South Africa (Kruger National Park)	-	1 scene	best correlation: band 2: R^2=0.44; modelling of biomass: CK: RMSE= 830 kg ha^{-1}, OK: RMSE=1008 kg ha^{-1}, multiple regression: RMSE=1374 kg ha^{-1}
Verbesselt et al. 2006	SPOT-VGT, 10-day	empirical regression	VIs (RVI, NDVI, SAVI), single	mean herbaceous	tropical grassland,	533 sites, each with 100 plots (50	South Africa	-	5 years	Integrated VIs (rain season): R^2 up to 0.69

	compo-sites		date + integrated	biomass at the end of the rain season	tree savannah	cm × 60 cm): yearly estimates of total herba-ceous biomass	(Kruger National Park)			(best: I-RVI); single-date VIs (end of rain season): R^2 up to 0.47
Wessels et al. 2006	AVHRR	empirical regression – geometric means regression	I-NDVI	herbaceous biomass	savannah	522 sites, plots 50 m × 60 m: vegetation composition, structure, herba-ceous biomass	South Africa (Kruger National Park)	R: regression not transferable to other years, rela-tionship changed between growth seasons; P: regression better for indivi-dual sites than for landscape group	15 years	Individual sites: average R^2=0.42, landscape groups: average R^2=0.26, multiple variables (+ tree cover): average R^2=0.36, allowing different equa-tions for different years: R^2=0.5 (smoothed field data: R^2=0.56)
Baccini et al. 2008	MODIS	empirical – Random Forest regression tree model + multiple regression	7 MODIS spectral bands (459–2155 nm)	AGB	tropical forest, xeric shrubland	942 MODIS pixels used (field data ave-raged from 3 plots, total of 1440 forest inventory plots)	Tropical Africa (between ca. 13° N and 20° S)	R/P: big areas covered, with one model quite good results	4 years	Regression tree model: R^2=0.82, linear regression: R^2=0.71
Xu et al. 2008	MODIS	empirical regression – linear, power, exponential, quadratic, cubic, logarithmic	NDVI (MVC for period July–September)	grass production	grassland	2790 sample plots (1 m × 1 m) for grass and 10 m × 10 m for shrubs	China	P: individual models performed much better than national model	1 year	Best regional models: correlation coefficients: 0.62–0.78; estimation precision: regional models: ~80%, national model: 47%

Table A-2: Overview of studies for biomass estimation in semi-arid regions using medium-resolution optical data.

Study	Data used	Approach	Variables used	Information derived	Land cover	Field data	Country/ Area	Repeatability (R)/ Portability (P)	Time covered	Accuracy
Prince and Astle 1986	Landsat TM	empirical regression – linear	ratio TM7/TM5	herb biomass	open tree and shrub savannah, woodland savannah	3 sites (12 km × 12 km), with 20 plots (200 m × 200 m) with 30 plots (0.5 m × 0.5 m): live green and dead AGB	Botswana	R/P: Different regression equations for each site and each year	2 years	Variation accounted for by the regression models: (i) with site factor: ~76%, (ii) multi-temporal without site factor: ~70%, (iii) predictive equations: maximum 84%
Franklin and Hiernaux 1991	Landsat TM	radiative transfer (Li-Strahler canopy reflectance model) + allometric equations	average crown area, tree density	foliage and above-ground woody biomass	wooded grassland, woodland	20 field sites	Sahel + Sudan	P: assumptions of Li-Strahler model (stand characteristics) need to be calibrated at each site	2 years	Results compared favourably to field measurements and literature
Anderson et al. 1993	Landsat TM	empirical – univariate regression, 3 approaches	NIR-red difference, NIR/red ratio, NDVI	above-ground biomass	rangeland	study site of 42 km² with 240 sample plots	Colorado, USA	R: greenness strata approach applicable for three periods, the other two approaches not so stable	3 years	Sample point: R^2= 0.16; Spectral class: R^2=0.96 (significant for one period); Greenness strata: R^2=0.71–0.95 (significant for all periods)
Pereira et al. 1995	Landsat TM	empirical regression – linear was best	NDVI	biomass	shrubland	12 sampling sites (120 m × 120 m or 90 m × 90 m), each with 6 line transects with 36 plots	Portugal	P: equation only valid for shrubland, not for other land cover types	1 scene	R^2=0.76
Todd et al. 1998	Landsat TM	empirical regression –	NDVI, GVI, BI, WI, red band	AGB	semi-arid shortgrass	12 sites (6 grazed, 6 ungrazed), size	Colorado, USA	-	1 scene	Grazed sites: R^2= 0.62–0.67, ungrazed sites:

		linear			steppe	90 m × 90 m, each with 15 clippings of 0.25 m²				R^2=0.35, all sites + grazing info: R^2=0.7 (red)
Moleele et al. 2001	Landsat TM	empirical regression – linear	greenness, brightness, NDVI, PVI, TM5/TM7, TM5+TM7, TM5-TM7 (best)	green AGB: grass + 3 browse layer	hardveld, sandveld, recent alluvium	Grass biomass: 0.5 m quadrats, green browse (woody) biomass: 112.5 m² plots	Botswana	-	2 years	Best correlation (TM5-TM7): browse layer: 0.47–0.72, total AGB: 0.6, grass: not good, predictive equation: total AGB: 0.36
Qi and Wallace 2002	Landsat ETM+	empirical – multivariate regression	fractional cover + NDSVI + canopy height (from NIR)	biomass	grass dominated arid rangeland	10 study sites	South-eastern Arizona, USA	-	1 scene	R^2=0.93
Wylie et al. 2002	Landsat TM, field radio-meter	empirical – (1) field data + radiometer: plot estimate, (2) quadratic regression: plot–Landsat	NDVI	grassland biomass	grassland	step (1): 54 biomass measurements (unburned, ungrazed); step (2): 64 biomass measurements	Great Plains, USA	P: Model applied over large area	1 year	(1): R^2=0.85, (2): R^2=0.92
Calvão and Palmeirim 2004	Landsat TM	empirical regression – least-squares linear regression	Spectral bands, NDVI	total living, woody, total, litter biomass	shrubland	19 sampling sites (end of the dry season)	Portugal	-	1 scene	Leaf biomass: R^2= 0.53 (TM7), R^2=0.59 (NDVI); Woody biomass: R^2 >0.92 (TM7, TM5, TM3); Total biomass: R^2=0.88 (TM7, TM2, TM3); Total living biomass: R^2>0.90 (TM7, TM3)

Samimi and Kraus 2004	Landsat	empirical regression – nonlinear	134 indices (from Landsat DNs, radiance, and reflectance)	grass / foliage / woody / total AGB	savannah	4 study areas, total of 74 test sites	South Africa, Zimbabwe	P: Extension of the model to an additional region improved the coefficients of determination	1 scene for each site	High correlation of several indices to grass (R^2 up to 0.85) and foliage biomass (R^2 up to 0.84); no significant correlation for woody and total AGB
Suganuma et al. 2006	-	-	SBA, CC, LAI	woodland biomass	open woodland	35 plots: tree biomass	Australia	-	1 year	SBA: R^2>0.99, CC: R^2>0.94, LAI: R^2>0.92
Aranha et al. 2008	Landsat TM	empirical regression – stepwise	NDVI	shrubs and young pine trees AGB	shrubland, young pine trees	400 plots of each 200 m²	Portugal	-	1 scene	Shrub biomass: R^2=0.36, pine tree biomass: R^2=0.24

Table A-3: Overview of studies for biomass estimation in semi-arid regions using high-resolution optical data (spaceborne and airborne).

Study	Data used	Approach	Variables used	Information derived	Landcover	Field data	Country/ Area	Repeatability	Time covered	Accuracy
Dancy et al. 1986	True colour aerial photography	empirical regression – exponential	RGB bands → percentage ground cover	grass/bush biomass	rangelands	none; reference – visual estimation of biomass from aerial imagery	Botswana	-	2 years	R^2=0.72
Thenkabail et al. 2004	IKONOS (four images, wet and dry season)	empirical regression – linear and non-linear	Different bands and indices	oil palm biomass	savannah, oil palm plantation	285 field plots (16 m × 16 m) from 2 study sites: tree height, age, DBH, stem height	West Africa	-	1 year	Best model exponential: R^2 up to 0.73; predictive power of models: 64-72%
Addink et al. 2007	HyMap (5m)	empirical Ridge regression, Lasso	Spectral ranges: 0.4–0.75 µm (13 bands), 1.1–1.45 µm (6 bands),	AGB	herbs, dense bushes	216 plots of each 5 m × 5 m	France	-	1 scene	R^2=0.47; results of band selection are not discussed

		regression	1.6–1.8 µm (3 bands)							
Beeri et al. 2007	HyMap (7.6–8.7m)	empirical regression – linear	bNDVI, nNDVI, $CR_{B991–B1306}$	PV and NPV biomass	Moderately grazed pastures, mixed-grass prairie	8 plots (10 m × 10 m), for each two strips of 1 m × 10 m clipped	USA	-	1 day	Total biomass: 18% error (CR), NDVI tended to overestimate biomass
Ozdemir 2008	Quickbird	empirical regression – linear, multi-variate	Tree attributes: crown area, shadow area	stem volume	semi-arid open forest	Study area (25 km²), 61 plots: DBH, tree height – stem volume derived using stem volume table	Turkey	-	1 scene	Shadow area: R^2 up to 0.67; crown area: R^2 up to 0.51; Multivariate regression: R^2=0.67
Cho and Skidmore 2009	HyMap (4m)	empirical regression	VIs (e.g. NDVIs, MSAVI, SARVI, NDVI), red-edge positions	grass/herb biomass production	grass/herbs	Mediterranean mountain ecosystem	Italy (Majella National Park)	predictive capability for the other year was weak	2 years	VIs: high correlation only for a single year, R^2 up to 0.58; red-edge and linear extrapolation: more robust, R^2=0.62
Nijland et al. 2009	HyMap (5m)	empirical regression model – (ridge regression)	Spectral bands	AGB	Mediterranean forest, dense shrubs, herbs and shrubs	227 field plots	Southern France	-	1 scene	Use of optimal pixel size (95m/65m) resulted in error reduction of 17%

Table A-4: Overview of studies for biomass estimation in semi-arid regions using SAR data.

Study	Data used	Approach	Variables used	Information derived	Landcover	Field data	Country/ Area	Repeatability/ Portability (R/P)	Time covered	Accuracy
Frison et al. 1998	ERS-WSC	ecosystem model + backscatter model – inversion	10-day back-scattering coefficient	total herbaceous AGB	herbaceous vegetation	50 km × 50 km study region with 4 sites, each 1 km²	Sahel, Mali	-	4 years	Error of biomass estimation ~33%
Frison et al. 2000	SSM/I, ERS-WSC	ecosystem model + backscatter model – inversion	10-day back-scattering coefficient	herbaceous AGB	herbaceous vegetation	4 sites (25 km × 25 km), average AGB from several 1 km² plots	Sahel, Mali	-	3 years	Error of biomass estimation ~58%
Svoray et al. 2001	ERS-2 (from 3 seasons)	empirical regression – linear	backscatter	AGB, green leaf biomass (GVD)	forest, shrubs, dwarf shrubs, herbaceous vegetation	Field data + literature	Israel	-	1 year	C-Band backscatter better related to GVD: R^2=0.85
Santos et al. 2002	JERS-1	empirical regres-sion – sigmoid and logarithmic	radar backscatter	AGB	forest-savannah contact zone	68 field plots	Brazil	P: method can not be applied to other transition zones	2 scenes	Logarithmic/sigmoid function: R^2= 0.66/0.68
Jarlan et al. 2003	ERS scattero meter	water balance model, radiative transfer model	backscatter + rainfall data	herbaceous biomass	annual grass layer and sparse woody layer	4 sites (25 km × 25 km): standing her-baceous biomass, vegetation cover	Sahel, Burkina Faso, Mali	P: model used for 350 000 km² region	10 years	R^2=0.92 (absolute mean error of 130 kg ha^{-1} dry mass), consis-tency check with NDVI data: R^2=0.71
Cronin 2004	AIRSAR (L/P-band)	empirical regression – non-linear + radar backscatter model	backscatter	total, branch, trunk, leaf and small branch AGB	semi-arid woodland	34 sites with 50 m × 50 m plots: tree height, DBH, species + allometric equations	Australia	-	1 year	Empirical HV: total biomass (R^2 0.18–0.61), P-HV: R^2= 0.61, L-HV: R^2=0.57, All others R^2 <0.41; for branch biomass best: 0.45
Collins et al. 2009	AIRSAR (L/P-	empirical regression - linear	backscatter	AGB	open-forest savannah	30 plots, size of 30 m × 30 m or 50 m ×	Australia	-	1 day	Strongest: L-HV: R^2=0.92

	band)					50 m				
Mitchard et al. 2009	ALOS PALSAR (12.5m, HH/HV)	empirical regression	backscatter	woody biomass (stems ≥10cm)	tropical forest – savannah transition, woodland	253 field plots	Cameroon, Uganda, Mozambique	P: consistency tested by applying other site's regressions: RMSE increased by 12-30% and remained low for AGB<150 Mg/ha	1 year	Individual regressions: best L-HV: R^2=0.61-0.76; using all data together: R^2=0.73 (for HV), R^2=0.56 (for HH), but less consistent

Table A-5: Overview of studies for biomass estimation in semi-arid regions using a combination of optical and radar data or modelling approaches.

Study	Data used	Approach	Variables used	Derived information	Landcover	Field data	Country/ Area	Repeatability/ Portability (R/P)	Time covered	Accuracy
Mougin et al. 1995, Lo Seen et al. 1995	AVHRR-GAC	ecosystem model (STEP) + canopy and soil reflectance models	VIs (NDVI, GEMI, SAVI, SR)	simulation of NDVI, AGB	semi-arid grassland	2 validation areas, standing AGB measured over 10 years	Sahel region	-	16 years	Model prediction vs. field data: r>0.9 (Mougin et al. 1995)
Nouvellon et al. 2001	Landsat TM, ETM+	ecosystem model	NDVI	simulation of carbon budgets	semi-arid grassland	field measurements of biomass	Arizona, USA	-	10 years	RMSE of 8.8 g dry mass m^{-2}
Svoray and Shoshany 2002, 2003	ERS-2, Landsat TM	water-cloud-model (WCM) + fractional cover; empirical relationship	backscatter + Landsat fractional cover	herbaceous AGB	herbaceous vegetation	57 plots of each 0.3 ha (33 natural herbaceous vegetation, 24 wheat and barley)	Israel	-	1 year	regression with ERS: R^2=0.66, WCM: ERS alone: R^2=0.84, with fractional cover: R^2=0.91
Feng et al. 2005	-	empirical – logarithmic	LAI	grassland AGB	semi-arid grassland	study site (1 km^2) with 5 plots (1 m^2): monthly LAI and AGB	Inner Mongolia	-	1 year	Mean relative error: 8.15%
Jarlan et al. 2008	SPOT-VGT	STEP model + radiative transfer model	NDVI	AGB	rangeland: herbaceous layer, sparse woody plants	13 sites (1 km^2), total of 126 points	Mali (Sahel)	R: applied over several years	5 years	R^2=0.78
Mangiarotti et al. 2008	ENVISAT-ASAR (WSM), SPOT-VGT	STEP model + radiative transfer and backscatter models (soil, vegetation)	backscatter, NDVI	green AGB	rangeland: herbaceous layer, sparse woody plants	test site (1 km^2) with 12 field plots (1 m^2): time-series of field data: AGB and LAI	Mali (Sahel)	-	1 year	good for growing period, but too high for sensecence period (error: 140–300 kg ha^{-1})
Chen et al. 2009	Landsat ETM+, JERS-1	empirical, multiple regression (linear model)	spectral bands + VIs + JERS-1 backscatter	biomass of shrub, grass, sparse woodland, mixed	low to high shrubs, grass, sparse woodland, rock, lichen	two sites (one for model development, one for validation and transferability test	Canada	P: transfer to second study site: good results ([3], [4])	1 year	[1] R^2=0.72, MedAPE=53%; [2] R^2=0.78, MedAPE=33%; [3] R^2=0.81 [4] R^2=0.59

Appendix B: Map of Vegetation Communities for the Study Areas

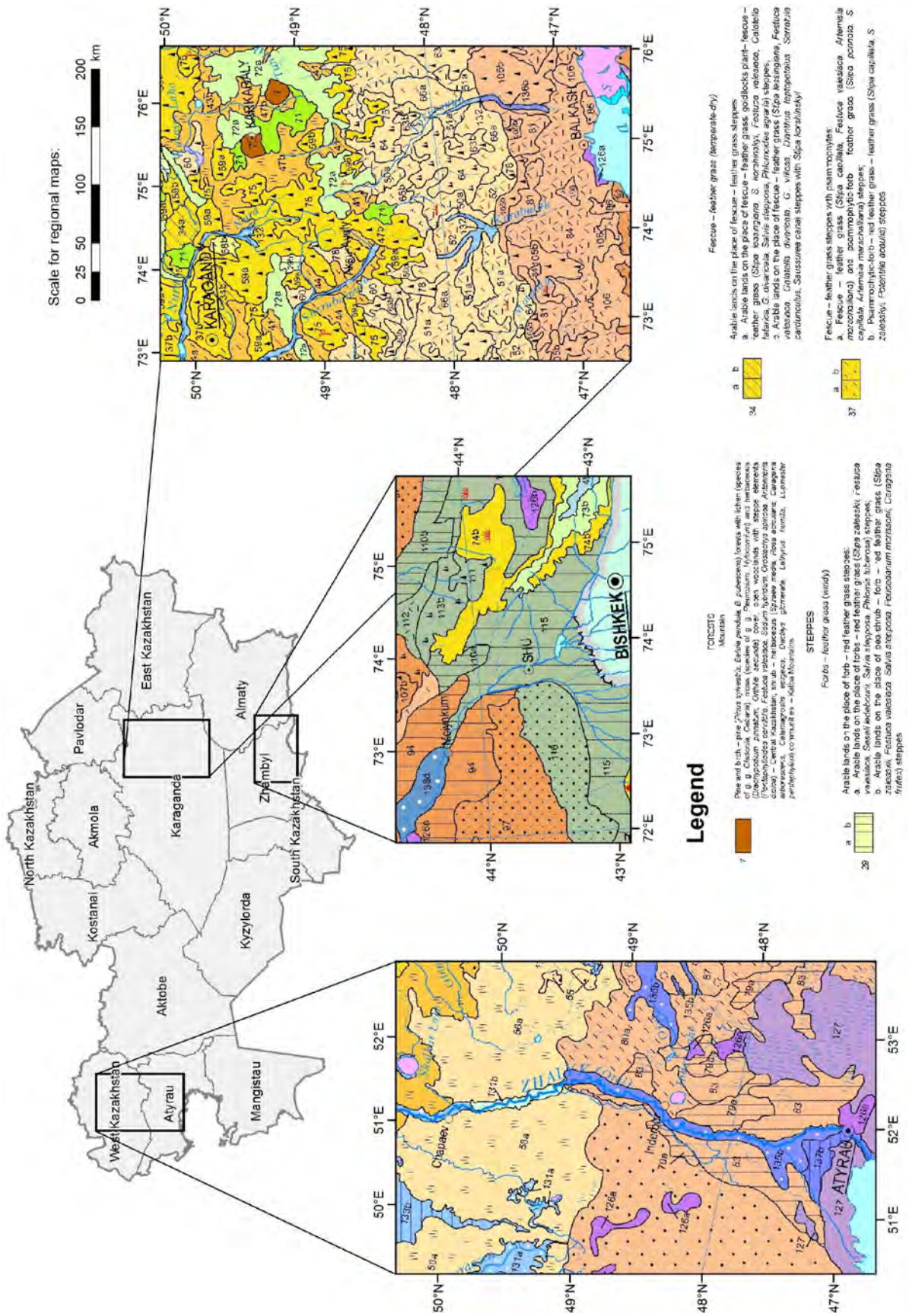

Figure B-1: Map showing the distribution of vegetation communities (Source: Volkova et al. 2010).

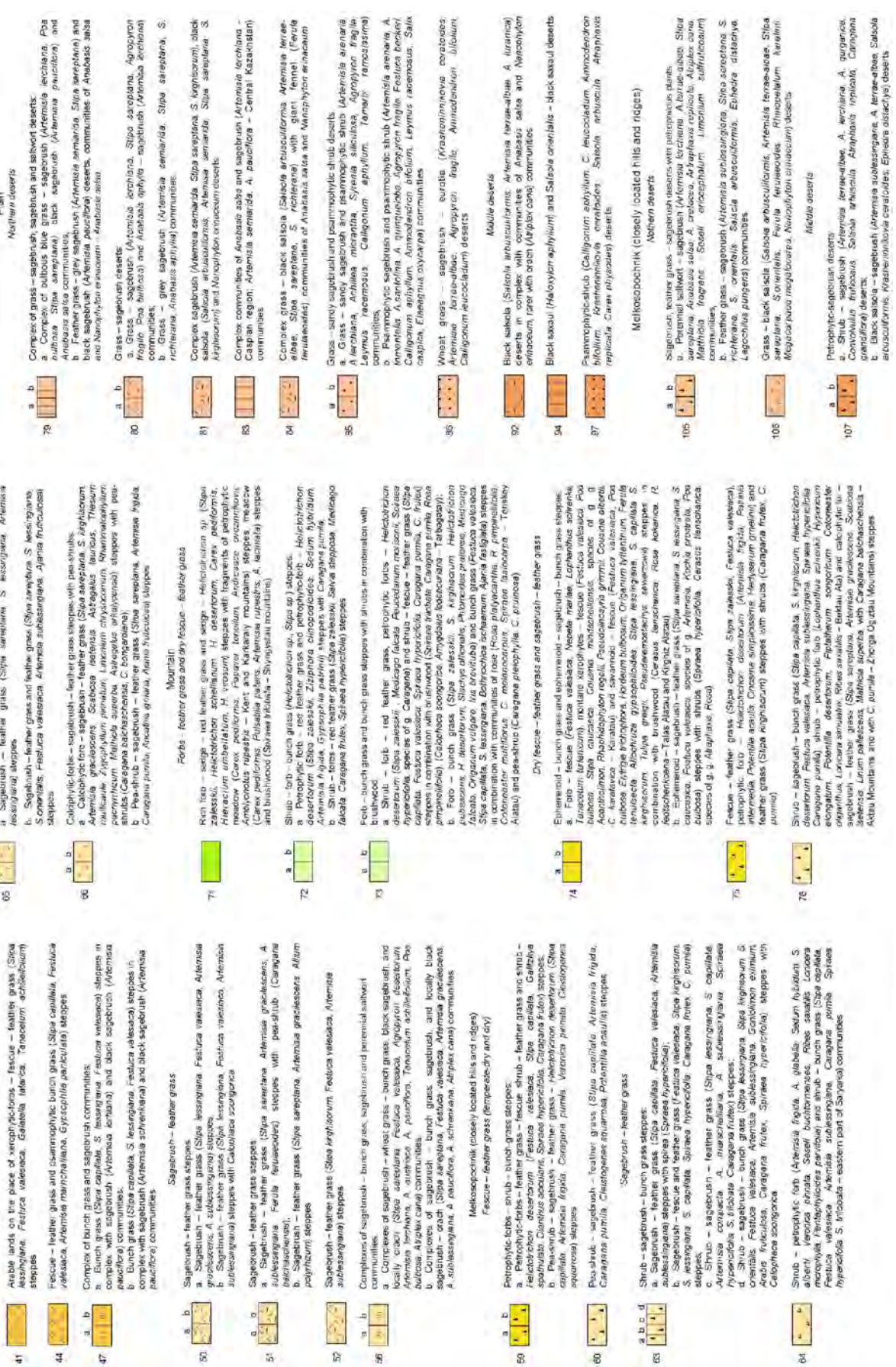

Figure B-1 (continued): Map showing the distribution of vegetation communities (Source: Volkova et al. 2010).

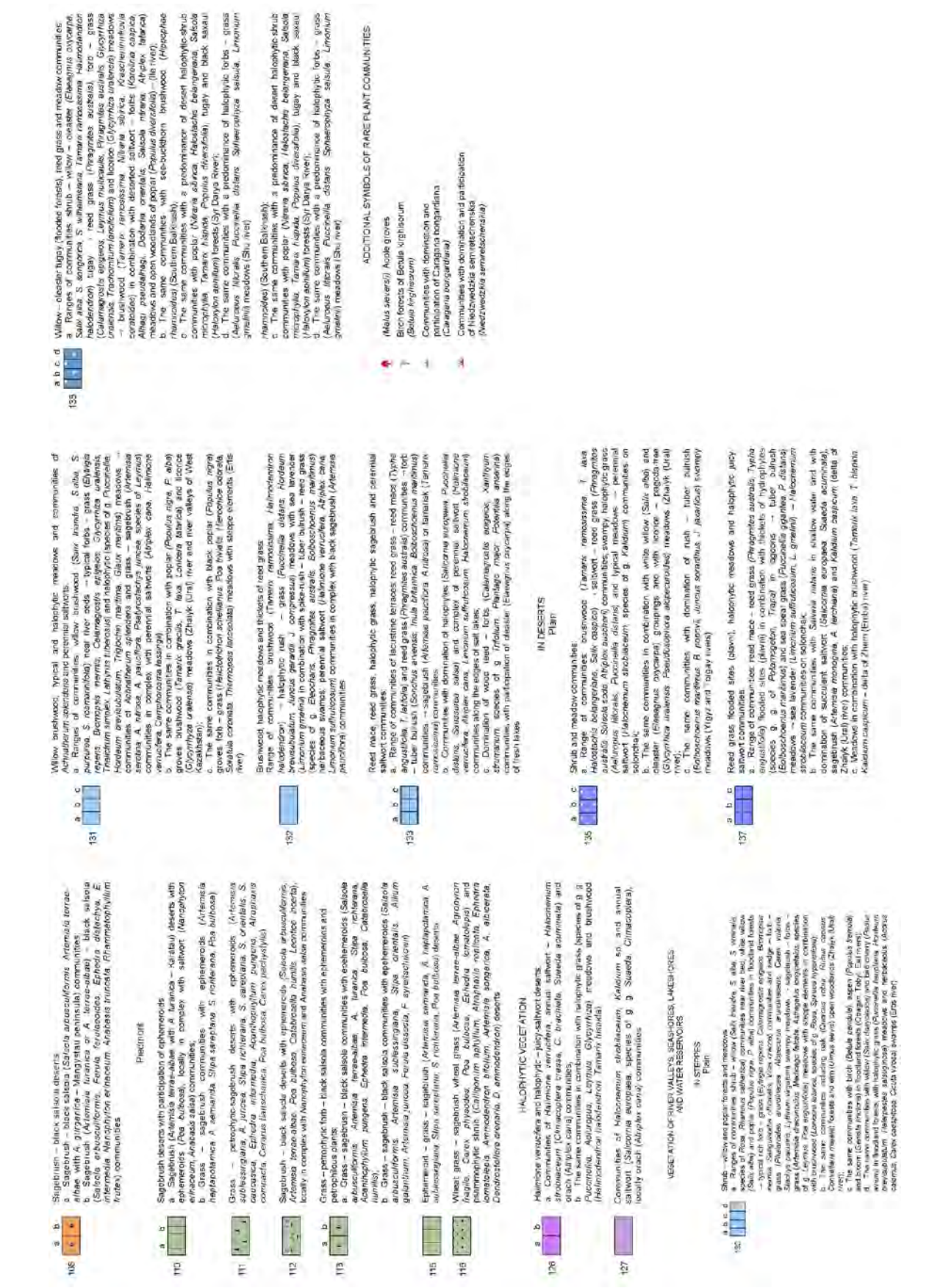

Figure B-1 (continued): Map showing the distribution of vegetation communities (Source: Volkova et al. 2010).

Appendix C: Test Site Tables

Table C-1: Test sites in study area Central Kazakhstan – geographic location, land cover class from the Central Asia land cover and land use map (Klein et al. 2012), and vegetation type number, vegetation communities, and main species from Volkova et al. (2010).

No.	Centre LAT [°]	Centre LON [°]	Land cover class	Veg. type no.	Vegetation communities	Main species
1	46.8108	74.7706	Sparse vegetation	126a	Communities of *Halimione verrucifera*, annual saltwort – *Halocnemum strobilaceum* and orach communities	*Halimione verrucifera, Halocnemum strobilaceum (Climacoptera crassa, C. brachiata, Suaeda acuminata), Atriplex cana*
2	46.8511	74.7563	Open shrubland	84	Complex grass – black salsola with giant fennel; communities of *Anabasis salsa* and *Nanophyton erinaceum*	*Salsola arbusculiformis, Artemisia terraealbae, Stipa sareptana, Stipa richterana, Ferula ferulaeoides, Anabasis salsa, Nanophyton erinaceum*
3	46.8743	74.8189	Open shrubland	84	[See No. 2]	[See No. 2]
4	47.9855	73.9753	Grassland	52	Sagebrush – feather grass steppes	*Stipa kirghisorum, Festuca valesiaca, Artemisia sublessingiana*
5	47.9753	73.8872	Grassland	52	[See No. 4]	[See No. 4]
6	48.0408	73.9332	Grassland	52	[See No. 4]	[See No. 4]
7	48.0902	73.8777	Grassland	66a	Calciphytic forbs – sagebrush – feather grass steppes with pea shrubs	*Stipa sareptana, Stipa kirghisorum Artemisia gracilescens, Scabiosa isetensis, Astragalus tauricus, Thesium multicaule, Zygophyllum pinnatum, Limonium chrysocomum, Rhammatophyllum pacnyrrhizum, Mathiola superba, Astragalus arkalycensis, Caragana balchaschensis, Caragana bongardiana*
8	48.8280	73.7285	Grassland	44	Fescue – feather grass and psammophytic bunch grass steppes	*Stipa cavillata, Festuca valesiaca, Artemisia marhchalliana, Gypsophila paniculata*
9	49.2243	73.3531	Grassland	72a	Petrophytic forb – red feather grass and petrophytic-forb – *Helictotrichon desertorum* steppes *with Caragana pumila*	*Helictotrichon desertorum, Stipa zalesskii, Ziziphora clinopodioides, Sedum hybridum, Artemisia frigida, Gypsophila patrinii, Caragana pumila*
10	48.9932	73.4470	Sparse vegetation	44	[See No. 8]	[See No. 8]
11	48.9857	73.4870	Grassland	44	[See No. 8]	[See No. 8]

Table C-2: Test sites in study area South Kazakhstan – geographic location, land cover class from the Central Asia land cover and land use map (Klein et al. 2012), and vegetation type number, vegetation communities, and main species from Volkova et al. (2010).

No.	Centre LAT [°]	Centre LON [°]	Land cover at pixel	Veg. type no.	Vegetation communities	Main species
12	43.7613	73.5492	Sparse vegetation	94	Black saxaul and *Salsola orientalis* – black saxaul deserts	*Haloxylon aphyllum, Salsola orientalis*
13	43.8756	73.3916	Sparse vegetation	97	Psammophytic-shrub deserts	*Calligonum aphyllum, Calligonum leucocladum, Ammodendron bifolium, Krasheninnikovia ceratoides, Salsola arbuscula Atraphaxis replicate, Carex physodes*
14	43.3793	73.5887	Sparse vegetation	115	Ephemeroid – grass – sagebrush deserts	*Artemisia semiarida, Artemisia heptapotamica, Artemisia sublessingiana, Stipa sareptana, Stipa richterana, Poa bulbosa*
15	43.8708	74.0607	Sparse vegetation	115	[See No. 14]	[See No. 14]
16	43.9061	74.0372	Sparse vegetation	110a	Sagebrush deserts with ephemeroids, locally in complex with saltwort communities	*Artemisia terrae-albae, Poa bulbosa, Nanophyton erinaceum, Anabasis salsa*
17	44.2438	73.2393	Sparse vegetation	115	[See No. 14]	[See No. 14]
18	44.3282	72.9091	Grassland	138d	Willow – oleaster tugay, reed grass and meadow communities with a predominance of halophytic forbs – grass meadows	*Aeluropus littoralis, Puccinellia distans, Sphaerophyza salsula, Limonium gmelinii*
19	43.5418	73.7198	Sparse vegetation	115	[See No. 14]	[See No. 14]
20	43.2069	74.7444	Irrigated agriculture	115	[See No. 14]	[See No. 14]

Table C-3: Test sites in study area West Kazakhstan – geographic location, land cover class from the Central Asia land cover and land use map (Klein et al. 2012), and vegetation type number, vegetation communities, and main species from Volkova et al. (2010).

No.	Centre LAT [°]	Centre LON [°]	Land cover at pixel	Veg. type no.	Vegetation communities	Main species
21	48.5338	51.8584	Sparse vegetation	80a	Grass – sagebrush and *Anabasis aphylla* – sagebrush communities	*Artemisia lerchiana, Stipa sareptana, Agropyron fragile, Poa bulbosa, Anabasis aphylla*
22	48.5658	51.9724	Sparse vegetation	80a	[See No. 21]	[See No. 21]
23	48.3565	51.9266	Grassland	80a	[See No. 21]	[See No. 21]
24	50.1875	51.0561	Open shrubland	56a	Complexes of sagebrush – wheat grass – bunch grass, black sagebrush, and locally orach communities	*Stipa sareptana, Festuca valesiaca, Agropyron desertorum, Artemisia lerchiana, Artemisia austriaca, Artemisia pauciflora, Tanacetum achilleifolium, Poa bulbosa, Atriplex cana*
25	50.1985	50.9178	Rain-fed agriculture	56a	[See No. 24]	[See No. 24]
26	49.7407	51.2757	Grassland	56a	[See No. 24]	[See No. 24]
27	49.5338	51.4651	Sparse vegetation	56a	[See No. 24]	[See No. 24]
28	48.7080	51.4606	Sparse vegetation	85a	Grass – sandy sagebrush and psammophytic shrub communities	*Artemisia arenaria, Artemisia lerchiana, Achillea micrantha, Syrenia siliculosa, Agropyron fragile, Leymus racemosus, Calligonum aphyllum, Tamarix ramosissima*
29	47.9654	51.5524	Sparse vegetation	83	Complex communities of *Anabasis salsa* and sagebrush communities	*Anabasis salsa, Artemisia lerchiana*
30	47.5695	51.5905	Sparse vegetation	135b	Shrub and meadow communities in combination with white willow and oleaster groupings and with licorice – pagoda-tree meadows	*Tamarix ramosissima, Tamarix laxa, Halostachis belangeriana, Salix caspica, Phragmites australis, Salsola soda, Atriplex auscherii, Halocneum strobilaceum, Salix alba, Elaeagnus oxycarpa, Glycyrrhiza uralensis, Pseudosophora alopecuroides*

Appendix D: Foto Tables for Test Sites

June 2011: Test site 1, Study area Central Kazakhstan, LAT / LON: 46.8108° / 74.7706°

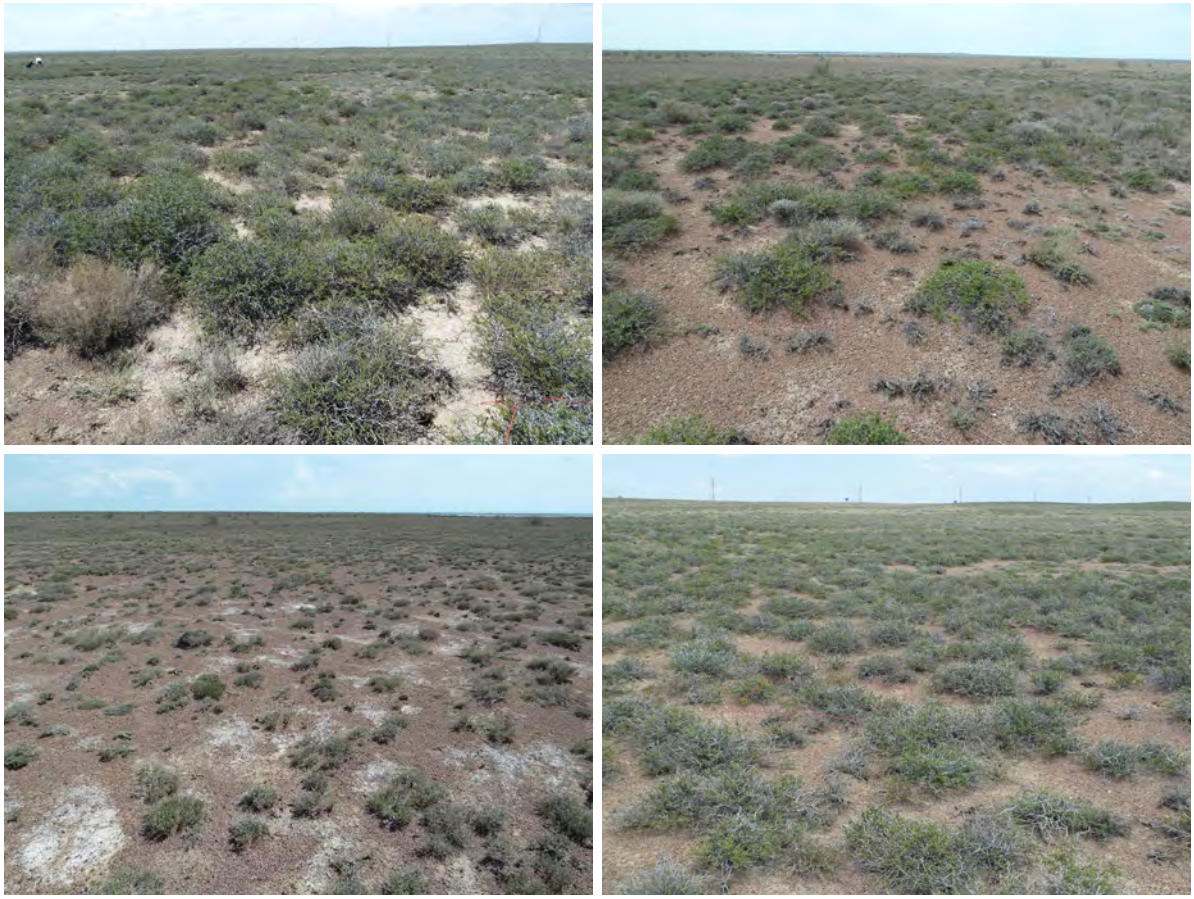

June 2011: Test site 2, Study area Central Kazakhstan, LAT / LON: 46.8511° / 74.7563°

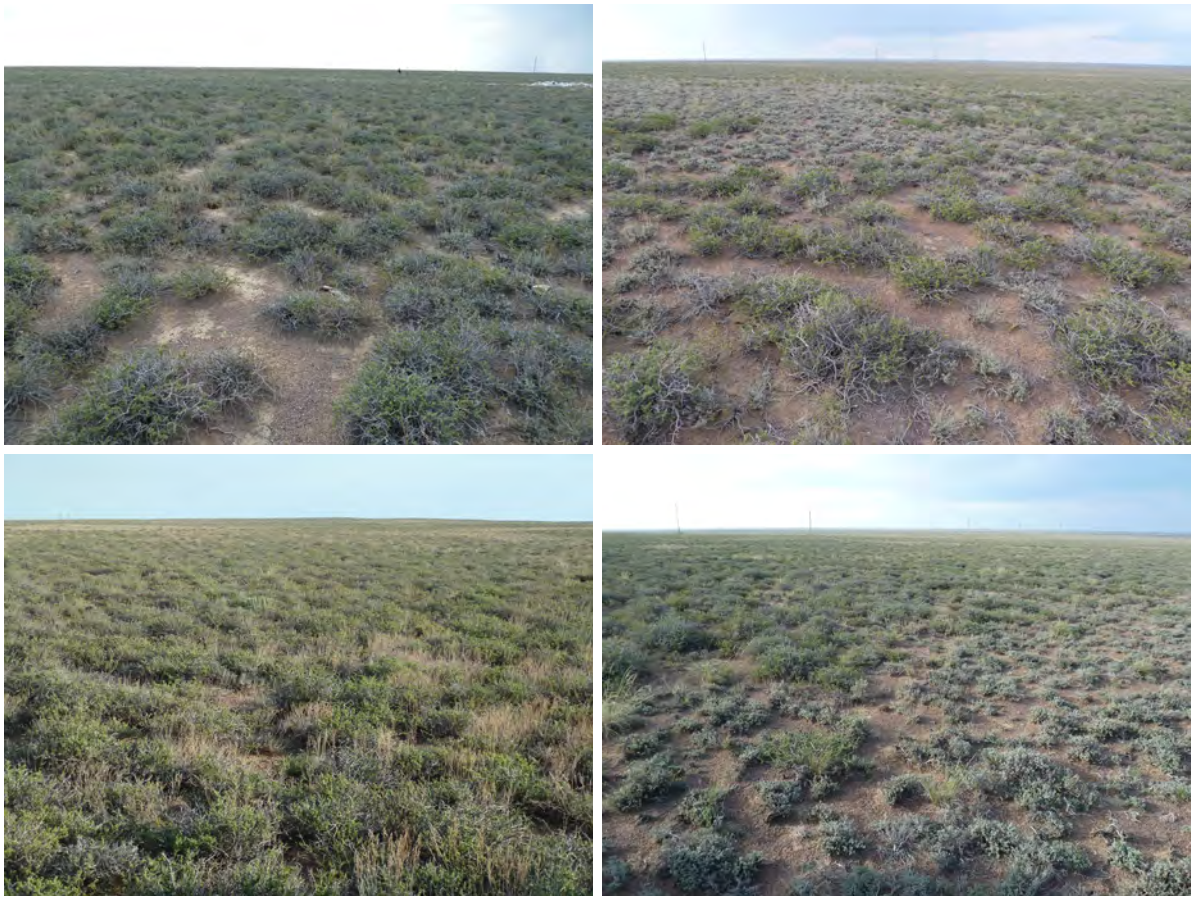

June 2011: Test site 3, Study area Central Kazakhstan, LAT / LON: 46.8743° / 74.8189°

June 2011: Test site 4, Study area Central Kazakhstan, LAT / LON: 47.9855° / 73.9753°

June 2011: Test site 5, Study area Central Kazakhstan, LAT / LON: 47.9753° / 73.8872°

June 2011: Test site 6, Study area Central Kazakhstan, LAT / LON: 48.0408° / 73.9332°

June 2011: Test site 7, Study area Central Kazakhstan, LAT / LON: 48.0902° / 73.8777°

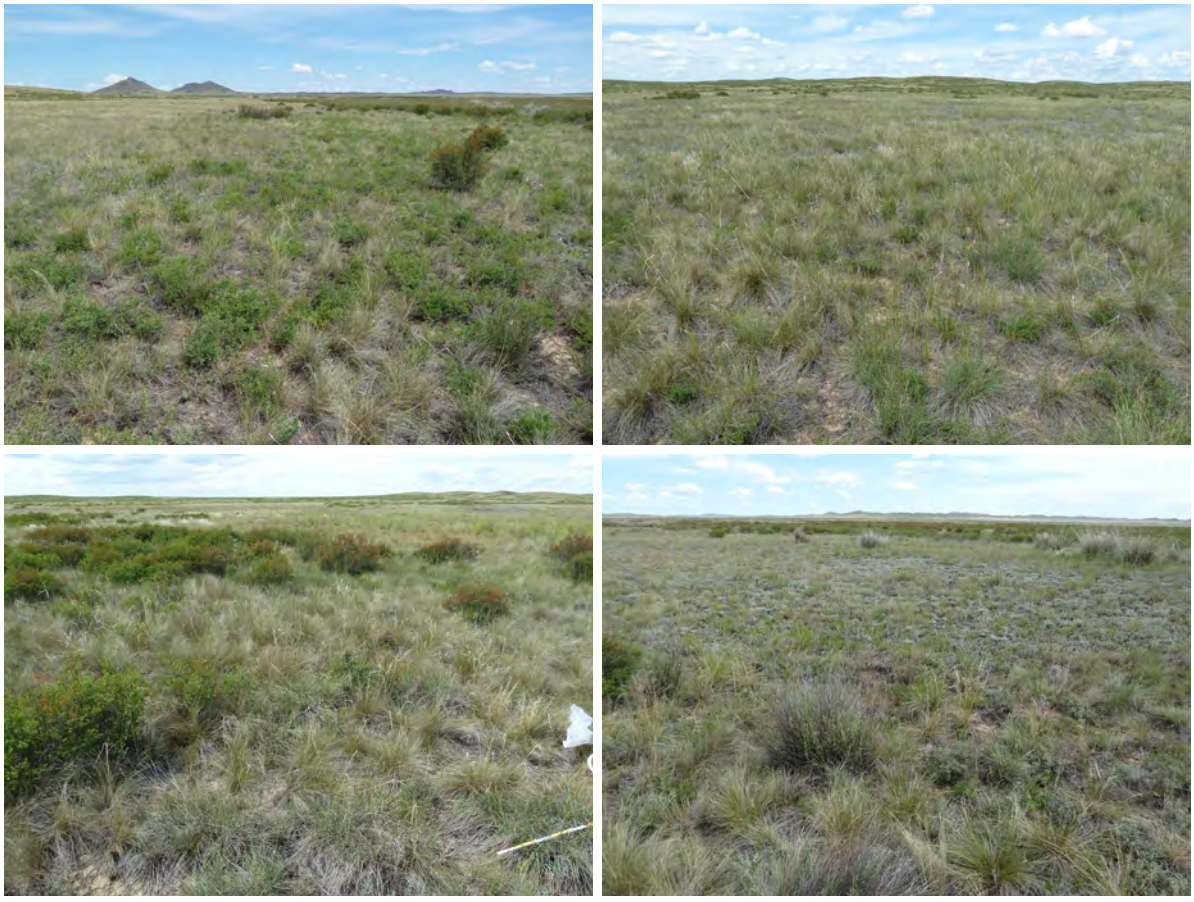

June 2011: Test site 8, Study area Central Kazakhstan, LAT / LON: 48.8280° / 73.7285°

June 2011: Test site 9, Study area Central Kazakhstan, LAT / LON: 49.2243° / 73.3531°

June 2011: Test site 10, Study area Central Kazakhstan, LAT / LON: 48.9932° / 73.4470°

June 2011: Test site 11, Study area Central Kazakhstan, LAT / LON: 48.9857° / 73.4870°

June 2011: Test site 12, Study area South Kazakhstan, LAT / LON: 43.7613° / 73.5492°

June 2011: Test site 13, Study area South Kazakhstan, LAT / LON: 43.8756° / 73.3916°

June 2011: Test site 14, Study area South Kazakhstan, LAT / LON: 43.3793° / 73.5887°

June 2011: Test site 15, Study area South Kazakhstan, LAT / LON: 43.8708° / 74.0607°

June 2011: Test site 16, Study area South Kazakhstan, LAT / LON: 43.9061° / 74.0372°

June 2011: Test site 17, Study area South Kazakhstan, LAT / LON: 44.2438° / 73.2393°

June 2011: Test site 18, Study area South Kazakhstan, LAT / LON: 44.3282° / 72.9091°




June 2011: Test site 19, Study area South Kazakhstan, LAT / LON: 43.5418° / 73.7198°



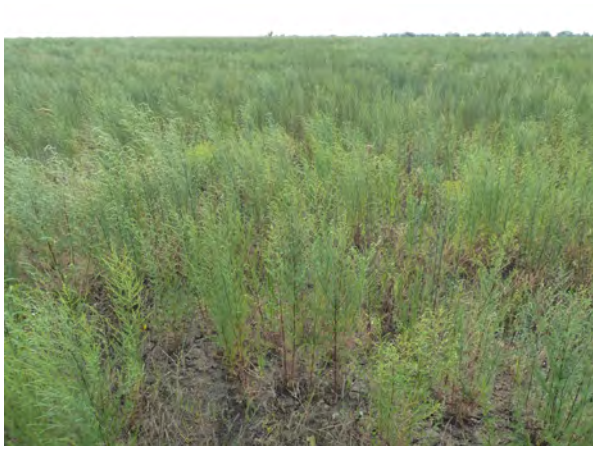


June 2011: Test site 20, Study area South Kazakhstan, LAT / LON: 43.2069° / 74.7444°

June 2011: Test site 21, Study area West Kazakhstan, LAT / LON: 48.5338° / 51.8584°

June 2011: Test site 22, Study area West Kazakhstan, LAT / LON: 48.5658° / 51.9724°

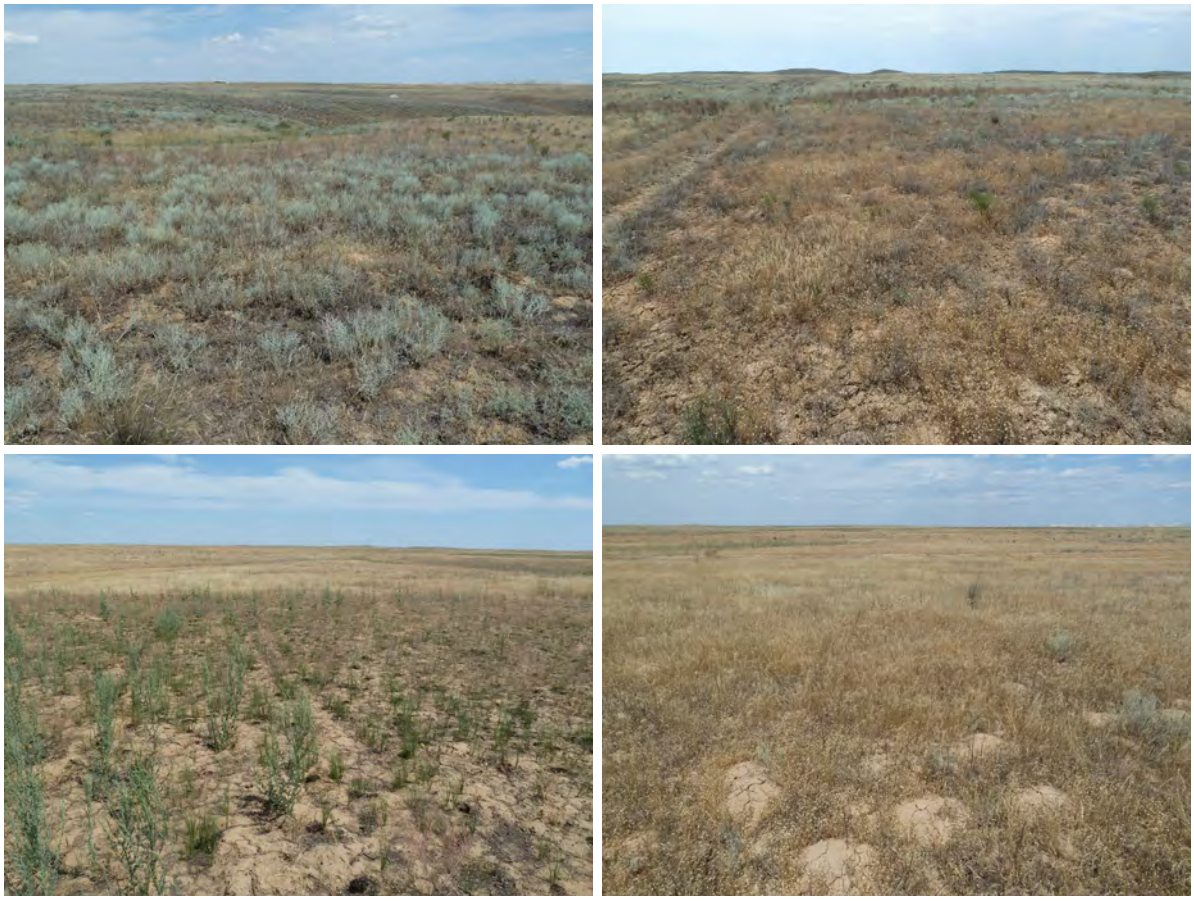

June 2011: Test site 23, Study area West Kazakhstan, LAT / LON: 48.3565° / 51.9266°

June 2011: Test site 24, Study area West Kazakhstan, LAT / LON: 50.1875° / 51.0561°

June 2011: Test site 25, Study area West Kazakhstan, LAT / LON: 50.1985° / 50.9178°

June 2011: Test site 26, Study area West Kazakhstan, LAT / LON: 49.7407° / 51.2757°

June 2011: Test site 27, Study area West Kazakhstan, LAT / LON: 49.5338° / 51.4651°

June 2011: Test site 28, Study area West Kazakhstan, LAT / LON: 48.7080° / 51.4606°

June 2011: Test site 29, Study area West Kazakhstan, LAT / LON: 47.9654° / 51.5524°

June 2011: Test site 30, Study area West Kazakhstan, LAT / LON: 47.5695° / 51.5905°

Appendix E: Field Protocols

Field protocol – Biomass Sub-Plots (Version: 19.10.2010)

Field site No. B-	**Sub plot No.** B-	**Biomass class** O low O medium O high	**Date**	**GPS-Point No.**
Coordinates	Lat (N)	Lon (E)		

Surface coverage (Sub-Plot size: **1m²**)							
green medium dry	O Bare Soil	O Litter	O Grass O Herbs O Shrubs O gr O me O dr	O Grass O Herbs O Shrubs O gr O me O dr	O Grass O Herbs O Shrubs O gr O me O dr	O Herbs O Shrubs O Trees O gr O me O dr	O Shrubs O Trees O O gr O me O dr
Height [cm]	---	---	O 3-15 O 15-30 O 30-50 O 50-80 O 80-120	O 3-15 O 15-30 O 30-50 O 50-80 O 80-120	O 3-15 O 15-30 O 30-50 O 50-80 O 80-120	O 15-30 O 30-50 O 50-80 O 80-120 O 120-200 O >200: _____	O 15-30 O 30-50 O 50-80 O 80-120 O 120-200 O >200: _____
Cover [%]							

Soil and surface description			
Soil Moisture	O dry O moist O very moist	Snow cover	O none O powder snow cover O snow height < 5 cm O snow height 5 – 40 cm O snow height > 40 cm
Topography (Slope /Terrain)	O flat: 0 - 7 % O gentle slope: 8 - 13 % O moderate slope / undulating - rolling: 14 - 20 %		O steep slope / rolling - hilly: 21 - 55 % O very steep / steeply dissected hilly - mountainous: 56 -140 %

Photographs							
Photo	**Photo No.**	Photo	**Photo No.**	Photo	**Photo No.**	Photo	**Photo No.**
GPS		Plot side 1		→ N		→ S	
Plot nadir		Plot side 2		→ E		→ W	

Biomass measurements **subtract weight of bag [g]:**

Sample No.: <Sub-plot-No> + <running No>

Sample No. (mark also the bag !!!)	Content	Condition	**Fresh weight [g] - NETTO -**	**Dry weight [g] - NETTO -**
B-	Grass / herbs	green		
B-	Grass / herbs	dry		
B-	Shrubs	stems/branches – live		
B-	Shrubs	stems/branches – dead		
B-	Shrubs	leaves – live		
B-	Shrubs	leaves – dead		
B-	Litter	---		

Field protocol – Biomass Transects (Version: 19.10.2010)

Field site No. B-		GPS-Track No.		Date
Start	Lat (S)	Lon (E)	GPS No.	No. of Photos (GPS, N, E, S, W, Transect)
End	Lat (S)	Lon (E)	GPS No.	No. of Photos (GPS, N, E, S, W, Transect)

Comments	
(please indicate No. of point if local observation)	

Distance between Observations: 1m (→ No. = Distance from Start Point)

Biomass classes: 0 - bare, 1 - low, 2 - medium, 3 - high

No.	Class	No.	Class	No.	Class	No.	Class	No.	Class	No.	Class	No.	Class	No.	Class
0		30		60		90		120		150		180		210		240	
1		31		61		91		121		151		181		211		241	
2		32		62		92		122		152		182		212		242	
3		33		63		93		123		153		183		213		243	
4		34		64		94		124		154		184		214		244	
5		35		65		95		125		155		185		215		245	
6		36		66		96		126		156		186		216		246	
7		37		67		97		127		157		187		217		247	
8		38		68		98		128		158		188		218		248	
9		39		69		99		129		159		189		219		249	
10		40		70		100		130		160		190		220		250	
11		41		71		101		131		161		191		221		251	
12		42		72		102		132		162		192		222		252	
13		43		73		103		133		163		193		223		253	
14		44		74		104		134		164		194		224		254	
15		45		75		105		135		165		195		225		255	
16		46		76		106		136		166		196		226		256	
17		47		77		107		137		167		197		227		257	
18		48		78		108		138		168		198		228		258	
19		49		79		109		139		169		199		229		259	
20		50		80		110		140		170		200		230		260	
21		51		81		111		141		171		201		231		261	
22		52		82		112		142		172		202		232		262	
23		53		83		113		143		173		203		233		263	
24		54		84		114		144		174		204		234		264	
25		55		85		115		145		175		205		235		265	
26		56		86		116		146		176		206		236		266	
27		57		87		117		147		177		207		237		267	
28		58		88		118		148		178		208		238		268	
29		59		89		119		149		179		209		239		269	

No.	Class
270	
271	
272	
273	
274	
275	
276	
277	
278	
279	
280	
281	
282	
283	
284	
285	
286	
287	
288	
289	
290	
291	
292	
293	
294	
295	
296	
297	
298	
299	
300	
301	
302	
303	
304	
305	
306	
307	
308	
309	

No.	Class
310	
311	
312	
313	
314	
315	
316	
317	
318	
319	
320	
321	
322	
323	
324	
325	
326	
327	
328	
329	
330	
331	
332	
333	
334	
335	
336	
337	
338	
339	
340	
341	
342	
343	
344	
345	
346	
347	
348	
349	

No.	Class
350	
351	
352	
353	
354	
355	
356	
357	
358	
359	
360	
361	
362	
363	
364	
365	
366	
367	
368	
369	
370	
371	
372	
373	
374	
375	
376	
377	
378	
379	
380	
381	
382	
383	
384	
385	
386	
387	
388	
389	

No.	Class
390	
391	
392	
393	
394	
395	
396	
397	
398	
399	
400	
401	
402	
403	
404	
405	
406	
407	
408	
409	
410	
411	
412	
413	
414	
415	
416	
417	
418	
419	
420	
421	
422	
423	
424	
425	
426	
427	
428	
429	

No.	Class
430	
431	
432	
433	
434	
435	
436	
437	
438	
439	
440	
441	
442	
443	
444	
445	
446	
447	
448	
449	
450	
451	
452	
453	
454	
455	
456	
457	
458	
459	
460	
461	
462	
463	
464	
465	
466	
467	
468	
469	

No.	Class
470	
471	
472	
473	
474	
475	
476	
477	
478	
479	
480	
481	
482	
483	
484	
485	
486	
487	
488	
489	
490	
491	
492	
493	
494	
495	
496	
497	
498	
499	
500	
501	
502	
503	
504	
505	
506	
507	
508	
509	

No.	Class
510	
511	
512	
513	
514	
515	
516	
517	
518	
519	
520	
521	
522	
523	
524	
525	
526	
527	
528	
529	
530	
531	
532	
533	
534	
535	
536	
537	
538	
539	
540	
541	
542	
543	
544	
545	
546	
547	
548	
549	

No.	Class
550	
551	
552	
553	
554	
555	
556	
557	
558	
559	
560	
561	
562	
563	
564	
565	
566	
567	
568	
569	
570	
571	
572	
573	
574	
575	
576	
577	
578	
579	
580	
581	
582	
583	
584	
585	
586	
587	
588	
589	

No.	Class
590	
591	
592	
593	
594	
595	
596	
597	
598	
599	
600	
601	
602	
603	
604	
605	
606	
607	
608	
609	
610	
611	
612	
613	
614	
615	
616	
617	
618	
619	
620	
621	
622	
623	
624	
625	
626	
627	
628	
629	

Field site No. B-

No.	Class
630	
631	
632	
633	
634	
635	
636	
637	
638	
639	
640	
641	
642	
643	
644	
645	
646	
647	
648	
649	
650	
651	
652	
653	
654	
655	
656	
657	
658	
659	
660	
661	
662	
663	
664	
665	
666	
667	
668	
669	
670	

No.	Class
671	
672	
673	
674	
675	
676	
677	
678	
679	
680	
681	
682	
683	
684	
685	
686	
687	
688	
689	
690	
691	
692	
693	
694	
695	
696	
697	
698	
699	
700	
701	
702	
703	
704	
705	
706	
707	
708	
709	
710	
711	

No.	Class
712	
713	
714	
715	
716	
717	
718	
719	
720	
721	
722	
723	
724	
725	
726	
727	
728	
729	
730	
731	
732	
733	
734	
735	
736	
737	
738	
739	
740	
741	
742	
743	
744	
745	
746	
747	
748	
749	
750	
751	
752	

No.	Class
753	
754	
755	
756	
757	
758	
759	
760	
761	
762	
763	
764	
765	
766	
767	
768	
769	
770	
771	
772	
773	
774	
775	
776	
777	
778	
779	
780	
781	
782	
783	
784	
785	
786	
787	
788	
789	
790	
791	
792	
793	

No.	Class
794	
795	
796	
797	
798	
799	
800	
801	
802	
803	
804	
805	
806	
807	
808	
809	
810	
811	
812	
813	
814	
815	
816	
817	
818	
819	
820	
821	
822	
823	
824	
825	
826	
827	
828	
829	
830	
831	
832	
833	
834	

No.	Class
835	
836	
837	
838	
839	
840	
841	
842	
843	
844	
845	
846	
847	
848	
849	
850	
851	
852	
853	
854	
855	
856	
857	
858	
859	
860	
861	
862	
863	
864	
865	
866	
867	
868	
869	
870	
871	
872	
873	
874	
875	

No.	Class
876	
877	
878	
879	
880	
881	
882	
883	
884	
885	
886	
887	
888	
889	
890	
891	
892	
893	
894	
895	
896	
897	
898	
899	
900	
901	
902	
903	
904	
905	
906	
907	
908	
909	
910	
911	
912	
913	
914	
915	
916	

No.	Class
917	
918	
919	
920	
921	
922	
923	
924	
925	
926	
927	
928	
929	
930	
931	
932	
933	
934	
935	
936	
937	
938	
939	
940	
941	
942	
943	
944	
945	
946	
947	
948	
949	
950	
951	
952	
953	
954	
955	
956	
957	

No.	Class
958	
959	
960	
961	
962	
963	
964	
965	
966	
967	
968	
969	
970	
971	
972	
973	
974	
975	
976	
977	
978	
979	
980	
981	
982	
983	
984	
985	
986	
987	
988	
989	
990	
991	
992	
993	
994	
995	
996	
997	
998	
999	

Appendix F: Figures of Annual NPP, Annual NPP Deviation, and Monthly NPP Anomalies for 2003–2011

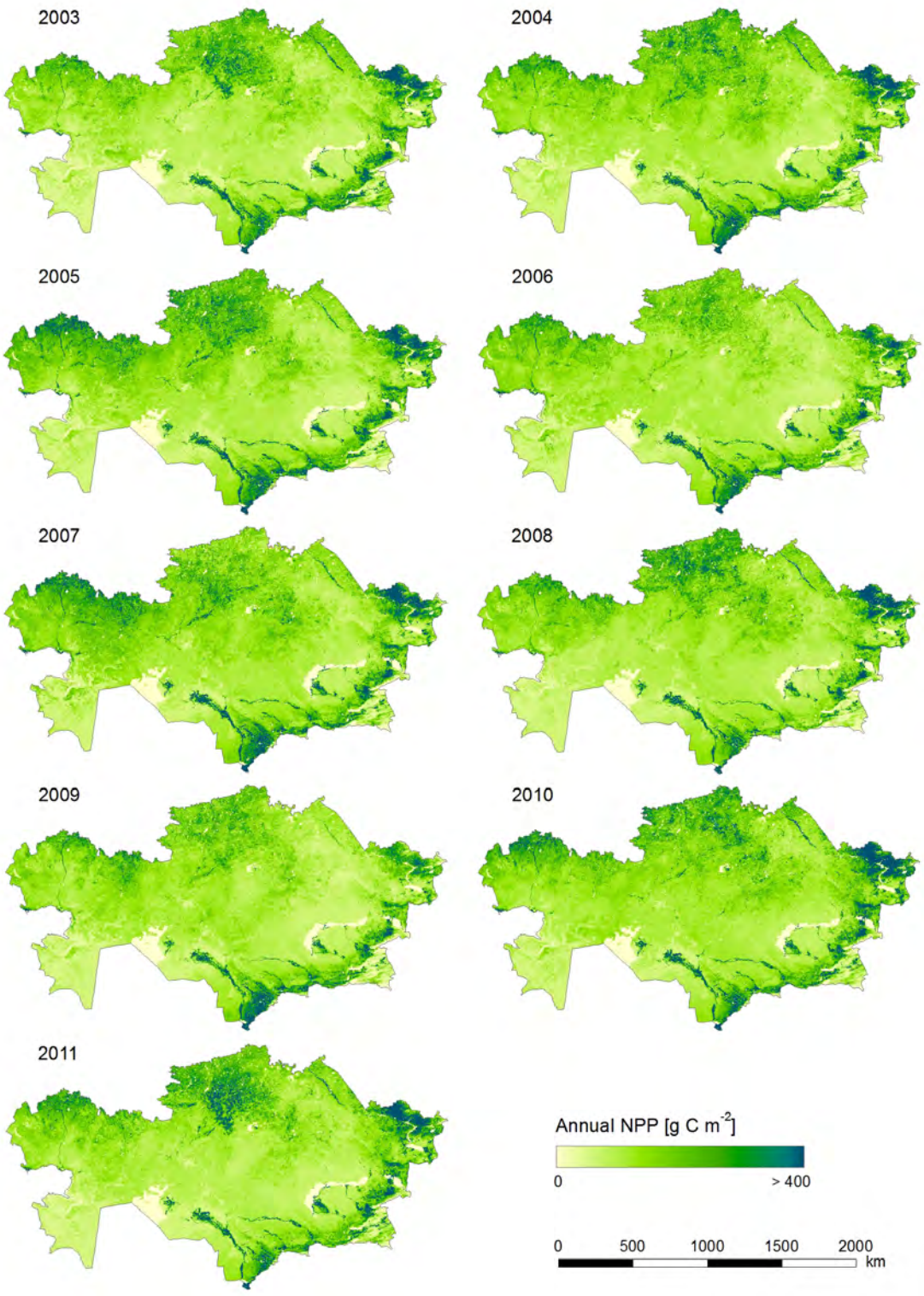

Figure F-1: Annual NPP in Kazakhstan for the years 2003–2011 modelled with BETHY/DLR.

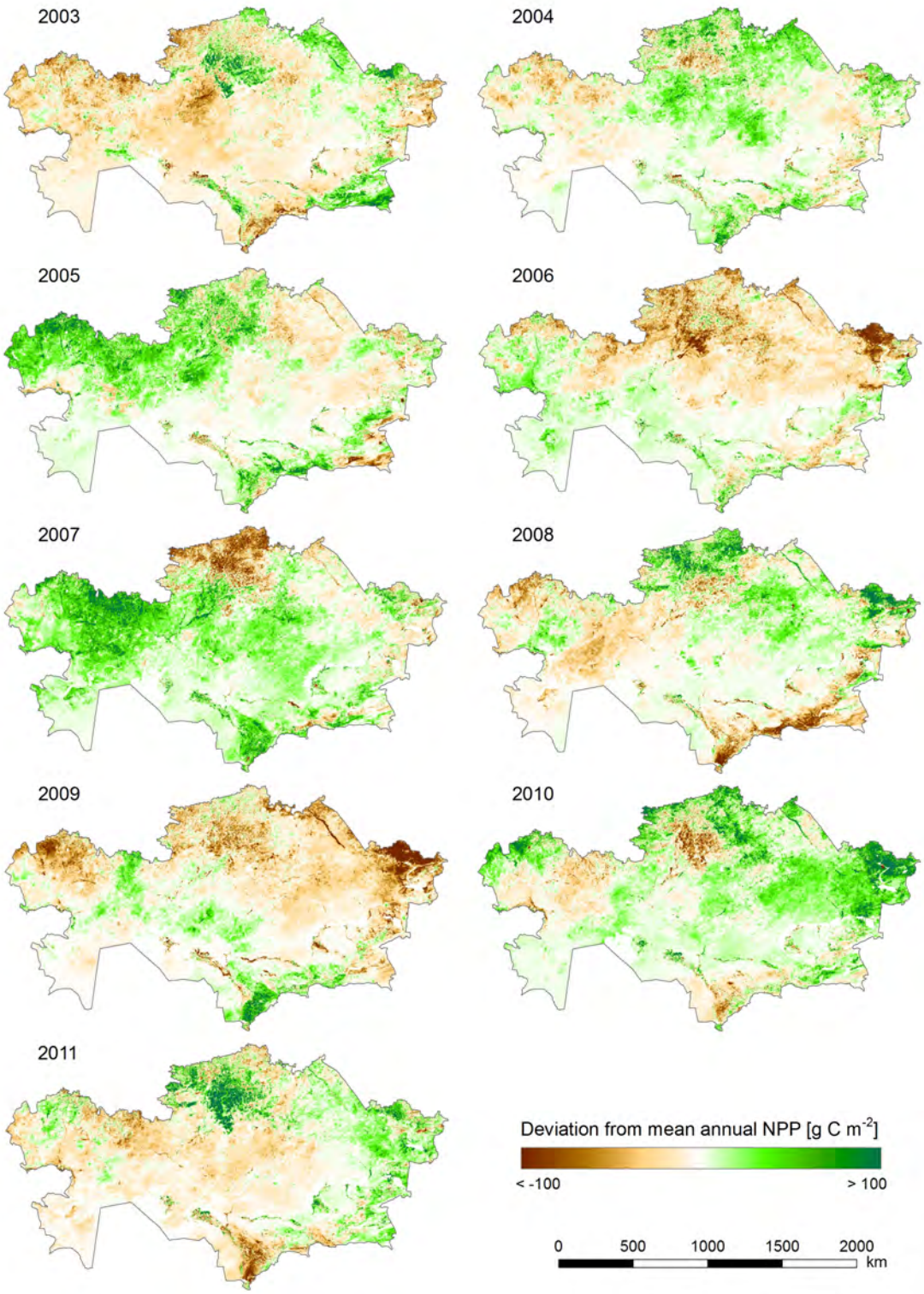

Figure F-2: Absolute deviation from the mean annual NPP in Kazakhstan for the years 2003–2011. Deviation is given in relation to the mean annual NPP for the 2003–2011 time period.

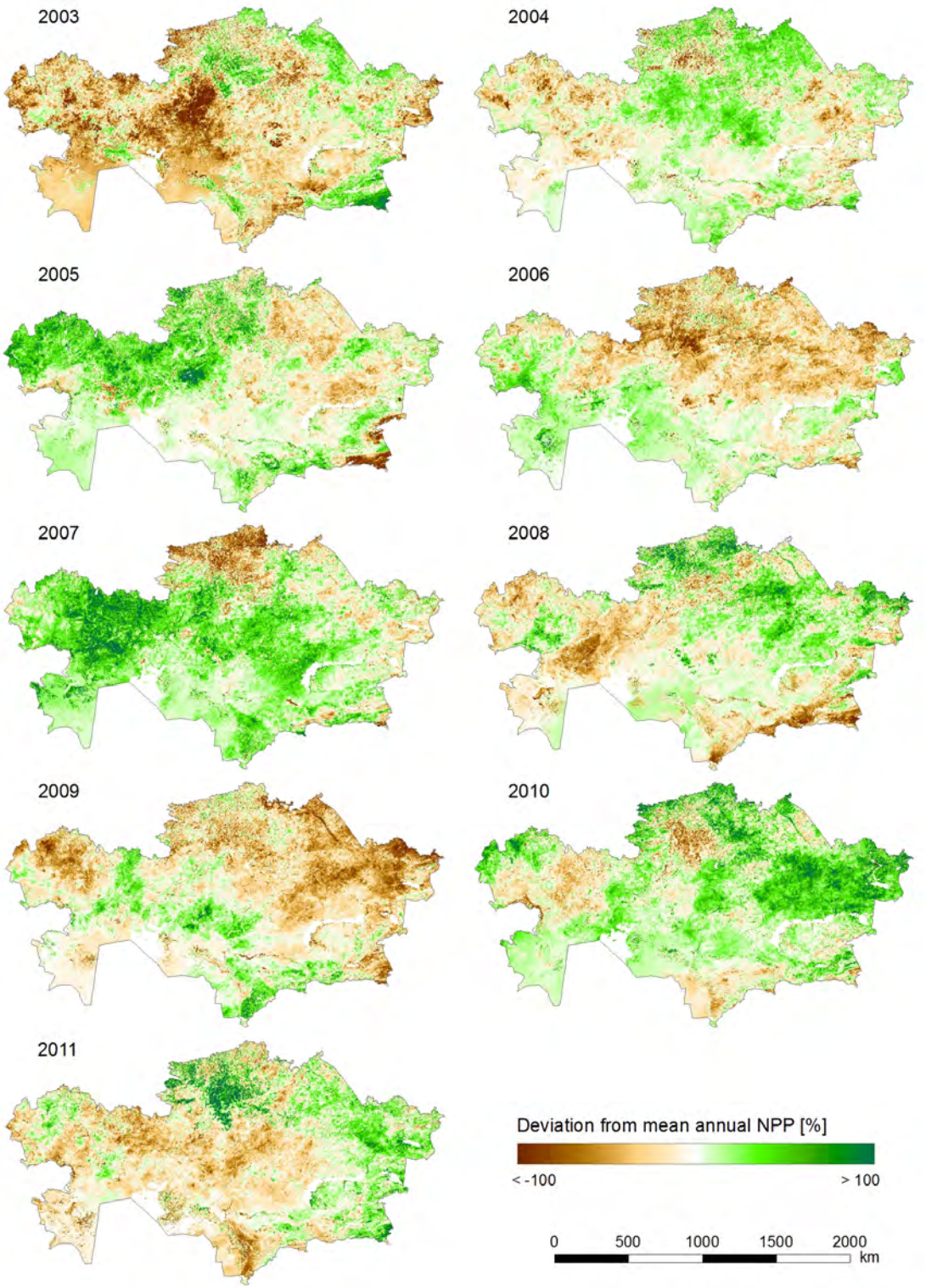

Figure F-3: Relative deviation from the mean annual NPP in Kazakhstan for the years 2003–2011. Percentage deviation is given in relation to the mean annual NPP for the 2003–2011 time period.

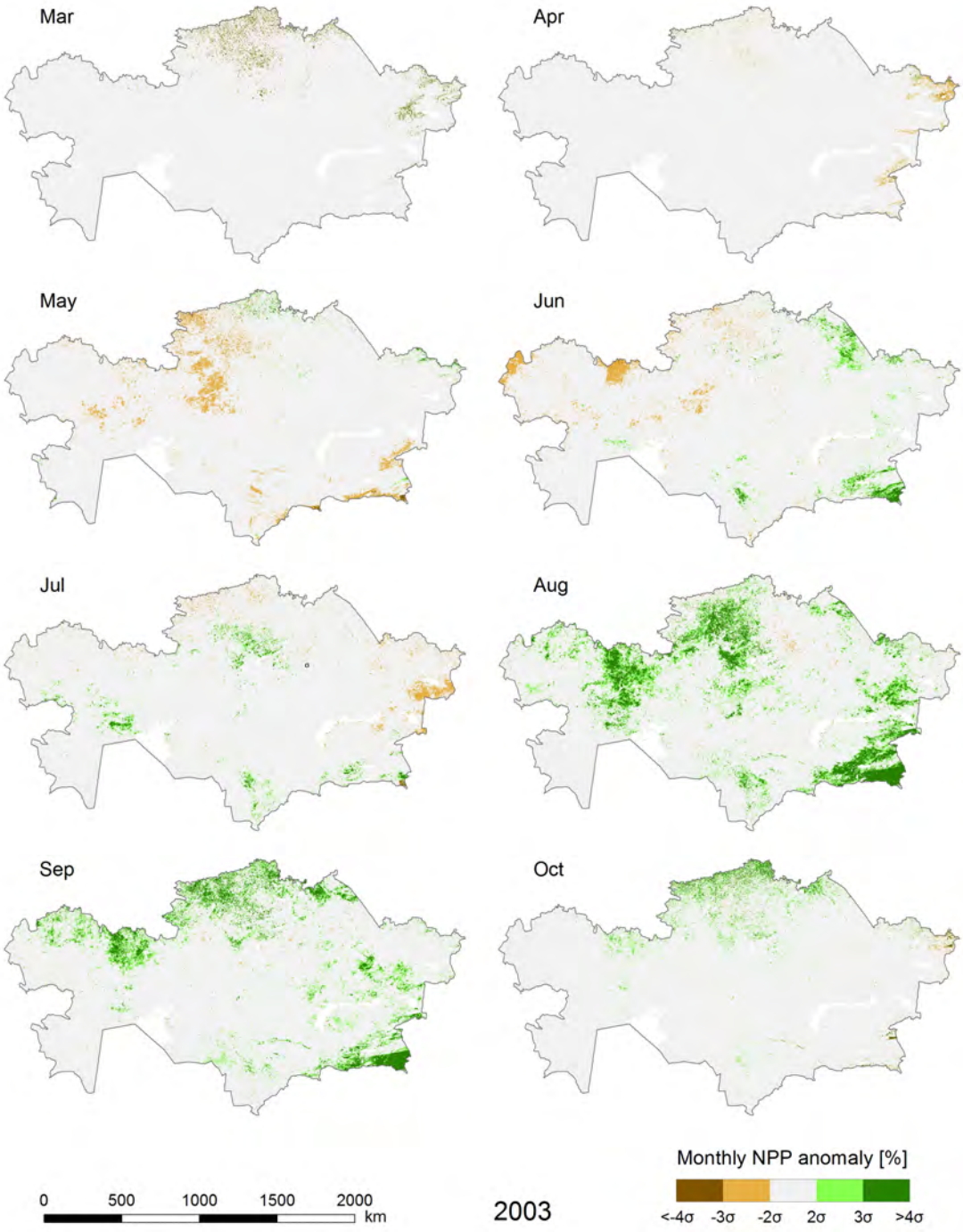

Figure F-4: Monthly NPP anomalies in Kazakhstan for March to October 2003.

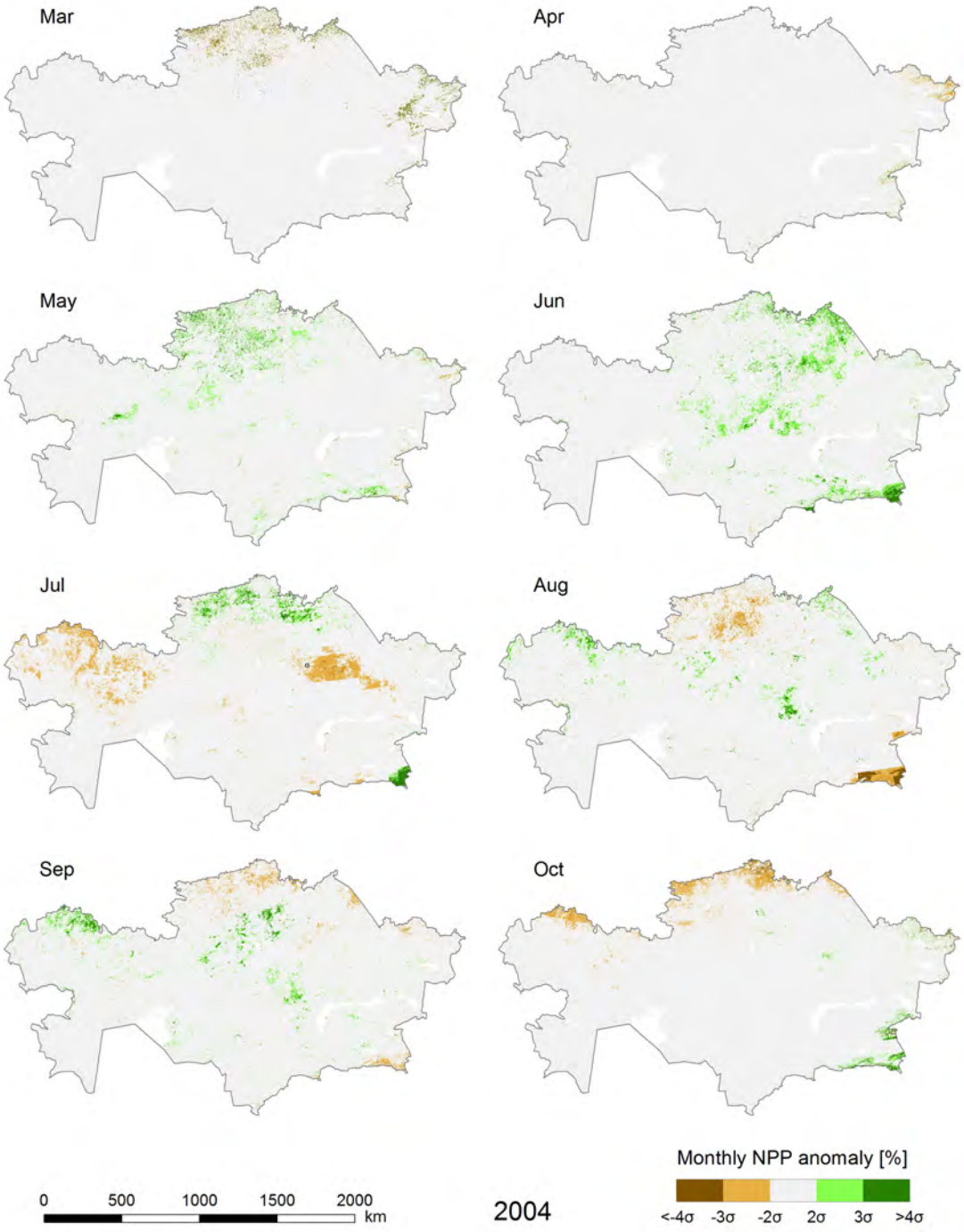

Figure F-5: Monthly NPP anomalies in Kazakhstan for March to October 2004.

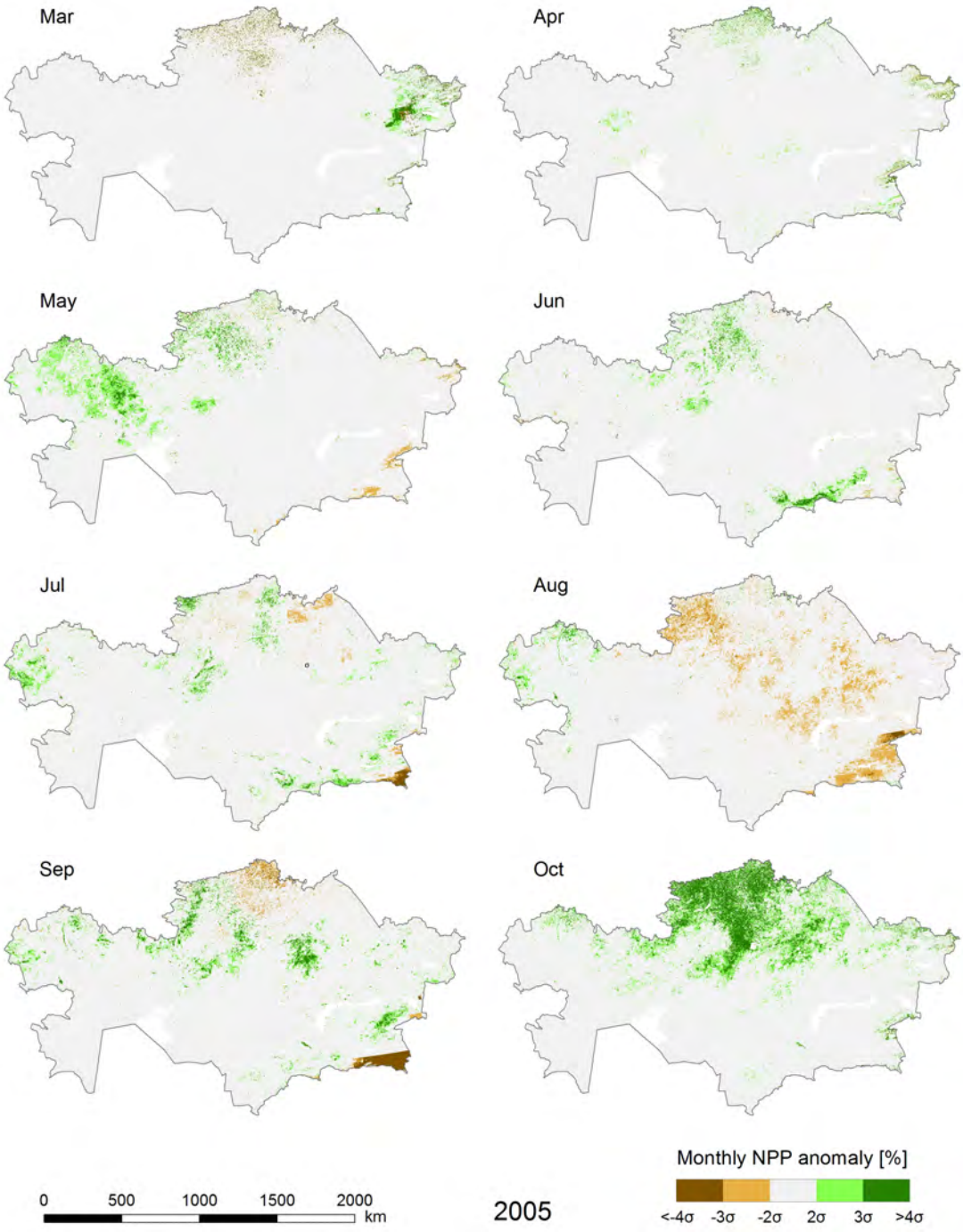

Figure F-6: Monthly NPP anomalies in Kazakhstan for March to October 2005.

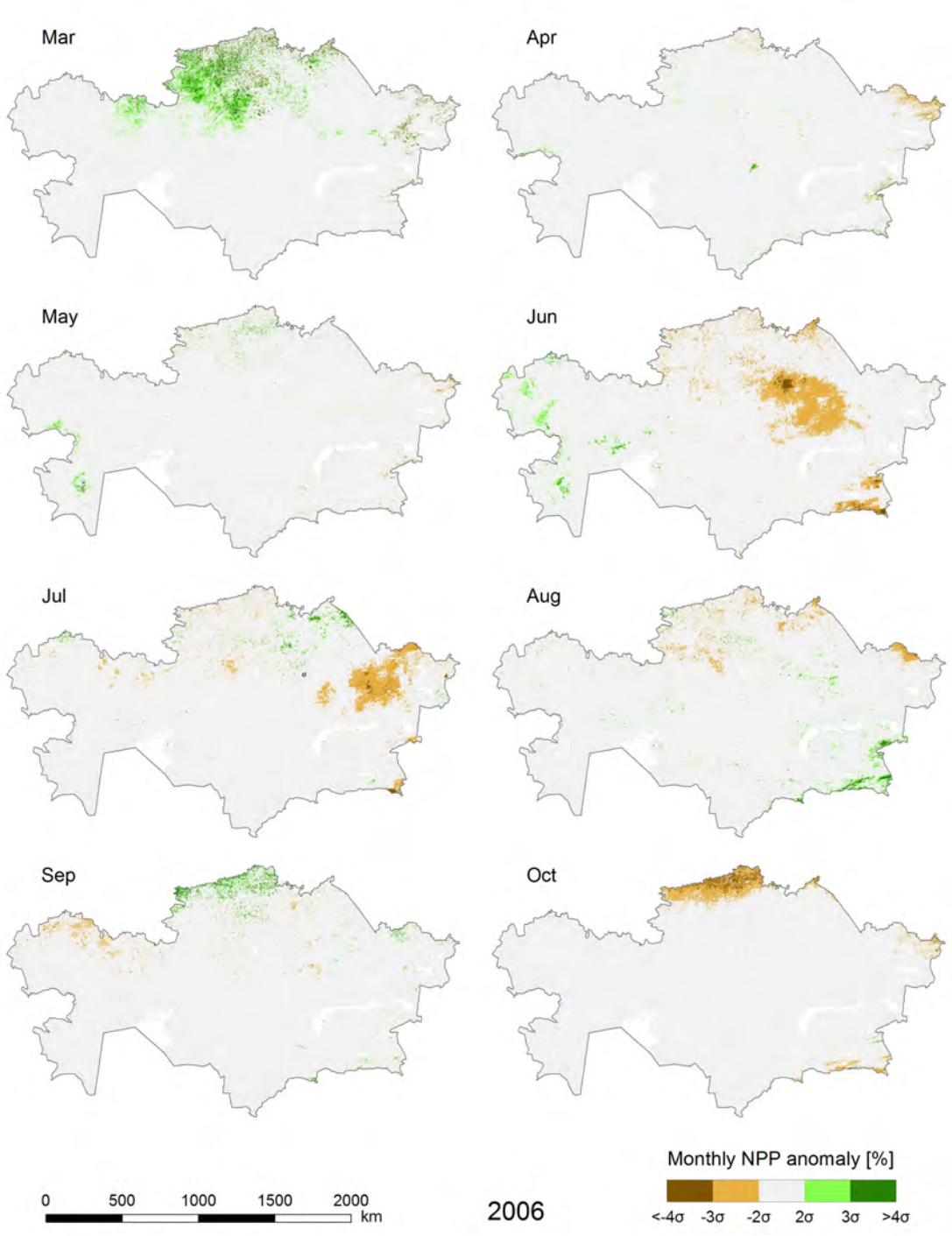

Figure F-7: Monthly NPP anomalies in Kazakhstan for March to October 2006.

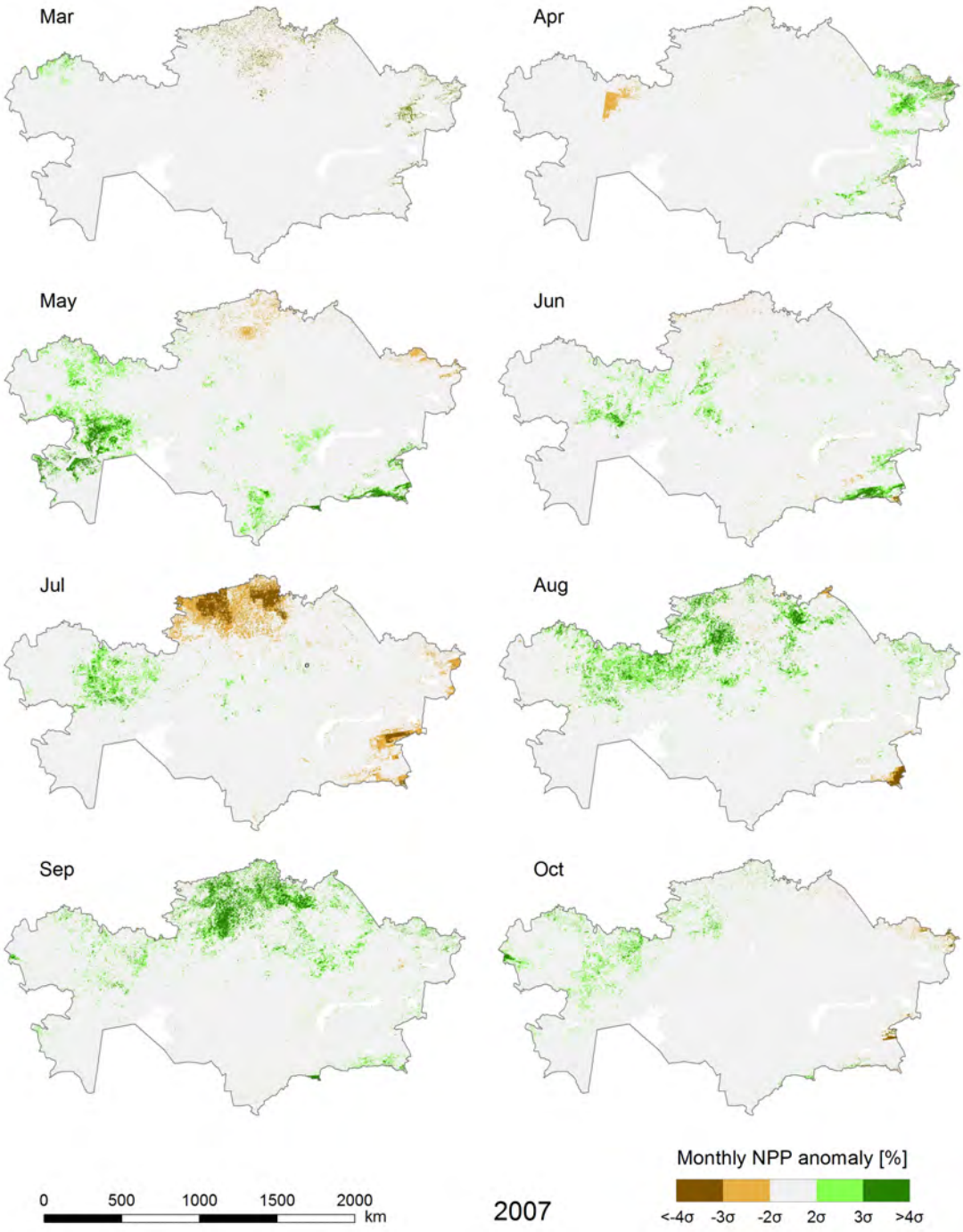

Figure F-8: Monthly NPP anomalies in Kazakhstan for March to October 2007.

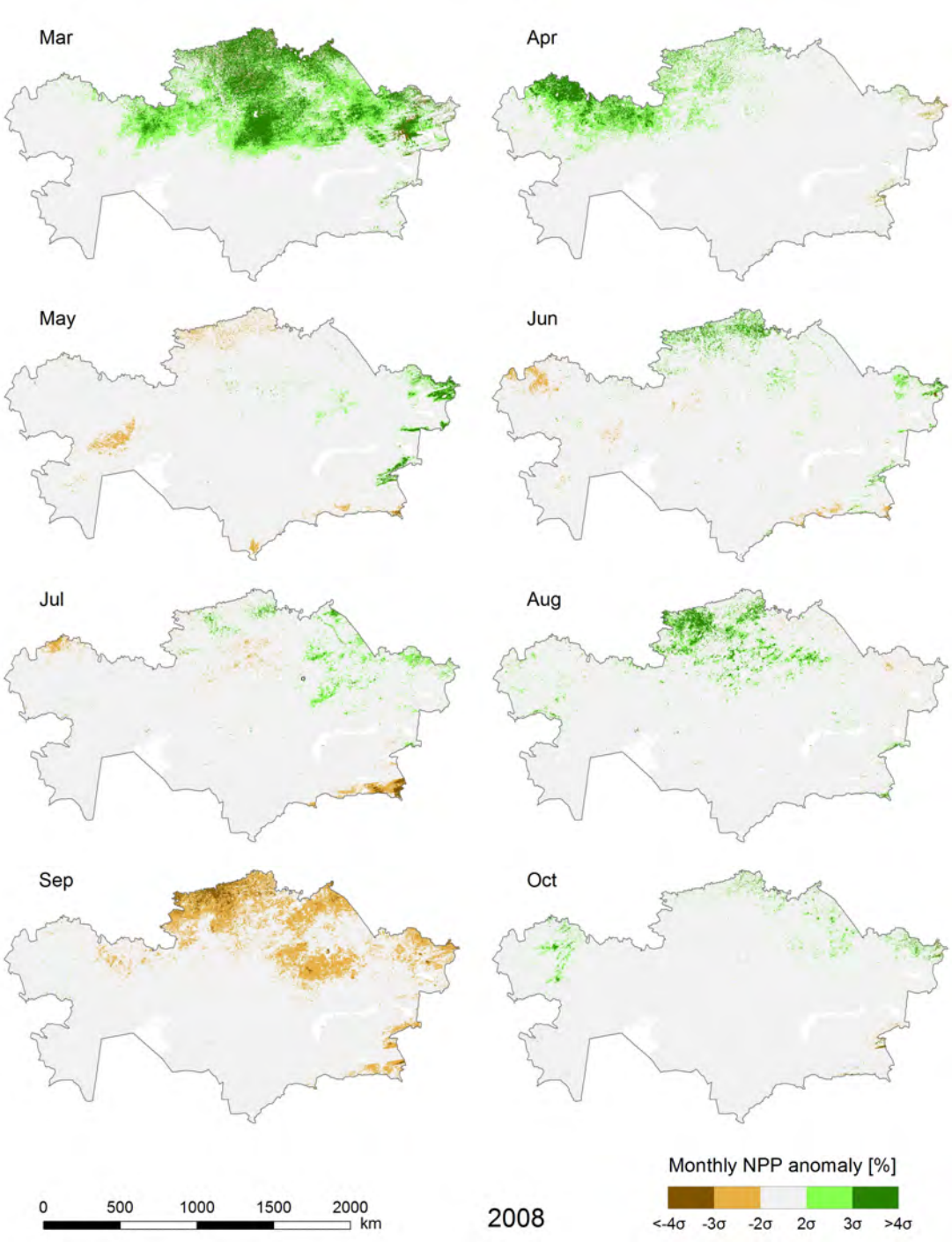

Figure F-9: Monthly NPP anomalies in Kazakhstan for March to October 2008.

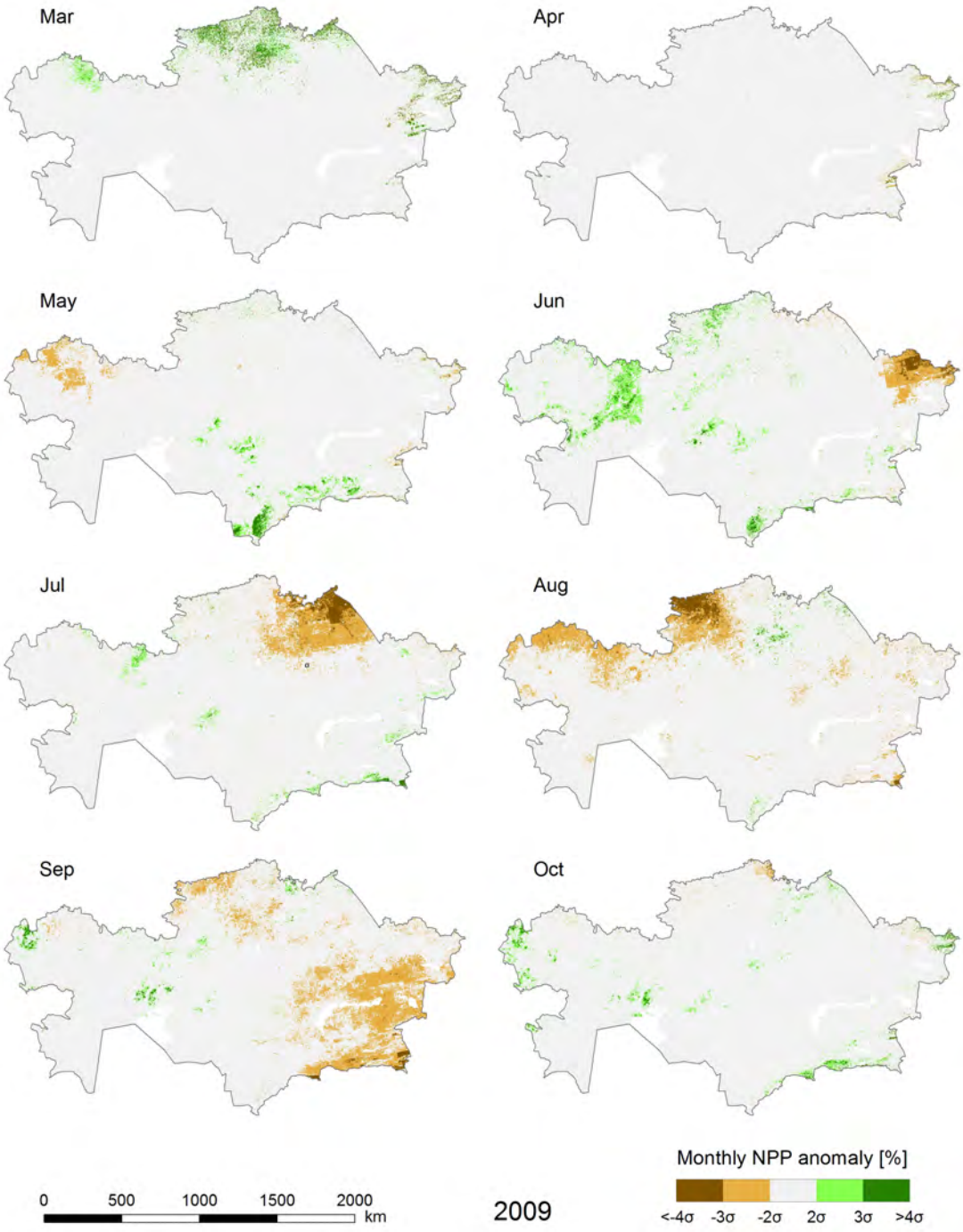

Figure F-10: Monthly NPP anomalies in Kazakhstan for March to October 2009.

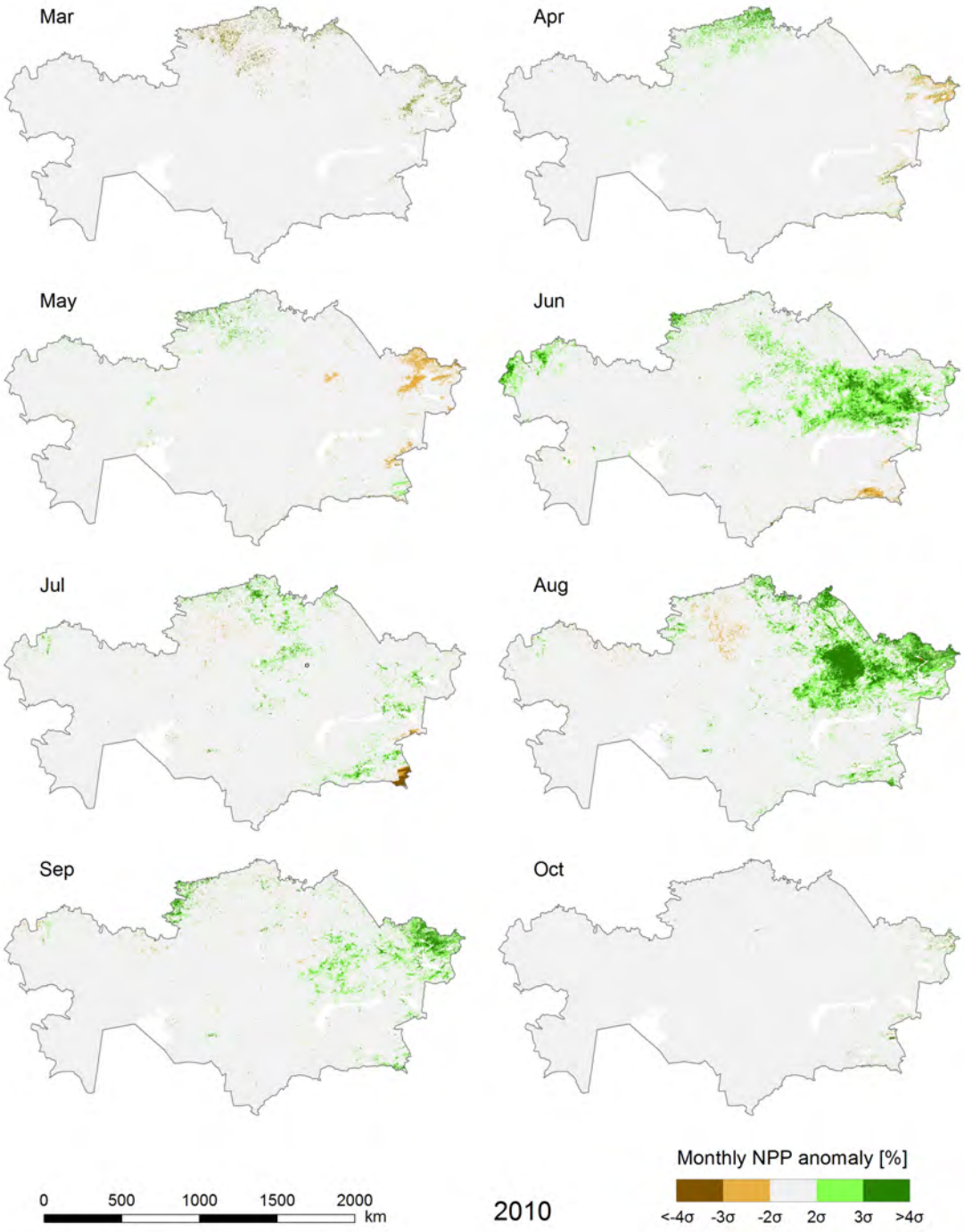

Figure F-11: Monthly NPP anomalies in Kazakhstan for March to October 2010.

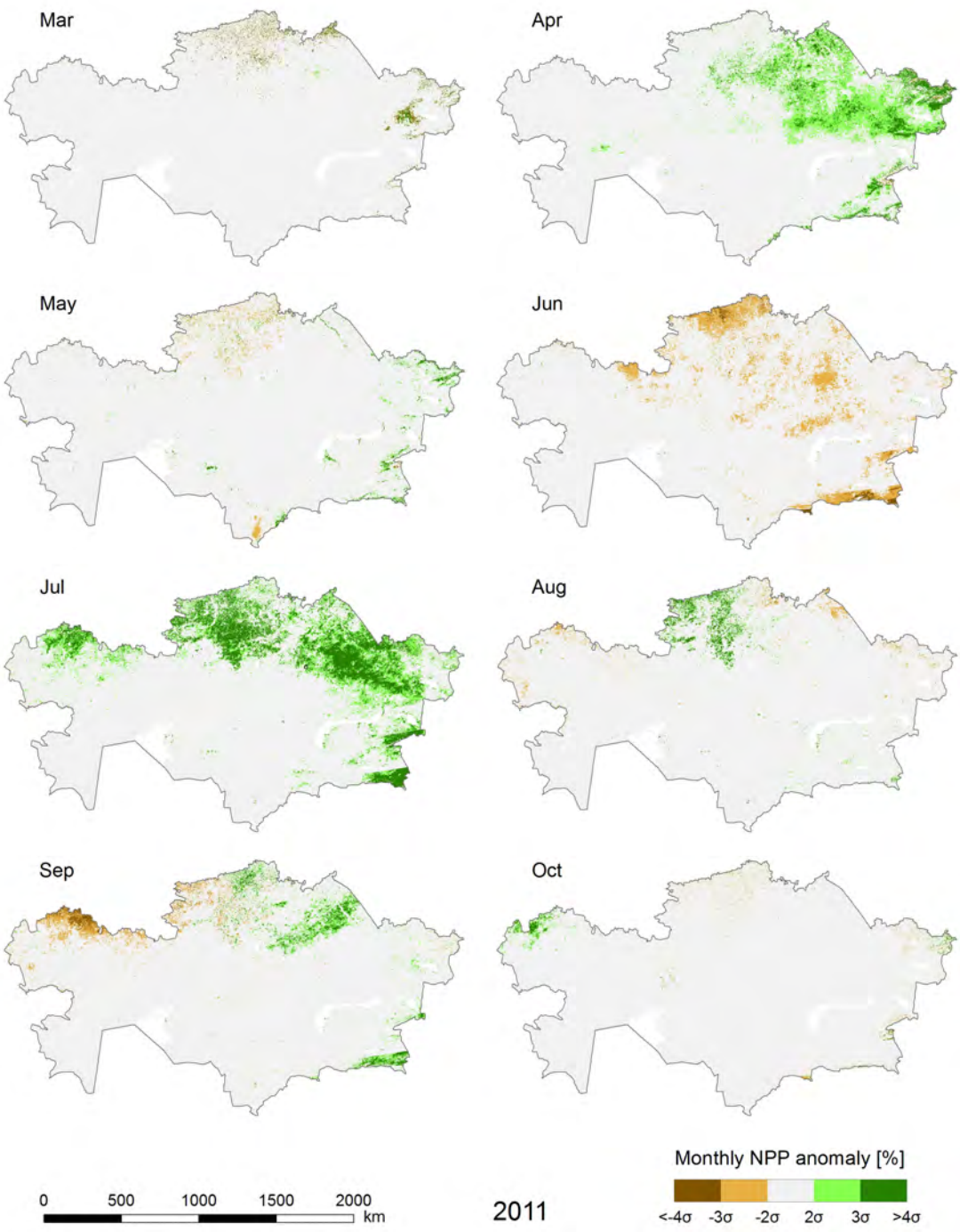

Figure F-12: Monthly NPP anomalies in Kazakhstan for March to October 2011.